THE INTERACTION OF SIMPLE GASES WITH HOT METAL FILAMENTS

by

MELVYN ROYSTON PAINTER

A dissertation submitted for the
Degree of Doctor of Philosophy
in the
Department of Chemistry
of the
University of Aston
in Birmingham

August, 1973.

SUMMARY

The interaction of iodine, methyl bromide, methyl cyanide and methyl iodide with tantalum, tungsten, molybdenum and platinum filaments has been studied in a magnetron system. The interaction of two of these compounds, iodine and methyl iodide, with tantalum filaments has also been studied in an ultra high vacuum system.

The study of the surface ionisation of iodine and the methyl compounds in the magnetron revealed the mechanisms of ion formation for the bromide, cyanide and iodide negative ions from these compounds. Adsorption and dissociation on the filament surface were found to be important in the ion formation reaction.

The study in the ultra high vacuum system consisted of observing the thermal desorption of neutral species from the surface and the effects of gas adsorption on the electron work function of this surface. The study of the thermal desorption of iodine and methyl iodide revealed the presence of adsorbed molecular iodine and from a quantitative analysis of this reaction the surface coverage of the desorbing species, the order of reaction and the enthalpy and entropy of activation for the desorption reaction were ascertained.

The effect of the vapours of all the compounds mentioned above on the various surfaces employed was observed using both thermionic emission and contact potential measurements and the most important factor determining the emission properties was found to be the formation of carbides by reaction of the metal with the methyl group. The physical and thermionic emission properties of tantalum carbide have been studied in detail.

-o-

PREFACE

This dissertation, which is being submitted for the degree of Doctor of Philosophy in the University of Aston in Birmingham, is an account of the work done under the supervision of Professor F. M. Page in the Department of Chemistry of the University of Aston in Birmingham from August, 1970 to August, 1973. Except where references are given in the text, the work described herein is original and has not been nor is being submitted for a degree at any other University.

M.R. Painter

M. R. Painter
August, 1973.

ACKNOWLEDGEMENTS

I wish to express my gratitude to Prof. F. M. Page for his guidance and encouragement during the past three years.

I should also like to thank my accomplices, Tony Chamberlain and Mike P. E. Houghton for their well meaning advice and help during this period.

Last, but by no means least, I should like to thank my wife Jacky for her patience and encouragement during the pursuance of my researches and for typing this thesis.

-o-

CONTENTS

1.0. Introduction

-o-

TABLES

-o-

FIGURES

-o-

1.0. INTRODUCTION

1.1. The Interaction of Gases with Metal Surfaces

The objective of this thesis was the study of the reaction of certain gas phase molecules with metal surfaces. From many studies it is clear that the gas-metal surface reaction can be divided into two main categories, the adsorption of the gas onto the metal surface and the desorption of the adsorbed products from the surface.

1.1.1. The Adsorption Reaction (1)

When two immiscible phases are brought into contact it is nearly always found that the concentration of one of the phases is greater at the interface than in its bulk. This tendency for accumulation to take place is called adsorption and its occurrence is due to the atoms in any surface being subjected to unbalanced forces of attraction perpendicular to the surface plane.

It is usual to classify adsorption into two basic types, physical adsorption and chemical adsorption, but this classification is not distinct, the main difference being that electron transfer takes place between the adsorbed species and the surface only in chemisorption.

Chemisorption, being a chemical reaction, may require an appreciable activation energy, whereas physical adsorption, which is a Van der Waals type interaction, requires no activation energy.

Considering more closely the adsorption reaction, if the gas is present above the surface at a pressure, P, then the number of molecules colliding with a unit area of the surface will be given by kinetic theory$^{(2)}$ as $P/(2\pi mkT)^{\frac{1}{2}}$. If the sticking probability, S, is defined as the fraction of collisions resulting in chemisorption then the rate of adsorption is given by,

$$\left(\frac{dn}{dt}\right)_{ads} = \frac{S.\ P}{(2\pi mkT)^{\frac{1}{2}}} \qquad - \qquad (1\text{-}1)$$

Only rarely is S equal to unity (and is generally $\leqslant 0.4$ $^{(3)}$) and this can be attributed to several factors. If the adsorption is activated then only those molecules possessing the necessary activation energy, the Boltzmann factor, will be adsorbed. It may also be that a particular gas molecule-surface configuration is necessary or that the molecule collides with an occupied site thus inhibiting reaction and in both of these cases S will be less than unity.

The sticking probability may therefore be written,

$$S = \sigma .\ f(\theta)\ \exp\ (-E_a/RT) \qquad - \qquad (1\text{-}2)$$

Hence,

$$\left(\frac{dn}{dt}\right)_{ads} = \frac{\sigma .P}{(2\pi mkT)^{\frac{1}{2}}}\ f(\theta)\ .\ \exp\ (-E_a/RT) \ - \quad (1\text{-}3)$$

Where σ is the condensation coefficient, E_a the activation energy for adsorption and $f(\theta)$ a function of the surface coverage, θ, represents the probability that collision occurs at a vacant site.

The condensation coefficient may be an empirical quantity but it is also possible to formulate it using the absolute reaction rate theory. This theory gives the rate of adsorption as (4),

$$\left(\frac{dn}{dt}\right)_{ads} = n_g \cdot n_s \cdot f(\theta)\,\frac{kT}{h}\,\frac{F_a^{\ddagger}}{F_g F_s}\,\exp\left(-E_a/RT\right) \qquad - \quad (1\text{-}4)$$

where n_g is the gas phase concentration (=P/kT), n_s is the total number of surface sites and $F_a^{\ddagger}$, F_g, F_s are the partition functions of the activated complex for adsorption, the gas phase molecule and the surface respectively. This last quantity can be set equal to unity.

Therefore,

$$\sigma = \left(\frac{2\pi mkTn_s^2}{h^2}\right)^{\frac{1}{2}} \cdot \left(\frac{F_a^{\ddagger}}{F_g}\right) \qquad - \quad (1\text{-}5)$$

This describes the configurational or entropy effect mentioned above.

1.1.2. The Desorption Reaction

When the bond between an adsorbed species and the surface is broken the species enters a region of rapid electron exchange (5). During the traverse through this region the energy band associated with the surface-radical bond shifts and narrows until it attains the unperturbed, discrete nature characteristic of the gas phase species. After moving a distance of the order of the molecular diameter the electron exchange ceases and the probability that the species is desorbed as a neutral particle, a positive ion or a negative ion will be determined by the free energy of formation of the particular species.

It is more useful to consider the desorption reactions of these three types of particle individually.

1.1.2.1. Desorption of Neutral Particles

Physical adsorption is generally a reversible process and therefore the desorbing species is usually the species previously adsorbed.

In the case of a chemisorbed atom or molecule chemical reaction, leading to decomposition, may occur, for example carbon monoxide is adsorbed without dissociation(6) whilst carbon dioxide is adsorbed as carbon monoxide molecules and oxygen atoms(7).

The rate of desorption of a particular species, desorbing via a first order reaction, can be shown to be of the form,(4)

$$\left(-\frac{dn}{dt}\right)_{des} = n_a \cdot \frac{kT}{h} \frac{F_d^{\ddagger}}{F_a} \exp\left(-E_d/RT\right) \qquad - \quad (1\text{-}6)$$

where n_a ($= n_s f'(\theta)$) is the number of adsorbed species available for desorption, E_d is the activation energy for desorption and $F_d^{\ddagger}$, F_a the partition functions of the activated complex for desorption and the adsorbed species respectively.

Unlike chemisorption, desorption is always an activated process. The activation energies for these two processes are related via the heat of adsorption,

$$E_d = E_a + q \qquad - \quad (1\text{-}7)$$

so that in the limiting case where $E_a = 0$ then $E_d = q$.

1.1.2.2. Desorption of Charged Particles

The desorption of charged particles from a metal surface is generally called surface ionisation. The desorption of an electron can be treated in a similar way to the desorption of heavier charged species.

In a similar way to above, the absolute reaction rate theory can be utilised to formulate rate equations for the emission of positive and negative ions(8).

For the desorption of negative ions,

$$\left(-\frac{dn_-}{dt}\right)_{des} = n_a \frac{kT}{h} \cdot \frac{F_-^{\ddagger}}{F_a} \cdot \exp -\frac{(\chi + E_d - E)}{RT} \quad - \quad (1\text{-}8)$$

and positive ions,

$$\left(-\frac{dn_+}{dt}\right)_{des} = n_a \frac{kT}{h} \cdot \frac{F_+^{\ddagger}}{F_a} \cdot \exp -\frac{(\chi + E_d + I)}{RT} \quad - \quad (1\text{-}9)$$

where E is the electron affinity and I the ionisation potential of the desorbing species and $F_-^{\ddagger}$, $F_+^{\ddagger}$ are the partition functions of the activated complexes for the desorption of negative and positive ions respectively.

There is an equilibrium at the surface and an equation, usually called the Saha-Langmuir equation, may be written to describe the equilibrium ratio of any of the emitted particles, neutral particles, positive ions, negative ions and electrons by combining two or more of the equations in the preceding section.

1.2. Theoretical and Experimental Basis of Methods used for the Study of Gas Metal Reactions

In general these methods can be divided into those in which measurements are made on the system at equilibrium and those in which kinetic measurements are made when the system is disturbed from equilibrium. An example of the first is the study of surface ionisation in a flow system whilst the thermal desorption method is an example of the latter.

Although the gas metal reaction can be divided into the adsorption and desorption reactions the experimental methods are not so sharply divided and often a method yields information about both reactions.

In all of these methods the preparation of the surface is of the utmost importance as surfaces which are sufficiently active to enter into chemisorption are, by virtue of their high unsaturation, very prone to contamination.

There are two ways of obtaining a clean surface, in the first a contaminated surface is cleaned, either thermally or by chemical reaction, for example the removal of oxygen by reduction with hydrogen(9) or by bombardment with charged particles(10). The second method is to outgas a small speciment of the solid, in vacuo, just below that temperature at which it becomes volatile and then to heat it to a slightly higher temperature to form an evaporated film on the surface of the containing vessel(11).

1.2.1. Adsorption

The main information required is the amount of gas adsorbed, the sticking probability and the heat of adsorption.

Three main types of clean surface have been used to study adsorption; powders, evaporated films and filaments. The experimental techniques used normally differ as these three types of surface differ greatly in surface area, an average powder may adsorb 100cm.^{3} of gas, a film 0.1 cm.^{3}, whilst a typical filament, of 1cm.^{3} surface area, only 10^{-5}cm.^{3} of gas.

For this reason most volumetric studies of the amount of gas adsorbed have been carried out using powders(12) and evaporated metal films(13) although some measurements have been made using filaments(14). With filaments an alternative, more accurate method is to heat the filament and measure the quantity of gas adsorbed from the pressure rise(14). This latter method forms the basis of the thermal desorption method.

From these volumetric studies it is possible to obtain the surface coverage, θ , and the pressure as a function of time. From these the sticking probability, defined in equation (1-2) can be calculated as a function of θ . The adsorption of nitrogen (5) hydrogen(16) oxygen(17) and carbon monoxide(18) on various metals are examples of the systems studied in this way.

Measurements of the heat of adsorption are often carried out concurrently with surface coverage measurements as the two quantities are often interrelated. Heats of adsorption may be determined from adsorption isotherms, desorption rates or measured calorimetrically.

In the calorimetric method (1) either the heat liberated by adsorption is measured directly and isothermally (useful for powders) or heat loss prevented and the heat determined from the rise in adsorbent temperature (such adiabatic methods are useful for films(19) and filaments(20).

1.2.2. Desorption

1.2.2.1. Desorption of Neutral Particles

After an impinging molecule has fully accommodated with the surface there is a finite probability that it will desorb and this desorption reaction can be considered as part of an equilibrium involving adsorption and accommodation on the surface.

The rate of adsorption was shown to be given by,

$$\left(\frac{dn}{dt}\right)_{ads} = \frac{S.P}{(2\pi mkT)^{\frac{1}{2}}} \qquad - \quad (1\text{-}1)$$

The rate of desorption of molecules can be written(22),

$$\left(-\frac{dn}{dt}\right)_{des} = \frac{n}{\tau} \qquad - \quad (1\text{-}10)$$

where τ is the mean time of residence on the surface. Combining equations (1-1) and (1-10)

$$\frac{n}{\tau} = \frac{S.\ P}{(2\pi mkT)^{\frac{1}{2}}} \qquad - \quad (1\text{-}11)$$

Since the pressure, n and S may be evaluated from an adsorption isotherm then τ may be estimated$^{(21)}$. τ is defined as the mean lifetime on the surface but is also the reciprocal of the desorption rate constant.

$$\tau = \frac{1}{k_d} \exp\left(\frac{E_d}{RT}\right) \qquad - \quad (1\text{-}12)$$

Therefore from a study of τ as a function of temperature the activation energy for desorption may be found.

Other methods of studying desorption arise if, instead of viewing the adsorption in equilibrium, the rate of desorption of molecules is studied when no (or a negligible amount of) adsorption can occur.

This has been considered $^{(4)}$ and as given in equation (1-6) the rate is,

$$\left(-\frac{dn}{dt}\right)_{des} = \bar{d}.\ n^x.\ \frac{kT}{h} \cdot \frac{F_d^{\neq}}{(F_a)^x} \cdot \exp\left(\frac{-E_d}{RT}\right) \qquad - \quad (1\text{-}13)$$

where $\bar{d}$ is the transmission coefficient.

This assumes that the rate varies linearly with n, that is there is no interaction between adsorbed molecules in the desorption process.

The experimental rate will be of the form,

$$\left(-\frac{dn}{dt}\right)_{des} = n^x \cdot k_x \exp \frac{-E_d}{RT} \qquad - \quad (1\text{-}14)$$

This equation can be utilised in two ways. If the temperature is varied and the desorption rate and surface concentration measured as a function of temperature then the rate constant and the activation energy for desorption may be estimated. This is the basis of the thermal desorption measurements in this work and has been the basis of much work and many reviews(22-5) in which the theory and experimental procedure has been developed.

An alternative approach, developed by several workers(26-28) enables the study of the desorption reaction at constant temperature by supplying the necessary energy for desorption by allowing an electron beam to impinge onto the surface. This method, called electron impact desorption, can often yield information about the temperature dependence of the desorption energy and the transmission coefficient.

1.2.2.2. Desorption of Charged Particles

Langmuir and Kingdon(29) first observed the formation of positive ions on an incandescent tungsten surface. Since then numerous studies of both positive and negative surface ionisation have been conducted since this effect opens interesting possibilities for ion production as well as the detection of molecular and atomic beams(30).

The developments recently have followed two main directions. On the one hand there have been equilibrium studies in which the classes of molecules and metal surfaces for which ionisation occurs and the Saha Langmuir equation is valid have been extended(8,31). On the other hand there has been an attempt to study the mechanism of surface ionisation itself, for example by direct determination of the desorption and charge transfer probabilities for ions and atoms(32).

Most of the work has been on equilibrium systems and many reviews have been written(8,31,33-35). In this work interest will be concentrated on the formation of negative ions and the determination of their electron affinities or other energy terms involved in the energy change of the rate determining step. It will be of interest to study not only the equilibrium between negative ions and neutral species but also that between the negative ions and electrons.

Combining the experimental equation for the rates of emission of electrons and negative ions (in terms of current) yields an experimental equation of the form,

$$\frac{J_e}{J_i} = \frac{T^2}{P} . C . \exp\left(- \frac{E}{RT}\right) \qquad - \quad (1\text{-}15)$$

where C is a constant.

An equation of this form is derived theoretically in section (3).

Of the procedures available for studying this equilibrium at hot metal filaments the space charge method of Glockler and Calvin(36) is the most simple. This requires only the determination of the current-voltage characteristic of a space charge limited diode both with and without the presence of an electronegative gas. From this the contribution made to the total current by the negative ions may be calculated. However this method has the limitation that the ions must constitute an appreciable fraction of the total current.

The basis of many measurements used to study negative ion formation is the magnetron method introduced by Sutton and Mayer(37) and developed by Page(38).

In this the negative ion current formed at the heated filament is compared with the thermionic electron current derived from the same source. The electrons and ions are separated by the use of a parallel magnetic field around a coaxial filament-grid-anode assembly. In the presence of the magnetic field only the ions are collected.

This method has been developed and made more versatile by the use of a mass spectrometer, instead of a magnetic field, to separate the ions and electrons (39-42).

More recently, the mechanisms of surface ionisation have been studied more directly. A method which has proved useful for this uses a pulsed molecular beam technique in an attempt to determine the mean residence time of both ions and atoms on metal surfaces.

Apparatus suitable for such measurements has been described (34) and results presented for both positive (5,32) and negative (32,43) ions. The method yields useful information but as yet has only been applied to simple molecules such as the halogens and alkali halides.

1.3. Methods used to study the Reactions of Iodine, Methyl Iodide and Methyl Cyanide with Metal Filaments

The interaction of iodine and the various methyl compounds above with metal filaments has been studied in several ways in order to elucidate the adsorption-desorption reaction of these systems, both at low temperatures (300°K) and elevated temperatures (1000 - 2000°K).

The adsorption and desorption of methyl iodide and iodine have been studied in an ultra high vacuum system, using the thermal desorption method to determine the rates and energetics of these reactions.

The reaction of all of the compounds mentioned above with incandescent metal filaments has been studied, using the magnetron method, in order to obtain information about the dissociative adsorption reaction and the mechanism of surface ionisation, to form the I^-, Br^- and CN^- ions, of these compounds on the filament at elevated temperatures.

Work function measurements were conducted in conjunction with both sets of experiments. The measurement of the thermionic work function forms an integral part of the magnetron method but these measurements on their own and work function measurements in the ultra high vacuum system, using both thermionic and contact potential difference methods, gave further information about the gas-metal reaction.

2.0. ELECTRON WORK FUNCTION MEASUREMENTS

In this section first the theory of the electron work function of a metal surface will be considered and then the experimental methods used for determining this value and changes in it due to gas adsorption will be discussed.

2.1. Theory of the Electron Work Function

The work function of a metal surface can be defined (44, 45) as the difference between the electrochemical potential, $\bar{\mu}e$, of an electron inside the surface and the potential energy of an electron outside the surface at an infinite distance in the absence of external electric fields. If χ is the work function, ϕ the electrostatic potential of the electron just outside the metal surface and e the electronic charge, then,

$$\chi = -\phi_{outer} - \bar{\mu}/e \qquad - \quad (2\text{-}1)$$

If the surface of the metal is considered more closely it will be seen that this consists of a double or dipole layer. This arises because the charges at the surface, the electrons, are screened from the interior by charges of opposite signs, the atom cores, located in the interior close to the surface. The result is a surface dipole layer, due to this asymmetry of charges, which gives rise to a potential jump at the surface.

To be removed from the highest occupied level in the surface (the Fermi level) to a point outside the surface, the electron must traverse this double layer. Equation (2-1) can be expanded to give,

$$\chi = (\phi_{inner} - \phi_{outer}) - \mu/e \qquad - \quad (2\text{-}2)$$

Where the electrochemical potential of the electron has been resolved into two terms, μ , the chemical potential (sometimes called the inner work function) of the electron which is independent of the surface and a term ϕ_{inner}, which depends upon surface conditions. The quantity (ϕ_{inner} - ϕ_{outer}) represents the potential difference between the inside and outside of the conductor and depends upon surface conditions as well as the structure of the interior, It is called the surface potential and will vary for different crystal faces and if adsorbed species are present on the surface.

Consider the presence of an adsorbed gas (1, 45). This adsorbate can modify the inherent dipole structure of the surface. Suppose there are n gas molecules adsorbed $cm.^{-2}$ and the molecule-surface atom dipole is aligned perpendicular to the conductor surface, then this approximates to a double charge layer of charge density, ne. If the dipole moment/adsorbed species is independent of concentration the system may be regarded as a capacitor, or dipole sheet, whose potential is proportional to the number of individual dipoles in a unit area.

The dipole moment, M, for a single adsorbed species is given by,

$$M = e.d \qquad - \quad (2\text{-}3)$$

where d = charge separation.

The total dipole moment/unit area, M_t, is therefore,

$$M_t = n.M = n.e.d. \qquad - \quad (2\text{-}4)$$

According to classical electrostatic theory the potential of the electron changes sharply from Φ to $\Phi \pm 4\pi nM$ on traversing the electrical double layer.

The potential drop across this double layer, ΔV, is therefore given by,

$$\Delta V = 4\pi nM \qquad - \quad (2\text{-}5)$$

ΔV is equal to the work function change, $\Delta \chi$, because it is the change in energy needed to remove an electron from the surface after forming the adsorbed layer.

The work function in the presence of the adsorbed layer is therefore given by,

$$\chi_{ads} = (\phi_{inner} - \phi_{outer}) - \frac{\mu}{e} \pm 4\pi nM \qquad - \quad (2\text{-}6)$$

If the negative end of the dipole produced on adsorption is directed away from the surface (an electronegative layer) then the work function is increased; if towards the surface (electropositive layer) it is decreased.

If M is in Debyes and $\Delta \chi$ in volts then the experimental dipole moment is given by,

$$M_{expt.} = \frac{10^{18} . \Delta \chi}{4\pi . 300. n} \qquad - \quad (2\text{-}7)$$

Using this equation it is therefore possible to find the dipole moment between the ad-atom and the surface using experimentally derived quantities, the surface concentration and the change in work function in the presence of the adsorbate.

2.2. Experimental Methods for the Determination of the Work Function and Work Function Changes due to Adsorption (34,44)

2.2.1. Thermionic Emission

The application of thermodynamics and statistical mechanics to the calculation of the saturated current density, J_s, for electrons emitted from a conductor at temperature, T, leads to the well known Richardson-Laue-Dushman equation,

$$J_s = AT^2(1 - \bar{r}_e) \exp(-\chi/kT) \qquad - \quad (2\text{-}8)$$

where, A = thermionic emission constant = $\dfrac{4\pi mk^2e}{h^3}$

(1.2×10^6. A.m.$^{-2}$deg.$^{-2}$)

$\bar{r}_e$ = zero field reflection coefficient

χ = work function

Several assumptions have been made in the derivation of this equation, the most important of which are that the surface of the conductor is uniform (i.e. a single crystal) and that the field necessary to produce saturation of the electron current is negligibly small (and may be set equal to zero).

The latter is the easier to make a correction for using the Schottky equation.

In figure (2-1) the potential energy of an electron moving normal to the surface is plotted as a function of distance from the surface. The solid curve is the result of imposing the field E on the image potential.

The difference between the potential maximum and the potential at infinity is $\frac{1}{2}(eE/\pi\varepsilon_0)^{\frac{1}{2}}$ where E is the applied potential (in V.m.$^{-1}$) and ε_0 the permittivity of vacuum. The work function can therefore be corrected using the equation,

$$\chi_0 = \chi_E + \frac{1}{2}\left(\frac{eE}{\pi\varepsilon_0}\right)^{\frac{1}{2}} \qquad - \quad (2\text{-}9)$$

or, inserting appropriate values,

$$\chi_0 = \chi_E + 3.79 \times 10^{-5}.\, E^{\frac{1}{2}} \qquad - \quad (2\text{-}10)$$

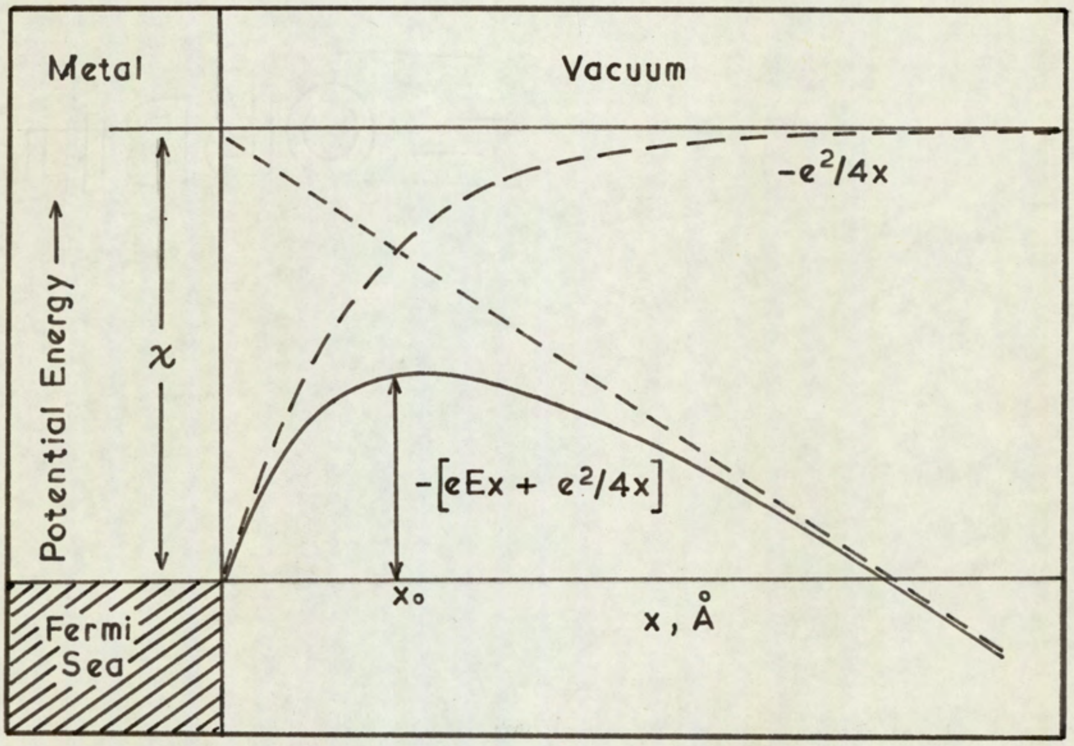

FIGURE (2-1) Modification of the Image Potential, $e^2/4x$, of an Electron Moving Normal to a Metal Surface as the Result of Imposition of a Field E, also Normal to the Surface.

If the surface of the emitter is uniform then from equation (2-8) a plot of experimental values of $\ln(J_s/T^2)$ as a function of $(1/T)$ will give a straight line from which can be calculated the "apparent" (or Richardson) work function,(46)

$$\chi^* = -k \cdot \frac{d(\ln J_s/T^2)}{d(1/T)} \qquad - \quad (2\text{-}11)$$

Equation (2-8) may be differentiated and substitution of the result into equation (2-11) gives the relationship between the true and apparent work function,

$$\chi^* = -T\left(\frac{d\chi}{dT}\right) - \frac{kT^2}{(1-\bar{r})} \cdot \left(\frac{d\bar{r}}{dT}\right) \qquad - \quad (2\text{-}12)$$

Herring and Nicholls (47) suggest that $\bar{r}$ is small compared to unity and also that it is not dependent upon temperature so this expression may be simplified,

$$\chi = \chi^* + T.\left(\frac{d\chi}{dT}\right) \qquad - \quad (2\text{-}13)$$

The apparent emission constant A^* is related to the true emission constant A by the relationship,

$$A = \frac{A^*}{(1-\bar{r}_e)} \cdot \exp\left(\frac{1}{k} \cdot \frac{d\chi}{dT}\right) \qquad - \quad (2\text{-}14)$$

Most experimental emitters for which thermionic constants have been determined have been polycrystalline metals, the surfaces of which are far from uniform. These surfaces consist of patches which have different work functions. In the theoretical approach to thermionic emission for such a surface there are two limiting cases:

(1) The applied field at the surface is much stronger than the patch field (the field outside the emitter arising from the difference in work function of adjacent sites).

(2) The applied field is weak compared to the patch field.

These cases yield work function values, χ^{**} and $\bar{\chi}^{**}$ respectively which are related to χ but by quantities such as the fractional surface area and fractional emission current of the patches which cannot be determined experimentally.

It can be seen that in order to determine the work function by thermionic emission the temperature of the surface must be varied and if this method is used to determine work function changes there are two factors to consider:

(1) Work function changes can only be measured at temperatures where thermionic emission is measurable and at this temperature many adsorbed films may be destroyed. This is particularly true for electronegative species which may increase the work function of the surface. It has been useful for studying electropositive layers such as those of alkali metals, where lowering of the work function occurs.

(2) If adsorption does occur at the elevated temperatures required for thermionic emission then variation of the temperature may cause the surface coverage to change. If the surface concentration of adsorbed species is n molecules cm.$^{-2}$, then at equilibrium,

$$n = v . \tau \qquad - \quad (2\text{-}15)$$

where v = bombardment rate from gas phase

τ = mean lifetime of adsorbed species on surface.

The variation of τ with temperature is normally expressed by the Frenkel equation, (2)

$$\tau = \tau_0 \exp\left(\frac{\pm Q}{RT}\right) \qquad - \quad (2\text{-}16)$$

where Q = heat of adsorption

τ_0 = constant (vibration time of adsorbed molecule with surface) $\simeq 10^{-13}$ sec.

Therefore,

$$n = v\tau_0 \exp\left(\frac{\pm Q}{RT}\right) \qquad - \quad (2\text{-}17)$$

Interpretation of work function changes found by the temperature dependence of electron emission is therefore not simple but it is possible providing the above factors are taken into account.

2.2.2. Contact Potential Difference

Consider two isolated and electrically neutral conductors, A and B, with electrochemical potentials, $\bar{\mu}_A$ and $\bar{\mu}_B$. If these are placed in electrical contact and attain thermal and electrical equilibrium, then,

$$\bar{\mu}_A = \bar{\mu}_B \qquad - \quad (2\text{-}18)$$

This will be brought about by the transfer of electrons from the conductor with the highest electrochemical potential. It has been shown that the work function can be written as,

$$\chi = \phi_{inner} - \phi_{outer} - \frac{\mu}{e} \qquad - \quad (2\text{-}2)$$

The electron current will continue to flow until (ϕ^A_{inner} - ϕ^B_{inner}) is equal to the initial difference ($\bar{\mu}_A - \bar{\mu}_B$) and then there will be an electrical potential difference between A and B (or rather two points, just outside the surfaces of A and B). There is a double layer of charge at the junction due to this electron transfer.

From figure (2-2) it can be seen,

$$\phi^A_{inner} - \phi^B_{inner} = \chi_A - \chi_B = V_{AB} \qquad - \quad (2\text{-}19)$$

where V_{AB}, the difference in work functions, is called the contact potential difference between the two surfaces.

The surface of a real conductor will consist of patches of different work functions and for a particular patch, i, equation (2-2) can be written,

$$\chi_i = \phi^i_{inner} - \phi^i_{outer} - \frac{\mu_i}{e} \qquad - \quad (2\text{-}20)$$

The average work function, $\bar{\chi}$, can be found by summing over all patches, each of fractional area f_i.

$$\bar{\chi} = \sum_i (f_i \cdot \chi_i) \qquad - \quad (2\text{-}21)$$

Equation (2-19) can then be written,

$$\bar{V}_{AB} = (\bar{\chi}_A - \bar{\chi}_B) \qquad - \quad (2\text{-}22)$$

Suppose now that A and B are not in actual physical contact but are otherwise connected electrically and that a potential $V_{ext.}$ is introduced into the external circuit.

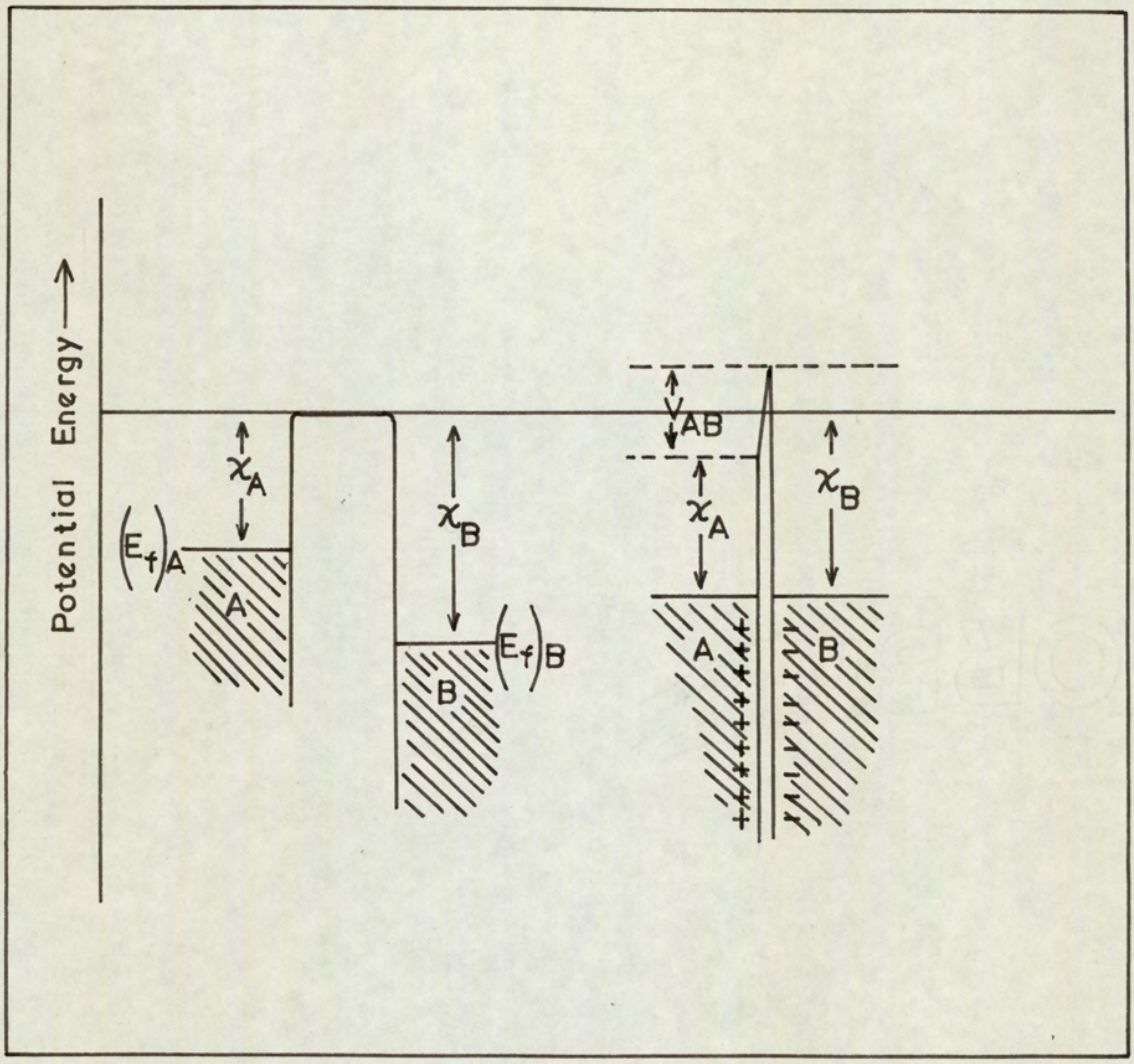

FIGURE (2-2) Contact Potential, V_{AB} between conductors A& B

Equation (2-22) now becomes,

$$\overline{V}_{AB} + V_{ext} = (\overline{\chi}_A - \overline{\chi}_B) + V_{ext}. \qquad - \quad (2\text{-}23)$$

This equation forms the basis of several experimental methods as it can be seen that when $V_{AB} = -V_{ext.}$ then,

$$(\overline{\chi}_A - \overline{\chi}_B) = -V_{ext} \qquad - \quad (2\text{-}24)$$

The difference in the work function of the two surfaces is given by an experimental parameter, V_{ext}.

This contact potential can be measured in several ways (44) but the most convenient method is the electron beam retarding potential method.

2.2.2.1. Electron Beam Method of measuring the Contact Potential Difference

This method is based on the determination of the anode current-voltage characteristics of a diode.

To understand how this method gives contact potential measurements the theory of the plane parallel diode must be considered. An ideal diode consists of two plane parallel, infinitely long, electrodes, one at high temperature emitting electrons thermionically and the other at a distance, d, from the emitter collecting these electrons. The current-voltage characteristics of such a diode can be divided into three regions;

(a) Retarding field region.
(b) Space charge limited current region.
(c) Saturated current region.

The distribution of the electric field between the two parallel electrodes is shown in figure (2-3) (47a).

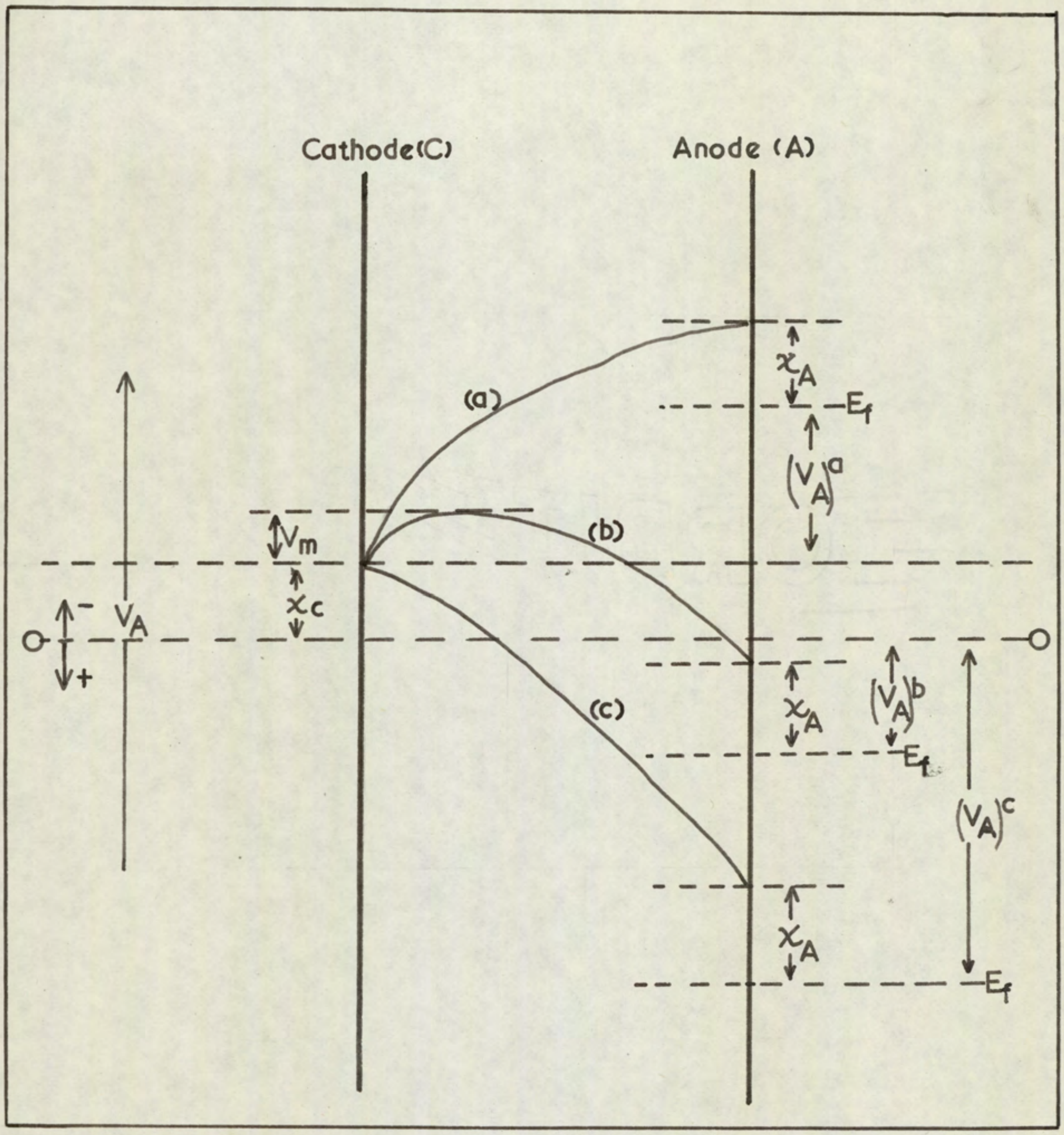

FIGURE (2-3) Electric Field Distribution between Two Parallel Electrodes

(a) Retarding Field.
(b) Space Charge Limited Region.
(c) Saturated Field Region.

In the retarding field region the potential barrier which must be overcome for an electron to be emitted from the cathode and collected by the anode is equal to $\left[-(V_A)^a + \chi_A\right]$. Using equation (2-8) the current density in the retarding field region is, at a cathode temperature, T,

$$J_{ret} = AT^2 (1 - \bar{r}_e) \exp -\left(\frac{-(V_A) + \chi_A}{kT}\right) \qquad - \quad (2\text{-}25)$$

or,

$$J_{ret} = J_{sat} \exp \left(\frac{(V_A)^a - \chi_A + \chi_c}{kT}\right) \qquad - \quad (2\text{-}26)$$

The current in the retarding field region is exponentially dependent upon the applied voltage, A plot of $\ln(J_{ret})$ against V_A will give a straight line, the slope of which gives the temperature of the emitter, This in fact represents a measure of the energy distribution of the emitted electrons, this exponential dependence of J_{ret} upon V_A shows that the energy distribution is Maxwellian.

In the space charge region there exists, in front of the cathode, an electron cloud, called a space charge, owing to the fact that more electrons are emitted than are transported to the collector. Combined with this space charge there is a potential minimum, V_m.

The current density, J_{sp} is

$$J_{sp} = AT^2 (1 - \bar{r}_e) \exp -\left(\frac{(\chi_c - V_m)}{kT}\right) \qquad - \quad (2\text{-}27)$$

or,

$$J_{sp} = J_{sat} \exp \left(\frac{V_m}{kT}\right) \qquad - \quad (2\text{-}28)$$

The solution to this equation is not simple and the region is of little quantitative importance.

When a sufficiently high anode voltage is applied all the electrons emitted by the cathode are collected at the anode and the electron current is given by the equation,

$$J_{sat} = AT^2 \ (1 - \bar{r}_e) \ \exp - \left(\frac{\chi_c}{kT} \right) \qquad - \quad (2\text{-}29)$$

It has been shown for two metals in electrical contact,

$$\overline{V}_{AC} = (\overline{\chi}_C - \overline{\chi}_A) \qquad - \quad (2\text{-}30)$$

From equations (2-25) and (2-29) the relationship between the retarding field current density and that in the saturated field, in terms of the contact potential difference, is,

$$J_{ret} = J_{sat} \ \exp \left(\frac{V_A - \overline{V}_{AC}}{kT} \right) \qquad - \quad (2\text{-}31)$$

Thus when the applied field equals the contact potential difference, the retarding field and saturated field currents are equivalent.

By proper choice of experimental conditions the space charge region can be made very small so that only the retarding field and saturated current regions are apparent in the current-voltage characteristic. This is shown in figure (2-4) and an apparatus which fulfils the requirements is described by Shelton $^{(48)}$.

The 'knee' in the current-voltage curve will occur when the electrostatic potential energy of an electron in the vacuum just outside the metal surface of the anode is equal to the potential energy of a similar electron at the cathode.

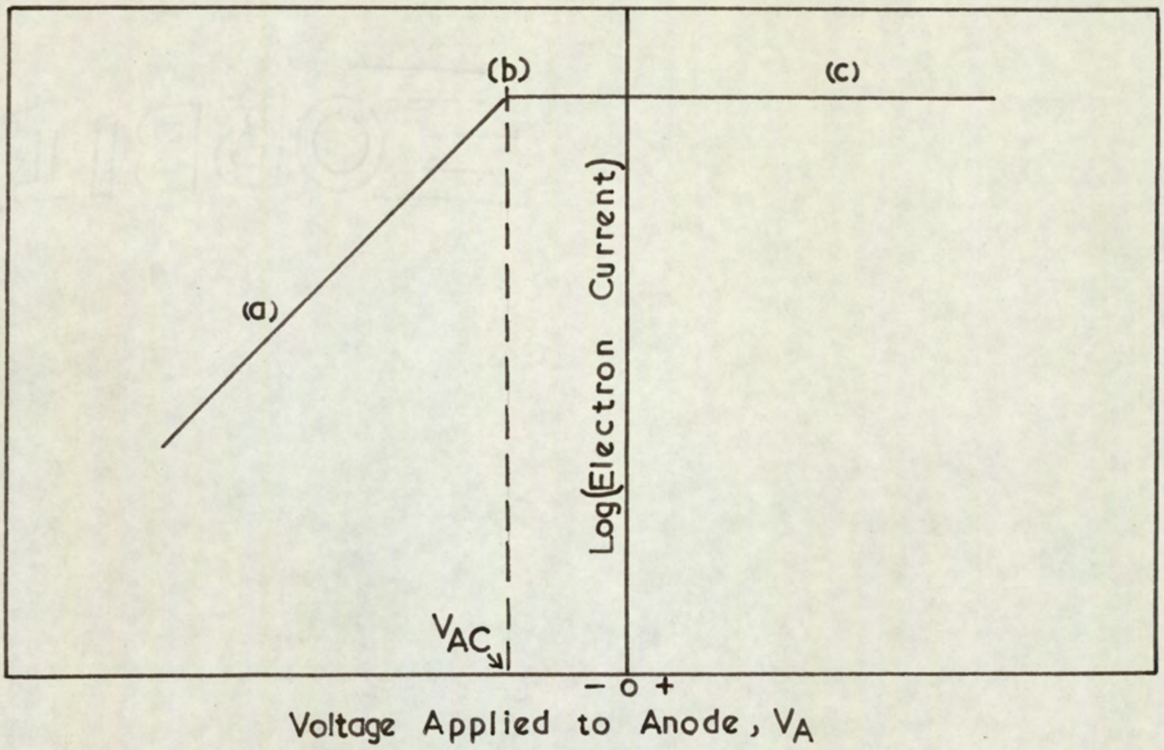

FIGURE (2-4). Current-Voltage Characteristic Plot.

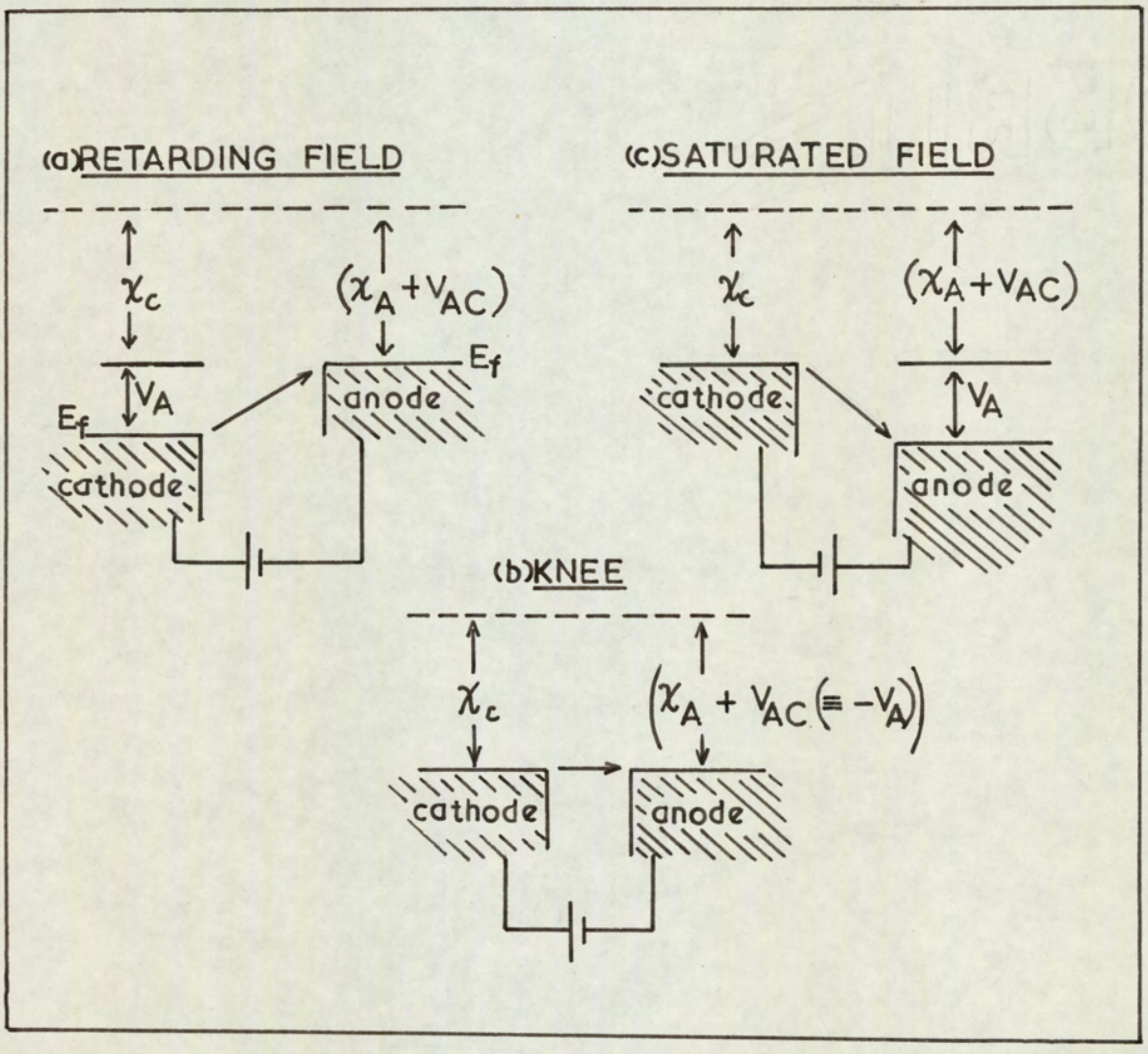

FIGURE (2-5). Potential Energy Diagrams.

$$\phi^{A}_{outer} = \phi^{C}_{outer} \qquad - \quad (2\text{-}32)$$

This will occur when,

$$\overline{V}_{AC} = - V_A \qquad - \quad (2\text{-}33)$$

The potential energies in the retarding field region, the knee and the saturated field region can be made clearer by the use of diagrams in figure (2-5).

If the work function of the emitter is a function of temperature for the temperature range under study then,

$$\chi_C = \chi_A + \overline{V}_{AC}\ (T) \qquad - \quad (2\text{-}34)$$

3.0. THE INTERACTION OF ELECTRONEGATIVE GASES WITH HOT METAL SURFACES : NEGATIVE SURFACE IONISATION(8)

In the presence of a gas, a filament emitting electrons thermionically is also found to emit ions (positive or negative, depending upon the nature of the surface and substrate) which are formed at the surface in a process called surface ionisation. Many studies have been made on this phenomenon and the theory of such processes is quite well developed although its application to all but simple cases is complex. If the substrate is an electronegative species, negative surface ionisation predominates.

Consider a substrate, A, interacting with the metal surface, which in the simplest case is assumed to be an inert source of electrons, to produce a negative ion A^- which is then desorbed into the gas phase.

$$A_{(g)} \longrightarrow A_{(s)} + C \rightleftharpoons A^-_{(s)} \longrightarrow A^-_{(g)}$$

The overall energy change in this reaction, $E(A_{(g)} \rightarrow A^-_{(g)})$, is called the electron affinity of the species A and is defined as the decrease in energy of the system relative to the infinitely separated molecule and an electron.

An equilibrium constant for the reaction can be formulated,

$$K = \frac{[A^-]}{[A]\,[e]}$$

These quantities may be identified with the fluxes of ions and electrons out of a small element of volume near the filament surface (measured ion and electron currents) and the flux of neutral species into this element of volume (calculated from kinetic theory and measured pressure). The heat of reaction, which is the required electron affinity, may then be evaluated by the method of statistical mechanics.

This simple treatment of ion formation assumes the filament surface to be inert and the substrate A not to be adsorbed or dissociate on the metal surface. In practice it has been found that these phenomena do occur (38,49) and a theoretical treatment must take these into account.

3.1. Energetic Treatment of Ion Formation oh a Metal Surface

Consider the formation of the negative ion A^-, by surface ionisation from the substrate A B where adsorption and dissociation of AB and adsorption of the residue B can all occur. If the residue B is adsorbed for a finite length of time, then this reaction may be separated from ion formation and the heat of adsorption of B must be taken into account in the energetic treatment. The overall reaction can now be written,

$$AB_{(g)} + e_{(m)} \rightarrow A^-_{(g)} + B_{(m)} \qquad - \quad (3\text{-}3)$$

The overall energy change will not now be the electron affinity of A as previously but will be the energy change between the initial and final states of this reaction, of which the electron affinity of A is only a part. The reaction mechanism can be considered as adsorption of AB onto the filament surface, dissociation of the molecule and formation of A^- on the surface followed by desorption of A^-, and perhaps B, into the gas phase. All possible steps are shown in the energy level diagram, figure (3-1).

If all of the mentioned steps occur then the overall energy change, W, is given by,

$$W = \chi + D - E - Q_B \qquad - \quad (3\text{-}4)$$

where χ is the work function of the surface, D is the bond dissociation energy of AB, E is the electron affinity of A and Q_B is the heat of adsorption of the fragment B. W and χ may

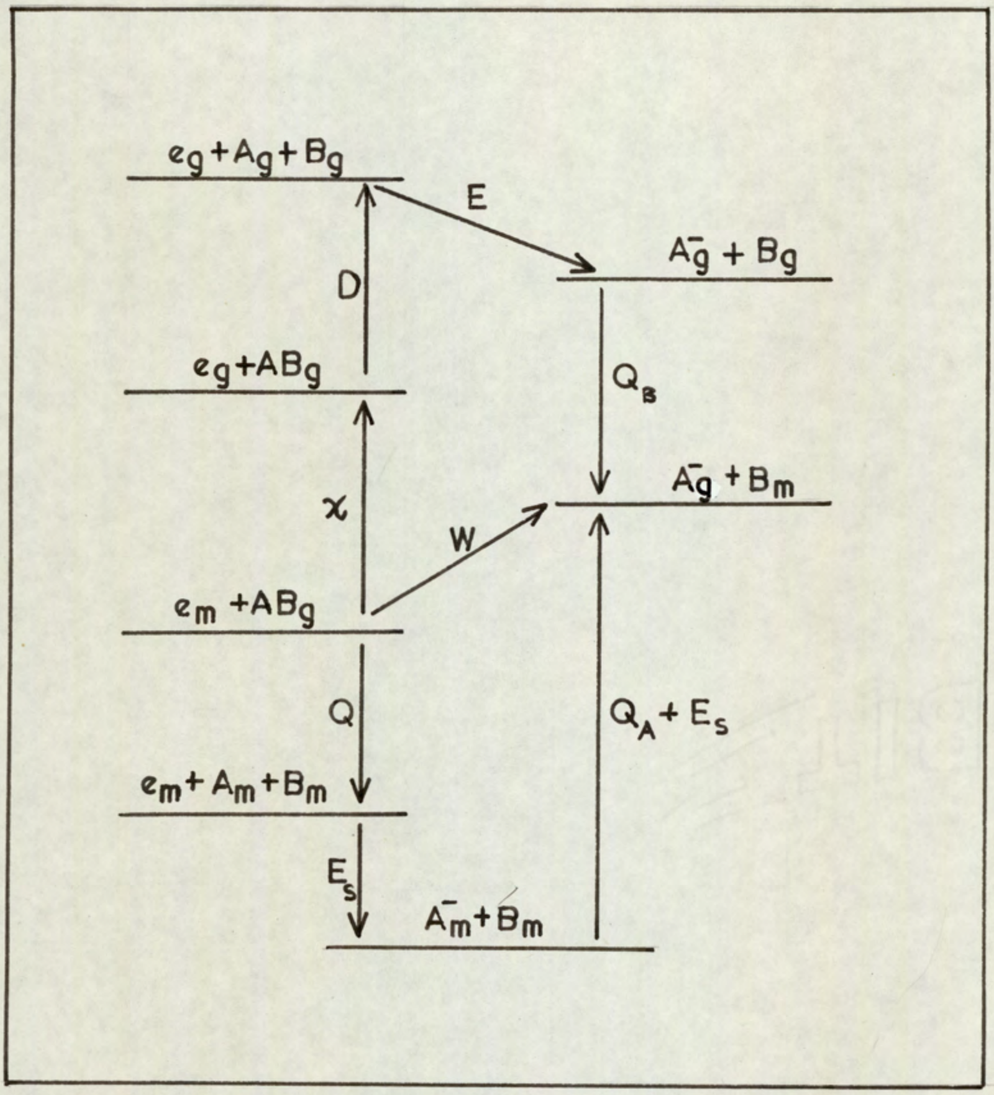

FIGURE (3-1). Energy Level Diagram for Ion Formation at a Surface.

be determined experimentally from measured ion and electron currents but the energetics of none of the intermediate surface reactions are known, The apparent electron affinity E' is given by $(\chi - W)$, therefore,

$$E' = E + Q_B - D \qquad - \quad (3\text{-}5)$$

This is a generalised mechanism and the actual steps involved will vary, depending upon the substrate and conditions.

3.2. The Rate of Emission of Electrons and Ions

Using the mechanism of ion formation suggested above and the energy changes involved, rate laws controlling the emission of electrons and ions can be formulated. Two approaches are used, a simple kinetic approach using the Langmuir adsorption isotherm and an alternative approach, using the transition state theory, leading to a rate equation in terms of the molecular properties of the reactants and products and the overall energy change.

3.2.1. Kinetic Treatment of Ion Formation

The ion current may be identified with the rate of emission of negative ions and the electron current with the rate of emission of electrons. The emission equation for electrons is given in equation (2-8). Assuming the reflection coefficient to be small compared to unity and that if the ion precursor is adsorbed on the surface with a fractional coverage θ , so that only a fraction $(1 - \theta)$ of the surface may emit electrons, the current density is,

$$J_e = A_e T^2 (1 - \theta) \exp -(\chi/RT) \qquad - \quad (3\text{-}6)$$

The ion precursor may be desorbed as a neutral species or a negative ion. If Q_n is the heat of desorption of the ion then the ion current density is,

$$J_i = C . \theta . \exp -(Q_n/RT) \qquad - \quad (3\text{-}7)$$

where C is a constant.

Langmuir assumed that the rate of adsorption of a gas phase species was proportional to the number of available adsorption sites whilst the rate of desorption was proportional to the number of adsorbed species. At equilibrium this leads to the equation,

$$\left(\frac{\theta}{1 - \theta}\right) = \frac{k_1 p}{k_2} \qquad - \quad (3\text{-}8)$$

where θ is the fractional coverage, p the gas phase pressure and k_1, k_2 the rate constants for adsorption and desorption respectively. If E_a is the activation energy for adsorption and E_d that for desorption then,

$$\frac{\theta}{1-\theta} = \frac{k'_1 p \ \exp\left(-E_a/RT\right)}{k'_2 \ \exp\left(-E_d/RT\right)} \qquad - \quad (3\text{-}9)$$

or since

$$E_d = Q_{AB} + E_a \qquad - \quad (3\text{-}10)$$

where Q_{AB} is the heat of adsorption of AB

$$\left(\frac{\theta}{1-\theta}\right) = k'p \ \exp\left(+Q_{AB}/RT\right) \qquad - \quad (3\text{-}11)$$

or

$$p = \left(\frac{\theta}{1-\theta}\right) k'' \ \exp\left(-Q/RT\right) \qquad - \quad (3\text{-}12)$$

The equilibrium constant for ion formation can be written in terms of experimental quantities,

$$K = \frac{[A^-]}{[A]\,[e]} = \frac{J_i}{J_e \cdot p} \qquad - \quad (3\text{-}13)$$

Therefore from equations (3-6), (3-7) and (3-12),

$$\frac{J_e \cdot p}{J_i} = \frac{A_e T^2}{C\,k''} \exp\left(\frac{-(\chi + Q_{AB} - Q_n)}{RT}\right) \qquad - \quad (3\text{-}14)$$

The heat of adsorption of AB can be split into its component parts,

$$Q_{AB} = Q_A + Q_B - D \qquad - \quad (3\text{-}15)$$

as can the heat of desorption of the negative ion which may be equated to the work done in desorbing neutral A and an electron and combining them in the gas phase.

$$Q_n = Q_A + \chi - E \qquad - \quad (3\text{-}16)$$

Hence,

$$\frac{J_e p}{J_i T^2} = \frac{A}{Ck''} \cdot \exp\left(-\left(\frac{E + Q_B - D}{RT}\right)\right) \qquad - \quad (3\text{-}17)$$

From equation (3-16), $(E + Q_B - D) = E'$, the apparent affinity.

Therefore, assuming the temperature dependence of A/Ck'' to be negligible compared with that exhibited by the exponential term, the energy term E' may be evaluated graphically from a semi-log plot of $\dfrac{J_e p}{J_i T^2}$ against $1/T$.

The evaluation of the pre-exponential term parameters may be more difficult.

3.2.2. The Absolute Reaction Rate Theory applied to the Emission of Electrons and Ions from a Metal Surface (8) (section 4.4)

The application of statistical mechanics to the calculation of the rate of a reaction (4) involves two stages, the definition of a transition state and the calculation of the frequency with which reacting species pass through this stage. The reactants are assumed to be in thermodynamic equilibrium with the activated complex in the transition state whilst the formation of products from the activated complex is an irreversible reaction.

$$A \rightleftharpoons A^{\ddagger} \longrightarrow \text{products} \qquad - \quad (3\text{-}18)$$

The equilibrium constant for this reaction is,

$$K^{\ddagger} = \frac{[A^{\ddagger}]}{[A]} = \frac{F'^{\ddagger}}{F_A} \cdot \exp\left(-\frac{\epsilon^{\ddagger}_0}{kT}\right) \qquad - \quad (3\text{-}19)$$

where $F'^{\ddagger}$, F_A are the complete, rational partition functions of the activated complex and reactant and $\epsilon_0^{\ddagger}$ the difference in their ground state energy levels at $0^{o}K$. The concentration of the activated complex is therefore,

$$[A^{\ddagger}] = [A] \cdot \frac{F^{\ddagger}}{F_A} \cdot \exp\left(-\frac{\epsilon_0^{\ddagger}}{kT}\right) \qquad - (3\text{-}20)$$

The rate of reaction is the rate at which the activated complexes can cross the energy barrier between the reactants and products,

$$\text{Rate} = \nu\,[A^{\ddagger}] \qquad - (3\text{-}21)$$

The motion of the complex along the reaction coordinate over the energy barrier can be treated as a weak vibration of one of the bonds leading, in a forward direction, to completion of the reaction. The partition function $F^{\ddagger}$ contains one term which represents this weak vibration. In the case of a weak vibration the full expression for the partition function simplifies to $kT/h\nu$ where ν is the frequency of the vibration. Combining this fact with equations (3-20) and (3-21),

$$\text{Rate} = [A] \cdot \frac{kT}{h} \cdot \frac{F^{\ddagger}}{F_A} \cdot \exp\left(-\frac{\epsilon_0^{\ddagger}}{kT}\right) \qquad - (3\text{-}22)$$

where $F^{\ddagger}$ is the partition function of the activated complex for all modes except the vibrational mode leading to reaction.

This equation can be applied to the rates of emission of electrons and ions from a metal surface.

3.2.2.1. The Emission of Electrons

The potential gradient near the surface of an emitter in the presence of an applied field is shown in figure (2-1). An electron leaving the filament is subjected to the external field and its own image field at the surface and the combination of these two opposed fields leads to a maximum in the potential energy of the electron. This is known as the Schottky barrier and is considered as the transition state for emission of an electron.

The partition function, F_e, for an electron in the metal is given by the equation,

$$F_e = [e] \cdot \exp\left(-\delta/kT_s\right) \qquad - \ (3\text{-}23)$$

where $[e]$ is the electron concentration at the surface, T_s, the temperature and δ a complex function of the Fermi level of the surface. The work function, per mole of electrons, χ, will be given by,

$$\chi = N(\epsilon_o - \delta) \qquad - \ (3\text{-}24)$$

The electron in the transition state will have three degrees of translational freedom, one of which is the rate determining motion, so that,

$$F'^{\ddagger} = \frac{kT_s}{h\nu} \cdot (F^{\ddagger}_{e,t}) \qquad - \ (3\text{-}25)$$

The translational partition function is $\left(\frac{2\pi m_e kT_s}{h^2}\right)^{\frac{1}{2}}$ per degree of freedom and introducing a factor of 2 to allow for the spin degeneracy of the electron the rate equation becomes,

$$\left(-\frac{dn_e}{dt}\right) = \frac{2 \cdot kT_s}{h} \cdot \frac{2\pi m_e kT_s}{h^2} \exp\left(-\frac{\chi}{NkT_s}\right) \qquad - \ (3\text{-}26)$$

If the reflection coefficient is now introduced and it is noted that the emission current is the rate of emission multiplied by the charge on the electron, then,

$$J_e = \frac{4\pi m_e k^2 . T_s^2 . e}{h^3} (1 - \bar{r}_e) \exp -(\chi / RT_s) \qquad - (3\text{-}27)$$

which is identical with the emission equation, (2-8).

3.2.2.2. The Emission of Ions

The emission of ions is conveniently discussed by first considering the surface to be covered by ion precursors and then later considering the influence of temperature and surface coverage on the rate of emission.

The reaction on the surface to form the transition complex may be written,

$$A_s + e_s \rightleftharpoons (A^-)^{\ddagger} \longrightarrow A_g^- \qquad - (3\text{-}28)$$

and the equilibrium constant associated with this equation is,

$$K^{\ddagger} = \frac{[A^{\ddagger}]}{[A_s]\,[e]} = \frac{F_i^{\prime\ddagger}}{F_A . F_e} . \exp -\frac{(\epsilon_o + \epsilon)}{kT_s} \qquad - (3\text{-}29)$$

Where ϵ_o and ϵ represent the difference between the ground state energy and that in the transition state for the electron and substrate respectively. When the surface bond is broken the species A enters a region of rapid electron exchange between the metal and acceptor orbital of A (in the case of a halogen this will be an outer p orbital). The transition state for the formation of a negative ion can be considered as the furthest point from the surface where this electron exchange is still possible (5).

Using the same method as in section (3.2.2.1) the rate equation for the emission of ions is,

$$\left(- \frac{dn_-}{dt}\right) = \frac{kT_s}{h} . [A_s] . \frac{F_i^{\ddagger}}{F_A} . \exp\left(- \frac{(\epsilon_o - \delta + \epsilon)}{kT_s}\right) \qquad - (3\text{-}30)$$

If the zero of potential energy is taken as the transition state the algebraic sum of the energy terms may be equated to the sum of the work function, χ , the heat of desorption, E_d and the electron affinity of the ion precursor, E.

Therefore, since,

$$\chi = N(\epsilon_o - \delta) \quad \text{and} \quad (E - E_d) = N\epsilon$$

it follows,

$$\left(-\frac{dn_-}{dt}\right) = \frac{kT_s}{h}[A_s] \cdot \frac{F_i^{\ddagger}}{F_A} \cdot \exp\left(-\frac{(\chi + E_d - E)}{RT_s}\right) \qquad - (3\text{-}31)$$

If the process of ion formation represents only a minor perturbation of the adsorption-desorption equilibrium of the ion precursors then the concentration, $[A_s]$, of such precursors may also be evaluated by the reaction rate theory.

In the simplest case, when the negative ion is formed by the simple addition of an electron to the precursor, which is itself identical with the gaseous substrate, then the rate equation for adsorption is,

$$\left(\frac{dn}{dt}\right)_{ads} = ([C_s] - [A_s]) \cdot [A_g] \cdot \frac{kT_g}{h} \cdot \frac{F_a^{\ddagger}}{F_sF_g} \cdot \exp\left(-\frac{E_a}{RT}\right) - (3\text{-}32$$

Similarly, the rate equation for desorption is,

$$\left(-\frac{dn}{dt}\right)_{des} = [A_s] \cdot \frac{kT_s}{h} \cdot \frac{F_d^{\ddagger}}{F_A} \cdot \exp\left(-\frac{E_d}{RT_s}\right) \qquad - \quad (3\text{-}33)$$

where $[C_s] - [A_s]$	represents the number of sites available for adsorption per unit area.
$[A_s]$	is the surface concentration per unit area.
$[A_g]$	is the gas phase concentration of A
$F_a^{\ddagger}$, $F_d^{\ddagger}$	are the partition functions of the activated complexes for adsorption and desorption.

The process of ion formation is considered to be occurring under conditions of low surface coverage so that $[C_s] - [A_s] \simeq [C_s]$ and the interaction between neighbouring species can be neglected.

Combining equations (3-31), (3-32) and (3-33) the final equation for the rate of emission of ions can be found, noting from kinetic theory that $[A_g] = P/kT_g$ and assuming, as is generally found, that the adsorption reaction is non activated, then the rate is given by,

$$\left(- \frac{dn_{-}}{dt} \right) = \frac{[C_s] \, . \, P}{h} \, . \, \frac{F_i^{\ddagger} \, . \, F_a^{\ddagger}}{F_g \, . \, F_d^{\ddagger}} \, . \, \exp \left(- \frac{(\chi - E)}{RT} \right) \qquad - \ (3\text{-}34)$$

The ion current will therefore be given by,

$$J_i = \frac{[C_s] \, . \, P \, . \, e}{h} \, . \, \frac{F_i^{\ddagger} \, . \, F_a^{\ddagger}}{F_g \, . \, F_d^{\ddagger}} \, . \, \exp \left(- \frac{(\chi - E)}{RT} \right) \qquad - \ (3\text{-}35)$$

This emission equation applies to a substrate which does not dissociate during ion formation nor does adsorption of a residue occur, but the theory may be modified to take these phenomena into account.

The values of the partition functions and the terms involved in them will depend upon the internal structure of the molecules and their mobility on the surface in the adsorbed state and in the transition states for ion formation, adsorption and desorption. Often simplification can be made, for example, the rotational, electronic and vibrational partition functions in the activated complexes for adsorption and desorption and the gas phase partition function are not likely to differ to any great extent.

3.2.3. The Attainment of Equilibrium at the Surface

Both the theoretical methods (thermodynamic and kinetic) for obtaining expressions to determine the electron affinity include the assumption that the particles incident from the gas phase on the surface of the ion emitter are adsorbed on this surface and, during adsorption, reach thermal and electrical equilibrium with the adsorbent.

This may be justified indirectly by the experimental values obtained for the electron affinities which agree with those obtained by other methods (e.g. photodetachment (50) and shock tube (51) studies) and directly by the demonstration that the initial energy distribution of the emitted particles is Maxwellian and corresponds to the filament temperature.

The ionic energy distribution may be determined using the retarding field technique described in section (2.2.2.1) and such experiments for both the ion (52, 53) and electron (48) emission have shown that the initial energy distribution of the particles is Maxwellian.

In experiments using a high resolution energy analyser, both alone (54) and linked to a mass spectrometer (55), a similar result was obtained for the initial energy distribution of thermoelectrons, K^+, Li^+, Cs^+ and Cl^- ions (both from Cl_2 and KCl).

3.3. Experimental Study of Surface Ionisation and Thermionic Emission by the Magnetron Method

Equations (3-27) and (3-35) describe the rate of emission of electrons and negative ions respectively and they can be combined to give,

$$\frac{J_e P}{J_i T^2} = \frac{k 4 \pi m_e}{h^2 [C_s]} \cdot \frac{F_i^{\ddagger} \cdot F_a^{\ddagger}}{F_g \cdot F_d^{\ddagger}} \cdot \exp\left(\frac{-E}{RT}\right) \qquad - \ (3\text{-}36)$$

The electron affinity, E (or the apparent electron affinity, E', if the process is not simple direct capture) may therefore be obtained from a plot of $\ln(J_e/J_i T^2)$ against T^{-1}.

The following data is therefore required;

(1) The electron current as a function of temperature.

(2) The ion current as a function of temperature.

(3) The true temperature of the emitting filament.

Further information may be obtained from a measurement of:

(1) The dependence of the thermionic currents upon the substrate pressure.

(2) The dependence of the values of the apparent electron affinity on the filament material. For example, tungsten, tantalum, molybdenum and platinum filaments may be used to give an indication of the importance, or otherwise, of adsorption on the filament surface in the surface ionisation process.

The magnetron method is capable of providing all of this information.

3.3.1. Measurement of the Ion and Electron Currents - the Theory of the Magnetron

A thermionic vacuum tube having a uniform magnetic field perpendicular to its electric field is known as a magnetron.

There are two types of magnetron; one with plane parallel electrodes and the other with the cathode and anode arranged coaxially. The latter type has been used in this work although a planar magnetron has been used by several workers (56, 57).

A diagram of the magnetron is shown in figure (3-2).

The ions and electrons are emitted with negligible initial velocities from the filament and then accelerated to the anode by an electric field E. When the external magnetic field is applied the charged particles will suffer an additional acceleration, perpendicular to the direction of this field. It is convenient to use cylindrical coordinates, r, θ and Z to discuss the electron and ion trajectories under the influence of these two fields.(58)

Let the radius of the filament be a and that of the outer anode, b. If V is the potential on the anode and v the velocity of the ions, then the law of conservation of energy requires that,

$$\tfrac{1}{2}mv^2 + eV = 0 \qquad - \quad (3\text{-}37)$$

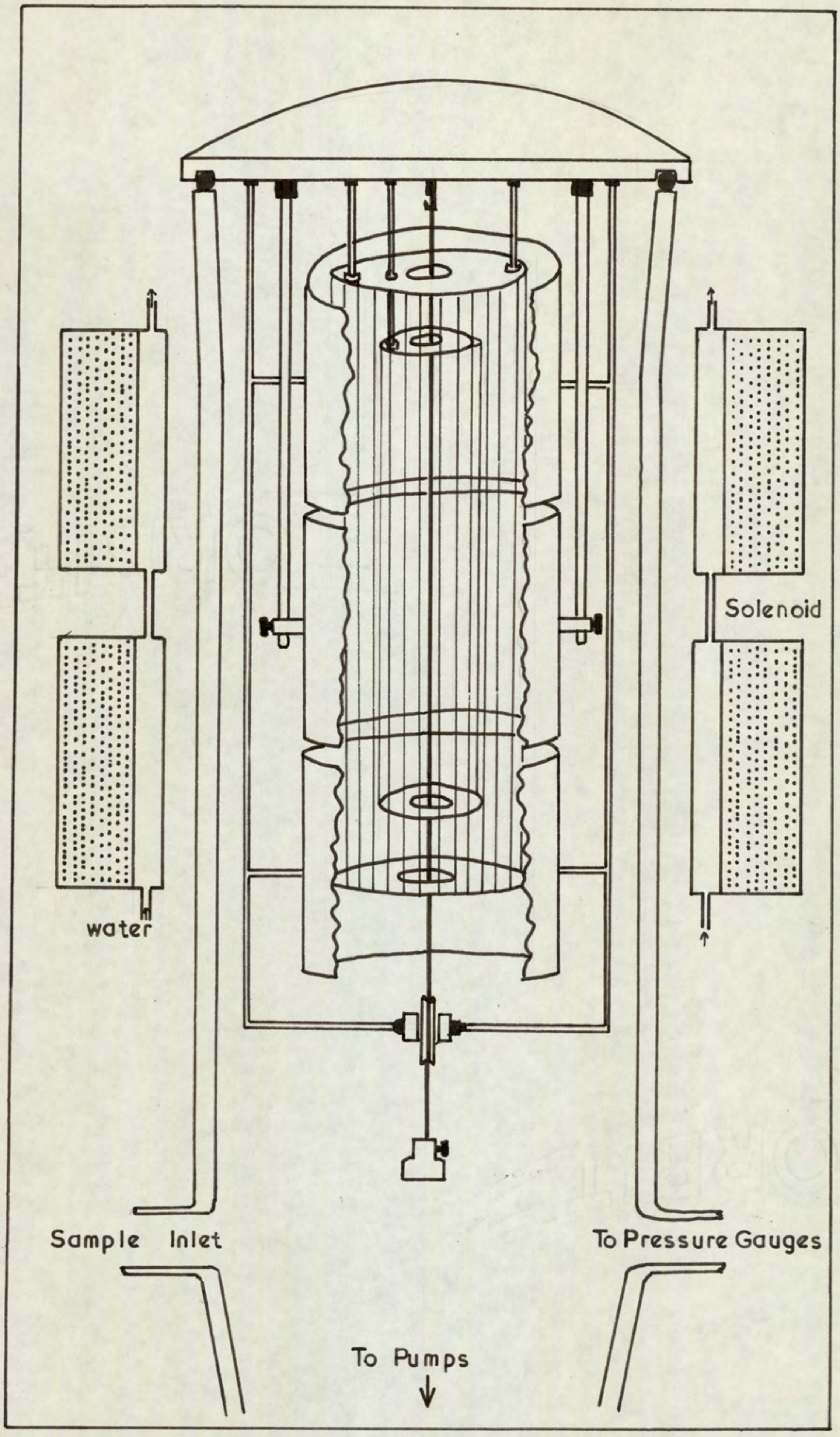

FIGURE (3-2). The Magnetron.

assuming that the potential of the emitter is zero. Using cylindrical coordinates and taking into account the effect of the magnetic and electric fields on the ion, then,

$$\tfrac{1}{2}m\left(\frac{d^2r}{dt^2} + r^2\frac{d^2\theta}{dt^2}\right) + eV = 0 \qquad - (3\text{-}38)$$

The torque about the axis is due to the magnetic field and is equal to $-e\mu_0 r\frac{dr}{dt}H$ and this may be equated to the rate of increase of angular momentum.

$$m\frac{d}{dt}\left(r^2\frac{d\theta}{dt}\right) = -e\mu_0 r\left(\frac{dr}{dt}\right)H \qquad - (3\text{-}39)$$

$$r^2\frac{d\theta}{dt} = -\frac{e}{m}\mu_0 H\int_a^r r\,.\,dr \qquad - (3\text{-}40)$$

$$r^2\frac{d\theta}{dt} = -\frac{e}{m}\mu_0 H\left(\frac{r^2 - a^2}{2}\right) \qquad - (3\text{-}41)$$

This may be combined with equation (3-38) to obtain,

$$\frac{d^2r}{dt^2} = -\left(\frac{2e}{m}\right)V - \left(\frac{e}{m}\mu_0 H\right)^2\left(\frac{r^2 - a^2}{2r}\right)^2 \qquad - (3\text{-}42)$$

The electron paths are circles perpendicular to the filament axis and when the distance from the axis is a maximum, $\frac{dr}{dt}$ is zero.

Let this distance be r, then,

$$\frac{r_o^2 - a^2}{2r_o} = \left(\frac{-V_o}{(e/2m)\;\mu_o^2 H^2}\right)^{\frac{1}{2}} \qquad - (3\text{-}43)$$

where V_o is the potential at r_o.

Similarly, the "cut-off" field, H_c, is given by,

$$H_c = \frac{(8V_b)^{\frac{1}{2}}}{\mu_o\left(\frac{b^2 - a^2}{2b}\right)^2\left(\frac{e}{m}\right)^{\frac{1}{2}}} \quad - \quad (3\text{-}44)$$

where V_b is the potential of the outer anode and since the radius of the outer anode is large compared to that of the filament,

$$H_c = \left(\frac{8mV_b}{\mu_o eb^2}\right)^{\frac{1}{2}} \quad - \quad (3\text{-}45)$$

In the "cut-off" condition an electron leaving the filament would just fail to reach the anode. This "cut-off" condition is independent of the potential distribution between the anode and cathode so that the presence of space charge, or other electrodes, will not alter the conditions. In the magnetron used in this work two grids were placed symmetrically between the filament and anode to prevent the build up of space charge in the "cut-off" condition when the electrons do not reach the anode (8). Such a space charge could affect the emission of negative ions from the filament.

Under normal conditions of operation in the saturated field region the cut-off field for electrons was found to be about 27.0 Gauss. Under similar conditions the cut-off field for an ion such as Cl^- would be $> 10^5$ Gauss.

The total current (ions and electrons) can therefore be measured in the absence of the magnetic field whilst the ion current may be measured in the presence of the magnetic field.

3.3.2. Measurement of Filament Temperature

The accurate measurement of the temperature of the emitting filament is fundamental to the determination of activation energies by the magnetron method. In this method the temperature was measured optically using a disappearing filament pyrometer (Leeds and Northrup - type 8630 (6530 Å filter)).

The filament was ~15 cm. long but emission measurements were only made from the middle 5 cm. section over which the temperature will be uniform (59)

The true filament temperature will always be higher than the measured temperature because of absorption of some of the emitted radiation by the glass wall of the vacuum system through which the temperature is measured and because the spectral emissivity of the surface is less than unity.

These errors can be corrected for by use of the equation, (60)

$$\frac{1}{T} - \frac{1}{S_\lambda} = \frac{\lambda}{C_2} \ln(\varepsilon_{\lambda,t} \cdot A_\lambda) \qquad - \quad (3\text{-}46)$$

where T is the true (or blackbody) temperature

S_λ is the optical temperature measured at wavelength

C_2 is a constant (1.43879 ± 0.00019 cm.°K)

A_λ is the absorption coefficient (0.92)

$\varepsilon_{\lambda,t}$ is the emissivity coefficient at a particular wavelength and temperature

Data to correct the measured temperature to the true temperature may be found for most metals. Graphs of S (°C) against T (°K) are shown in figure (3-3) for tantalum (60, 61), tungsten (62) molybdenum (62) and platinum (63).

3.3.3. Measurement of Pressure

The ultimate pressure of the vacuum system was $< 1 \times 10^{-6}$ mm.Hg. The pressure during an experiment was in the range $10^{-5} - 10^{-2}$ mm.Hg. Three gauges were used to cover this range; a Pirani gauge (10^{-1} - 5×10^{-4} mm.Hg) a Penning gauge ($10^{-3} - 10^{-7}$ mm.Hg) and a Baratron differential pressure gauge. General aspects of pressure measurements using these gauges are discussed later in section (8-5).

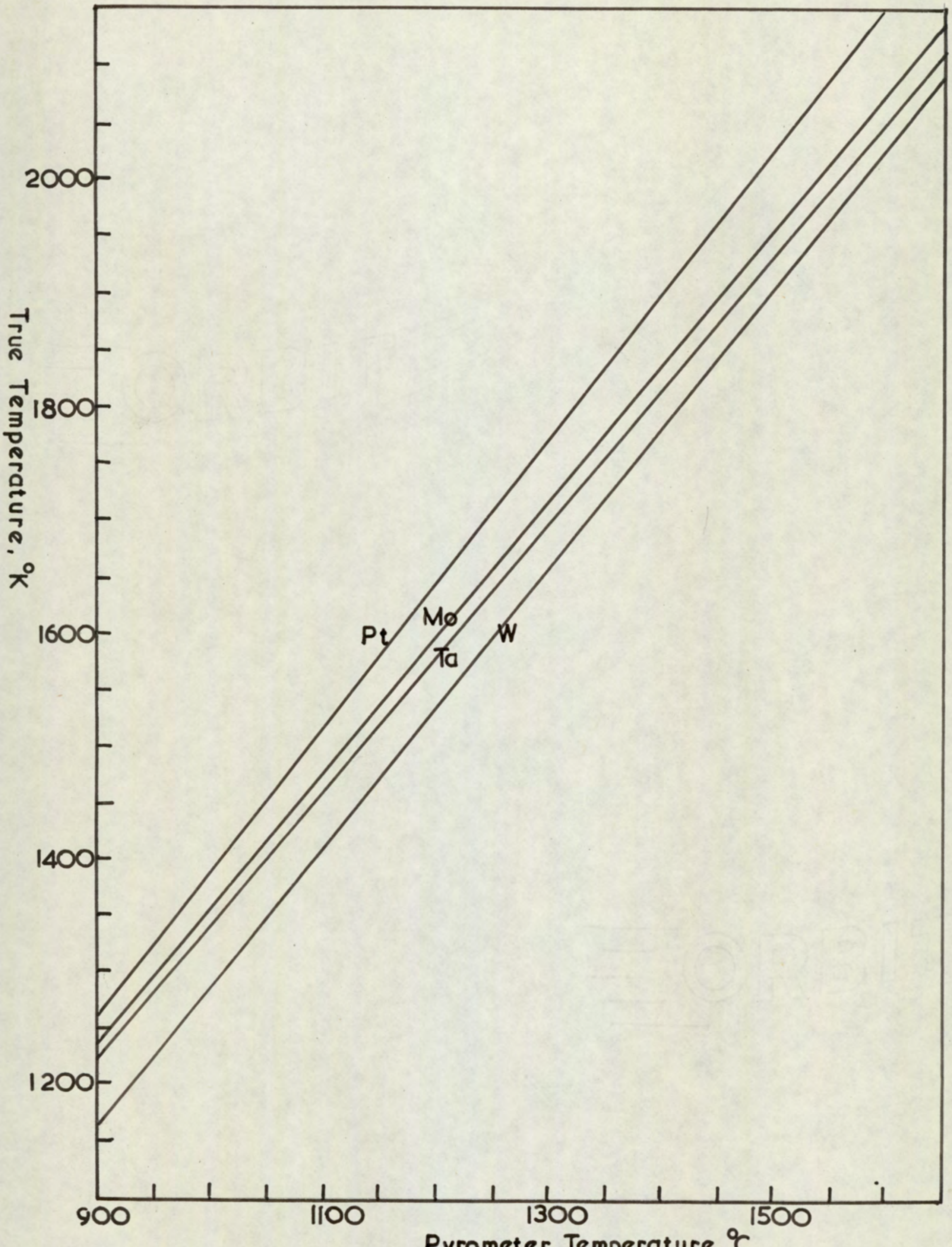

FIGURE (3-3). Emissivity & Absorption Temperature Correction

3.3.4. Design and Construction of the Magnetron

The cylindrical magnetron consists of a coaxial filament-grid-anode assembly mounted inside a glass vacuum envelope which is surrounded by an electromagnetic coil to generate the homogeneous magnetic field required to separate the ions and electrons.

3.3.4.1. The Vacuum System

The vacuum system must be capable of producing a background pressure well below the desired working pressure.

A liquid nitrogen trapped, stainless steel mercury diffusion pump, backed by a liquid nitrogen trapped oil filled rotary pump was employed to produce background pressures of $< 1 \times 10^{-6}$mm.Hg which was adequate for working pressures of 5×10^{-5} and greater.

The magnetron assembly was mounted inside a "Q-Vac" vacuum container fitted with side arms for the Pirani and Penning gauges and also for the needle valve used to control the admission of gaseous samples into the vacuum system.

The vacuum system was not bakeable in its entirity but could be partially outgassed by the action of the hot filament which could heat surfaces in its proximity by conduction, radiation and electron bombardment.

3.3.4.2. The Magnetron Assembly

In a practical design of the magnetron the anode is split into three sections; only the central section is used to make measurements, the two outer sections ensure that parameters such as the filament temperature and electric field are constant along the entire length of the filament in the central region.

The anodes were fabricated from non-magnetic stainless steel and the split anode assembly, together with the grids were mounted on glass to metal seals in a $\frac{1}{4}$" metal plate. The electrical leadthrough from the central anode used to measure the emission currents was a silica glass seal with a long leakage path (leakage resistance $> 10^{14}$ ohm) and this was also sealed into the metal plate.

Several methods of fixing and aligning the filament were experimented with but a method that was found very successful both for ductile materials such as platinum and strong materials such as tungsten is shown in the diagram of the magnetron. A stainless steel pulley was mounted in a copper fork, so that it could rotate freely, with its outer edge aligned along the central axis of the magnetron. The upper end of the filament was clamped securely whilst its lower end was wound once around the pulley and a predetermined weight (determined by the strength of the filament) fixed to the free end, thus tensioning the filament.

3.3.4.3. The Magnet

Consideration must be given to the design of the magnet so that a uniform field may be obtained over the entire length of the collecting anode and thus achieve a sharp cut-off of the electron current.

If a single coil is employed, unless this is very long, there will be a considerable variation in the magnetic field over the length of the anode, as shown in figure (3-4) and therefore to achieve a uniform field, over the desired length, a Helmholtz type, double coil was constructed. By arranging the coils with a suitable separation, as shown in figure (3-5) a uniform magnetic field could be obtained.

Both the coils were wound on brass formers designed to allow water cooling during operation. The coils were 5 cm. wide with 1500 turns of 0.028" diameter enamelled copper wire and to obtain a uniform field over the 5 cm. length of the central anode the centres of the coils were 7 cm. apart.

3.3.5. Experimental Techniques

Prior to any measurements in the magnetron the filament was outgassed at high temperature ($> 2200^{o}$K, except for platinum which was outgassed at $\sim 2000^{o}$K). This treatment ensured

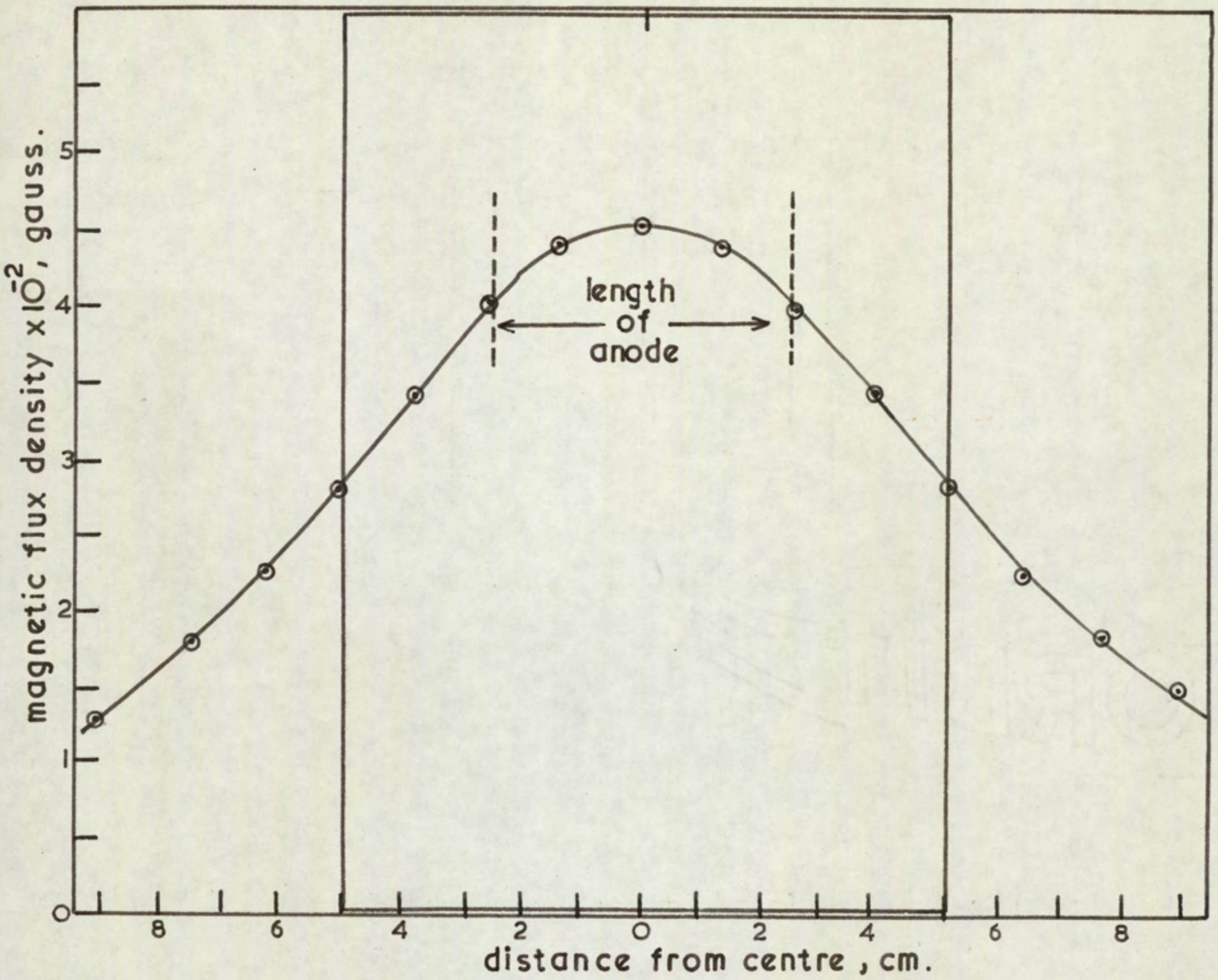

FIGURE (3-4) Magnetic Field Along Axis of Single Coil.

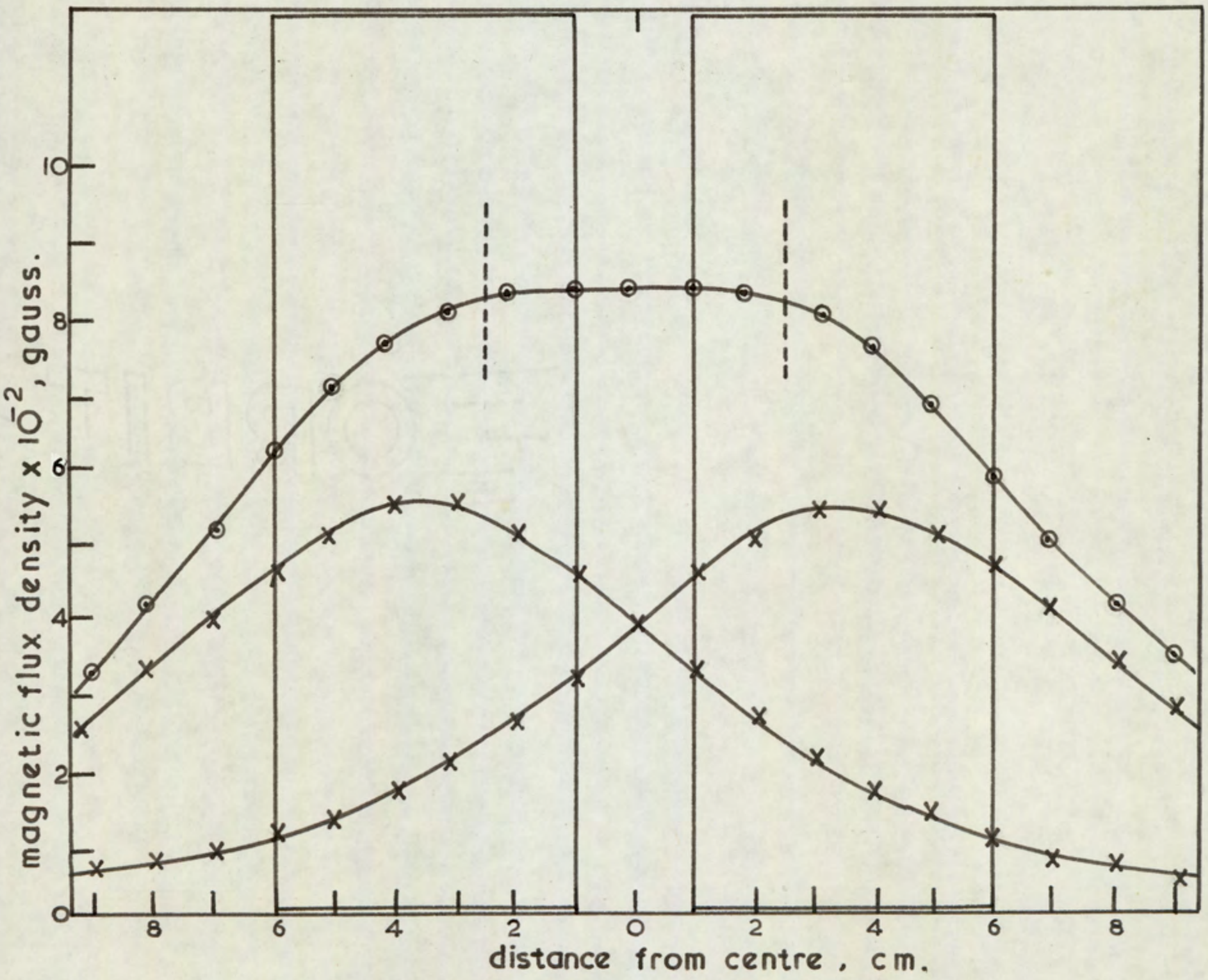

FIGURE (3-5) Magnetic Field Along Axis of Double Coil.

stabilisation of the crystal structure of the filament.

The apparent work function of the filament was then determined using the method described in section (2.2.1). This temperature dependence of the electron emission, although reproducible, could not be described as a fundamental property of the filament because of the polycrystalline nature of the emitter surface but it was a well defined quantity.

After this preparation procedure the sample gas was allowed into the system at the working pressure and the whole system allowed to equilibriate. A continuous flow method was employed to reduce the possibility of contamination due to decomposition at the hot filament.

To determine the apparent electron affinity the substrate pressure was fixed and the ion and total currents measured as a function of temperature, both for increasing and decreasing temperatures.

The external electrical circuitry required to obtain these quantities is shown in figure (3-6). The anode currents were measured using an AVO D.C. amplifier (10^{-13} - 10^{-7}A.) together with a galvanometer (10^{-8} - 10^{-4} A.) and the grid currents could also be monitored using a similar galvanometer. Power for the magnet was supplied by ten, 12v. heavy duty storage batteries.

In order to facilitate experimental measurements it was found convenient to calibrate the temperature of the filament as a function of the current through it (I_f), as measured using a shunt resistor and a digital voltmeter. The optical temperature was measured in the presence of the sample gas, corrected to the true temperature and then a plot of I_f against T2 made. This was found to be linear over a large temperature range and could be used for several experiments before being checked.

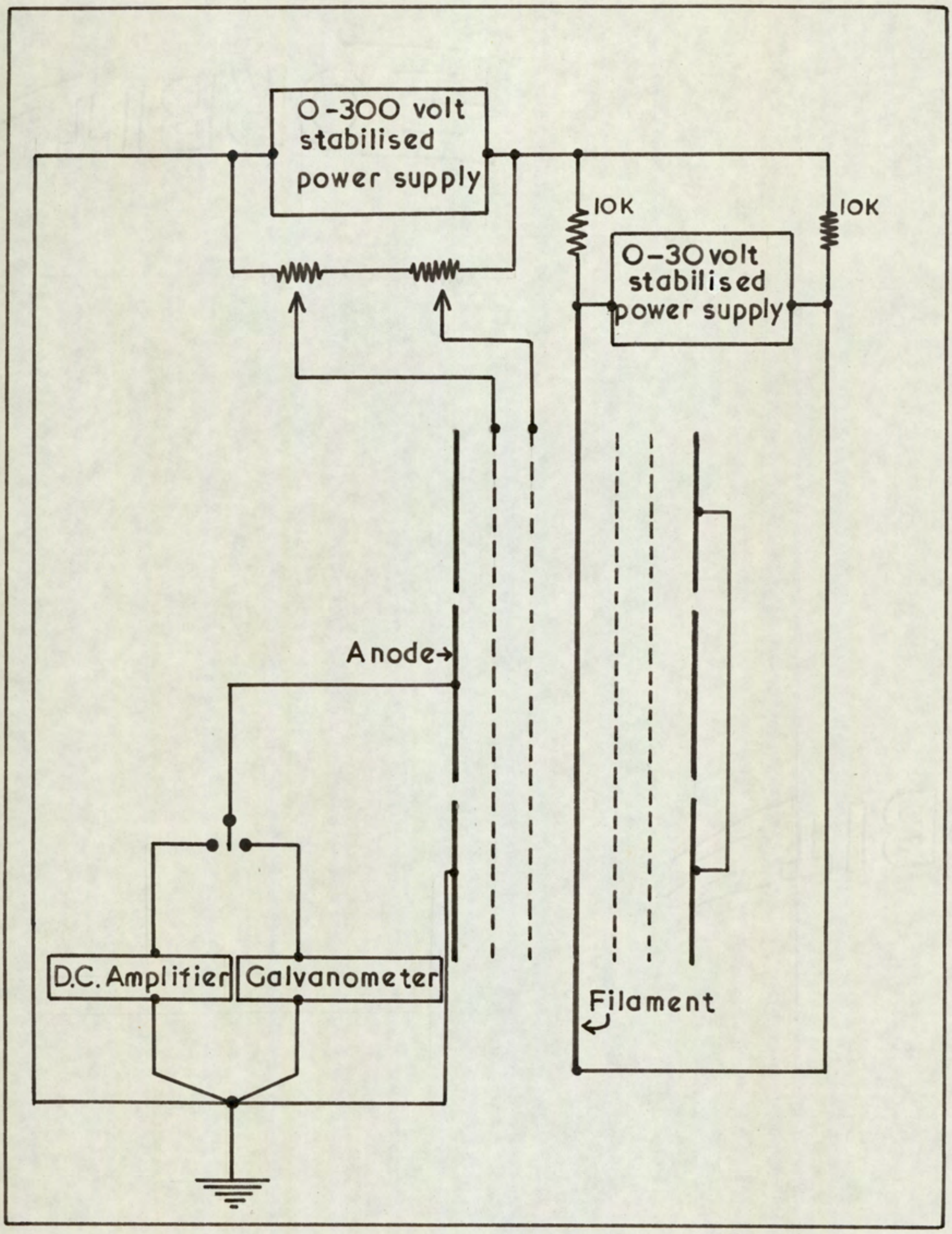

FIGURE (3-6) Magnetron – Electrical Circuit.

4.0. THERMAL DESORPTION

4.1. Introduction to Thermal Desorption

Thermal desorption studies are an important, sensitive tool for investigating the interaction of gases with solid surfaces (25). From the interpretation of thermal desorption data considerable information can be obtained about the nature of adsorbed gas species and the kinetics of the surface rate processes leading to the appearance of molecules in the gas phase, in particular rates of desorption, the order of reaction and the activation energies and entropies for desorption.

Gases such as hydrogen have been shown to be adsorbed on metallic surfaces in the atomic state (64), whilst gases such as carbon monoxide have been shown to adsorb without dissociation (18). Other gases such as iodine have been shown to adsorb on certain metals in both molecular and atomic bonding states (65,66). Thermal desorption data can reveal the presence of various phases of adsorbed gas species and a complete analysis will provide the population and kinetic parameters for each of these phases.

The thermal desorption data is obtained by measuring the flux of the gases that are evolved from the surface under study and the temperature of the surface as a function of time. The detector for this measurement can be either a partial pressure or a total pressure instrument.

This data can be obtained with relative ease but the interpretation of such data in order to obtain a kinetic rate expression for the desorption reaction presents considerable difficulties for a real system. This difficulty stems from the complications that are introduced by the dynamics of the vacuum system, the measurement of the surface temperature and the mathematical treatment of the data.

The following mathematical treatment is based upon the theory of the absolute reaction rate and accommodates the dynamics of the experimental vacuum system.

4.2. Theory of Thermal Desorption (25, 67)

In any pumped system the rate of change of pressure is determined by the difference between the rates at which gas enters and leaves the system, and, given time, the system will settle down to a steady state. In the desorption experiment this equilibrium is disturbed by a change in the condition of one surface in the system and a transient change in pressure results.

If the vacuum system could be considered as a completely closed system then during the flash the number of molecules desorbed from the filament could be obtained from the ideal gas law,

$$PV = n\,RT \qquad - \quad (4\text{-}1)$$

If the pressure change is ΔP, then the number of molecules will be given by,

$$\frac{\Delta n}{A} = \frac{\Delta P . V}{kT} \text{ molecules.cm.}^{-2} \qquad - \quad (4\text{-}2)$$

where A = area of filament

In a real vacuum system however there will always be a state of dynamic equilibrium which is disturbed by the flash. If the system is completely sealed and subject to pumping, the pressure after the flash will fall exponentially.

$$P_t = P_o . \exp\left(\frac{S_t t}{V}\right) \qquad - \quad (4\text{-}3)$$

where P_t = pressure at time t
P_o = pressure at time t = 0
S = pumping speed at time t
V = volume of system.

S_t includes all types of pumping; these may be due to an actual pump or an unintentional pumping source, for example, a vacuum gauge or the surfaces of the vacuum system. At the same time there will be a leak rate, L, into the system, usually due to outgassing.

At equilibrium,

$$\frac{dN}{dt} = -\frac{S}{V}.N + L \qquad - \quad (4-4)$$

During the 'flash' the rate of change of the total number of particles present is given by,

$$\frac{dN}{dt} = -A\frac{dn}{dt} - \frac{S}{V}.N + L \qquad - \quad (4-5)$$

It is assumed that the thermal desorption experiment occurs in a time interval during which the rate of readsorption on the filament is negligible.

The change dN/dt is proportional to the change in pressure in the system which will be measured at some point distant from the desorbing source. This means the desorbing molecules must undergo many collisions with the surface of the vacuum system before reaching the detector and therefore the pressure change recorded by the detector will be due to molecules in thermal equilibrium with the vacuum envelope.

If the ambient temperature is To, then from the ideal gas law,

$$N = \frac{P.V}{kTo} \qquad - \quad (4-6)$$

differentiating with respect to time

$$\frac{dN}{dt} = \frac{V}{kTo} \cdot \frac{dP}{dt} \qquad - \quad (4-7)$$

Substituting into equation (4-5),

$$\frac{dP}{dt} \cdot \frac{V}{kTo} = -A\frac{dn}{dt} - \frac{S}{V} \cdot \frac{PV}{kTo} + L \qquad - \quad (4-8)$$

Rearranging this equation,

$$\left(-\frac{dn}{dt}\right) = \frac{V}{AkTo}\left(\frac{dP}{dt} + \frac{S}{V} . P - \frac{LkTo}{V}\right) \qquad - \quad (4\text{-}9)$$

At a steady state prior to the flash the pressure will be at an equilibrium pressure given by Peq. At this pressure all leaks are balanced by all types of pumping.

Prior to the flash, $\frac{dP}{dt} = 0$; $\frac{dn}{dt} = 0$; $P = Peq$

Therefore from equation (4-6)

$$P_{eq} = \frac{LkTo}{S} \qquad - \quad (4\text{-}10)$$

Substituting this into equation (4-9) letting $\Delta P = (P - Peq)$ when P is the instantaneous pressure

$$\left(-\frac{dn}{dt}\right) = \frac{V}{AkTo}\left(\frac{d(\Delta P)}{dt} + \frac{S}{V}(\Delta P)\right) \qquad - \quad (4\text{-}11)$$

This equation gives the rate of desorption in terms of several quantities all of which are amenable to experimental evaluation.

V : The volume of the apparatus obtained from the estimated internal dimensions.

ΔP : Evaluated from the pressure immediately prior to the flash and the instantaneous pressure recorded during the experiment.

$\frac{d(\Delta P)}{dt}$: The derivative of the pressure trace.

S : The pumping speed of the system for the species being desorbed. This is evaluated from the decrease in pressure as a function of time immediately after the heating cycle has finished. This may not be exactly correct as the clean filament will constitute a pumping source at this stage whilst during the flash it will not. Because of the small surface area of the filament this effect is likely to be small for the short period involved.

Equation (4-11) can be rearranged for the purposes of computation. If the maximum recorded pressure is ΔP_m then the equation may be written,

$$\left(-\frac{dn}{dt}\right) = \frac{S.\Delta P_m}{AkT_o}\left(\frac{V.\frac{d(\Delta P)}{dt}}{S\Delta P_m} + \frac{\Delta P}{\Delta P_m}\right) \qquad - \quad (4\text{-}12)$$

A typical pressure-time curve will have the appearance shown below in figure (4-1).

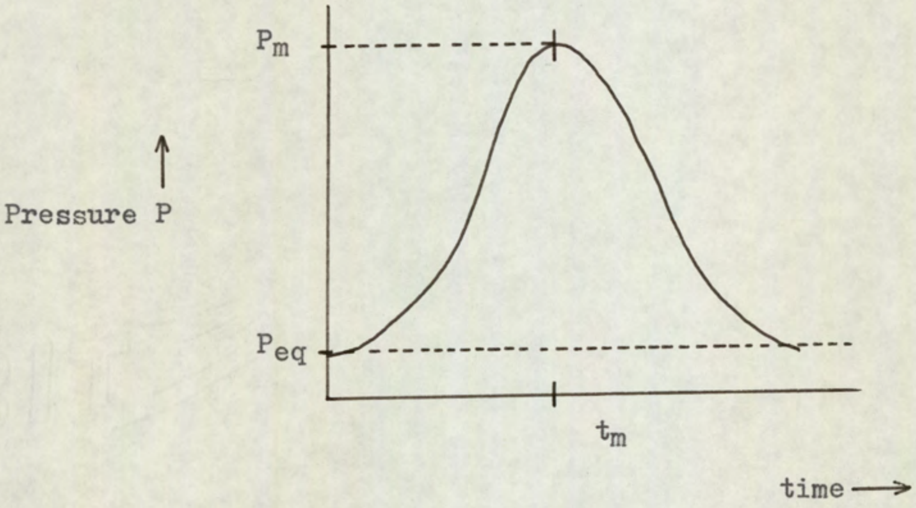

Figure (4-1)

At a certain time, t_m, the pressure curve has a maximum value given by ΔP_m, and at this time the derivative of the pressure-time curve is zero.

$$\left(-\frac{dn}{dt}\right)_{t_m} = \frac{S\Delta P_m}{AkT_o}\cdot\left(\frac{V\ .\ 0}{S\Delta P_m} + 1\right) \qquad - \quad (4\text{-}13)$$

$$\left(-\frac{dn}{dt}\right)_{t_m} = \frac{S\Delta P_m}{AkT_o} \qquad - \quad (4\text{-}14)$$

Therefore, equation (4-12) may be rewritten,

$$\left(-\frac{dn}{dt}\right)_t = \left(-\frac{dn}{dt}\right)_{tm} \left(\frac{V.\frac{d(\Delta P)}{dt}}{SPm} + \frac{\Delta P}{\Delta Pm} \right) \qquad - \quad (4\text{-}15)$$

From this equation (4-15) the rate of desorption of a gas species as a function of time can be evaluated from the pressure changes in a system under carefully controlled conditions.

The surface coverage, in molecules .cm^{-2} can be determined by integration of the desorption rate equation. The initial surface coverage, n_o, will be given by integration over the entire desorption reaction.

$$n_o = \int_o^{tz} \left(-\frac{dn}{dt}\right)_t dt \qquad - \quad (4\text{-}16)$$

where tz is the time at which the experimental desorption rate approaches zero.

It can be seen this integral gives the area under the desorption rate-time curve shown below in fig. (4-2).

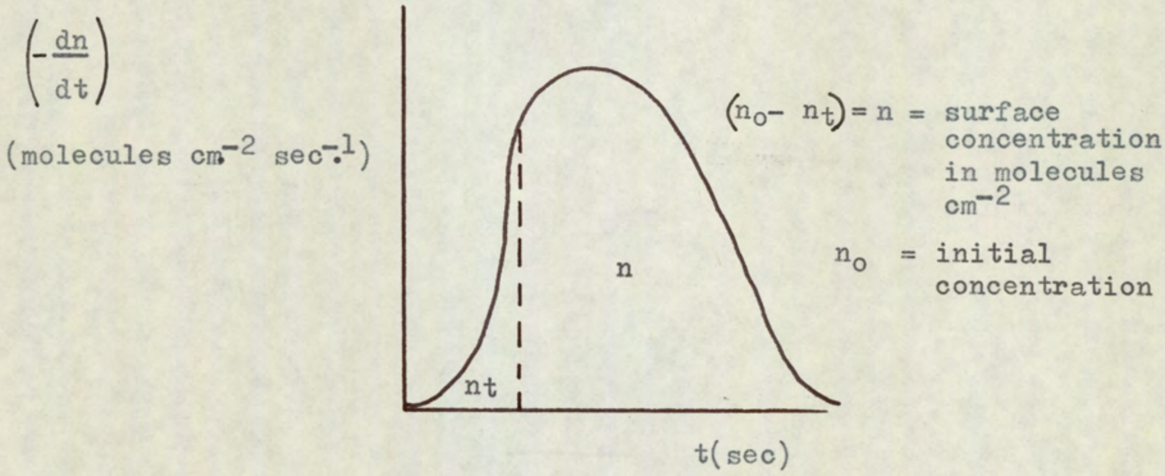

Figure (4-2)

The surface concentration at any time t, n, will be given by the integral

$$n = \int_{t}^{tz} \left(- \frac{dn}{dt}\right)_t . \ dt \qquad - \quad (4\text{-}17)$$

$$\therefore \quad n = \int_{o}^{tz} \left(- \frac{dn}{dt}\right)_t . \ dt - \int_{o}^{t} \left(- \frac{dn}{dt}\right)_t . \ dt \qquad - \quad (4\text{-}18)$$

or,

$$n = (n_o - n_t) \qquad - \quad (4\text{-}19)$$

This integration procedure was carried out using a computer program to evaluate the two integrals in equation (4-18) by numerical integration and then evaluate the difference $(n_o - n_t)$ to give the instantaneous surface concentration n.

At any time therefore the instantaneous rate of desorption $\left(- \frac{dn}{dt}\right)_t$ is known from equation (4-15) and the surface concentration from equation (4-18) so that the rate constant for desorption k_d for a reaction of order x may be calculated from the relation

$$-\left(\frac{dn}{dt}\right)_t = k_d . \ n^x \qquad - \quad (4\text{-}20)$$

4.3. The Thermal Transient

The preceding section was concerned with the evaluation of the rate equation for desorption under isothermal conditions. During the thermal desorption reaction the section of the surface under examination, usually a filament is raised in temperature during a predetermined programme so that the temperature is always known as a function of time, although not necessarily analytically. Equation (4-20) which describes the desorption of gas under isothermal conditions loses validity as the "rate constant, k_d is a function of temperature of the surface.

The order of the reaction remains a valid concept but the rate constant must be replaced by a more slowly varying parameter, namely the Arrhenius energy of activation defined by,

$$E_d = RT^2 . \left(\frac{d(\ln k_d)}{dT}\right) \qquad - \quad (4\text{-}21)$$

The rate equation can then be rewritten,

$$\left(-\frac{dn}{dt}\right)_t = n^x . A . \exp\left(-\frac{E_d}{RT}\right) \qquad - \quad (4\text{-}22)$$

where A, the pre-exponential factor and E_d, the activation energy are experimentally determined, temperature independent quantities.

The important experimental quantity, E_d, can be determined by two methods. Rearranging equation (4-22) and taking logarithms, the following equation is obtained,

$$\ln\left(\frac{(-dn/dt)_t}{n^x}\right) = \ln.A - \frac{E_d}{RT} \qquad - \quad (4\text{-}23)$$

Using equations (4-15) and (4-18) together with the known temperature programme it can be seen a plot of $\ln\left(\frac{(dn/dt)_t}{n^x}\right)$ against $1/T$ for the correct value of x will yield a straight line of slope $- E_d/R$, and hence E_d may be evaluated.

The activation energy may also be calculated from a single point calculation.

Differentiation of equation (4-20) with respect to time gives:

$$\left(- \frac{d^2n}{dt^2}\right) = n^x \cdot \frac{dk_d}{dt} + x \cdot k_d \cdot n^{x-1} \cdot \frac{-dn}{dt} \qquad - \quad (4\text{-}24)$$

$$= n^x \cdot \frac{dk_d}{dT} \cdot \frac{dT}{dt} + x \cdot k_d \cdot n^{x-1} \cdot \frac{-dn}{dt} \qquad - \quad (4\text{-}25)$$

$$= k_d n^x \left\{\frac{d(\ln k_d)}{dt} \cdot \frac{dT}{dt} + \frac{x}{n} \cdot \frac{-dn}{dt}\right\} \qquad - \quad (4\text{-}26)$$

$$\left(- \frac{d^2n}{dt^2}\right) = \left(- \frac{dn}{dt}\right)\left(\frac{d(\ln k_d)}{dT} \cdot \frac{dT}{dt} + \frac{x}{n} \cdot \frac{-dn}{dt}\right) \qquad - \quad (4\text{-}27)$$

at the maximum in the desorption rate - time curve $\left(- \frac{d^2n}{dt^2}\right)$ passes through zero so that

$$0 = \left(- \frac{dn}{dt}\right)_{max} \cdot \left(\frac{d(\ln k_d)}{dT} \cdot \frac{dT}{dt} + \frac{x}{n} \cdot \left(- \frac{dn}{dt}\right)_{max} \right) \qquad - \quad (4\text{-}28)$$

Rearranging:

$$\frac{d(\ln k_d)}{dT} = -\frac{dt}{dT} \cdot \frac{x}{n} \cdot \frac{dn}{dt} \qquad - \quad (4\text{-}29)$$

From equation (4-21)

$$E_d = RT^2 \cdot \frac{d(\ln k_d)}{dt} \qquad - \quad (4\text{-}30)$$

or,

$$E_d = \frac{x.RT^2}{\beta\, n} \left(\frac{dn}{dt}\right)_{max} \qquad - \quad (4\text{-}31)$$

where x = order of reaction

β = $\frac{dT}{dt}$ at the maximum in the desorption rate curve

n = surface concentration at $\left(\frac{dn}{dt}\right)_{max}$

$\left(\frac{dn}{dt}\right)_{max}$ = maximum value of $\frac{dn}{dt}$

T = the temperature corresponding to the value of $\left(\frac{dn}{dt}\right)_{max}$

4.4. The Absolute Reaction Rate Theory (4)

To provide a deeper insight into the mechanism of the desorption reaction and to obtain values for the experimental entropy and enthalpy of activation for the reaction, the theory of reaction rates can be applied. This theory attempts to calculate the rate constant from first principles.

The rate, r, for a chemical reaction of several reacting species can be written,

$$r = k(C_A^a \cdot C_B^b \ldots\ldots\ldots) \qquad - \quad (4\text{-}32)$$

where C_A, C_B are the concentrations of the reactants.

a, b are the orders of reaction for the respective reactants.

k is the rate constant and is in fact a function of temperature.

It was first suggested by Arrhenius that in any reacting system there existed an equilibrium between inert and 'active' species which contained enough energy, called the activation energy, to undergo reaction. If a model for equilibrium between these 'activated' species and the inert reactant molecules is set up then the variation of the rate constant with temperature is of the form shown in equations (4-21) and (4-22).

$$k = A \exp\left(- \frac{E_A}{RT}\right) \qquad - \quad (4\text{-}33)$$

Although this equation was originally derived experimentally, an equation of the same form can be derived from the absolute reaction rate theory.

This theory is based on the idea that a chemical reaction is characterised by an initial state which passes over, by continuous change, an energy barrier along the reaction coordinate into the final state.

At some point along the reaction coordinate there is some critical intermediate state in the sense that if this state is obtained there is a high probability that the reaction will continue to completion. This critical state is usually called the activated complex and the reaction can be represented by the diagram below:

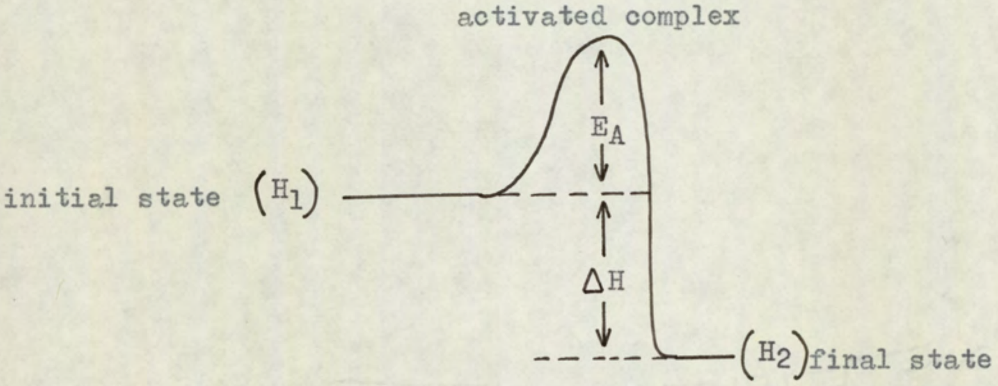

It is more correct to consider the free energies of the initial, activated and final states and the free energy of activation $\Delta G^{\ddagger}$.

It can be seen that in neither case does E_A or $\Delta G^{\ddagger}$ bear any direct relationship to the overall 'energy' change ΔH or ΔG.

The activated complex is regarded as an ordinary molecule having all the usual thermodynamic properties with the exception that motion in one direction, along the reaction coordinate leads to decomposition; motion in either direction leads to a more stable state.

The rate of reaction can be written:

$$r = \begin{bmatrix}\text{concentration of}\\ \text{activated complex}\end{bmatrix} \quad x \quad \begin{bmatrix}\text{frequency of}\\ \text{crossing barrier}\end{bmatrix} \qquad -(4\text{-}34$$

$$= c^{\ddagger} . \frac{\bar{v}}{\delta}$$

where $c^{\ddagger}$ = concentration

δ = width of barrier

$\bar{v}$ = mean velocity of crossing

Consider the region near the top of the energy barrier.

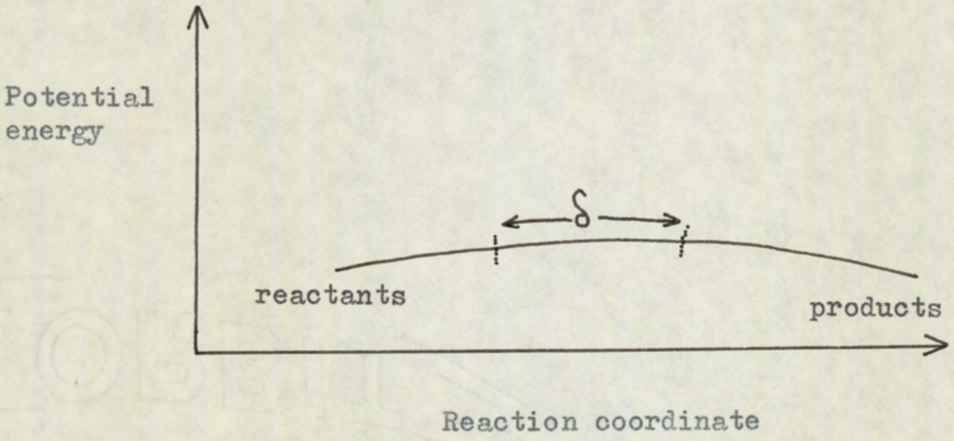

If a flat portion of length δ of the reaction coordinate is defined as comprising the activated state, then the average lifetime of the complex, τ , is given by

$$\tau = \frac{\delta}{\bar{v}} \qquad - \quad (4\text{-}35)$$

The rate of reaction is then $c^{\ddagger}/\tau$. The mean velocity of the activated complexes crossing the barrier is found from kinetic theory to be $(kT/2\pi m)^{\frac{1}{2}}$.

The rate of reaction is therefore given by

$$r = c^{\ddagger} . \left(\frac{kT}{2\pi m}\right)^{\frac{1}{2}} . \frac{1}{\delta} \qquad - \quad (4\text{-}36)$$

Since it was postulated earlier that the reactants are always in equilibrium with the activated complex it is possible to express the equilibrium constant for a system of ideal substances as,

$$K^{\ddagger} = \frac{c^{\ddagger}}{C_A C_B} \qquad - \quad (4\text{-}37)$$

The equilibrium constant can also be expressed as the ratio of the probabilities of the molecules existing as either reactants or an activated complex, that is, the ratio of the partition functions.

$$K^{\ddagger} = \frac{F^{\ddagger}_{abs}}{F_{A_{abs}} F_{B_{abs}}} \qquad - \quad (4\text{-}38)$$

These are absolute partition functions, that is the equation assumes that the energy levels of all the species are expressed in terms of the same zero. It is more practical to measure energies relative to the energies of the molecules at absolute zero.

Therefore,

$$K^{\ddagger} = \frac{F'^{\ddagger}}{F_A F_B} . \exp\left(\frac{-\epsilon_o}{kT}\right) \qquad - \quad (4\text{-}39)$$

where ϵ_o represents the difference in the zero energy levels per molecule between the activated complex and the reactants.

Combining equations (4-32) and (4-36) an equation for the rate constant is obtained

$$k = \frac{C^{\ddagger}}{C_A C_B} \cdot \left(\frac{kT}{2\pi m}\right)^{\frac{1}{2}} \cdot \frac{1}{\delta} \qquad - \quad (4\text{-}40)$$

Combining this with equation (4-39) , remembering equation (4-37)

$$k = \left(\frac{kT}{2\pi m}\right)^{\frac{1}{2}} \cdot \frac{1}{\delta} \; \frac{F'^{\ddagger}}{F_A F_B} \cdot \exp\left(-\frac{\epsilon_o}{kT}\right) \qquad - \quad (4\text{-}41)$$

$F'^{\ddagger}$ is the complete partition function for the activated complex and this can be expressed as the product of the partition function for the normal degrees of freedom of the complex and the partition function for motion along the reaction coordinates, leading to reaction

$$F'^{\ddagger} = F^{\ddagger} \cdot f_t \qquad - \quad (4\text{-}42)$$

The partition function for translational motion is given by

$$f_t = \sum_{\substack{i \\ \text{levels}}} g_t . \exp\left(- \epsilon_t /kT\right) \qquad - \quad (4\text{-}43)$$

Where g_t is the degeneracy and ϵ_t the absolute energy of the ith level. As the translational energy levels are very closely spaced this summation can be replaced by an integration and it can be shown that the partition function for one degree of translational freedom along the length of coordinate, δ is:

$$f_t = \left(\frac{2\pi mkT}{h^2}\right)^{\frac{1}{2}} \cdot \delta \qquad - \quad (4\text{-}44)$$

Therefore from equation (4-41)

$$k = \left(\frac{kT}{2\pi m}\right)^{\frac{1}{2}} \cdot \left(\frac{2\pi mkT}{h^2}\right)^{\frac{1}{2}} \cdot \delta \cdot \frac{1}{\delta} \cdot \frac{F^{\ddagger}}{F_A F_B} \cdot \exp\left(-\frac{\epsilon_o^{\ddagger}}{kT}\right)$$

or,

$$k = \frac{kT}{h} \cdot \frac{F^{\ddagger}}{F_A F_B} \cdot \exp\left(-\frac{\epsilon_o^{\ddagger}}{kT}\right) \qquad - \quad (4\text{-}45)$$

A well known relationship in thermodynamics is

$$\Delta G = - RT \ln K$$

or $$K = \exp(-\Delta G/RT) \qquad - \quad (4\text{-}46)$$

Where the free energy change of a reaction for the reactants and products in their standard states is related the equilibrium constant for the reaction.

The equilibrium constant in this case is

$$K^{\ddagger} = \frac{C^{\ddagger}}{C_A C_B} = \frac{F^{\ddagger}}{F_A F_B} \exp\left(-\frac{E_o^{\ddagger}}{RT}\right) \qquad - \quad (4\text{-}47)$$

$$\therefore \quad k = \frac{kT}{h} \cdot \exp\left(-\frac{\Delta G^{\ddagger}}{RT}\right) \qquad - \quad (4\text{-}48)$$

Where $\Delta G^{\ddagger}$ represents the free energy difference between the reactants and the activated complex when both of these are in their standard states.

Since the free energy change for any reaction can be expressed in terms of the enthalpy and entropy changes, equation (4-48) can also be expressed in terms of these.

$$k = \frac{kT}{h} \exp\left(\frac{\Delta S^{\ddagger}}{R}\right) \cdot \exp\left(-\frac{\Delta H^{\ddagger}}{RT}\right) \qquad - \quad (4\text{-}49)$$

Equations (4-45) and (4-49) are of great use and importance in the analysis of desorption data.

To allow for the fact that not all activated complexes may in fact undergo the transition to products, the transmission coefficient, $\bar{d}$, is introduced so that equation (4-49) becomes

$$k = \bar{d}.\frac{kT}{n} \exp\left(\frac{\Delta S^{\ddagger}}{R}\right) \exp\left(-\frac{\Delta H^{\ddagger}}{RT}\right) \qquad - \quad (4\text{-}50)$$

The transmission coefficient may or may not be a function of temperature and this will be discussed later.

4.5 Application of Absolute Reaction Rate Theory to the Desorption Reaction

Desorption from an adsorbed layer of molecules on a solid surface can be considered as involving an activated state in which the molecule attached to an adsorption site acquires the necessary configuration and activation energy to permit it to escape from the surface.

The two simplest cases of desorption are;

$$A_{ads} \rightleftharpoons A^{\ddagger} \longrightarrow A_{des} \text{ (1st order)} \qquad - \quad (4\text{-}51)$$

$$A_{ads} + A_{ads} \rightleftharpoons (A - A)^{*} \longrightarrow A_{2des} \text{ (2nd order)} \qquad - \quad (4\text{-}52)$$

In a general form the equilibrium constant, $K^{\ddagger}$, for these reactions can be written,

$$K^{\ddagger} = \frac{C^{\ddagger}}{(n)^x} = \frac{F^{\ddagger}}{(F_A)^x} \qquad - \quad (4\text{-}53)$$

where n = concentration of adsorbed molecules.cm^{-2}

$C^{\ddagger}$ = concentration of activated molecules.cm^{-2}

x = order of reaction

The rate of desorption, using equation (4-45) is,

$$\left(-\frac{dn}{dt}\right) = n^x \frac{kT}{h} \cdot \frac{F^{\ddagger}}{(F_A)^x} \exp\left(-\frac{\epsilon_o^{\ddagger}}{kT}\right) \qquad - \quad (4\text{-}54)$$

Alternatively, using equation (4-49) the rate of desorption is given by,

$$\left(\frac{-dn}{dt}\right) = n^{x} \cdot \frac{kT}{h} \exp\left(\frac{\Delta S^{\ddagger}}{R}\right) \exp\left(\frac{-\Delta H^{\ddagger}}{RT}\right) \qquad - \quad (4\text{-}55)$$

Several types of behaviour may be considered. If the reaction is first order, $x = 1$ and two cases may be considered (1).

(1) If the complexes and adsorbed molecules possess identical degrees of freedom and similar vibration frequencies on the surface, then $F^{\ddagger} = F_A$.

(2) The activated complex may be less strongly bound to the surface than the adsorbed molecule and therefore possess greater freedom of movement. In this case $F^{\ddagger}/F_A > 1$. In the extreme case where the complex has translational and rotational freedom and the adsorbed molecule has not, $F^{\ddagger}/F_A$ may have a value of 10^3 to 10^4.

In the case of a second order reaction, $x = 2$ and three types of behaviour may be considered.

(1) If the complexes and adsorbed species are both immobile and only vibrations of high frequency occur, $F^{\ddagger} = F_A = 1$.

(2) The complex may be mobile while the adsorbed molecules are immobile. In this case $F_A = 1$ but $F^{\ddagger} > 1$. The rate will then be greater than case (1).

(3) Both molecules and complexes may be mobile, a possible example of this is the desorption of hydrogen chemisorbed on metal surfaces as atoms. In this case two degrees of translational freedom are lost in forming the complex tending to make $F^{\ddagger}/F_A^2 < 1$. Although this may to some extent be offset by the rotational partition function, the rate of desorption would be rather slower than in the first case.

4.6. Experimental Determination of Energy, Enthalpy and Entropy of Activation

The activation energy can be determined as shown in section (4.3) from the relationship,

$$E_d = RT^2 \cdot \frac{d(\ln k_d)}{dT} \qquad - \quad (4\text{-}21)$$

Taking logarithms of equation (4-49)

$$\ln k_d = \ln T + \ln \frac{k}{h} + \frac{\Delta S^{\ddagger}}{R} - \frac{\Delta H^{\ddagger}}{RT} \qquad - \quad (4\text{-}56)$$

and differentiating with respect to temperature

$$\frac{d(\ln k_d)}{dT} = \frac{1}{T} + \frac{\Delta H^{\ddagger}}{RT^2} \qquad - \quad (4\text{-}57)$$

Equating equations (4-21) and (4-57)

$$\frac{E_d}{RT^2} = \frac{1}{T} + \frac{\Delta H^{\ddagger}}{RT^2} \qquad - \quad (4\text{-}58)$$

$$E_d = \Delta H^{\ddagger} + RT \qquad - \quad (4\text{-}59)$$

The experimental rate equation is given by,

$$r_d = \left(- \frac{dn}{dt}\right) = k_d \cdot (n)^x \qquad - \quad (4\text{-}60)$$

Taking logarithms of this equation and comparing the result to equation (4-56),

$$\ln\left(\frac{(-dn/dt)}{(n)^x\ T}\right) = \ln\frac{k}{h} + \frac{\Delta S^{\ddagger}}{R} - \frac{\Delta H^{\ddagger}}{R} \qquad - \quad (4\text{-}61)$$

It can be seen that a plot of $\ln\left(\frac{(-dn/dt)}{(n)^x\ T}\right)$ against $\left(\frac{1}{T}\right)$ will give a straight line of slope $-\Delta H^{\ddagger}/R$ from which $\Delta H^{\ddagger}$ can be evaluated.

If equation (4-61) is rearranged then it is possible to evaluate the entropy of activation, $\Delta S^{\ddagger}$.

$$\Delta S^{\ddagger} = R\left(\ln\frac{(-dn/dt)}{(n)^x\ T} + \frac{\Delta H^{\ddagger}}{RT} - \ln\frac{k}{h}\right) \qquad - \quad (4\text{-}62)$$

Thus, if the correct units are chosen, it is possible to calculate the experimental entropy of activation $\Delta S^{\ddagger}$ from the experimental value of $\Delta H^{\ddagger}$ (or E_d using equation (4-59)) and the experimentally determined rates of desorption and surface concentration.

4.7. The Experimental Study of Thermal Desorption

4.7.1. Experimental Data Required

The thermal desorption reaction experiment consists of permitting gas to adsorb onto a metal surface and then desorbing the adsorbed species by raising the filament temperature through a controlled temperature programme.

Before any quantitative kinetic information can be obtained about the desorption reaction the experimental results must provide the following information:

(1) The temperature of the surface under study as a function of time.
(2) The gas density in the system as a function of time.
(3) The pumping speed of the system for the gases involved in the desorption reaction.

4.7.1.1. Measurement of the Filament Temperature

The determination of the filament temperature as a function of time, during the course of the experiment, is of the utmost importance for the evaluation of the thermodynamic parameters, E_d, $\Delta H^{\ddagger}$ and $\Delta S^{\ddagger}$. Since the temperature as a function of time does not appear in any of the rate expressions its exact form is not important other than that the value of dT/dt must exceed zero.

The most common method of increasing the temperature of the surface is by resistance heating $^{(15 - 18)}$, the power in this case develops from the electrical potential applied across the filament and the current flowing through it. When using this form of heating there are two important factors to consider. First, the filament should be of sufficient length so that the portion of the filament where the temperature variation is the greatest, that is at the ends where heat is conducted away by the filament supports, represents only a small fraction of the total length. This problem has been studied by Erhlich (22) under conditions of steady state and conditions similar to those encountered in 'flash' desorption, i.e. temperature rapidly changing with time, and it was found that the temperature was significantly more uniform, over a larger portion of the filament, in the latter case.

Secondly, the temperature of the filament at any instant may be determined from the measurement of the instantaneous filament resistivity. This is obtained from the ratio of the voltage across the filament, the current through it and a knowledge of the physical dimensions of the filament. It should be remembered (22, 68) that because of the temperature variation along the length of the filament there will be a resistance change during the temperature cycle.

Of these two considerations the temperature gradients at the ends of the filament are the most disturbing and warrant further consideration later.

4.7.1.2. Measurement of Gas Density in the System

The pressure change in the system was measured with an AEI-GEC Penning trigger discharge gauge. The control unit had linear scales, each covering a decade of pressure in the range 10^{-4} - 10^{-13} mm.Hg and also a logarithmic scale in the range 10^{-10} - 10^{-5} mm.Hg. Although the linear scales were more sensitive, the pressure increase during the desorption cycle was generally greater than one decade of pressure and therefore the log scale was employed. The control unit had an output for each mode of operation and in the logarithmic mode the output was 0.2 volts/decade of pressure.

The gauge was calibrated for dry air, which is mainly nitrogen, and thus the gauge calibration would not be expected to hold for any other gas composition. This type of gauge has been calibrated for gases such as O_2, N_2, He, Ar and CO (69,70,71) but unfortunately no data could be found to correct the apparent measured pressures, nor could any means be found of calculating the gauge sensitivity for different gases.

The ion current in a trigger discharge gauge is generally considered to be related to the pressure by the relationship, (71,72)

$$i_+ = kp^n \qquad - \quad (4\text{-}63)$$

where,

i_+ = measured ion current.
k = constant dependent upon control unit and gauge.
n = constant dependent upon the gas species.

Ideally, $n = 1$ but experimentally it is generally found to be greater than unity. It has been shown by several authors (69) that there are several values of n depending upon the pressure. These are called different "discharge modes" of the gauge and typical values for n are shown below for the pressure range $10^{-4} - 10^{-10}$ mm.Hg.

n	gas
1.19	N_2
1.11	CO
1.23	H_2
1.15	He

These values of n are average values and it is thought that there are several overlapping linear regions ($n = 1$) throughout the pressure range studied.

Gauge calibration in the ultra high vacuum range is not to be undertaken lightly as the experimental methods are very difficult. There are several methods used for accurate gauge calibration, the two most important being calibration against a mass spectrometer and a dynamic method depending upon the leak rate through an orifice, of known dimensions, in a thin plate. Both of these methods can be used down to 10^{-10} mm.Hg, the former down to 10^{-12} mm.Hg, but this could not be undertaken in this work because of the lack of the necessary equipment.

It has been stated that the relative intensities of the ion currents measured in the trigger gauge are in rough accord with the ionisation probabilities of the species in question. A search of the literature, however, did not reveal any data on iodine or methyl iodide of a suitable nature so that in this work it has been assumed that the gauge sensitivity for these two gases is the same as that for air. This may or may not introduce an error into the calculations.

4.7.1.3. Measurement of Pumping Speed

The total pumping speed of a vacuum system is the sum of all the various modes of pumping. These modes include not only the vacuum pumps but also pumping due to the pressure measuring devices and pumping, due to adsorption, by various surfaces in the vacuum system.

The pumping speed is defined by the equation below and the units are usually litres.sec^{-1}.

$$P_t = P_o \exp\left(- \frac{t \ S_p}{V}\right) \qquad - \quad (4\text{-}64)$$

where, P_t = pressure at time t.

P_o = pressure at time t = 0.

S_p = pumping speed at time t and pressure P_t.

V = effective volume of vacuum system.

This equation can be rearranged in a logarithmic form,

$$\ln\left(\frac{P_t}{P_o}\right) = \frac{S_p \ . \ t}{V} \qquad - \quad (4\text{-}65)$$

For a range of pressure where S is independent of the pressure then,

$$S = \frac{V}{(t_2 - t_1)} \ln. \left(\frac{P_{t_1}}{P_{t_2}} \right) \qquad - \quad (4\text{-}66)$$

where P_{t_1} and P_{t_2} represent the pressures at the beginning and end of the time interval defined by $(t_2 - t_1)$.

The observed form of the desorption trace will be dependent both upon the rate at which the temperature of the filament is increased and the total pumping speed of the system. For a closed system in which the pumping speed is zero no gas will be removed during the 'flash' and the desorption trace will have a form similar to that shown in figure (4-3). It can be seen that the gas species was adsorbed on the surface in several different states, each with a different desorption energy. In the situation where $S \rightarrow 0$, equation (4-11) becomes,

$$\left(- \frac{dn}{dt} \right) = \frac{V}{AkT_o} \cdot \frac{d(\Delta P)}{dt} \qquad - \quad (4\text{-}67)$$

and the initial surface concentration is directly proportional to the measured pressure increase.

$$n_o = \frac{V}{AkT_o} \cdot \Delta P_m \qquad - \quad (4\text{-}68)$$

A flow system exists where the pumping speed is greater than zero and an example of a desorption trace for this condition is shown in figure (4-4). It can be seen that in a dynamic system better resolution of the individual binding states is obtained, but in order to obtain quantitative results the pumping speed of the system must be known.

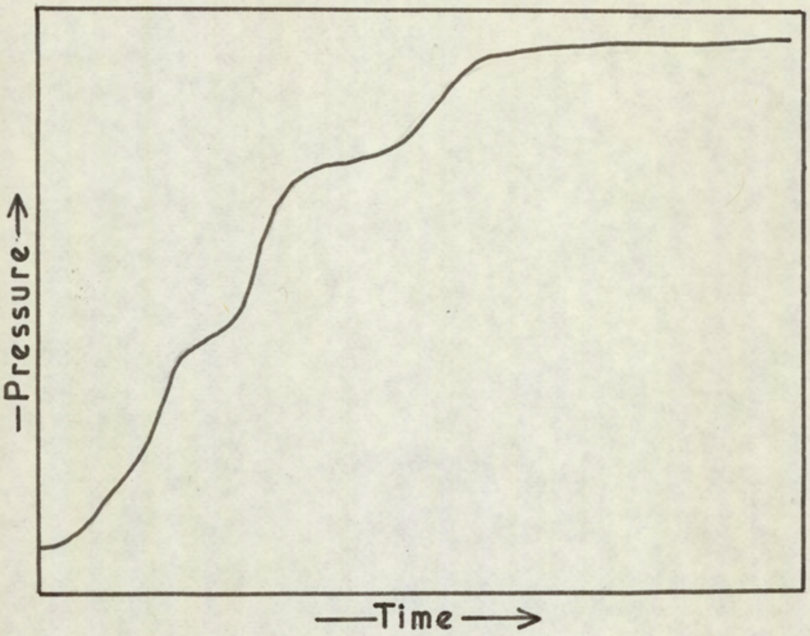

FIGURE (4-3).Desorption of Gases , S=O

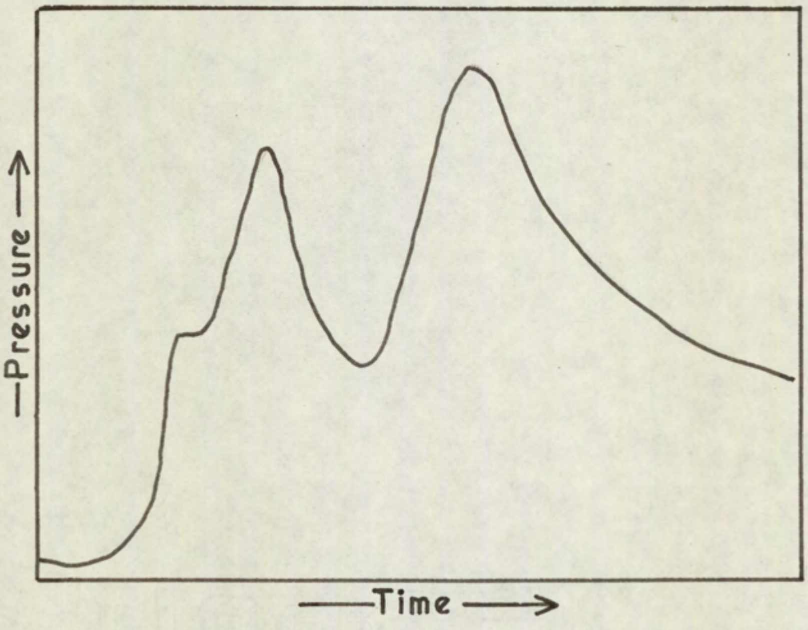

FIGURE (4-4) Desorption of Gases , S>O

4.7.2. The Experimental Apparatus

The ultra high vacuum system was to be used to study the desorption reactions of methyl iodide and iodine and the effect of these gases on the work function of a tantalum surface. Therefore the experimental apparatus must fit the needs of both areas of study and there are several major considerations which should be borne in mind.

The desorbed gases from the filament will make a number of collisions with the walls and surfaces within the vacuum system before reaching the pressure gauge. Reaction of the gases with these surfaces could lead to errors in the determination of the pressure change and composition of gas and hence to misleading results; for example, both carbon monoxide (73) and atomic hydrogen (3) adsorb strongly on glass walls and should be avoided in these cases.

The placement of the pressure measuring gauge too near the desorption filament could lead to erroneous measurements due to electrical effects and/or the effect of the angular and energy distribution of the emitted molecules. By placing the gauge some distance from the desorption chamber these effects may be overcome, but now the conductance of the connecting tubing must be taken into consideration. It can be shown (3) that the average transit time calculated from the dimensions and geometry of the apparatus used is of the order of several milliseconds which is short compared to the reaction time of one second.

Provision should be made for heating the system to a temperature of at least 250°C for some period of time. This is an important prerequisite for the attainment of very low pressures as the bakeout helps to desorb gases, especially water vapour from various internal surfaces of the system and thus reduce the internal leak rate.

4.7.2.1. The Vacuum System

Two sorption pumps were used as roughing pumps and a combination of a titanium sublimation pump and a Ferranti FJD15 getter ion pump was used to obtain the ultra high vacuum required. The gauge used was an AEI-GEC model V315 trigger discharge gauge. A diagram of the apparatus is shown in figure (4-5).

The sorption pumps were chosen as they were free from sources of hydrocarbon contamination. The two pumps were connected in series and could be isolated from one another by an elastomer valve, V_1.

To obtain the lowest pressures with this type of pump the zeolite must be activated by baking out at a temperature of 280°C in the presence of dry, boiled-off nitrogen. This temperature ensured removal of all adsorbed gases, especially water vapour but was not high enough to degrade the zeolite structure.

In operation, the pumps were used in series and cooled in liquid nitrogen. The entire system was purged with dry boiled-off nitrogen to free the system of inert gases and after this operation had been completed the pressure could be reduced to a value of 10^{-6} mm.Hg.

Once the pressure had been reduced to a limiting value by the sorption pumps the system was isolated from these and the getter ion pump brought into operation. Using this pump, pressures of $< 10^{-8}$ mm.Hg were attainable without baking the system. The pump and its associated magnet are able to withstand continuous temperatures of 300°C and it is operated throughout the bakeout cycle.

The bakeout cycle consisted of raising the temperature of the entire system at a rate of approximately 50°C.hour^{-1} to a temperature of 250°C. After an initial pressure rise to 10^{-4} mm.Hg the pressure slowly dropped and the bakeout was continued at least until there was no further apparent decrease in pressure and was

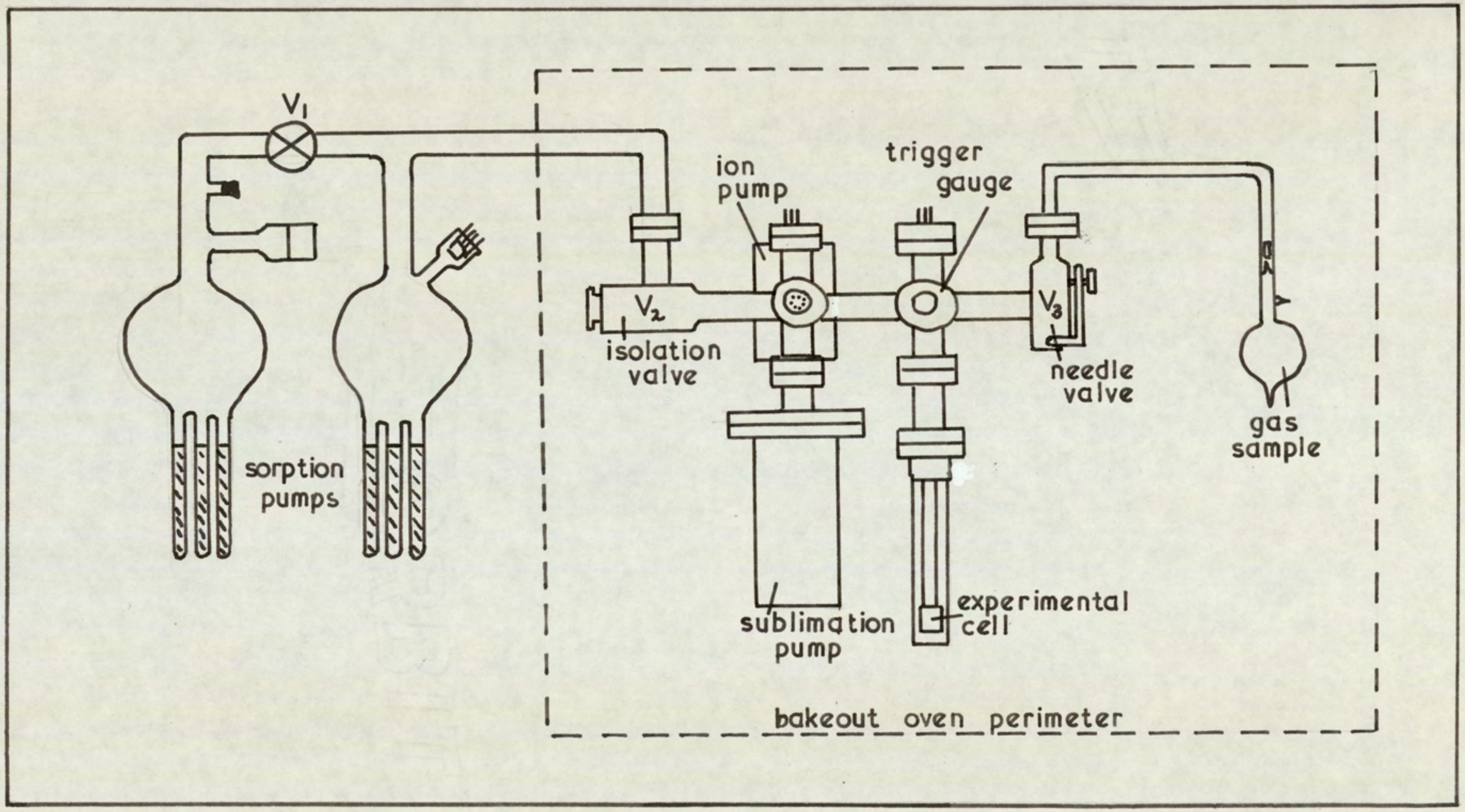

FIGURE (4-5). The Ultra High Vacuum System often prolonged for several days to ensure complete outgassing of all the internal surfaces.

During this high temperature bakeout all parts of the system that would be operated at elevated temperatures were outgassed, at, or above, their operating temperatures, until no further pressure rises were discernable. This operation was carried out for the flash desorption/work function filaments and also the titanium sublimation pump filaments. At the end of the bake-out cycle the temperature was reduced, at a rate of $50^{o}C.hour^{-1}$, to the ambient temperature. The titanium sublimation pump was then used in conjunction with the getter ion pump to reduce the pressure in the system to its ultimate value.

During operation of this pump the stainless steel pump body is immersed in liquid nitrogen and a clean titanium film is then deposited on the walls of the pump chamber by resistance heating of one of the filaments for approximately 1½ minutes.

Using these two pumps the ultimate pressure was found to be 2×10^{-12} mm.Hg as measured on the trigger gauge.

Three types of pressure gauge were in use on the vacuum system. In the sorption pump low vacuum line was a Pirani gauge for measuring pressures in the range $10^{-1} - 10^{-3}$ mm.Hg, whilst in the high vacuum side of the sorption pumps a hot filament ionisation gauge was used to monitor pressures in the range $10^{-3} - 10^{-7}$ mm.Hg. These two gauges were only used to ensure the correct pumpdown procedure before the system was closed at valve, V_2.

In the ultra high vacuum part of the system the Penning discharge gauge, capable of measuring pressures in the range $10^{-4} - 10^{-13}$ mm.Hg, was employed.

4.7.2.2. The Experimental Cell

The reaction cell was designed to study the effects that the adsorbed gas species have on the work function of a metal surface and also the thermal desorption reaction from the same surface. The electron beam method was used to determine the

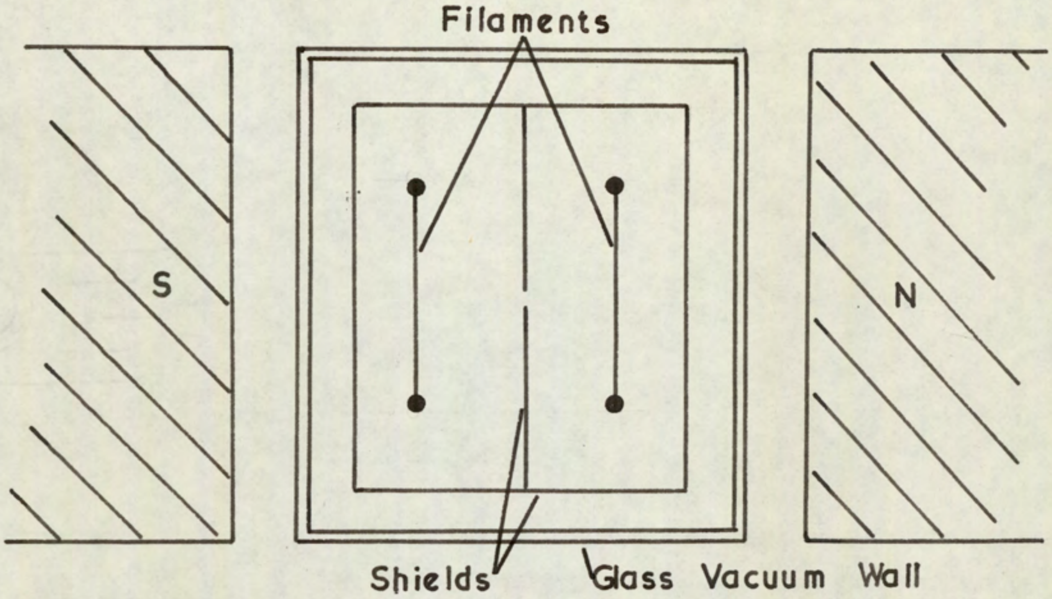

FIGURE (4-6) Planar Triode.

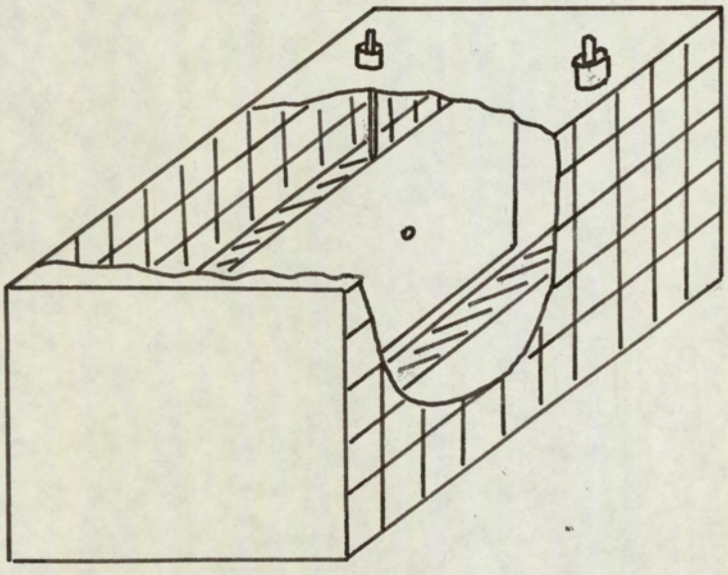

FIGURE (4-7). Cutaway of Experimental Cell.

contact potential difference between the surface under study and a reference tantalum filament, the work function of which was determined by thermionic measurements.

The experimental apparatus used was similar to that reported by Shelton (48) and is in the form of a planar triode. This is illustrated in figures (4-6) and (4-7). The 3000 gauss magnet was placed so that the magnetic and electric fields were normal to the surface of the sheet metal filaments. Provision was made for heating both filaments so that either could be used for the flash desorption or work function measurements.

The upper and lower portions of the cell were constructed from a high purity copper sheet, the sides were constructed from stainless steel mesh so that the temperature of the hot filaments could be measured using a pyrometer and the grid and filaments were constructed from tantalum sheet, .005" and .001" thick respectively.

4.7.2.3. Work Function and Thermal Desorption Measurements in the Planar Triode

For these measurements one filament was used as the thermionic emitter and the other as the collector. The cell was symmetrical and the role of the filaments was interchangeable. A positive accelerating potential, with respect to the emitting filament, was applied to the shields and the grid containing the aperture and the triode characteristic plot was obtained by variation of the potential of the emitter with respect to the collector. Thermionic work function measurements were carried out in the saturated field fegion.

The electrical circuit used for these measurements is shown in figure (4-8). The current for the emitter was supplied by two 12 volt heavy duty storage batteries that were connected in parallel.

In this apparatus factors giving rise to curvature near the breakpoint in the current-voltage characteristic are virtually eliminated. As a result of the electrostatic and magnetic field

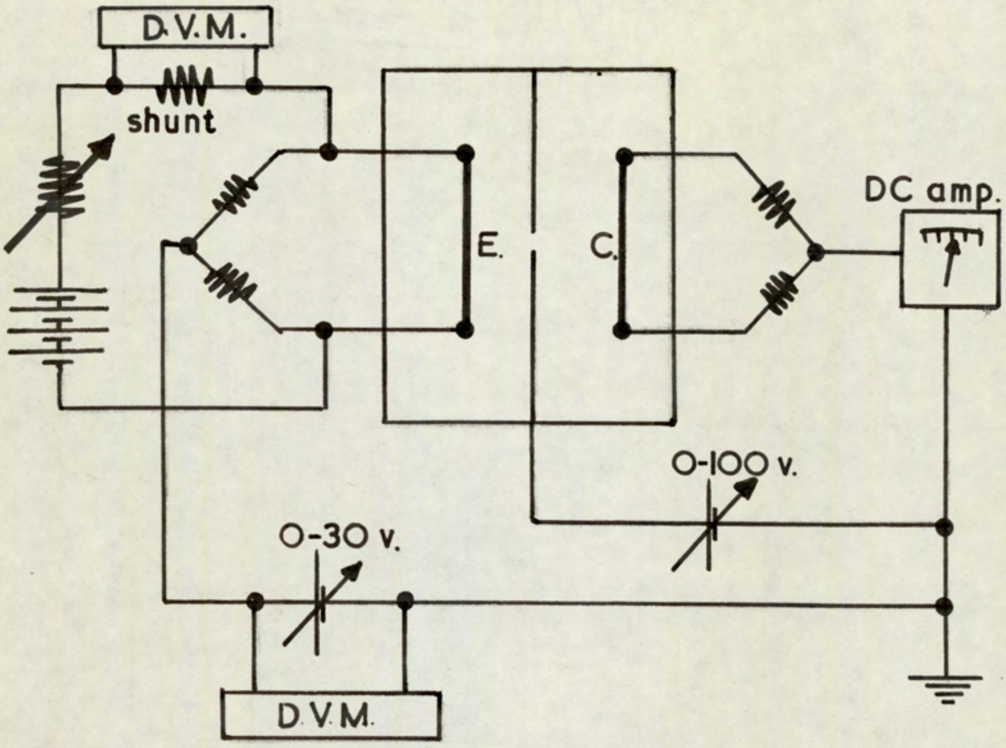

FIG.(4-8) Electrical Circuit – Work Function Measurements

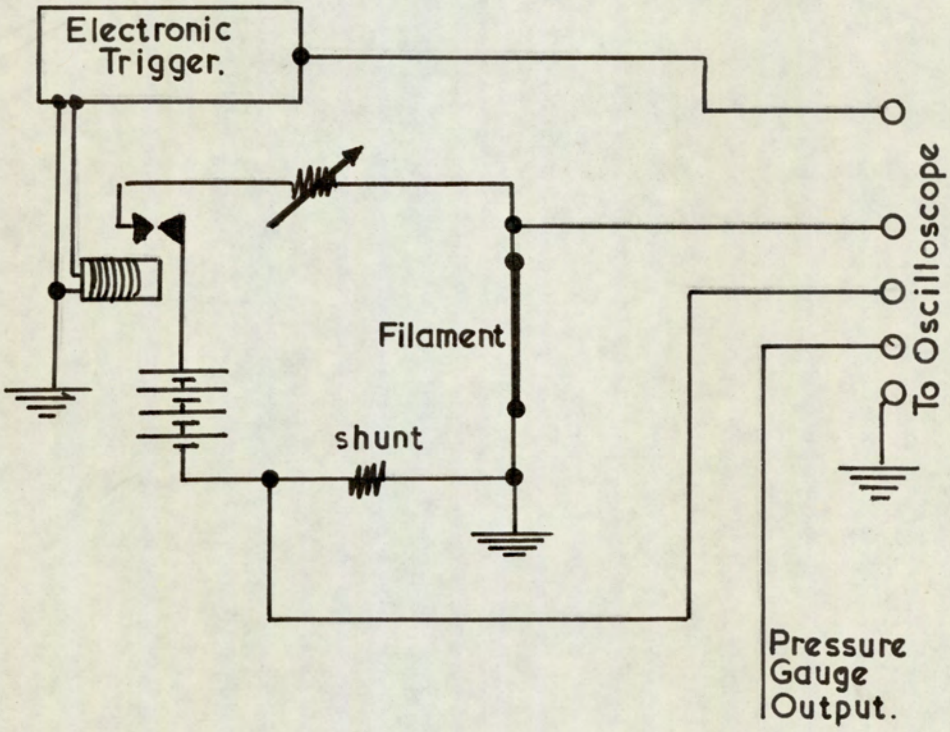

FIG.(4-9) Electrical Circuit – Thermal Desorption Measurements orientation the only electrons that were measured by the collector were those formed by a beam whose area was defined by the dimensions of the aperture. The electrons are tightly contained in spirals parallel to the magnetic field due to the effect of the crossed fields (75).

Because of these factors a very flat, saturated field region, a sharp breakpoint and a straight line for $\ln(J_{ret.field})$ against $V_{ret.}$ were obtained. It has been suggested that the magnetic field could affect the emission properties of the cathode but this has been shown not to be true (76).

There is also the possibility that secondary electron emission may occur from the intervening electrode, invalidating saturated current values and electron energy distribution measurements, but providing the emitter-grid accelerating voltage is kept to a low value (e.g. $\leqslant$ 10 volts) then the secondary electron current will be well below the primary electron current at all levels (67).

As stated above, either of the two filaments used in the work function measurements could be used for thermal desorption studies. The length of these filaments (2 cm.) is not as long as is desirable for use in thermal desorption reactions but the use of a longer filament was not practical.

The electrical circuit used in these experiments is shown in figure (4-9). A Tektronix Oscilloscope (type 545-A) with a type M1 four trace plug-in preamplifier unit was used to display, on the same time base, the following data:

(1) The voltage drop across a standard shunt resistor. This will give the current through the filament.

(2) The voltage across the input leads to the filament.

(3) The voltage output from the logarithmic scale of the trigger gauge.

The oscilloscope trace was recorded on photographic film.

4.7.3. Experimental Techniques

The techniques used to determine thermal desorption and work function data are given below.

4.7.3.1. Thermal Desorption Measurements

The following procedure was adopted:

(1) The filament in use was flashed repeatedly at high temperature until the pressure rise caused by heating the filament was small and consistent and the background pressure was in the 10^{-10} mm.Hg range.

(2) The sample gas was admitted into the system by use of the needle valve, V_3, until the desired pressure (usually in the 10^{-8} mm.Hg range) was obtained. The Pressure was kept constant for the desired adsorption time and after this time had elapsed the gas supply was turned off and the pressure was reduced to the value obtained prior to the gas dosing (P_B).

(3) The filament was flashed using the method shown in section (4.7.2.3) and the thermal desorption trace recorded photographically.

Prior to any measurement or series of measurements the sample gas was admitted into the system, at a pressure of $\sim 10^{-8}$ mm.Hg for several hours whilst the filament was flashed repeatedly. This ensured that the system was at equilibrium, especially with regard to the adsorption and desorption of the sample gas on the inner surfaces of the vacuum system.

4.7.3.2. Work Function and Contact Potential Measurements

Prior to the work function measurements both filaments were operated continuously for many hours at high temperatures ($>2300^\circ$K) to ensure complete outgassing of the filament and its supports. After this treatment pressures of $3 - 5 \times 10^{-10}$mm.Hg could be maintained with the emitter at its usual operating temperature of 1300 - 2000°K.

A set of characteristic curves for the clean filaments was then determined. From these curves it was possible to determine the following information;

(1) The Richardson work function, χ_E^{**} from a plot of $\ln\left(\frac{J_e}{T_e^2}\right)$ against $\frac{1}{T}$ using either saturated current or values in the retarding field region.

(2) The contact potential difference between the thermionic emitter and the collector and hence the work function of the collector, χ_c^{**} (T).

(3) The temperature dependence of the emitter work function.

Experiments were performed with a thermally cleaned collector and also with the collector after gas had been allowed to adsorb onto the surface for various times at various pressures. In some experiments the characteristic curves were monitored for a clean filament and then continuously during adsorption to determine the change in contact potential. At the end of such an experiment it was possible to carry out a flash desorption experiment and in this way the results of both techniques could be correlated.

Additional experiments were carried out in which the collector work function, as a function of temperature in the presence of adsorbed gas, was obtained. Two methods were used;

(1) A secondary, isolated (Teflon insulators and shielded) heating and measuring circuit was employed so that the collector current could be monitored during the heating cycle. Characteristic curves were determined at various collector temperatures in the range 300 - 1000°K in order to obtain the work function change due to any species adsorbing or desorbing in this temperature range.

(2) To eliminate any thermo-electric effects due to measuring the contact potential at various collector temperatures, similar experiments were performed but in these the collector was maintained at the desired temperature for a predetermined time and then allowed to cool to room temperature before recording the contact potential difference. For the pressure and time used in these experiments no appreciable readsorption would occur during the cooling cycle.

4.7.4. The Analysis of Experimental Data to obtain the Desorption Rate Equation

The results of the thermal desorption experiments were in the form of a photographic negative displaying the pressure, filament current and voltage drop across the filament as a function of time. Prints were made of these negatives on 8" x 10" Ilford grade 3 bromide paper.

The analysis of the photographs was greatly aided by the use of a Digico computer (employing the Mathchat language). This speeded up the analysis of the data, which although not complex involved much numerical manipulation.

A typical trace is shown in figure (5-1). All measurements were taken from these photographs.

4.7.4.1. Estimation of Filament Temperature

The resistance of a metal is generally a function of temperature. The resistance (in ohms) is related to the electrical resistivity (in ohms.cm.$^{-1}$) by the expression,

$$\rho_{Ta}(T) = R_{Ta}(T) \cdot \frac{A(T)}{l(T)} \qquad - \quad (4\text{-}70)$$

where $\rho_{Ta}(T)$ is the resistivity of the filament, $R_{Ta}(T)$ its resistance and A(T) and l(T) its cross sectional area and length respectively. It can be seen that all four terms of this equation are temperature dependent. It has been reported however that the linear expansion of tantalum in the temperature range 300 - 2400°K is 1.7% (77) which is well within the experimental error for the temperature estimation and can be ignored.

Therefore,

$$\rho_{Ta}(T) = R_{Ta}(T) \cdot \frac{A_o}{l_o} \qquad - \quad (4\text{-}71)$$

where l_o and A_o are the measured length and cross sectional area at 300°K.

The temperature dependence of the resistivity of tantalum has been determined experimentally (77). This is not a linear relationship but was found by computer, taking into account the dimensions of the filament (2.0 x 0.25 x 0.00254 cm.) to fit the equation shown below with a very low standard deviation.

$$\underset{(^{o}K)}{TEMP} = (0.493762 \times 10^2) + (0.853459 \times 10^4.R) + (0.153986 \times 10^6.R^2) + (0.121322 \times 10^7.R^3) + (0.380662 \times 10^7.R^4) \qquad - \quad (4\text{-}72)$$

This relationship is shown in figure (4-10). The resistance of the filament will be given by Ohm's law,

$$R_{Ta} = \frac{\text{voltage across filament}}{\text{current through filament}} = \frac{V_F}{I_F} \text{ ohms} \qquad - \quad (4\text{-}73)$$

It was not possible, however, to measure the voltage drop across the filament alone but only that across the filament, filament supports and copper conductors up to the vacuum leadthroughs. This quantity is called V_{Total}.

$$R_{Total}(T) = \frac{V_{Total}(T)}{I_F(T)} \qquad - \quad (4\text{-}74)$$

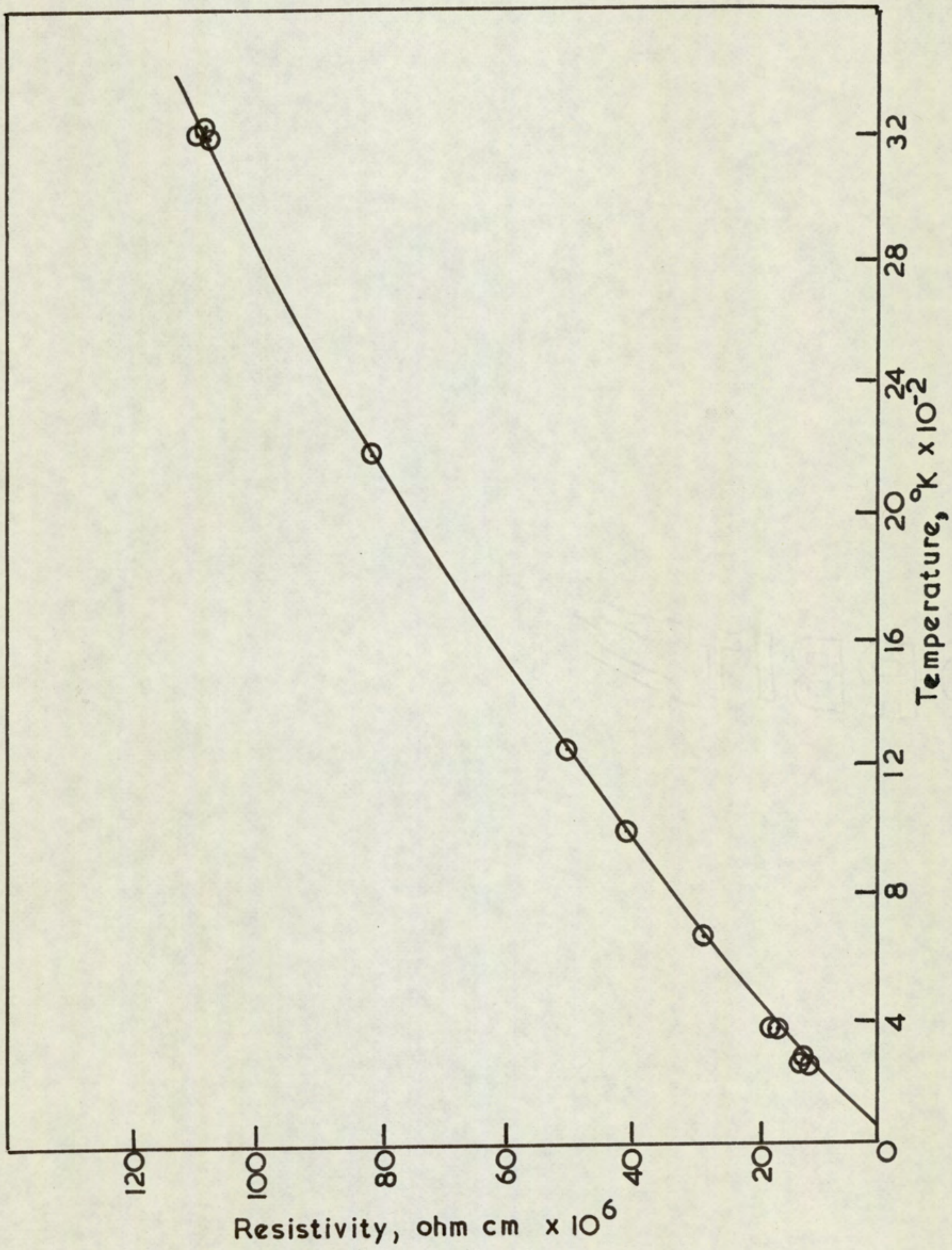

FIGURE (4-10) Electrical Resistivity of Tantalum

The total resistance can be separated into its constituent parts,

$$R_{Total}(T) = R(T)_{Ta} + R(T)_{\substack{\text{vacuum}\\ \text{leadthroughs}}} + R(T)_{\substack{\text{copper}\\ \text{conductors}}} + R(T)_{\substack{\text{filament}\\ \text{supports}}} + R(T)_{\text{contacts}}$$

\- (4-75)

It can be shown (67) that during the flash only the filament shows any appreciable temperature change, even the temperature of the stainless steel supports rises by only a few degrees. The only term that will be changing during the flash in equation (4-75) will be $R_{Ta}(T)$ and therefore this equation can be rewritten,

$$R(T)_{\text{total}} = R(T)_{Ta} + R(0)_{\text{Rest}}$$ - (4-76)

where $$R(0)_{\text{Rest}} = R_{\text{vac. l.}} + R_{\text{Cu. cond.}} + R_{\text{sup'ts}} + R_{\text{contacts}}$$ - (4-77)

It is possible to estimate the values of the first three terms on the right hand side of the equation from known dimensions and resistivity data, but not that of the term R_{contact}. This is the resistance of all the contacts in the circuit. From the dimensions of the filament however it is possible to estimate the value of $R(0)_{Ta}$ and since the value of $R(0)_{\text{total}}$ can be estimated from the initial values of the recorded trace then the value of $R(0)_{\text{rest}}$ can be evaluated. Using this value in equation (4-76) enables the filament temperature as a function of time to be obtained.

The following procedure was adopted. Measurements of the displacement of the current (I_{meas}) and voltage (V_{meas}) traces from the base lines were made at specified time intervals, usually 0.02 sec., from the enlarged photograph. The oscilloscope graticule (marked in 1cm. squares) was used to obtain the scaling factor (SF) to convert these to displacements (in cm.) of the oscilloscope trace. Using the amplification factors on the oscilloscope and the resistance of the standard shunt (0.0075Ω) the desired voltages, $V_{total}(T)$ and currents, $I_F(T)$, were obtained.

$$V_{total}(T) = \frac{V_{meas}(T) \times \text{amplification factor}}{\text{S.F.}} \quad \text{volts} \qquad - \quad (4\text{-}78)$$

and,

$$I_F(T) = \frac{I_{meas}(T) \times \text{amplification factor}}{\text{S.F.} \times 0.0075} \quad \text{amperes} \qquad - \quad (4\text{-}79)$$

Using the initial value of the current and voltage, $R(0)_{total}$ and hence $R(0)_{rest}$ were calculated. A computer program was written which utilised equation (4-72) and these values to tabulate the temperature of the filament as a function of time.

4.7.4.2. Estimation of Pressure

The logarithmic output from the pressure gauge was generally employed. This output was 0.2 volts per decade of pressure and if the amplifier-'scope sensitivity is set at 0.2 volts.cm.$^{-1}$ the pressure displacement will be, in a logarithmic form, 1 decade.cm.$^{-1}$.

The displacement of the pressure trace was measured over the same time intervals as the current and voltage traces. Using these values of $P_{meas.}$, together with the background pressure, P_B and the scaling factor, a computer program was used to tabulate values of the pressure P_t and relative pressure ΔP_t ($= P_t - P_B$) as a function of time, t.

4.7.4.3. Calculation of the Desorption Rate

The desorption rate was shown to be given by the equation,

$$\left(-\frac{dn}{dt}\right)_t = \left(\frac{dn}{dt}\right)_{tm} \left(\frac{V.\ \dfrac{d(\Delta P_t)}{dt}}{S\Delta P_m} + \frac{\Delta P_t}{\Delta P_m} \right) \qquad - \quad (4\text{-}15)$$

It has been shown in previous sections how S (4.7.1.3), ΔP_t and P_m (4.7.4.2.) may be evaluated. From P_t as a function of time it is possible to estimate $d(\Delta P_t)/dt$ either by graphical means or by a process of curve fitting and differentiation. The latter method, using a computer, was chosen as it was considered to be more accurate.

All of the values on the right hand side of equation (4-15) are known and hence $(-dn/dt)_t$ can be tabulated as a function of time.

4.7.4.4. Calculation of Surface Coverage

The surface concentration at any time, n, was shown to be,

$$n = \int_o^{tz} \left(\frac{-dn}{dt}\right)_t .\ dt - \int_o^{t} \left(\frac{-dn}{dt}\right)_t .\ dt \qquad - \quad (4\text{-}18)$$

In the previous section the rate of desorption was obtained as a function of time. The analytical expression relating these two quantities was obtained using a polynomial curve fitting program and numerical integration of this was used to evaluate the value of n at various times during the desorption reaction.

4.7.4.5. The Experimental Rate Equation

It has been shown in section (4-5) that the rate equation over the entire desorption reaction can be written,

$$\left(-\frac{dn}{dt}\right) = n^x \frac{kT}{h}\ \bar{d}.\ \exp\left(\frac{\Delta S^{\ddagger}}{R}\right) \exp\left(-\frac{\Delta H^{\ddagger}}{RT}\right) \qquad - \quad (4\text{-}55)$$

Using data obtained in sections (4.7.4.1) to (4.7.4.4) and equations (4-61) and (4-62) the two remaining unknowns in this equation, $\Delta H^{\ddagger}$ and $\Delta S^{\ddagger}$ may be evaluated and the experimental rate equation written in the form above.

5.0. RESULTS OF THERMAL DESORPTION EXPERIMENTS

5.1. Experiments on the Thermal Desorption of Background Gases

Before carrying out any experiments on iodine or methyl iodide, experiments were carried out in a "clean" system. The experimental tbchniques were identical to those employed when the sample gas was present.

A thermal desorption photograph of the residual gases is shown in figure (5-1).This spectrum was obtained after repeated flashing of the filament to ensure a clean surface and then allowing the residual gases to adsorb for one hour.

It can be seen there is a general fise in pressure between the start and finish of the flash, and superimposed upon this is a desorption peak at approximately 2000°K. This peak is qualitatively similar to the β_2 peak observed in previous work.(67) The nature of the desorbing species is unknown, and there was no means of determining experimentally the nature of the species. The peak maximum moves to lower temperatures as the coverage increases, pointing to a second order desorption reaction.

In order to try to remove this residual gas contamination the vacuum system was baked out again for 48 hours, at the end of which, after cooling, the pressure dropped into the 10^{-12} torr range. During the bakeout the filaments were vigorously outgassed. The peak was, however, still found to be present and therefore it was decided to continue with the experiments and use the results in this section to eliminate, as far as possible, the effects of the background adsorption and desorption upon the adsorption and thermal desorption of iodine and methyl iodide.

A series of photographs were taken for various adsorption times to give some idea of the increase in size of this peak with time.

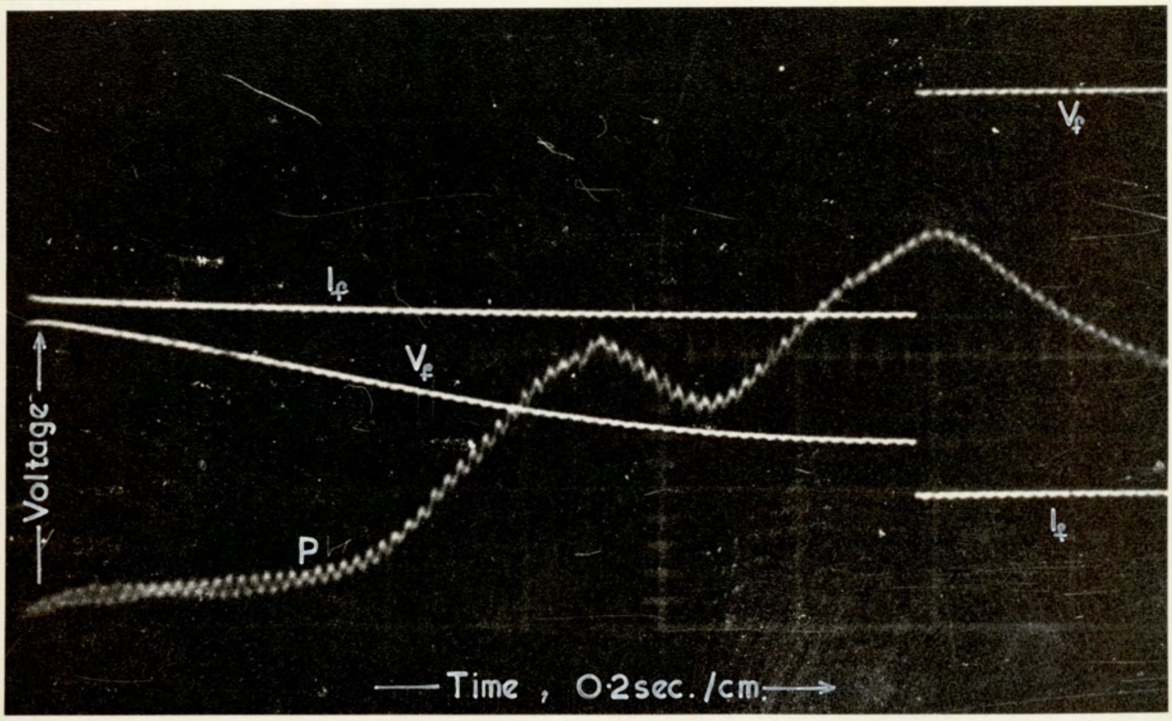

FIGURE (5-1) Thermal Desorption of Residual Gases

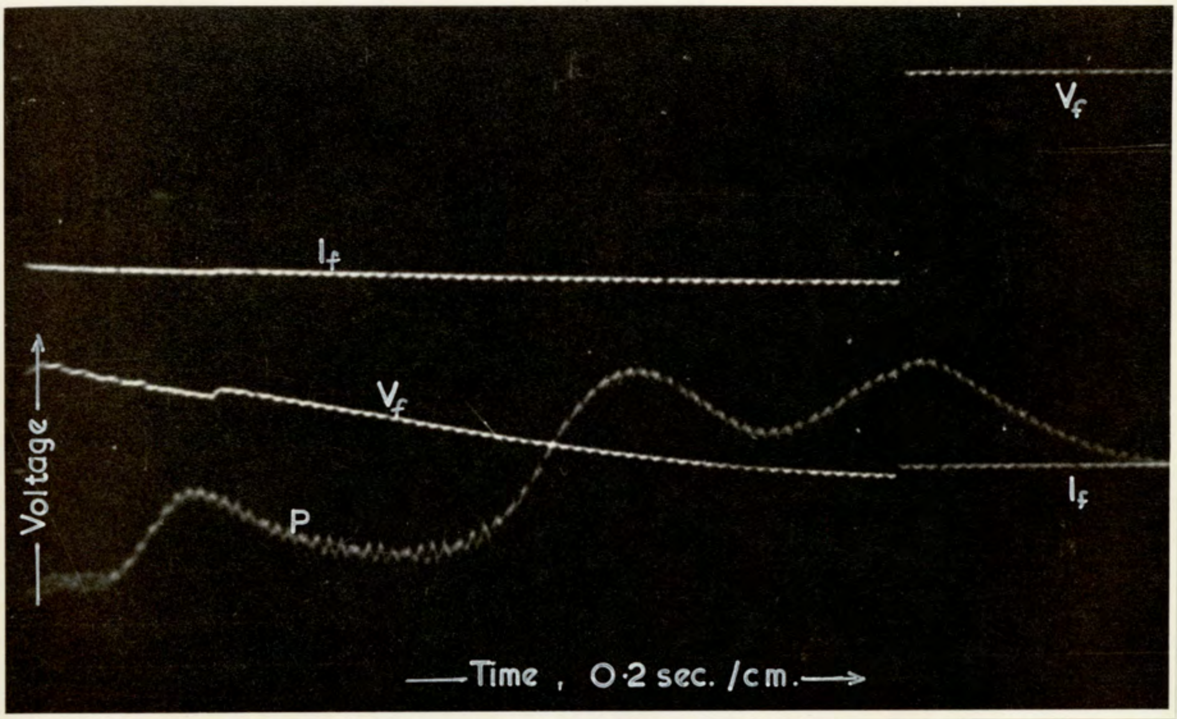

FIGURE (5-3) Thermal Desorption of Iodine

There appears to be only one peak, but because of the short filament used in this work and the subsequent importance of the temperature gradients at the ends of the filament, the pressure trace may encompass one or more desorption peaks.

It has been shown that the temperature variation along a filament is less during a flash than at steady state
It was not possible to determine the temperature along the filament during the flash but it was possible during the steady state operation of the filament. The temperature was measured with an optical pyrometer and the results corrected for emissivity and absorption. (60) The results obtained are shown in figure (5-2) It can be seen that the temperature is constant (± 10°K) over the middle 40% of the filament, but outside this range the temperature gradient is marked, approximately 30°K/mm. and over the end 1 - 2 mm. of the filament there is a large temperature gradient of approximately 1000°K/mm.

The temperature gradient during the flash will not be so great as this during the flash but the temperature gradient will still be a factor reducing the"resolution" of the thermal desorption apparatus.

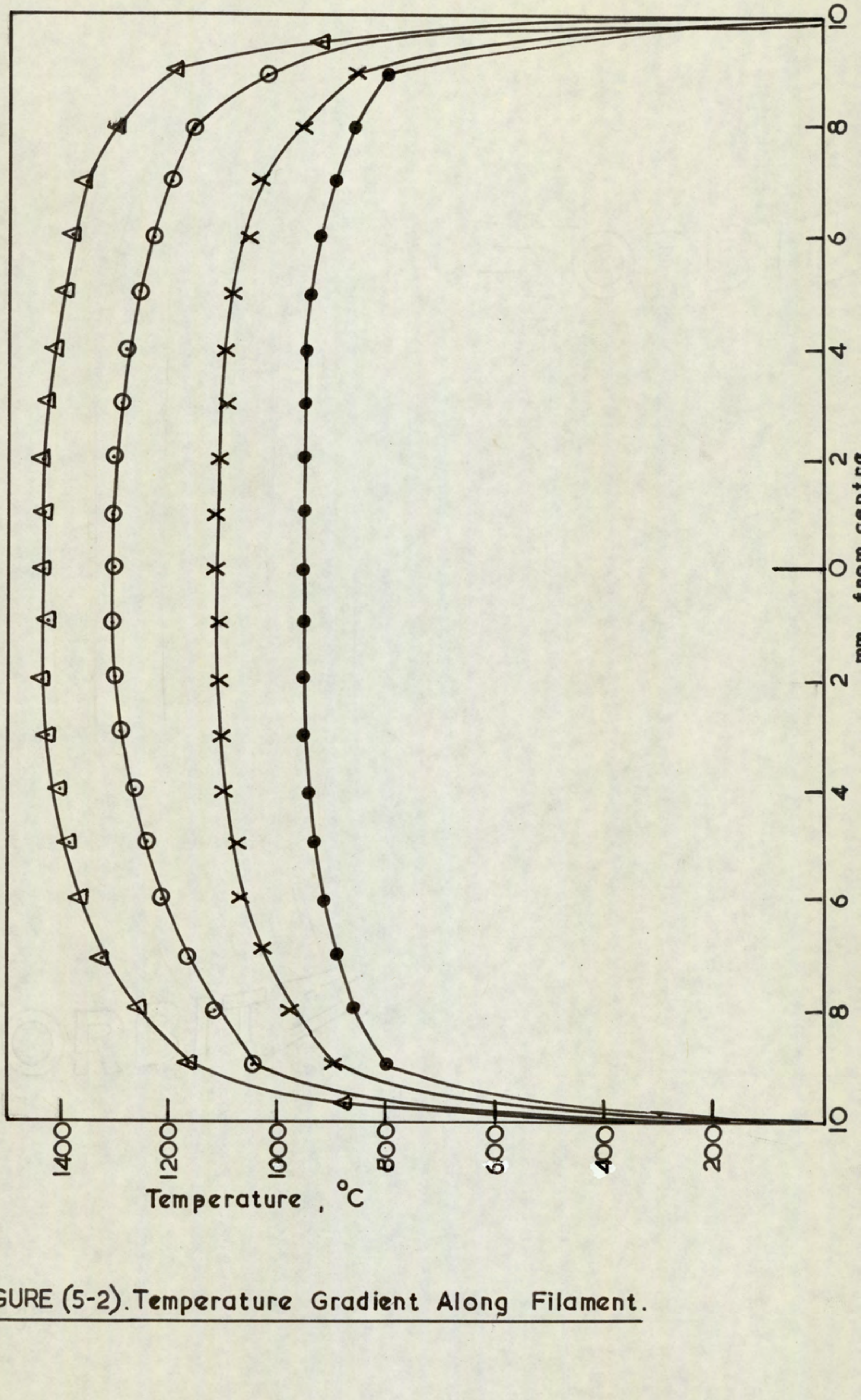

FIGURE (5-2). Temperature Gradient Along Filament.

5.2. Thermal Desorption of Iodine

In the previous section a single desorption peak with a maximum at about 1800 - 2000°K was observed. After the vacuum system had been saturated with iodine vapour for many hours the filament was flashed clean repeatedly and then the iodine was allowed to adsorb onto the filament at a pressure of 1 x 10^{-8} torr for one hour. The photograph is shown in figure (5-3)

It can be seen that the desorption trace now contains an additional peak with a maximum occuring at a temperature of approximately 700°K. The two peaks do not overlap to any great extent and therefore the analysis of the low temperature iodine peak should not present any difficulties due to this cause. A preliminary study of the desorption experiments showed:

(1) The temperature of the peak maximum of the iodine peak did not decrease with surface coverage and this points to a first order reaction.(18) The high temperature peak shows second order behaviour in this respect.

(2) The background peak grows much faster than the iodine peak. The background pressure was always in the range 1 - 3 x 10^{-10} torr whilst the iodine pressure was usually in the 10^{-8} torr pressure range. The sticking coefficient of iodine and the residual gases must therefore vary by several orders of magnitude.

(3) The whole of the spectrum is again superimposed on top of a general rise in pressure caused by desorption of gas from the filament supports and the rest of the cell. The mechanism could be by heat conduction, radiation or electron bombardment.

5.2.1. Quantitative Analysis of Iodine Desorption Data

Figure (5-4) shows the traces of two iodine desorption experiments, (18A3) and (18B6). Considering experiment (18B6) and using the methods previously outlined, the pressure and temperature can be obtained as a function of time and these results are shown in table (5-1). The background pressure for this experiment was 6.3×10^{-10} mm.Hg and a plot of ΔP against time is shown in figure (5-5). It can be seen that the iodine peak is superimposed on a gradual rise in pressure and also on the tail of the high temperature desorption peak, but by comparison with flash desorption pictures taken in the absence of iodine vapour the shape of the background is known and can be corrected for. The corrected trace of ΔP against time is shown in figure (5-6) together with the temperature-time relationship.

The temperature-time plot is almost linear in the range under study and follows the equation,

$$T = T_o + \beta t \qquad - \quad (5\text{-}1)$$

where $T_o = 290^\circ K$

$\beta = 1500^\circ K.sec.^{-1}$

t = time in seconds

The quantity $d(\Delta P)/dt$ was obtained by curve fitting and differentiating and the value of this as a function of time is shown in figure (5-7).

The pumping speed was obtained using equation (4-66) and was found to be 15 $l.sec.^{-1}$. Using these values, $(dn/dt)_t$ may be calculated as a function of time and this is shown in figure (5-8). The surface concentration was found by integration and this, together with the rate of desorption, is shown in table (5-2). The initial concentration, n_o, was estimated to be 7.7×10^{11} particles.cm.$^{-2}$.

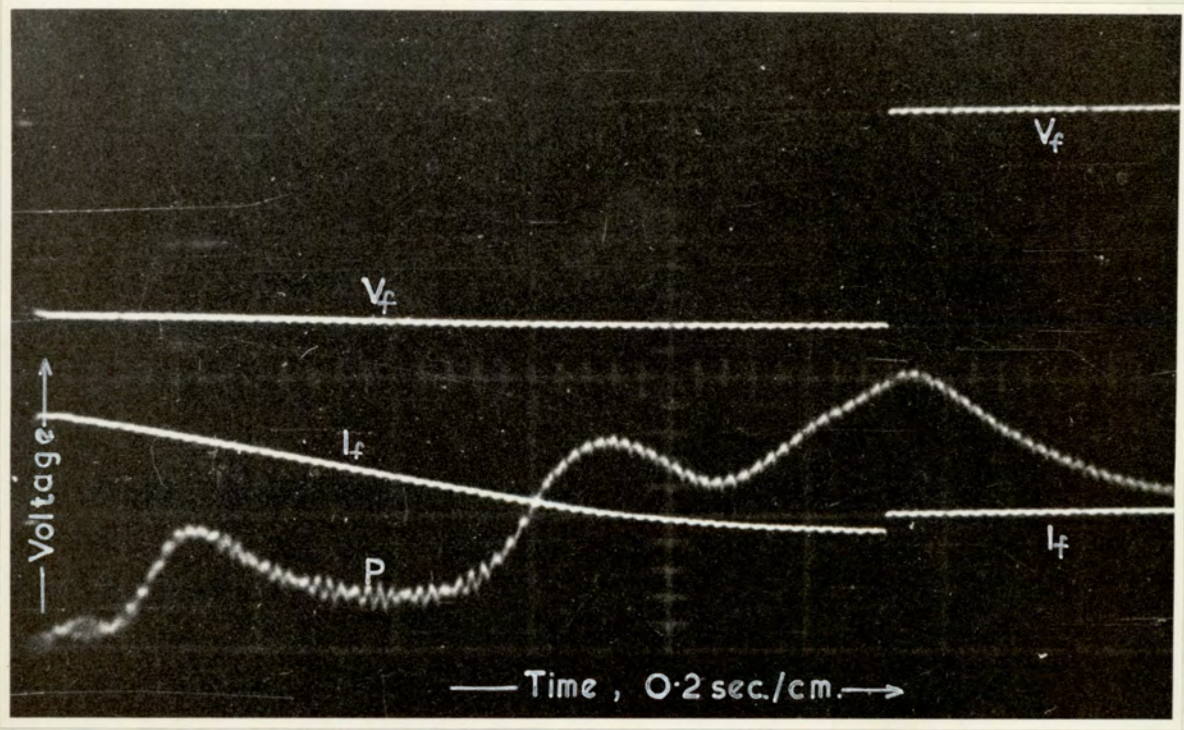

18A3

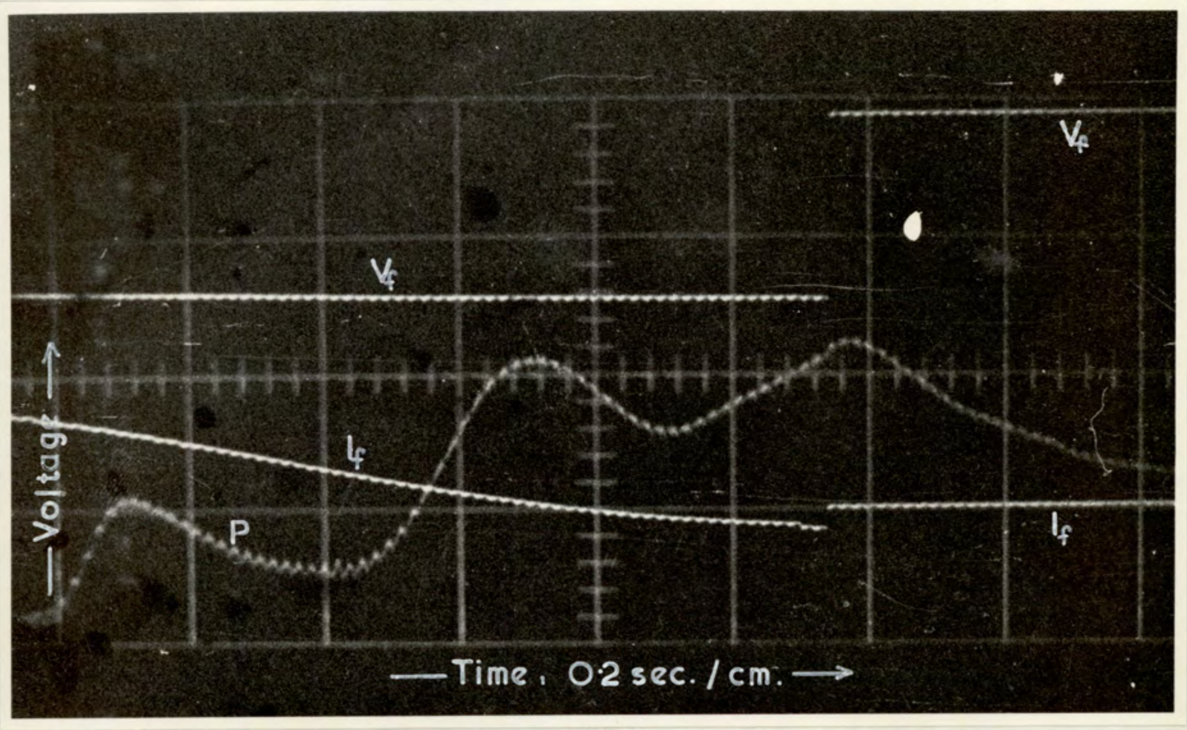

18B6

FIGURE (5-4). Iodine Thermal Desorption Experiments

TABLE (5-1)

EXPERIMENT 18B6 - EXPERIMENTAL AND CALCULATED DATA

Time, t (seconds)	$\Delta P \times 10^{10}$ (mm.Hg.)	$d(\Delta P/dt)_t \times 10^{+11}$ (mm.Hg.sec^{-1})
0.08	2.8	10.0
0.09	2.8	16.0
0.10	3.0	40.0
0.11	3.25	90.0
0.12	4.0	160.0
0.13	6.25	245.0
0.14	9.3	355.0
0.15	13.3	478.0
0.16	18.8	625.0
0.17	25.7	750.0
0.18	35.0	838.0
0.185	37.0	840.0
0.19	44.5	820.0
0.20	52.0	690.0
0.21	57.2	425.0
0.22	60.0	190.0
0.23	61.5	0.0
0.24	60.0	-13.0
0.25	57.5	-225.0
0.26	54.5	-275.0
0.27	50.5	-308.0
0.28	47.5	-326.0
0.29	42.3	-315.0
0.30	41.0	-300.0
0.31	38.8	-282.0
0.32	36.0	-275.0
0.33	33.1	-255.0
0.34	30.6	-245.0

TABLE (5-2)

EXPERIMENT 18B6 - EXPERIMENTAL AND CALCULATED DATA (CONTINUED)

Time, t (seconds	$(dn/dt)_t \times 10^{-11}$ (particles.sec^{-1})	Temperature, T (^oK)	Surface concentration $n \times 10^{-11}$ (particles.cm^{-2})
0.08	1.90	383	7.74
0.09	2.62	395	7.69
0.10	5.44	407	7.64
0.11	11.3	421	7.56
0.12	19.7	433	7.41
0.13	30.2	447	7.16
0.14	43.8	461	6.80
0.15	59.1	474	6.29
0.16	77.7	489	5.61
0.17	94.1	502	4.75
0.18	1o7.0	516	3.74
0.185	108.0	523	3.21
0.19	107.0	530	2.25
0.20	93.9	544	1.66
0.21	64.4	559	0.85
0.22	37.8	571	0.35
0.23	16.1	585	0.08
0.24	0.56	599	0.02
0.25	0.0	613	0.0
0.26	-	-	-

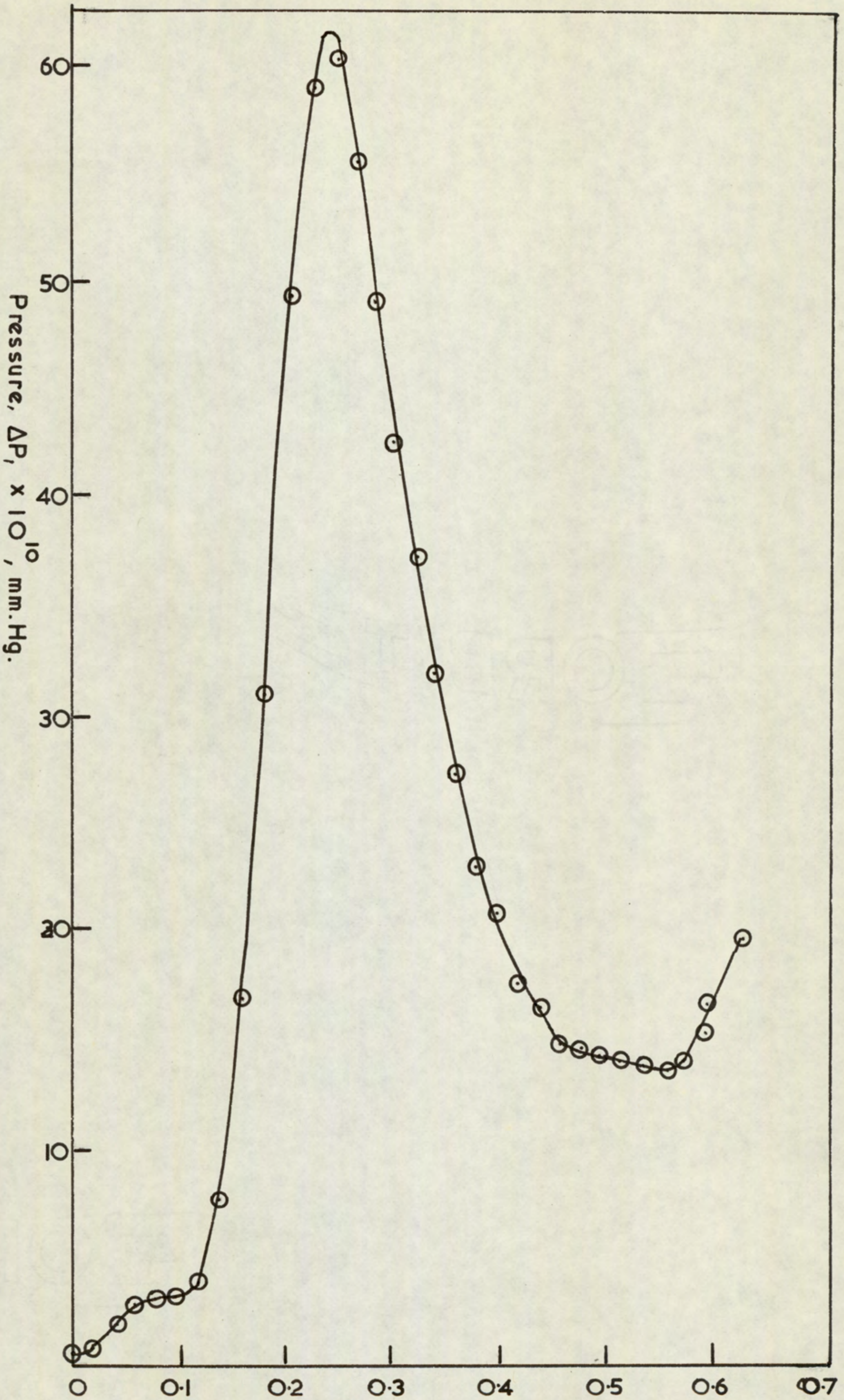

FIGURE (5-5). Experiment 18B6 Pressure-Time Curve

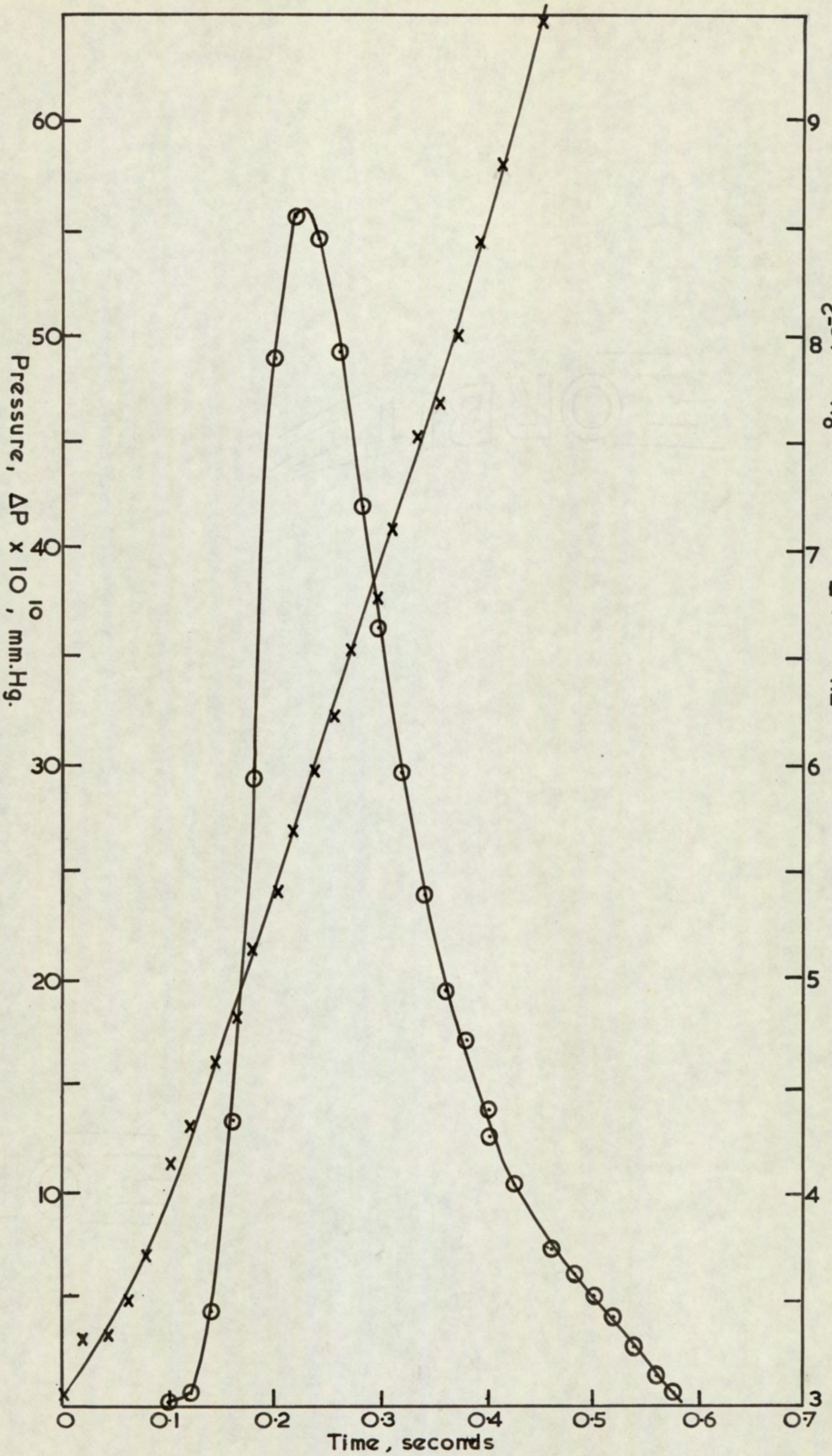

FIGURE (5-6) Experiment 18B6 Corrected Pressure & Temperature

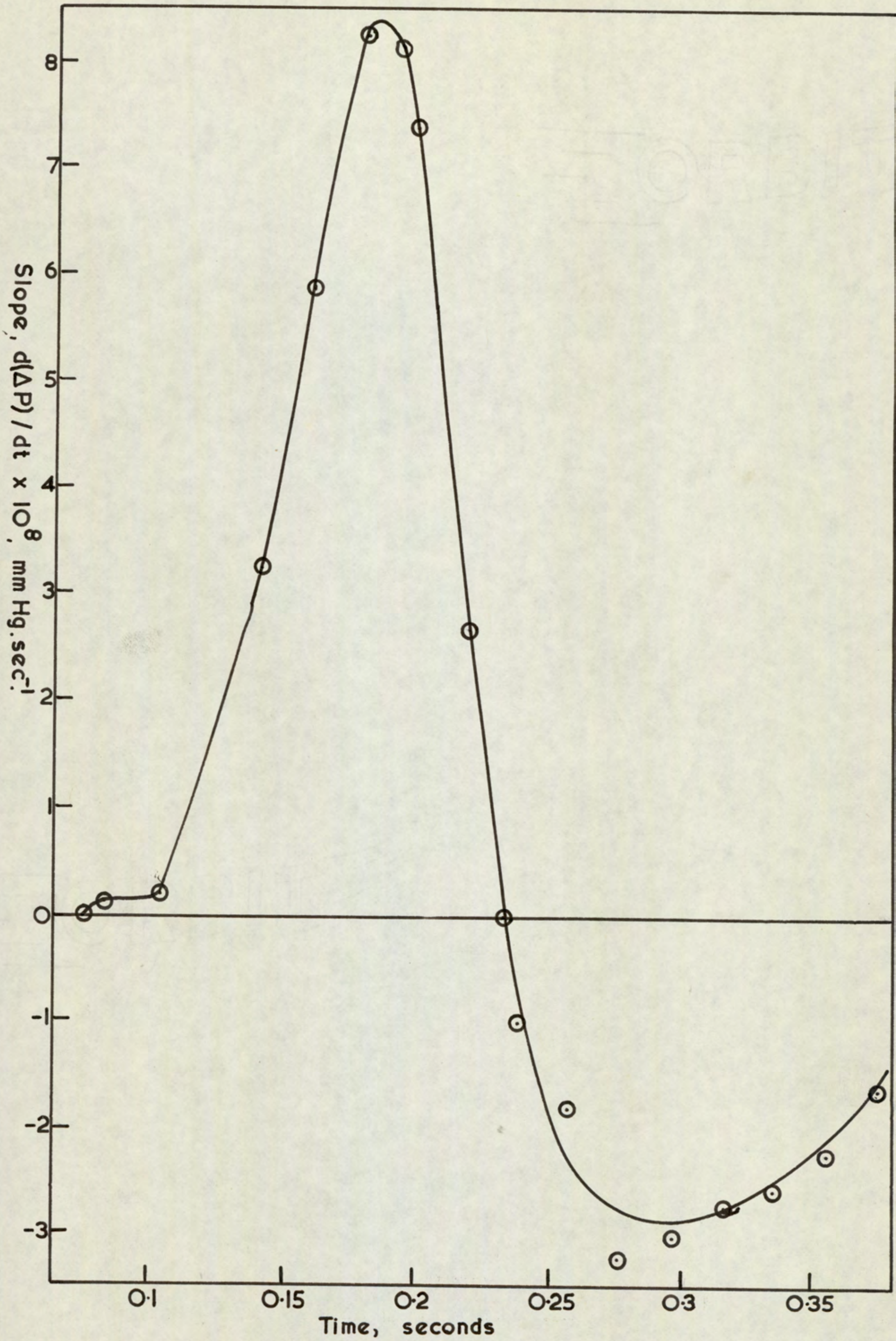

FIGURE (5-7). Experiment 18B6 d(ΔP)/ dt -Time Curve

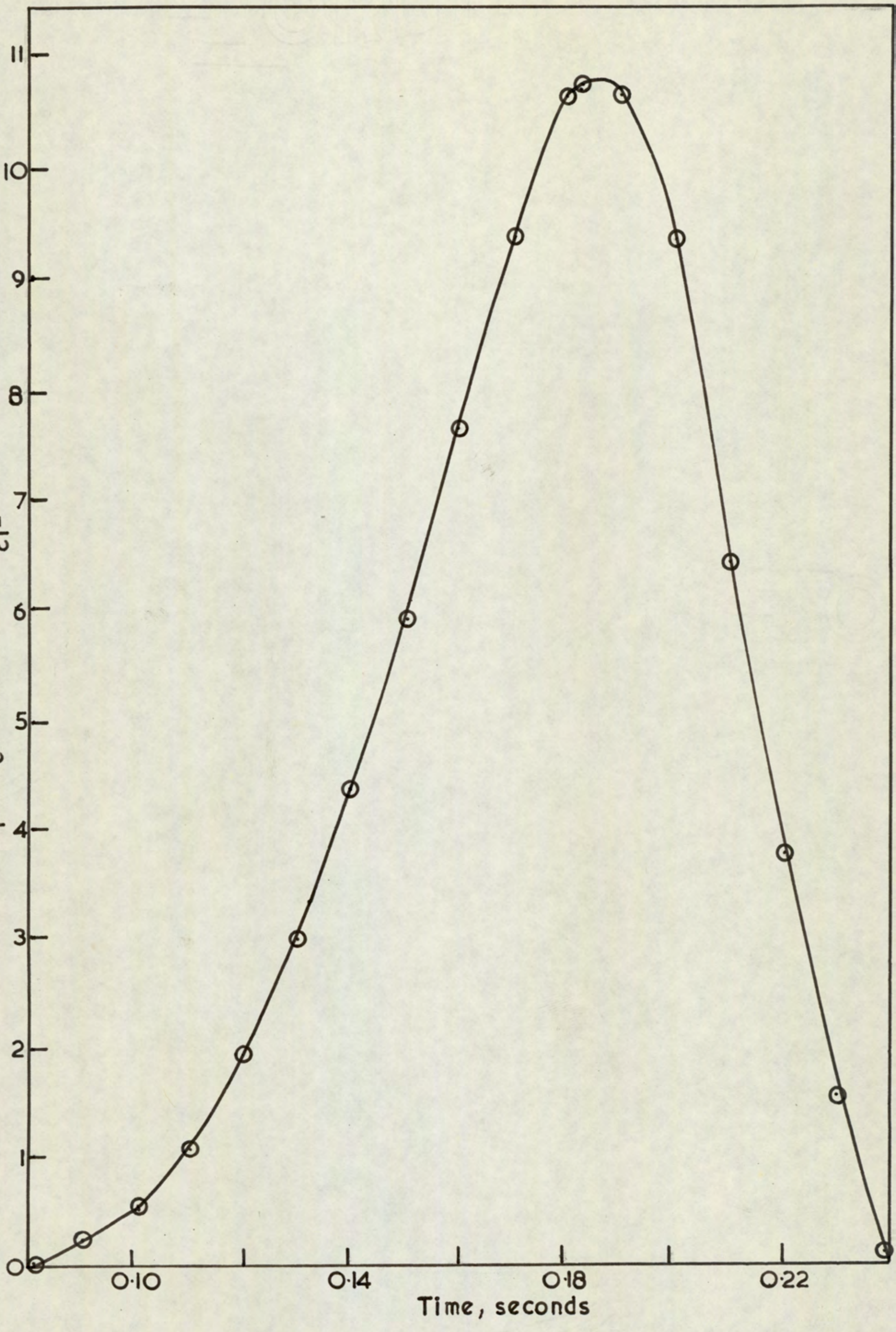

FIGURE (5-8). Experiment 18B6 Reaction Rate-Time Curve

5.2.2. Estimation of Thermodynamic Data from Iodine Desorption Experiments

The activation energy, enthalpy and entropy of activation were determined by the methods previously described.

A plot of $\ln\left(\frac{(-dn/dt)}{n^xT}\right)$ is shown in figure (5-9) for values of x of 1 and 2. It can clearly be seen that the plot for n = 1 is linear whilst that for n = 2 shows distinct curvature. The slope of the first order plot is $-\Delta H^{\ddagger}/R$.

From the graph,

$$\Delta H^{\ddagger} = -R\,.\,\frac{-2.303 \times 2}{0.00074} \qquad - \quad (5\text{-}2)$$

$$\therefore\ \Delta H^{\ddagger} = 52.2 \text{ KJ.mole}^{-1} \qquad - \quad (5\text{-}3)$$

Using equation (4-59) the activation energy can be estimated and was found to be 56.4 KJ.mole^{-1}.

The entropy of activation is calculated from equation (4-62) and was found to be -140 joule.deg.$^{-1}$mole^{-1}. The rate equation can then be written as below,

$$\left(\frac{-dn}{dt}\right)_t = n\,.\,\frac{kT}{h}\exp\left(\frac{-140}{R}\right).\ \exp\left(\frac{-52{,}200}{RT}\right) \qquad - \quad (5\text{-}4)$$

The fact that the reaction is first order is supported by the experimental observation that the temperature of the peak maximum of the desorption trace is independent of the initial surface coverage.

The activation energy may also be calculated using equation (4-31) and this gives a value of 54.2 KJ.mole^{-1}, in good agreement with that obtained graphically.

In this section it has been assumed that the average transmission coefficient, $\bar{d}$, in equation (4-55) is unity.

The experimental rate equation is of the form,

$$\left(\frac{-dn}{dt}\right) = n.\ A.\ \exp\left(-\frac{\Delta H^{\ddagger}}{RT}\right) \qquad - \quad (5\text{-}5)$$

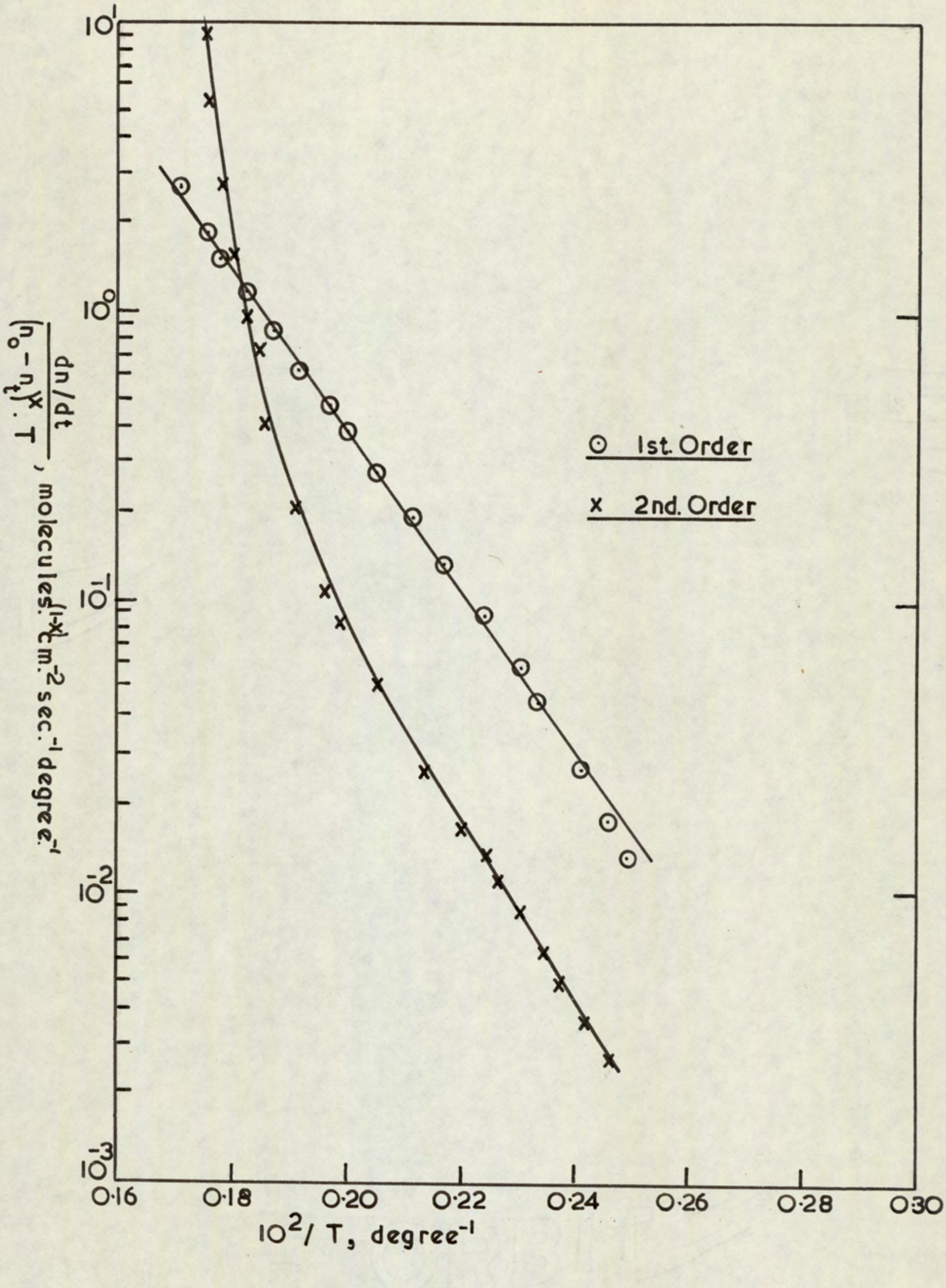

FIGURE (5-9) Experiment 18B6 - Order of Reaction Plot where A, the pre-exponential constant, is, by comparison with equation (4-55), given by,

$$A = \bar{d} \frac{kT}{h} \exp\left(\frac{\Delta S^{\ddagger}}{R}\right) \qquad - \quad (5\text{-}6)$$

Experimentally, $\bar{d}$ and $\Delta S^{\ddagger}$ cannot be separated, as,

$$\text{intercept (as } \frac{1}{T} \rightarrow 0) = \ln\bar{d} + \Delta S^{\ddagger}/R \qquad - \quad (5\text{-}7)$$

If $\bar{d}$ is not equal to unity, but constant, then only this last quantity $(\ln\bar{d} + \Delta S^{\ddagger}/R)$ may be obtained.

5.2.3. Summary of Iodine Flash Desorption Experiments

A similar analysis to that described in the previous sections has been carried out for other experiments in which the iodine was allowed to adsorb onto the filament for different lengths of time. In all of these experiments two peaks were observed, one of which could be attributed to iodine, the other, occurring at higher temperatures, to the adsorption of residual gases.

The experimental data is summarised in table (5-3), the derived data in table (5-4), whilst order of reaction plots are shown in figures (5-10) and (5-11). The first order plots always exhibit the greatest linearity, the second order plots showing distinct curvature over the whole temperature range.

The average value of the activation enthalpy found graphically was 47.2 (± 3.9) KJ.mole^{-1}, whilst calculations using equation (4-31) gave this quantity the value 42.5 (± 5.5) KJ.mole^{-1}.

This latter error is larger as this is derived from a single point determination and depends much more upon the absolute determination of the temperature than does the graphical method, an error of ± 3% in the temperature causing an error, because of the T^2 term, of ± 10% in the value of $\Delta H^{\ddagger}$.

TABLE (5-3)

Summary of Iodine Desorption Data

Expt. No.	Background Pressure, P_B $P_B \times 10^{10}$mm.Hg	Pressure Rise $\Delta P_m \times 10^{10}$mm.Hg	$T(\Delta P_m)$ ^oK
24-6	0.8	9.7	730
31-1	5.0	24.6	710
31-2	3.0	75.0	725
21-12	3.0	15.8	682
20-2	8.0	47.0	743
32.2	6.0	7.8	680
22-1	8.0	13.5	725
19-3	15.2	8.9	685
34-D-1	4.5	70.0	700
Average	-	-	710 P.E.=±20

TABLE (5-4)

Summary of Iodine Desorption Data

Expt. No.	$T_{\left(\frac{dn}{dt}\right)_{max}}$ °K	$n_o \times 10^{10}$ particles.cm.$^{-2}$	ΔH^{*} KJ.mole^{-1}	ΔS^{*} Joule deg.$^{-1}$mole^{-1}
24-6	592	12.8	51.0	159
31-1	575	33.2	47.7	159
31-2	595	9.6	54.3	151
21-12	558	28.2	42.0	172
20-2	580	68.5	50.2	167
32-2	550	16.7	38.0	188
22-1	630	28.0	-	-
19-3	555	16.4	42.5	161
34-D-1	590	97.5	52.2	145
Average	586 P.E.=18°K	-	47.2 P.E.=±3.9	163 P.E.=±8.7

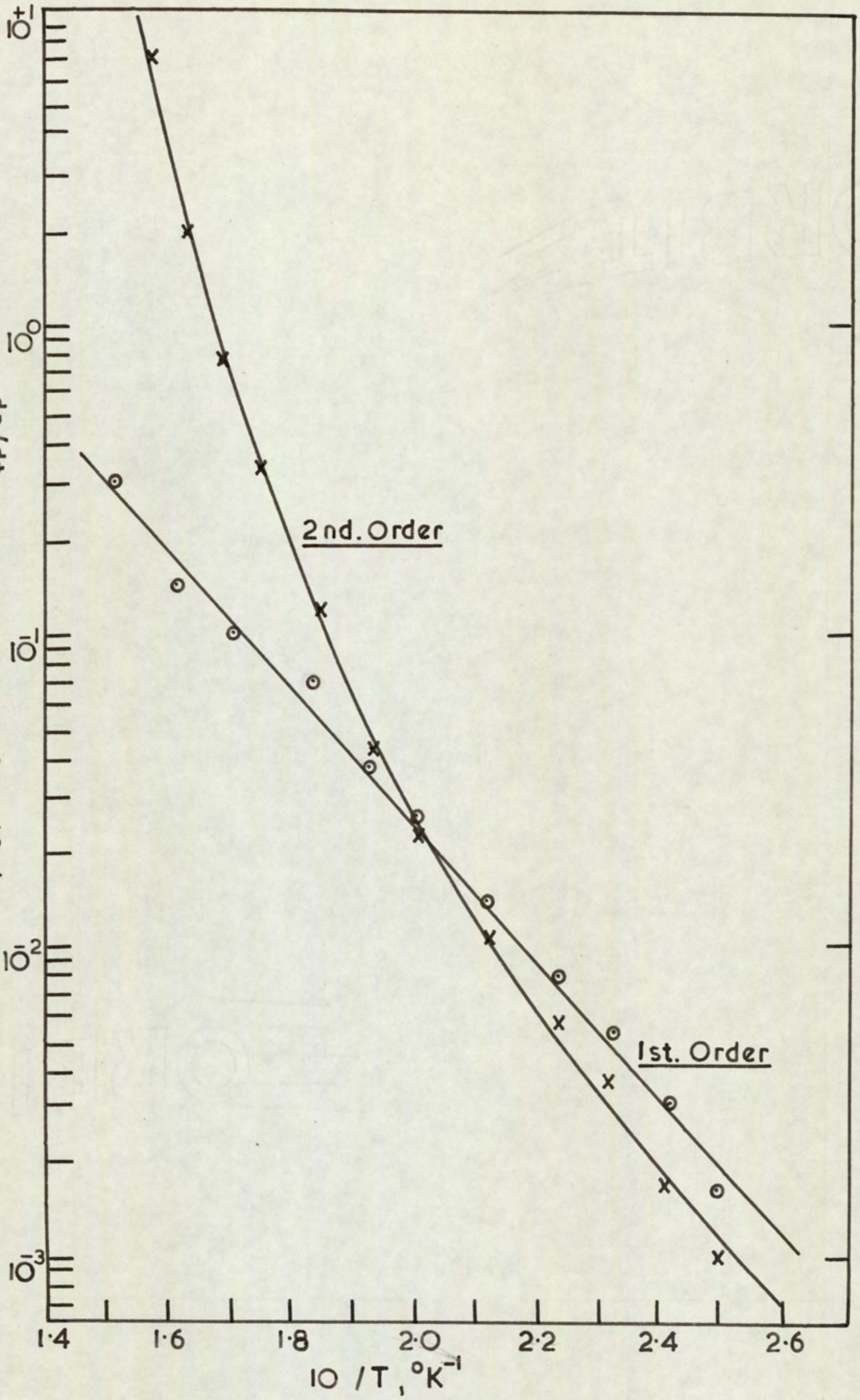

FIGURE (5-10) Experiment 19-3 Order of Reaction Plot

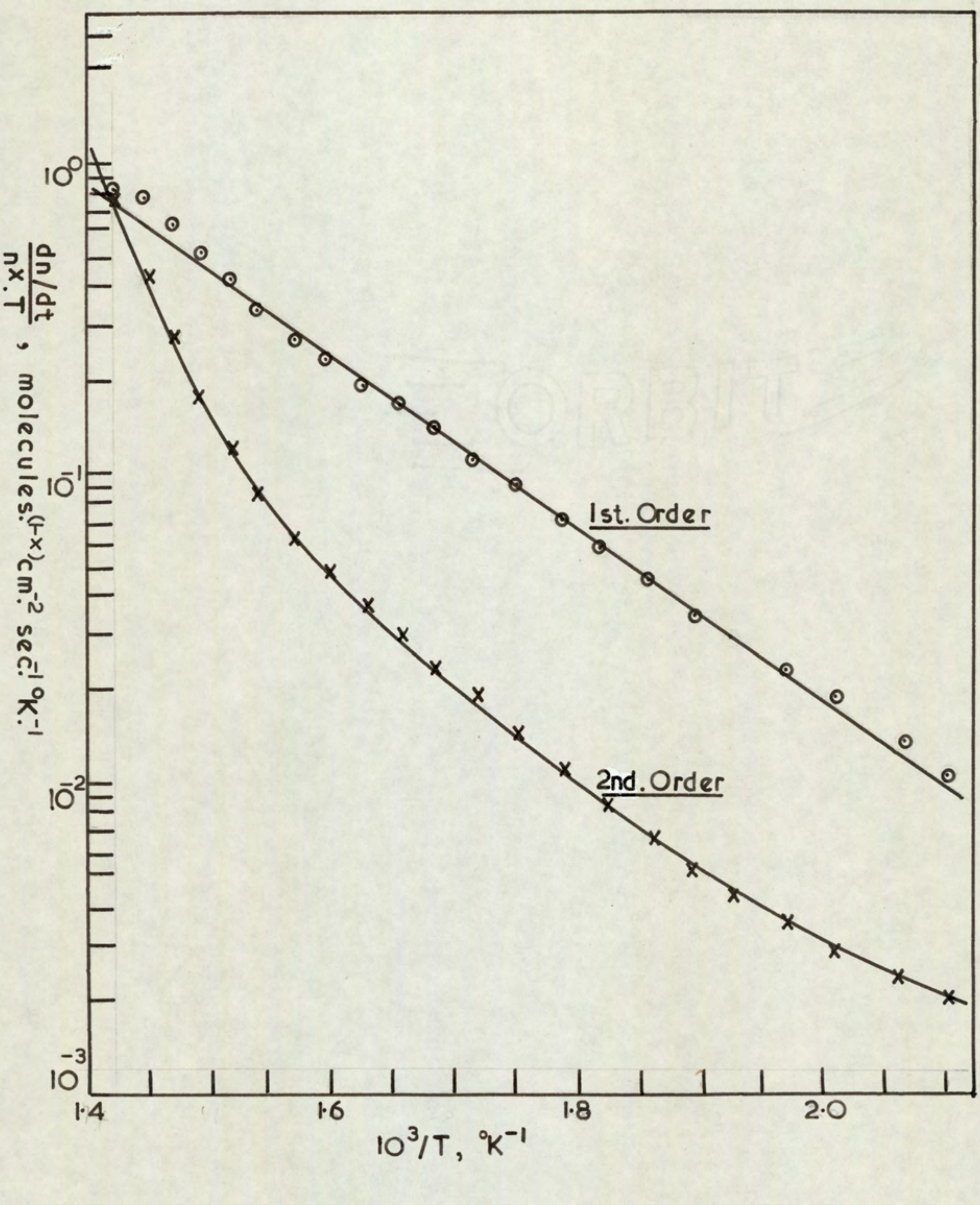

FIGURE (5-11). Experiment 20·2 -Order of Reaction Plot

5.2.4. Correlation of the Experimental Desorption Rate Equation with the Adsorption Rate Equation calculated from Kinetic Theory

The experimental desorption rate equation for molecular iodine is given by,

$$\left(-\frac{dn}{dt}\right)_{des.} = \frac{kT}{h} \, . \, n. \, \exp\left(-\frac{140}{R}\right) . \exp\left(-\frac{52,200}{RT}\right) \quad - \quad (5\text{-}8)$$

At room temperature (300°K) this can be simplified to,

$$\left(-\frac{dn}{dt}\right)_{des.} = 3.8 \times 10^{-3} . \, n \text{ molecules.cm.}^{-2}\text{sec.}^{-1} \quad - \quad (5\text{-}9)$$

The rate of adsorption, calculated from kinetic theory, assuming low coverage ($\theta \leqslant 0.1$) and non-activated adsorption, is given by,

$$\left(\frac{dn}{dt}\right)_{ads.} = \frac{s. \, P}{(2\pi mkT)^{\frac{1}{2}}} \quad - \quad (5\text{-}10)$$

and taking a typical pressure of 1×10^{-8} mm.Hg, the molecular weight, M, of iodine to be 254 a.m.u. and the sticking probability to be 0.4 (typically $\leqslant 0.4$ (1, 3)) then,

$$\left(\frac{dn}{dt}\right)_{ads.} = 5.0 \times 10^{11} \text{ molecules.cm.}^{-2}\text{sec.}^{-1} \quad - \quad (5\text{-}11)$$

When the equilibrium surface concentration of iodine, n_e, is reached,

$$\left(\frac{dn}{dt}\right)_{ads.} = \left(\frac{-dn}{dt}\right)_{des.}$$

Therefore, combining equations (5-9) and (5-11), n_e is found to be 1.3×10^{14} molecules.cm.$^{-2}$.

Using this data it is possible to calculate the rate of increase in surface concentration, (dn/dt), which will be given by,

$$\left(\frac{dn}{dt}\right) = \left(\frac{dn}{dt}\right)_{ads.} - \left(\frac{dn}{dt}\right)_{des.} \qquad - \quad (5\text{-}12)$$

Until n approaches n_e, the desorption rate is small compared to the adsorption rate, therefore if the adsorption rate is given correctly by kinetic theory, $(dn/dt) = 5.0 \times 10^{11}$ molecules.cm.$^{-2}$sec.$^{-1}$.

However, experimental values of n ranged up to $\sim 10^{12}$ molecules.cm.$^{-2}$ and as shown in figure (5-12) saturation of the surface with iodine molecules is reached at $\sim 10^{12}$ molecules.cm.$^{-2}$. However, the initial value of (dn/dt) was found to be 6×10^{8} molecules.cm.$^{-2}$sec.$^{-1}$, compared to 5.0×10^{11} above.

These discrepancies could be due to several causes, the most important of which are that the adsorption process may be activated or the sticking probability may be lower than expected.

If the process of adsorption is activated then it can be shown that the activation energy must be 12.2 KJ.mole^{-1}.

For a molecule to be permanently bonded to the surface it must lose, during its initial impact with the surface, an amount of energy exceeding its original thermal energy otherwise it will

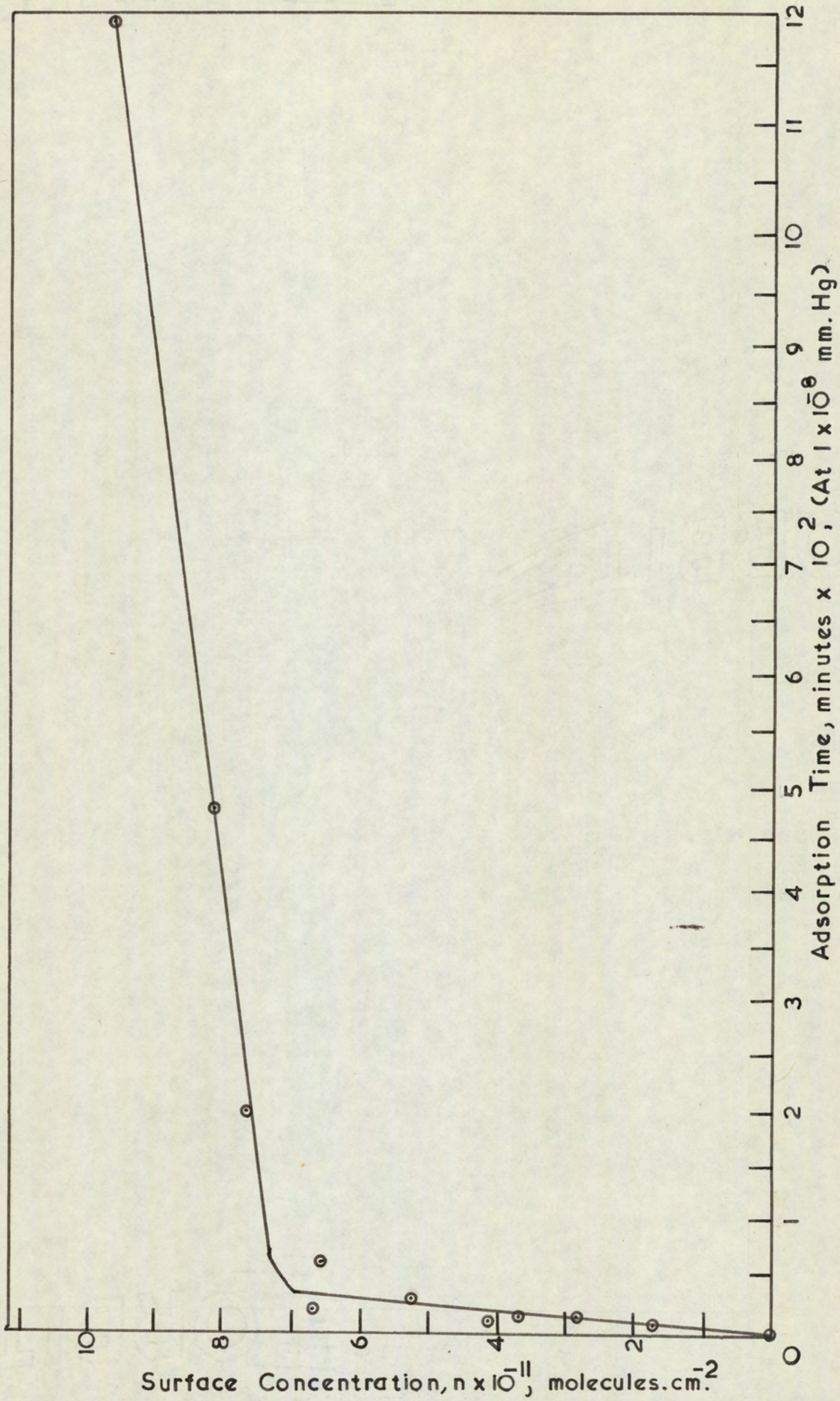

FIGURE (5-12) Surface Concentration as a Function of Adsorption Time desorb after one vibration. Energy transfer is found to be fairly efficient where the energy of interaction is high and collisions inelastic but is not so efficient at low interaction energies, such as those encountered for the I_2/Ta system and such an effect can result in a markedly lowered sticking probability.

5.2.5. Conclusions

The analysis of data obtained from photographs of the thermal desorption of iodine has yielded the following information:

(1) When iodine gas is allowed to adsorb onto a tantalum filament, the adsorbed species appears to exist in only one, low energy state which desorbs with a maximum rate at 600°K.

(2) The surface coverage was always found to be low for the conditions employed. The surface concentration was usually in the range 10^{10} - 10^{12} particles.cm.$^{-2}$ compared to the value of 10^{15} sites.cm.$^{-2}$ available to the adsorbing species.

(3) The desorption reaction was first order in the concentration of desorbing species.

(4) The enthalpy of activation was found to be 47.2 KJ.mole^{-1} and was independent of surface concentration.

(5) The entropy of activation was estimated to be -163 joule.deg.$^{-1}$mole^{-1}.

5.3. Thermal Desorption of Methyl Iodide

These experiments were carried out after the experiments on iodine so a thorough bakeout of the system was carried out to remove any iodine adsorbed on the walls of the vacuum system and the experimental cell. The bakeout was continued for 60 hours at a temperature of 240°C (Cu/Const. calibrated thermocouple) and during this time the ion pump was in continuous operation whilst the titanium sublimation pump and experimental filaments were outgassed rigorously for many hours.

After this preparation of the system, thermal desorption experiments were performed to determine the effects of residual gas adsorption. The primary objectives of these experiments were to ensure the complete removal of iodine from the system and to determine the presence of any other species that could affect the desorption trace due to methyl iodide.

5.3.1. Background Desorption prior to Methyl Iodide Experiments

The high temperature desorption peak which had been attributed, in section (5.1), to the desorption of residual gases, appeared to be much reduced in magnitude by the prolonged bakeout procedure adopted above in section (5.3). Figure (5-13) shows the desorption trace after 25 minutes residual gas adsorption. It can be seen that the high temperature peak shows up only as a shoulder on the pressure rise due to heating, by conduction or radiation, other parts of the experimental cell. The size of the shoulder did not grow appreciably for longer adsorption periods, for example one hour, and therefore this peak will not affect the low temperature desorption peak which will be seen to be present in the desorption of methyl iodide.

Flash desorption experiments were carried out for various residual gas adsorption times but the high temperature peak never approached the magnitude observed in the previous iodine desorption experiments. The iodine peak was barely detectable after long periods (up to 3 hours) of adsorption and this shows that the procedure adopted in section (5.3) was effective for the removal of residual gases.

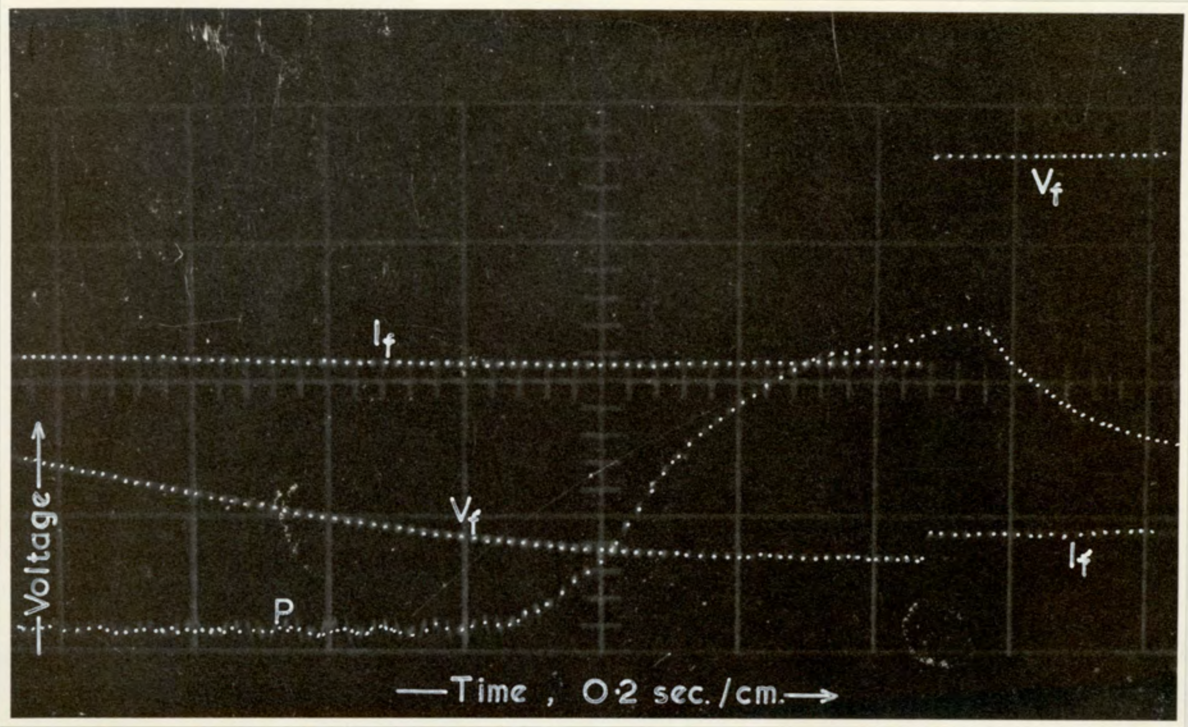

FIGURE (5-13) Thermal Desorption of Residual Gases

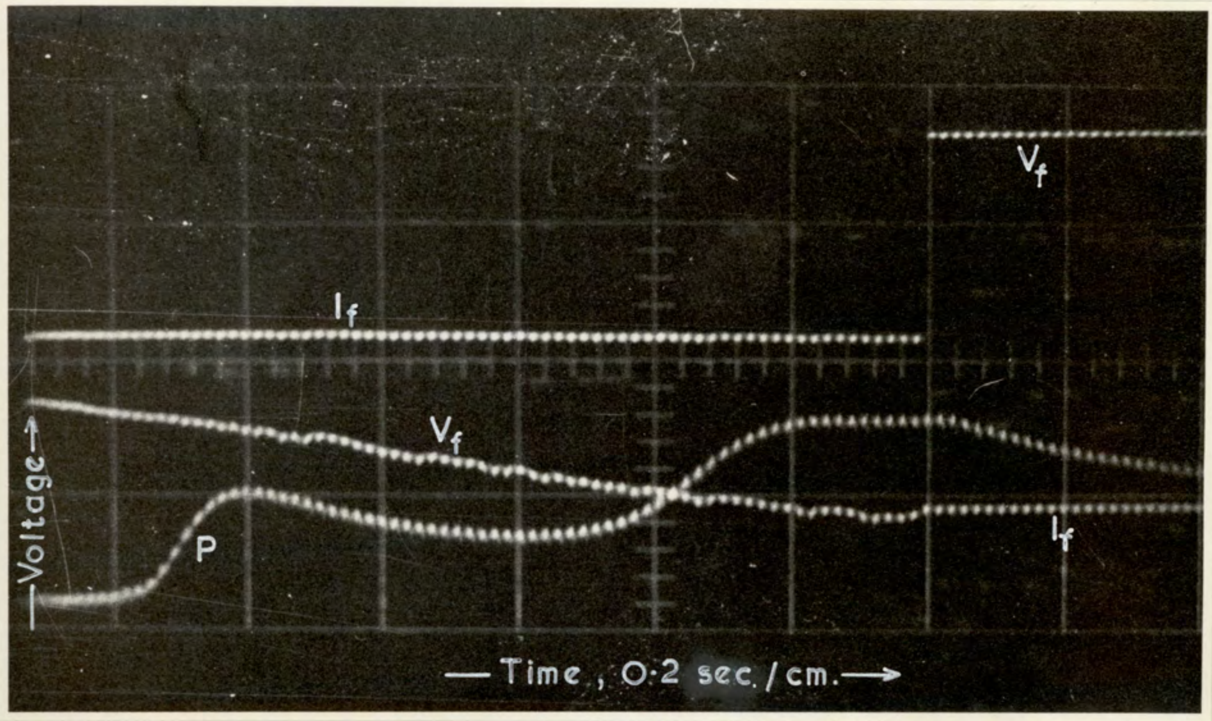

FIGURE (5-14) Thermal Desorption of Methyl Iodide

5.3.2. Quantitative Analysis of Methyl Iodide Desorption Data

Figure (5-14) shows a photograph of a methyl iodide desorption experiment. It can be seen that, as with the desorption of iodine, two peaks are discernable; a low temperature peak, attributed to the desorption of the adsorption products of methyl iodide and a high temperature peak, attributed to the desorption of residual gases and in this case perhaps, carbon residues from the adsorbed methyl group.

The data derived from the photograph of experiment (38-4) is shown in table (5-5). The background pressure for this experiment was 3×10^{-9} mm.Hg. A plot of the relative pressure, ΔP, as a function of time is shown in figure (5-15) and a plot of the low temperature desorption peak, corrected for background desorption, together with the temperature-time relation, is shown in figure (5-16).

For the pressure trace $d(\Delta P)/dt$ can be evaluated and using the values for ΔP_m (1.35×10^{-8} mm.Hg) the volume of the system (3.56 l.) and the pumping speed (29.0 l.sec.$^{-1}$) the desorption rate, and hence the surface concentration may be calculated for various intervals over the desorption peak. This data is shown in table (5-6) and figures (5-17) and (5-18). The initial surface concentration was found to be 3.1×10^{12} molecules.cm.$^{-2}$.

5.3.3. Estimation of Thermodynamic Data from Methyl Iodide Desorption Results

The activation enthalpy was determined from the plot of $\ln\left(\frac{(dn/dt)}{n^{x}T}\right)$ against $1/T$ shown in figure (5-19). The curve for $x = 1$ can be seen to be linear and from the slope of this curve the activation enthalpy was found to be 38.8 KJ.mole^{-1}.

Using this value, together with equation (4-59), the activation energy was found to be 43.5 KJ.mole^{-1} and together with equation (4-62) gave the value of -180 joule.deg.$^{-1}$mole^{-1} for the entropy of activation.

TABLE (5-5)

Experiment 38/4 - Experimental Data

Time, seconds	Pressure x 10^9, mm.Hg	Temperature, ^oK
0.00	3.0	305
0.02	3.0	309
0.04	3.0	333
0.06	3.0	346
0.08	3.0	377
0.10	3.0	414
0.12	3.1	447
0.16	3.3	492
0.20	4.4	534
0.22	7.5	558
0.24	10.1	586
0.26	13.1	607
0.28	16.0	636
0.30	16.8	665
0.32	17.3	705
0.36	16.6	784
0.38	15.6	825
0.40	14.4	856
0.44	12.7	932
0.48	11.2	1013
0.52	10.2	1097
0.56	9.4	1187
0.60	8.7	1256
0.64	8.3	1326
0.68	7.8	1421
0.72	7.6	1531
0.76	7.8	1581

TABLE (5-6)

Experiment 38/4 - Experimental and Calculated Data

Time, seconds	$d(\Delta P)/dt$, $mm.Hg.sec.^{-1}$	$dn/dt \times 10^{-12}$, $molecules.cm.^{-2}sec.^{-1}$	$n \times 10^{-11}$, $molecules.cm.^{-2}$	T, °K
0.10	0.0	0.0	31.0	426
0.12	2.8	0.56	30.9	452
0.14	3.3	1.18	30.7	475
0.16	7.7	2.03	30.4	500
0.18	13.3	11.4	29.1	525
0.20	90.0	17.2	26.2	555
0.22	113.8	21.3	22.3	582
0.24	137.3	27.9	17.3	610
0.26	160.8	22.6	12.3	640
0.28	87.8	17.8	8.3	673
0.30	44.0	13.9	5.1	708
0.32	10.0	9.4	2.8	745
0.34	-30.0	5.7	1.3	782
0.36	-55.9	3.0	0.8	820
0.38	-60.3	1.5	0.4	857
0.40	-50.7	0.5	0.05	845
0.42	-37.0	0.0	0.0	895

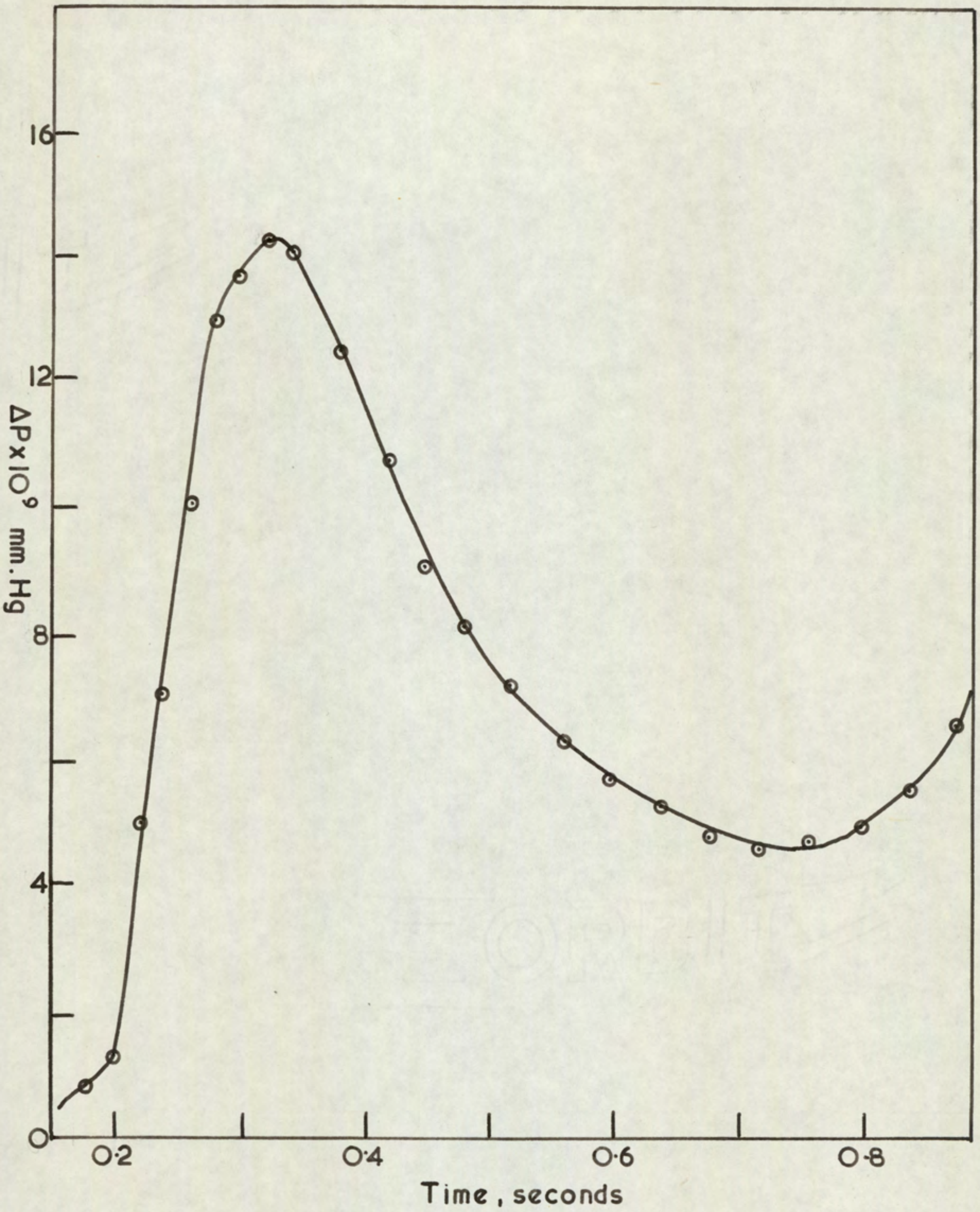

FIGURE (5-15). Experiment 38-4 Pressure-Time Curve

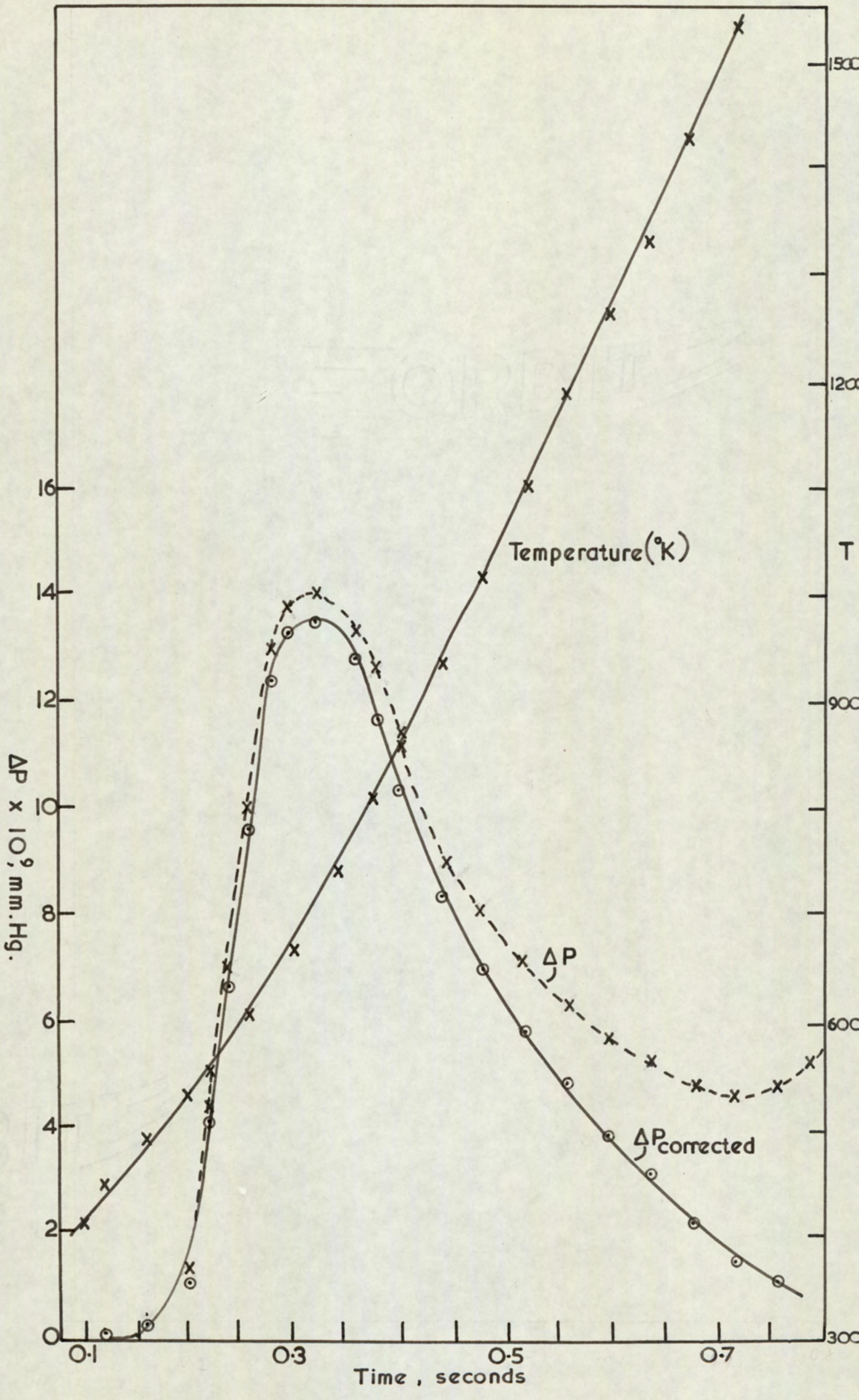

FIGURE (5-16) Experiment 38-4. ΔP and Temperature-Time Curves

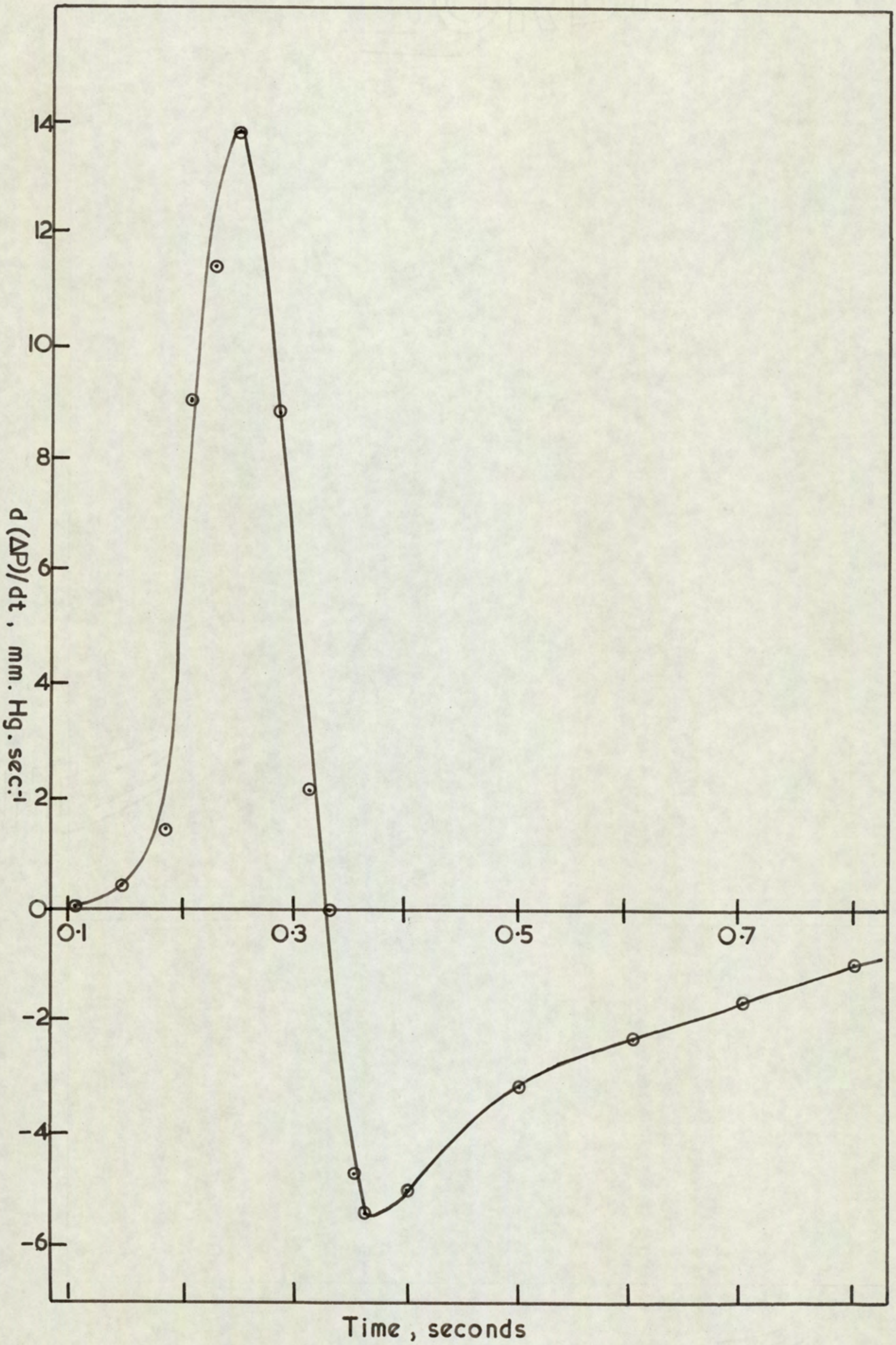

FIGURE (5-17). Experiment 38-4 d(ΔP)/dt – Time Curve

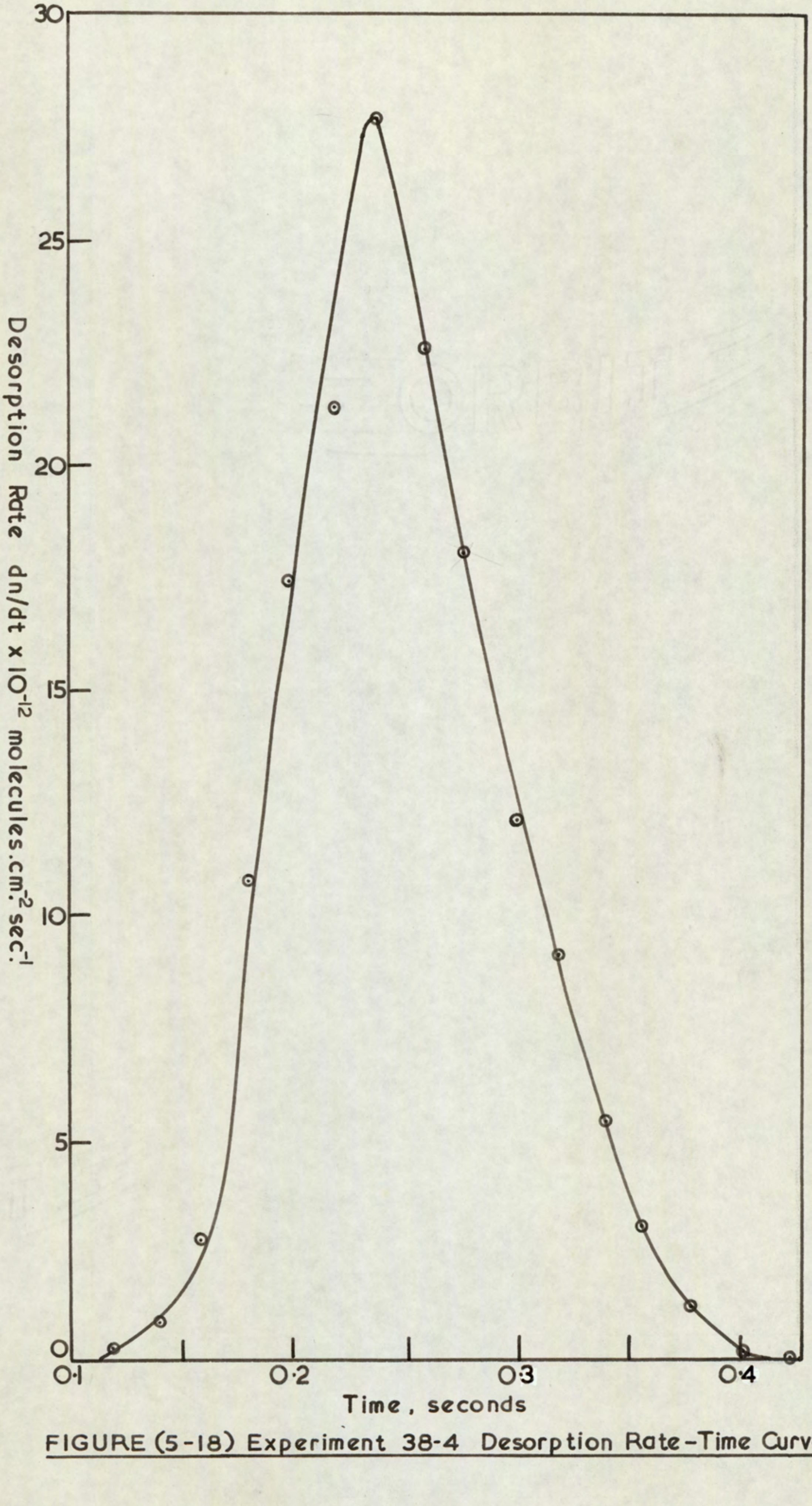

FIGURE (5-18) Experiment 38-4 Desorption Rate-Time Curve

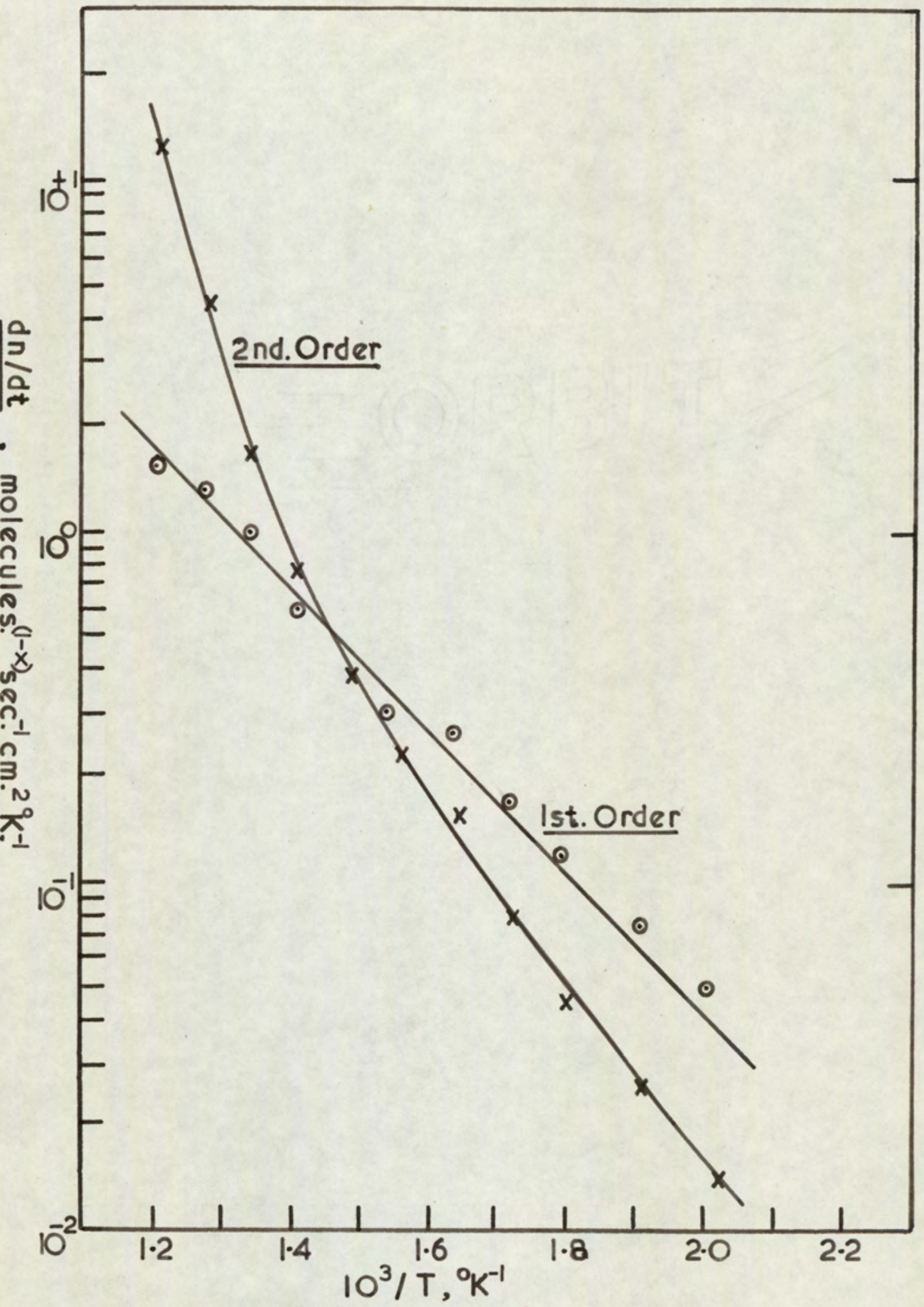

FIGURE (5-19). Experiment 38-4. Order of Reaction Plot

5.3.4. Summary of Methyl Iodide Desorption Data

The desorption traces of several other experiments were analysed in a similar way to that above and the important data is collected in table (5-7) where the average values are compared to the values found for the iodine desorption experiments. It can be seen that there is good agreement between all the important parameters, the temperatures at which the pressure and desorption rate are a maximum and the activation enthalpy and entropy.

TABLE (5-7)

Methyl Iodide Desorption Data

Expt. No.	$^{T}(P_m)$ ^oK	$^{T}\left(\frac{dn}{dt}\right)_{max}$ ^oK	$n_o \times 10^{-10}$ particles.cm.$^{-2}$	ΔH KJ.mole^{-1}	ΔS joule.deg.$^{-1}$mole^{-1}
38-4	725	565	310	38.8	180
38-1	690	590	12.8	49.2	160
37-8	702	580	26.0	52.5	152
Av'ge	705±10	579±7	-	46.8±3.4	164±8
Av'ge I_2 des.	710	586	-	47.2	163

5.3.5. Conclusions

The following conclusions can be drawn from an analysis of the thermal desorption of the residues after the adsorption of methyl iodide onto a tantalum filament;

(1) The thermal desorption pattern obtained after the adsorption of methyl iodide onto the tantalum filament closely resembled that obtained after the adsorption of iodine.

(2) A quantitative analysis of the low temperature desorption peak showed that the reaction was first order and occurred with an activation enthalpy of 46.8 (± 3.4) KJ.mole^{-1} and an activation entropy of -164 (± 8.2) joule.deg.$^{-1}$mole^{-1}.

(3) The pressure and desorption rate maximum occurred at the same temperature for both iodine and methyl iodide.

(4) The same species is desorbing in both the iodine and methyl iodide desorption experiments.

(5) No desorption peak which could be attributed to the desorption of the methyl radical, or any decomposition products of this, were observed. On adsorption it is most probable that fission of the carbon-iodine bond occurs. The methyl radical, together with a hydrogen atom, have been shown to be the initial adsorption products of methane on various metals (78,79,80) but the further decomposition of the methyl radical is slow (78,81).

The thermal desorption and decomposition of the methyl radical has also been studied but there is lack of agreement as to its fate. It has been reported to desorb with decomposition at 665°K (78) but other workers (82) have found that decomposition does not occur until 1200°K.

The low temperature peak found in the methyl iodide desorption experiments is identical in all respects to the iodine desorption peak and therefore it seems that the desorption of the methyl residue does not occur until higher temperatures where it may not be discernable from the background desorption.

6.0. DISCUSSION OF THERMAL DESORPTION RESULTS

6.1. The Applicability of Absolute Rate Theory to Desorption Reactions

The absolute reaction rate theory, using the methods of statistical mechanics predicts that the rate of a reaction will be given by

$$\left(-\frac{dn}{dt}\right) = (n_o - n_t)^x \, \bar{d} \, \frac{kT}{h} \cdot \frac{F^{\ddagger}}{F_{initial}} \cdot \exp\left(\frac{-E_o}{RT}\right) \qquad - \text{(6-1)}$$

Where $F_{initial}$ is the partition function of the adsorbed species and $F^{\ddagger}$ is the partition function of the activated complex (except that for translation along the reaction coordinate).

An alternative form of the rate equation, from which the experimental entropy and enthalpy were estimated is,

$$\left(-\frac{dn}{dt}\right) = (n_o - n_t)^x \, \bar{d} \, \frac{kT}{h} \exp\left(\frac{\Delta S^{\ddagger}}{R}\right) \exp\left(\frac{-\Delta H^{\ddagger}}{RT}\right) \qquad - \text{(4-55)}$$

where these two equations are related by the Sackur—Tetrode equation

$$(S_2 - S_1) = \Delta S = R \ln\left(\frac{F_2}{F_1}\right) \qquad - \text{(6-2)}$$

Equation (6-1) above was derived from a very general expression in order to obtain a form suitable for comparison with experimental rate parameters and was obtained at the expense of a number of assumptions.

The three main assumptions are,(26)

(1) There is equilibrium distribution of momentum of the reactants.

(2) The existence of a special partition function $F^{\ddagger}$ corresponding to the activated complex.

(3) The existence of an average transmission coefficient, $\bar{d}$.

Assumption (1) is fully justified if $E_A \geqslant 10RT$. In these experiments $RT = 5.0$ KJ.mole^{-1} compared with the activation energy of 52.2 KJ.mole^{-1}.

Assumption (2) may be considered as the definition of the activated complex. In the case of desorption the complex might be made up of atoms both of the adsorbate and substrate.

The activated complex for adsorption and desorption will be very similar and is generally assumed to be an immobile molecule attached to the surface. If the adsorbed film is also immobile the entropy of activation is numerically small as there is little difference between the initial and activated states and if the ratio $F^{\ddagger}/F_{initial}$ derived from rate measurements departs from unity by greater than $10^3 - 10^4$ then the required size of the activated complex may be unreasonable.

If the adsorbed film is mobile, however, $F^{\ddagger}/F_{initial}$ may depart widely from unity.

Assumption (3) is more difficult to appraise as defined in the classical limit $\bar{d}$ cannot, in general, be a constant but should be dependent upon the temperature as its value is affected by the interchange of translational and vibrational energy.

The experimentally determined frequency factor, A, is given by equation (5-7). This can be written in alternative form,

$$A = \bar{d} . \frac{kT}{h} . F^{\ddagger}/F_{initial} \qquad - \quad (6\text{-}3)$$

and if $A \ll (kT/h) \approx 10^{13}$, as found for these experiments then the reaction is called slow. If $\bar{d}$ is assumed to be constant and equal to unity the slowness of the reaction can be attributed to the small value of $F^{\ddagger}/F_{initial}$ which by equation (6-2) is equivalent to a large negative activation entropy.

6.2. The Activation Enthalpy

In section (5.2.4) it was concluded that the desorption reaction of iodine from a tantalum filament occurred by a first order process.

Likely rate controlling processes could be;

(1) The desorption of iodine atoms from an atomic film.

(2) The desorption of iodine molecules from a molecular film.

(3) The desorption of iodine molecules from an atomic film where the rate controlling step is not the formation of the molecular bond.

To decide which of these processes is most likely the energetics of the $I_2/I/Ta$ system must be studied more closely. The $I_2/I/W$ system has been studied by McCarroll who looked at the adsorption of iodine and the desorption of atomic and molecular iodine (65). Using known data for oxygen and iodine and a knowledge of the flash desorption behaviour of oxygen he showed that iodine could exist, undissociated on the surface of a metal up to 680°K. In these experiments the adsorption temperature was 300°K and the desorption reaction was essentially complete by 650°K, therefore the desorption of molecules from a molecular film must be considered further. If this were the mechanism desorption of molecules would cease around 700°K as above this temperature conversion to atoms would deplete the molecular film. The rate of depletion of molecules could then be written,

$$\frac{-d[I_2 \text{ surface}]}{dt} = \frac{d[I]}{dt} + \frac{d[I_2 \text{ gas}]}{dt} \qquad - (6\text{-}4)$$

It will be assumed that during the course of the desorption reaction in the range 400 - 650°K the molecular and atomic populations do not change.

McCarroll also noted the presence of an atomic film which desorbed at 1495°K, but in the experiments with I_2/Ta background desorption occurred at this temperature and no peak due to iodine atom desorption could be resolved. This does not preclude such an atomic bonding state which does seem most probable as it has been observed for other metals.

The binding energies of the different states involved in the Tantalum-Iodine system are best discussed by the use of a potential energy diagram. It is suggested that there are two possible binding states between iodine and tantalum, one in which the iodine molecule bond remains intact and the other in which this bond is broken and atomic adsorption occurs. The molecular state is the precursor to the atomic state. The potential energy diagrams are shown in figure (6-1) where the following symbols are used:

D_{I_2} = dissociation energy of the iodine bond.

D_{Ta-I} = dissociation energy of the surface bond.

Q_m = heat of adsorption of molecular iodine.

Q_A = heat of adsorption of atomic iodine.

E_m = molecular desorption energy.

E_A = atomic desorption energy.

Of these quantities only the dissociation energy of the iodine molecule in the gas phase is known accurately, but estimates can be made of some of the other quantities. Several attempts have been made to calculate heats of chemisorption (83,84). Much of the data for the adsorption of gases on metals (surface potentials, magnetic data, conductivity data and patterns of activity (1)) points to the formation of a covalent bond and using this assumption, together with the method of Eley (83) modified by Stevenson (84), the heat of adsorption of an iodine atom on tantalum has been calculated from the reaction,

$$2Ta_{(S)} + I_{2(g)} \longrightarrow 2TaI_{(S)} \qquad - (6\text{-}5)$$

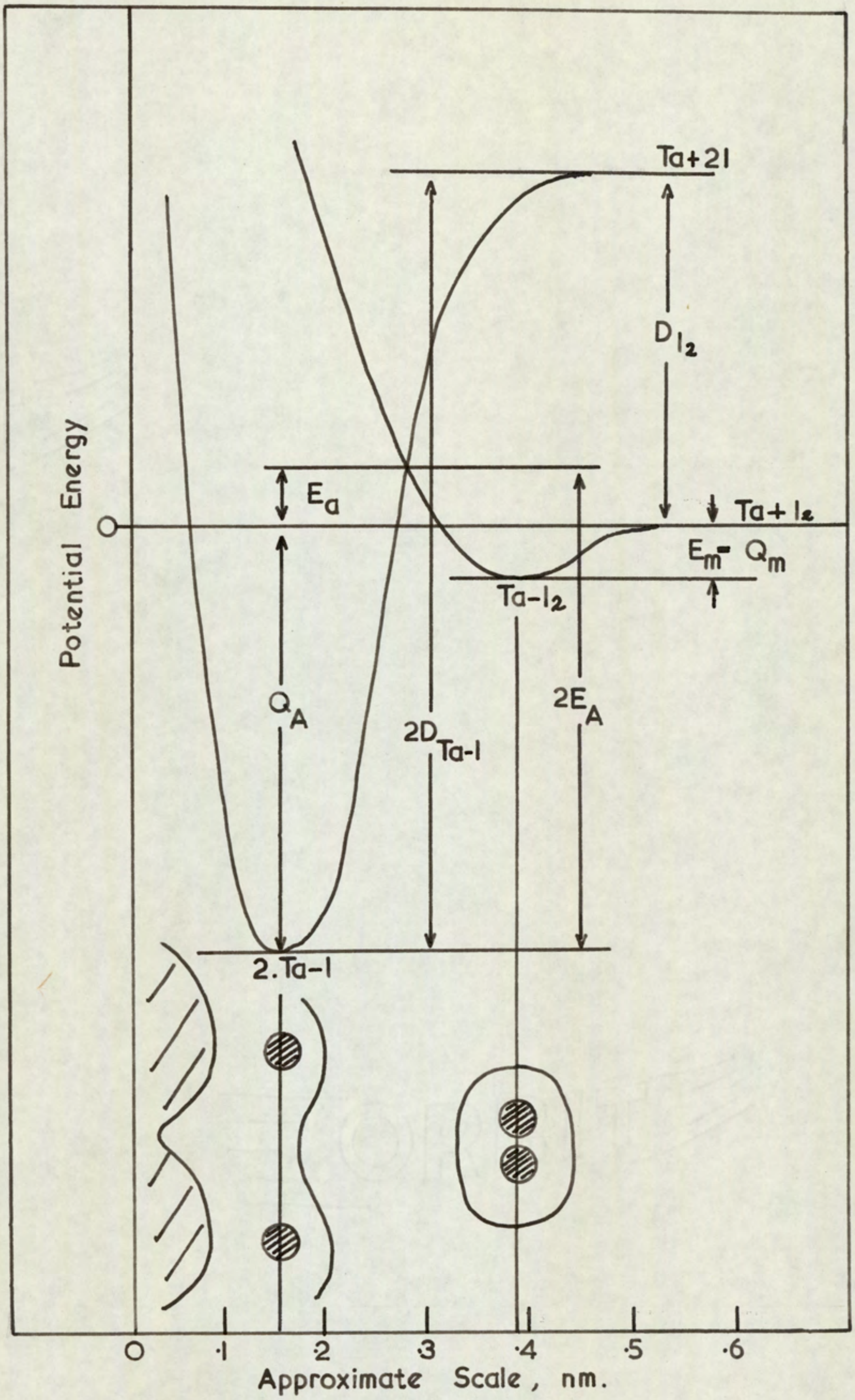

FIGURE (6-1) Potential Energy Diagram illustrating Physical and Chemical Adsorption of Iodine on a Tantalum Surface

The differential heat of adsorption at zero coverage is given by,

$$q_o = (2Q_A) = 2.E(Ta - I) - E(I - I) \qquad - \quad (6-6)$$

This equation assumes that no surface Ta-Ta bonds are broken during chemisorption and that surface metal atoms behave as if they possess free valencies. The energy of the surface bond may be evaluated using the Pauling equation for single bond energies,

$$E(Ta - I) = \tfrac{1}{2}\Big(E(Ta - Ta) + E(I - I)\Big) + 23.06(\varepsilon_{Ta} - \varepsilon_{I})^2 \quad - (6-7)$$

The last electronegativity term allows for the ionic contribution to the bond energy. Eley assumed that the electronegativity difference could be related to the surface dipole (at zero coverage), M, which may be obtained from the measured contact potential of the covered surface using the relationship,

$$M = \frac{V \,.\, 10^{18}}{2\,300.C_s} \qquad - \quad (6-8)$$

where V = c.p.d. in practical volts

C_s = surface concentration of adsorbed species.

Probably a more reliable method for obtaining electronegativity differences has been developed by Stevenson. It is based upon the association of the electronegativity of an atom with the energy of its first ionisation potential and electron affinity, which, for a metal, are both the same and equal to the work function.

Stevenson obtained,

$$\varepsilon = 0.355\phi \qquad - \quad (6-9)$$

where ϕ = the work function

0.355= scaling factor

The electronegativity of iodine has been determined using a similar method by Allred and Rochow. The value found for the work function of tantalum was 4.35 e.v. and $\varepsilon_I = 2.21$.

The value of E(Ta - Ta) can be calculated from the heat of sublimation of the metal using the relation,

$$E(Ta - Ta) = \frac{2}{12} \cdot \Delta H_{sublimation} \qquad - \quad (6\text{-}10)$$
$$= 130 \text{ KJ.mole}^{-1}$$

Using these values, E(Ta - I) is found to be 184 KJ.mole$(I)^{-1}$ and hence from equation (6-6), qo = 218 KJ.mole$(I_2)^{-1}$.

The experimental activation enthalpy is 52.2 KJ.mole^{-1} and if this is assumed to be the value for the desorption of one mole of iodine molecules this will be E_m in figure (6-1).

In figure (6-1) the relative position of the point A is as yet unknown. From this diagram it seems it is energetically more likely that the iodine is present on the surface as atoms although there will be an equilibrium between atoms and molecules. The activation energy for desorption of atoms is too high for this to be the possible desorption reaction and therefore the reaction must be desorption of molecules either from a molecular film or from an atomic film via a process in which the formation of the molecule is not rate determining. A possible rate determining step would be the breaking of one of the tantalum iodine bonds producing an activated complex, the reaction coordinate for which is the length of the Ta - I bond.

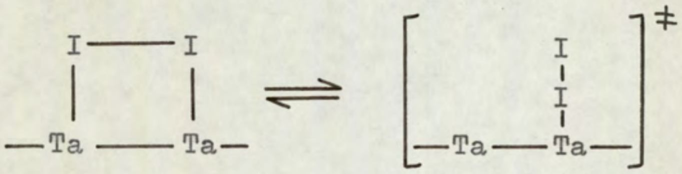

This would involve the breaking of a Ta - I bond but this would be partially compensated for by the increase in strength of the I - I bond and the redistribution of electrons around the Ta atoms. Using this model the activation energy of 52.2 KJ.mole^{-1} would seem to be reasonable.

From the results of the flash desorption of methyl iodide it was concluded that the same species was being observed as in the iodine experiments and this has now been shown to be iodine molecules.

This means that iodine must be mobile on the tantalum surface at 300^{o}K. The translation of the iodine atoms from site to site will be an activated process and the transition state for this could be a bridged iodine atom,

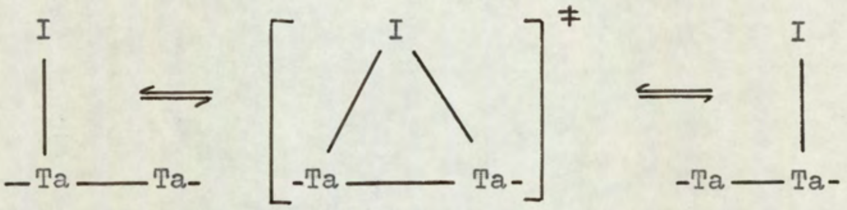

The rates of surface migration and activation energies for migration have been measured for several species and it has been shown that this latter quantity is always less than or equal to 0.2 x the activation energy for desorption, therefore for iodine, $E_{migration} \simeq 38$ KJ.mole^{-1}.

Assuming a first order reaction and a rate constant of 10^{13}sec.$^{-1}$

$$\left(\frac{d(mig)}{dt}\right) = I_s \cdot 10^{13} \exp\left(\frac{-38000}{R.300}\right) \qquad - \qquad (6\text{-}11)$$

$$\left(\frac{d(mig)}{dt}\right) \simeq I_s \quad \text{molecules.cm.}^{-2}\text{sec.}^{-1}$$

A typical value of the surface concentration was 10^{12}particles.cm.$^{-2}$ ($\theta = 0.001$) and therefore the iodine atoms migrating and forming molecules on the surface, prior to the desorption cycle can account for the desorption of iodine molecules following the adsorption of methyl iodide.

6.3. The Activation Entropy

The kinetic analysis of any reaction only gives information about the rate determining step. It is possible that the desorption reaction involves three stages:

1) Initial formation of iodine molecules from iodine atoms bonded to adjacent sites on the surface.
2) The formation of the activated complex from an adsorbed molecule.
3) The desorption of the complex from the surface into the gas phase.

Because of the apparent large, negative entropy change involved in the activation step there must be an appreciable difference between the properties of the adsorbed molecule and the activated complex. From the experimental entropy the ratio of the partition functions may be obtained,

$$\frac{F^{\ddagger}}{F_{\text{initial}}} = \text{Exp}\left(\frac{\Delta S^{\ddagger}}{R}\right) \qquad - \quad (6\text{-}12)$$

Inserting the experimental value of $\Delta S^{\ddagger}$ and also the value of the gas constant

$$\frac{F^{\ddagger}}{F_{\text{initial}}} = 10^{-9} \qquad - \quad (6\text{-}13)$$

It has been suggested that activated states for adsorption and desorption are immobile and possess no degrees of translational freedom parallel to the surface. If this is assumed and it is also assumed that the adsorbed iodine molecules were mobile and could be represented by a two dimensional ideal gas then the appropriate partition function could be calculated.

The partition function for translational motion is

$$F_{trans} = \left(\frac{2\pi mkT}{h^2}\right)^{\frac{1}{2}} . a \ / \text{ degree of freedom} \qquad - \quad (6\text{-}14)$$

Let a = 1 cm. and the standard state be 1 mole.cm^{-2}. For two degrees of freedom $F_{initial} = 2.5 \times 10^{-18}$ and assuming the vibrational partition functions to be very similar (these will be small compared to F_{trans}) then

$$\frac{F^{\neq}}{F_{initial}} = 5 \times 10^{-17}, \text{ or } \Delta S^{\ddagger} = -75.2 \text{ cal.deg}^{-1}\text{mole}^{-1} \qquad - \quad (6\text{-}15)$$

(This value cannot be compared with standard enthalpy changes and are of this magnitude because of the unusual standard state - 1 mole.cm^{-2}.)

The equation for F_{trans} is obtained from

$$F_{trans} = \int_{n=o}^{n=\infty} \exp\left(\frac{-h^2n^2}{8mkT}\right) .dn \qquad - \quad (6\text{-}16)$$

assuming all levels n = o to n = ∞ are accessible. However the translational motion of the iodine molecules will occur in a periodic field and will be an activated process. For migration to occur the value of n must exceed a certain minimum value (n_{min}) to allow for this activation energy.

$$F_{migration} = \int_{n=(n_{min})}^{n=\infty} \exp\left(\frac{-h^2n^2}{8mkT}\right) . \ dn \qquad - \quad (6\text{-}17)$$

This will account for the experimental ratio of 10^{-9} with both states immobile, the ratio is unity and with a completely mobile film the ratio is $\sim 10^{18}$. The activated state for migration will be similar to that for desorption. This time the reaction coordinate will be the position of the unbonded iodine atom.

These values have been calculated assuming that the transmission coefficient is unity but this may not be the case and any departure from unity will have the effect of numerically decreasing the activation entropy. If it is also temperature dependent this will affect the estimated values of both the entropy and enthalpy of activation.

Some studies have been carried out on the problem of interpreting the experimental enthalpy and entropy of activation. In the particular case of the electron induced desorption of hydrogen from nickel values of 52.6 $KJ.mole^{-1}$ and -236 $joule.deg.^{-1}mole^{-1}$ were obtained for the activation enthalpy and entropy respectively, assuming that the transmission coefficient was unity. Assuming this is not the case but that it in fact varies from 0.1 - 0.02 in the temperature range 690 - 830°K, produces values of 129$KJ.mole^{-1}$ and -16.7 $joule.deg.^{-1}mole^{-1}$ for the activation enthalpy and entropy. These values are not unique, but assuming the adsorption is non activated, the desorption enthalpy agrees with the measured heat of adsorption (85) of hydrogen on nickel and they prove the possibility of explaining the observed slow kinetics of desorption with a temperature dependent transmission coefficient without having to lend physical significance to experimental values of enthalpy and entropy, the values of $\Delta S^{\ddagger}$, in particular, being anomalously large.

6.4. Comparison with other Thermal Desorption Data

Many workers (25,65) when analysing thermal desorption data have used a simple rate equation,

$$-\frac{dn}{dt} = k_d\,(n_o - n_t)^x \;.\; \exp\,(-E/RT) \qquad - \qquad (6\text{-}18)$$

Solving this equation to find the temperature, T_p, at which the desorption rate is a maximum then,

$$\frac{E}{RT_p{}^2} = \frac{k_d}{\beta} \;.\; \exp \;.\; (-E/RT_p) \quad (\text{for } x = 1) \qquad - \qquad (6\text{-}19)$$

In order to obtain values of the activation energy the rate constant must be found and generally this has been assumed to equal kT/h ($\simeq 10^{13}$sec.$^{-1}$). This is derived from equation (6-1) assuming that $F^{\neq}/F_{initial} = 1$ which may be true for atomic desorption but not necessarily for molecular or second order reactions or those where changes in mobility on the surface may occur. kT/h at room temperature = 6.2×10^{12}.sec.$^{-1}$ and was supposed by Frenkel to be the period of vibration of the adsorbed molecule normal to the surface ($\simeq 10^{13}$.sec.$^{-1}$) (2).

For the range $10^{13} > k_d/\beta > 10^8$ ($^{o}K^{-1}$) then with a small (1%) error only,

$$E_d/RT_p = \ln\left(\frac{k_d T_p}{\beta}\right) - 3.64 \qquad - \quad (6\text{-}20)$$

Using the values, $\beta = 1.5 \times 10^3$ ^{o}K.sec.$^{-1}$, Tp = 530^{o}K and $k_d = 10^{13}$sec.$^{-1}$, then E_d is found to be 113 KJ.mole^{-1} compared to the experimental value of 52.2 KJ.mole^{-1} obtained graphically.

Using this equation but with the experimental rate constant and solving graphically then E = 54.3 KJ.mole^{-1}.

Hence it can be seen that the assumption of the value of a rate constant can lead to quite different activation energies. This has been shown to be true for other desorption reactions and has been attributed either to a low value of the transmission coefficient or to the fact that a particular orientation with respect to the surface must be achieved before desorption occurs (i,e. a large negative value for ΔS). The value of the rate constant has been discussed (25) and it has been shown that the assumption of $k_d = 10^{13}$ can lead to erroneous interpretations.

McCarroll in his work on the desorption of iodine from tungsten assumed that $k_d = 10^{13}$ and this accounts for the difference between the value obtained in this work (52.2 KJ.mole^{-1}) and McCarroll's value (125 KJ.mole^{-1}).

7.0. WORK FUNCTION MEASUREMENTS IN THE ULTRA HIGH VACUUM SYSTEM

7.1. Introduction

Work function measurements on clean tantalum and tantalum in the presence of adsorbed iodine and methyl iodide were carried out using two methods, both described in section (3.2).

Absolute work function values were determined from the temperature dependence of the thermionic emission current (section 3.2.1). Both Richardson (apparent) work function (χ^{**}) and effective work function ($\chi_{eff.}$) values were determined from this data.

Work function changes both with temperature and gas adsorption were determined using the electron beam retarding potential method (section 3.2.4.2).

To determine χ^{**} or $\chi_{eff.}$ then the temperature of the filament must be accurately known. The measurement of this is discussed in the next section.

7.2. The Measurement of Filament Temperature

There are several ways of measuring the emitter temperature;

(1) Direct measurement using an optical pyrometer.

(2) From the slope of the graph of $\ln(I_e)_{ret.}$ against the anode voltage in the retarding field region.

(3) Calculation of filament temperature from the power input.

The first two methods have been used, the third would be an impossible task because of end and radiation losses and temperature gradients in the filament.

7.2.1. Estimation of Filament Temperature using an Optical Pyrometer

In this method a Leeds and Northrup disappearing filament optical pyrometer, with a 0.653μ filter, was used to determine the brightness temperature of the filament.

The brightness temperature, S_λ, is connected to the true temperature, T, by the relationship,

$$\frac{1}{T} - \frac{1}{S_\lambda} = \frac{\lambda}{C_2} \ln(\epsilon_\lambda . A_\lambda) \qquad - \qquad (7\text{-}1)$$

where ϵ , the spectral emissivity and A_λ, the absorption coefficient of the glass vacuum wall are both functions of wavelength. The emissivity is also a function of temperature (60) following the relation,

$$\epsilon = -184 \times 10^{-8} . T + 0.414 \qquad - \qquad (7\text{-}2)$$

7.2.2. Estimation of Filament Temperature from Voltage-Ampere Characteristic Plots

In the retarding field region it has been shown (equation 3-51) that the electron current density is given by,

$$J_{Ret.} = AT^2 (1 - \bar{r}_e) \exp - \frac{(\chi_A - V_A)}{kT} \qquad - \qquad (7\text{-}3)$$

where T is the emitter temperature.
Rearranging,

$$\ln (J_{Ret.}) = \ln AT^2(1 - \bar{r}_e) - \frac{\chi_A}{kT} + \frac{V_A}{kT} \qquad - \qquad (7\text{-}4)$$

and differentiating,

$$\frac{d}{dVA} \cdot \left(\ln(J_{Ret.})\right) = \frac{1}{kT} \qquad - \quad (7-5)$$

Therefore a plot of $\ln(J_{Ret.})$ as a function of the anode voltage will give a straight line plot of slope $1/kT$, from which T may be evaluated.

7.2.3. Estimation of Filament Temperature - Comparison of Methods

A comparison of the two methods can be obtained from the results of two experiments, both of which are sets of characteristic curves for thermally cleaned filaments. In the first experiment (experiment (6)), filament (1) was the emitter and (2) the collector, whilst in the second experiment (experiment (33)), the roles of the filaments were reversed.

These are shown in figures (7-1) and (7-2) and it can be seen that as expected the plots of $\ln(J_e)$ against V_A in the retarding field region are linear and in the saturated field region the current collected is almost independent of the applied voltage. There is very little ambiguity in estimating the position of the knee, and hence little error in the value of V_{AC}.

The values of the temperature estimated using the optical pyrometer (T_{py}) and that calculated using the slope of the retarding field plot are given in table (7-1) together with the difference, ΔT, equal to $T_{py} - T_{calc}$ and the percentage difference.

Values of T_{calc} and T_{py} were generally within 2% agreement.

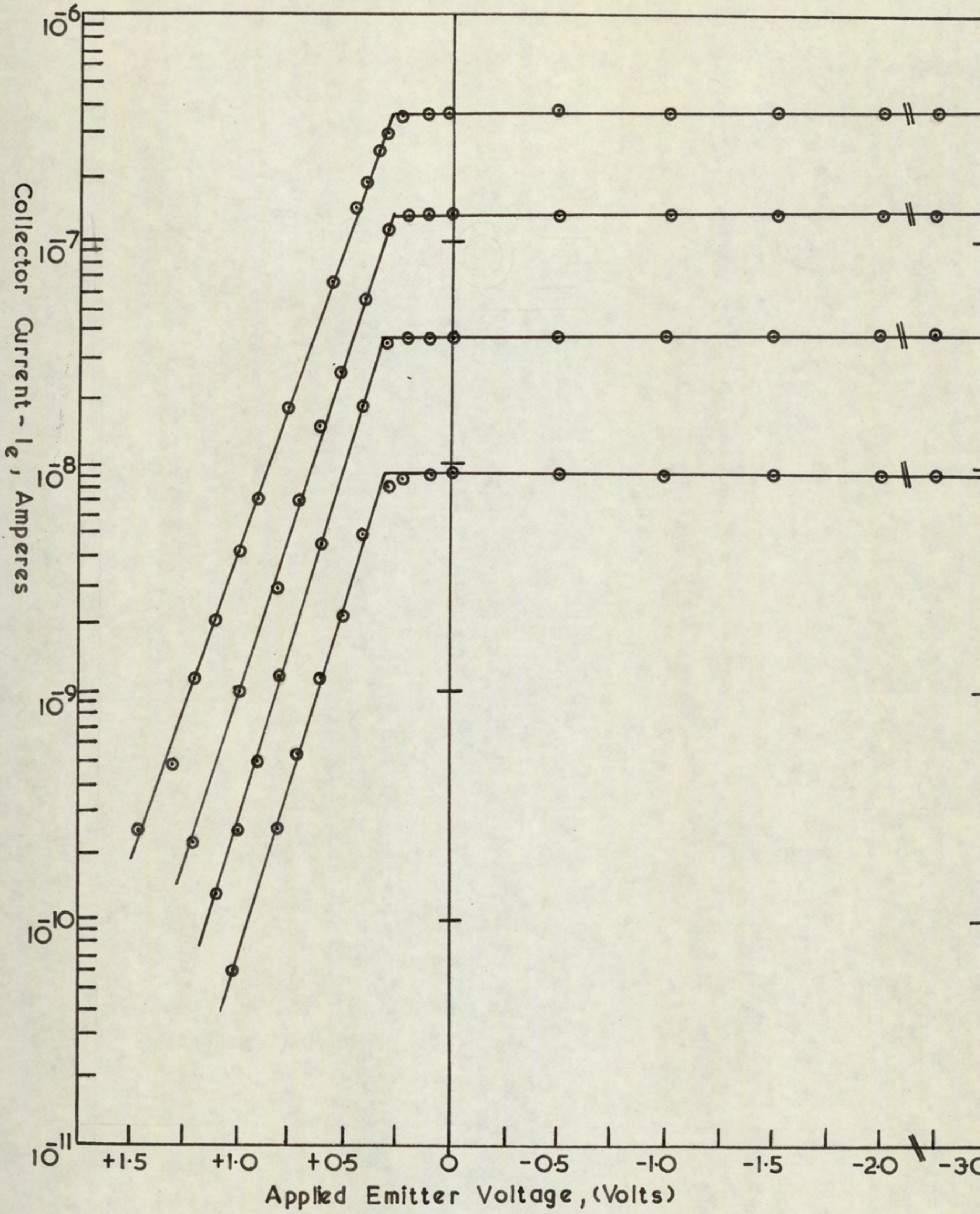

FIGURE (7-1) Characteristic Plots - Filament (1) Emitter
Filament (2) Collector

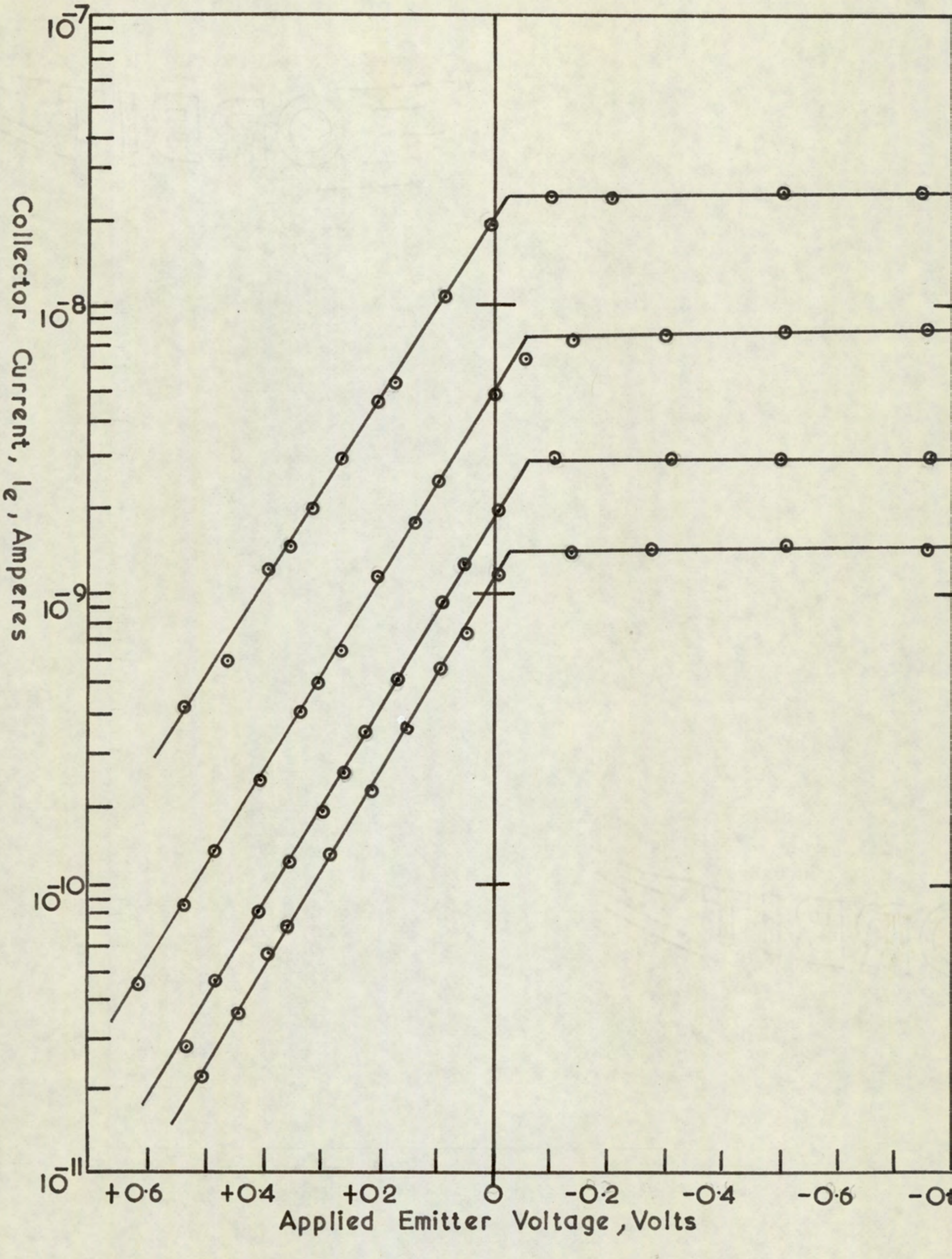

FIGURE (7-2) Filament (2) Emitter - Filament (1) Collector Characteristic Plots

TABLE (7-1)

Comparison of Pyrometer and Calculated Temperatures

Experiment (6)

T_{py} (^oK)	T_{calc} (^oK)	ΔT (^oK)	Error $\frac{\Delta T}{T_{py}} \times 100$
1750	1764	- 14	- 0.8
1683	1670	+ 13	+ 0.8
1633	1615	+ 18	+ 1.1
1566	1560	+ 6	+ 0.4

Experiment (33)

T_{py} (^oK)	T_{calc} (^oK)	ΔT (^oK)	Error $\frac{\Delta T}{T_{py}} \times 100$
1650	1630	+ 30	+ 1.8
1618	1590	+ 28	+ 1.75
1587	1560	+ 27	+ 1.75
1555	1530	+ 25	+ 1.65

Several problems were found in the determination of T_{calc}. The heating current was supplied via a stack of 12 v. storage batteries with a high wattage carbon block variable resistor to control the current through the filament. This was not a particularly stable supply and needed constant adjustment to ensure the constant electron emission required to obtain an accurate slope in the retarding field region. In this region the electron current is exponentially dependent upon both T^{-1} and V_A, both of which must be exceptionally stable for accurate temperature measurements.

Another problem was the presence of leakage currents which were independent of the electron current. These were especially troublesome in the 10^{-11}- 10^{-12}A. range and therefore more important at lower temperatures ($<1500^{\circ}$K). The leakage currents were caused partly by the vacuum electrical leadthrough insulators which were especially prone to moisture and partly to leakages in the experimental cell which appeared to depend both upon the applied voltage across the insulator and its temperature.

It was found overall that the pyrometric temperatures were more reproducible than the electron distribution method although the two methods gave good agreement.

7.2.4. Estimation of Filament Temperature - Current-Temperature Calibration Plots

The design of the planar triode and the position of the magnet made temperature measurement by direct observation during an experiment impossible. To overcome this problem a filament temperature-current calibration graph was employed.

If the filament is considered as an ideal black body emitter then the total radiation emitted, E_e, will be given by,

$$E_e = \sigma T^4 \qquad \text{watt.sec.}^{-1} \qquad - \quad (7\text{-}6)$$

The energy input to the filament, E_i, can be calculated from the electrical power input.

$$E_i = I_f^2 R = I_f \cdot V_f \quad \text{watt.sec.}^{-1} \qquad - \quad (7\text{-}7)$$

At steady state,

$$I_f^2 R = I_f V_f = \sigma T^4 \qquad - \quad (7\text{-}8)$$

Thus ideally a plot of $I_f R^{\frac{1}{2}}$ (or $(I_f V_f)^{\frac{1}{2}}$) against T^2 should yield a straight line graph.

Such a plot showed only slight curvature over the temperature range 1000 - 2000°K and once obtained enabled calculation of the filament temperature from the voltage drop across the filament and the current flowing through it.

The curvature is due to heat losses from the ends of the filament and the fact that the maximum in the distribution-wavelength plot is a function of temperature.

It was also found that a plot of I_f against T^2 was almost linear and very reproducible. Such plots are shown for filament (1) in figure (7-3) and filament (2) in figure (7-4).

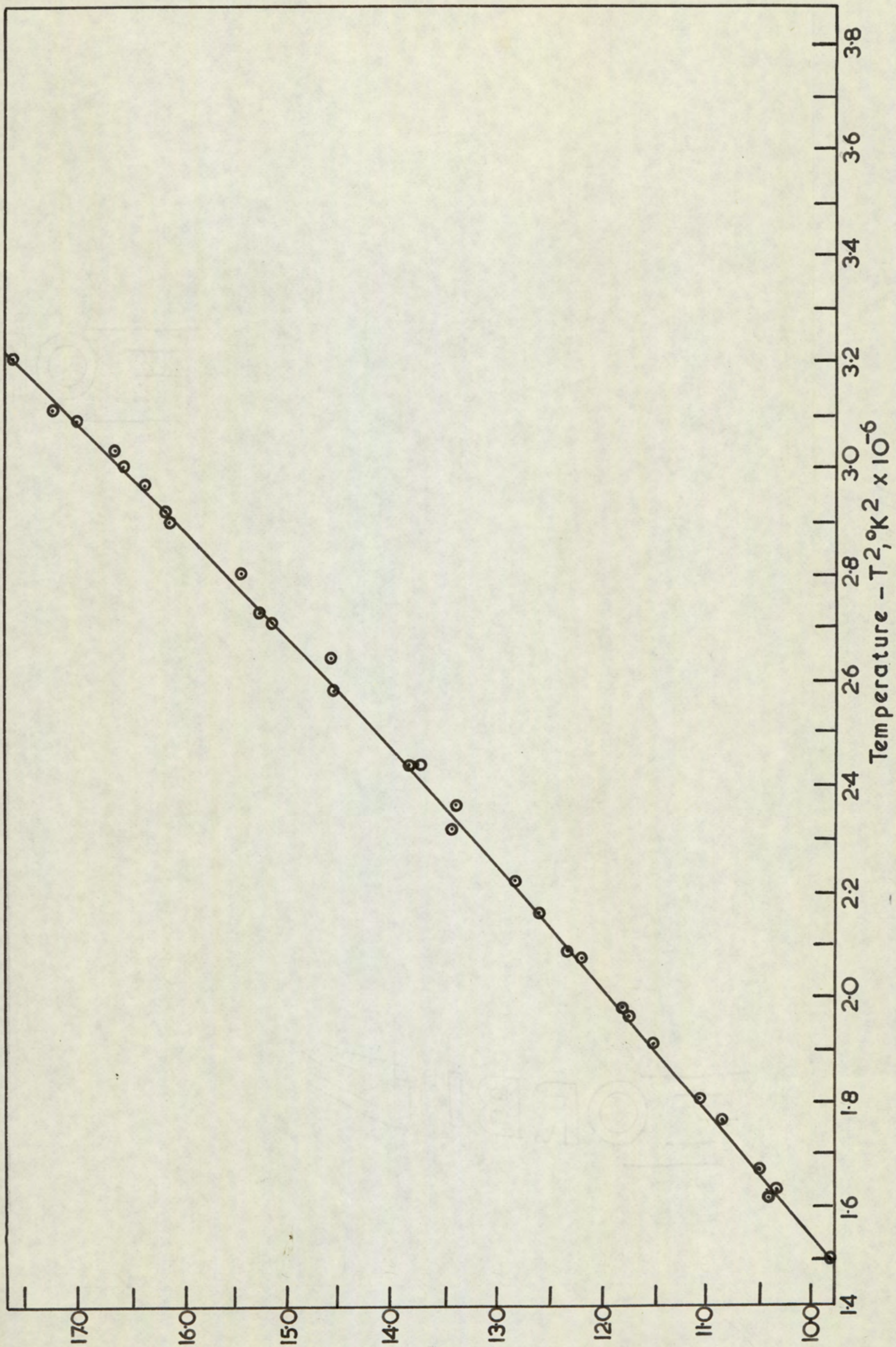

FIGURE (7-3). Filament (1) Current as a Function of T^2

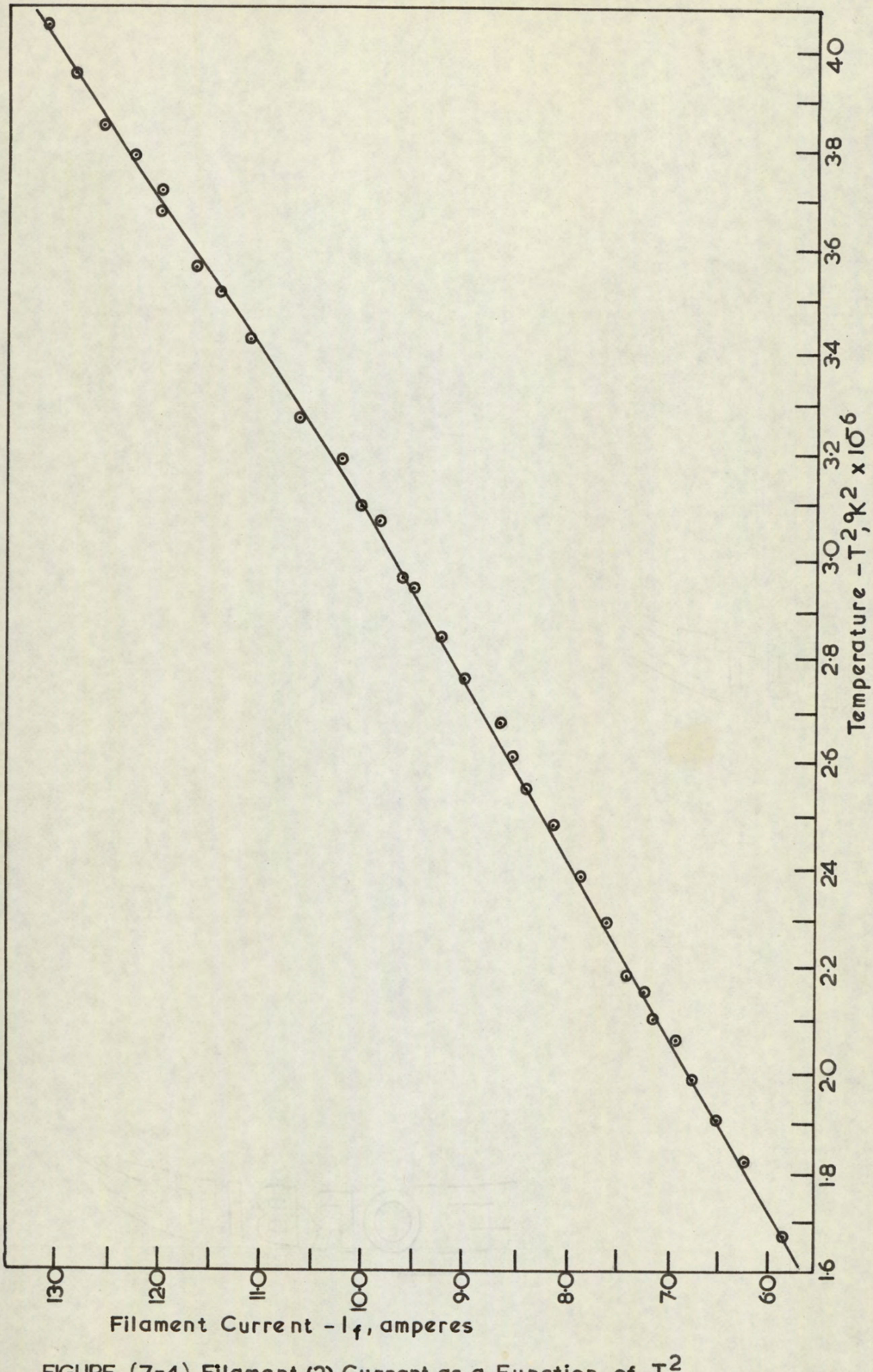

FIGURE (7-4) Filament (2) Current as a Function of T^2

7.3. Thermionic Emission Data for Clean Filament

Both filaments were flashed clean and outgassed and then Richardson and characteristic plots obtained to calculate values of χ^{**}, A^{**} and $\chi_{eff.}$.

7.3.1. Richardson Work Function of Clean Filament

A plot of $\ln(I_e/T^2)$ against T^{-1} yields a linear plot whose slope yields the work function, χ^{**}/R.

A typical plot is shown in figure (7-5) where χ^{**} was found to be 436 KJ.mole^{-1} (4.56 e.v.). The data for this plot is given in table (7-2).

The value of A^{**}, the intercept on the log (J_e/T^2) axis of the plot, is given by,

$$\frac{\ln A^{**} - \ln(J_e/T^2)}{10^4/T} = \frac{\chi^{**}}{R} \qquad - \quad (7\text{-}9)$$

A^{**} is calculated to be 30.0 A.cm.$^{-2}$deg.$^{-2}$ (values for other experiments gave values $1.0 < \log_{10} A^{**} < 2.0$).

The theoretical value of A is 120 A.cm.$^{-2}$deg.$^{-2}$ but agreement would only be expected for emission from a single crystal. There is no simple relationship between A and A^{**}.

TABLE (7-2)

Experiment (6) Data for Richardson Plot

I_e (A)	I_f (A)	T^2_{py} ($^oK^2$)	T (^oK)	$\frac{I_e}{T^2}$	$\frac{10^4}{T}$
3.0×10^{-7}	10.14	3.147	1774	9.55×10^{-13}	5.75
6.8×10^{-7}	10.68	3.310	1819	2.05×10^{-13}	5.50
4.4×10^{-7}	10.36	3.218	1794	1.37×10^{-13}	5.58
2.6×10^{-7}	10.04	3.124	1765	8.35×10^{-14}	5.67
1.35×10^{-7}	9.78	3.036	1743	4.44×10^{-14}	5.74
8.0×10^{-7}	9.39	2.904	1704	2.75×10^{-14}	5.88
4.4×10^{-8}	9.06	2.795	1672	1.59×10^{-14}	5.99
6.3×10^{-8}	8.68	2.660	1631	2.37×10^{-14}	6.13
1.75×10^{-8}	8.65	2.650	1628	6.61×10^{-15}	6.15
1.4×10^{-8}	8.54	2.613	1617	5.35×10^{-15}	6.18
8.4×10^{-9}	8.25	2.512	1585	3.34×10^{-15}	6.32
3.2×10^{-9}	7.90	2.400	1549	1.33×10^{-15}	6.46
1.5×10^{-9}	7.61	2.297	1515	6.53×10^{-16}	6.61
8.4×10^{-10}	7.28	2.177	1475	2.62×10^{-16}	6.79
5.7×10^{-10}	7.43	2.230	1493	3.77×10^{-16}	6.70
3.2×10^{-10}	7.10	2.105	1451	1.52×10^{-16}	6.89
1.35×10^{-10}	6.83	2.020	1421	6.7×10^{-17}	7.04
4.0×10^{-11}	6.47	1.900	1378	2.1×10^{-17}	7.26

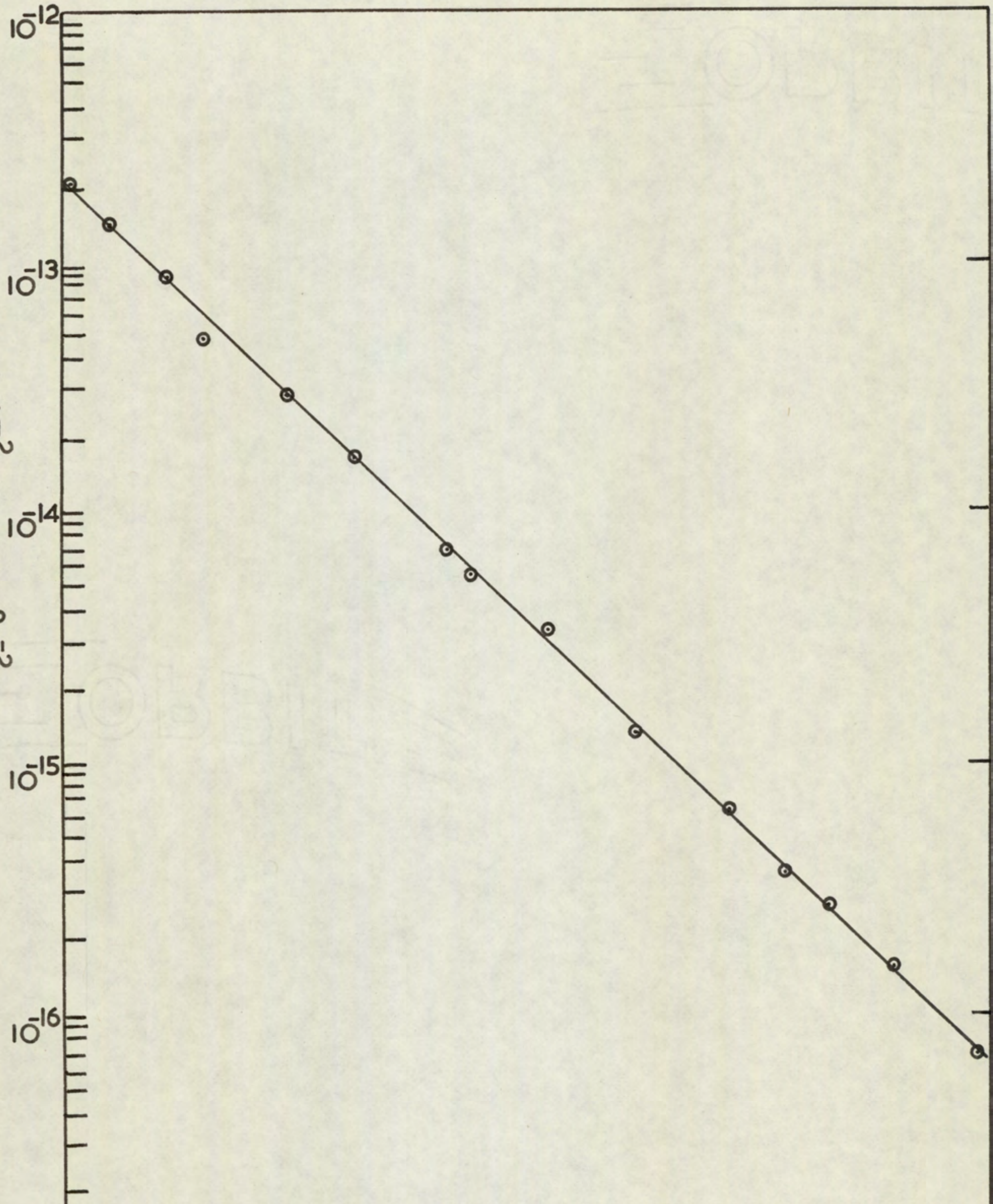

FIGURE (7-5) Richardson Work Function Plot - I_e / T^2 against T^{-1}

7.3.2. Analysis of Characteristic Current-Voltage Curves

The characteristic curves for filaments (1) and (2) are shown in figures (7-1) and (7-2). The temperature measurements appertaining to these plots are discussed in section (7.2.3.).

For the saturated current region;

(1) A Richardson plot can be made, using all the saturated current values, to find χ^{**}.

(2) The effective work function can be calculated for each characteristic curve.

$\chi_{eff.}$ is calculated from the equation,

$$J_e = 120.T^2 . \exp(-\chi_{eff}/kT) \qquad - \quad (7\text{-}10)$$

where J_e is the experimental electron current density. This can be rearranged,

$$\chi_{eff} = 1.984 \times 10^{-4} . T(2.079 + 2\log_{10}T + \log_{10}J_e) \qquad - \quad (7\text{-}11)$$

Effective work function values are useful where not enough points are available for a Richardson plot.

The two are related by the equation, (46)

$$\chi^{eff} = \chi^{**} + \frac{d(\chi_{eff})}{dT} . T \qquad - \quad (7\text{-}12)$$

In the retarding field region,

(1) Using the slope, $d(\ln J_e)/dV_A$, the temperature can be calculated for each curve.

(2) If enough points are available a Richardson plot may be made.

The contact potential difference V_{AC} $(= \chi_1 - \chi_2)$ may be obtained by extrapolation of the two linear regions to find the applied voltage at which they intersect.

The relevant data is shown in figure (7-6). Table (1) gives the data required for a Richardson work function plot and it is found, as shown in figure (7-7), $\chi^{\overset{1}{**}}$ = 447 KJ.mole^{-1} (4.62 e.v.). Table (2) shows the stages in calculating the effective work function values for each characteristic plot (a, the emitting area = 6.4×10^{-3}.cm.$^{-2}$)

Table (3) gives the contact potential values and hence the collector effective work function values.

From the change in the contact potential with temperature there appears to be a decrease in the effective work function with temperature. This could be caused by removal of contaminants with increasing temperature. In the range 1560 - 1750°K, $d\chi_{eff}/dT = 3 \times 10^{-4}$ volts.$^{o}K^{-1}$.

The Richardson function can also be obtained from a plot of $(I_e/T^2)_{Ret.}$ against T^{-1}. The barrier to emission in the retarding field region is higher than the emitter work function and is constant during the experiment and hence the current is unaffected by changes in the emitter work function. (48)

The data for these work function measurements is given in figure (7-6), Table (4). The results obtained using T_{calc} and T_{py} are compared and it can be seen that both lines have the same slope giving a value of $\chi^{\overset{1}{**}}$ = 443 KJ.mole^{-1} (4.60 e.v.). This compares with a value of 439 KJ.mole^{-1} (4.56 e.v.) and 444 KJ.mole^{-1} (4.78 e.v.), the higher value resulting in the assumption that A = 120 A.cm^{-2}.$^{o}K^{-2}$. The plots are shown in figure(7-7).

A similar analysis of experiment (33) for filament (2) shows that a Richardson plot of saturated current values gives $\chi^{\overset{2}{**}}$ = 495 KJ.mole^{-1} (5.15 e.v.).

The data for this and the Richardson plot for the retarding field currents are shown in figure (7-6), Table (5). The value of $\chi^{\overset{2}{**}}$ for the retarding field plots was 498 KJ.mole^{-1} (5.19 e.v.).

FIGURE (7-6)

Data for Analysis of Characteristic Plots

Table (1)

I_{sat} (A)	V_{AC} (V)	T^2 $\times 10^{-6}$ ($^oK^2$)	T_{py} (^oK)	I_e/T^2 ($A.^oK^{-2}$)	$10^4/T$ $^oK^{-1}$
9.2×10^{-9}	0.28	2.454	1566	3.7×10^{-15}	6.39
3.7×10^{-8}	0.29	2.668	1633	1.4×10^{-14}	6.13
1.29×10^{-7}	0.32	2.834	1683	4.55×10^{-14}	5.95
3.7×10^{-7}	0.33	3.064	1750	1.21×10^{-13}	5.72

Table (2)

I_e/T^2	$\frac{I_e}{aAT^2}$	$\log \frac{J_e}{AT^2}$	$\frac{5040}{T}$	χ_{eff} (e.v.)
3.7×10^{-15}	4.97×10^{-16}	-15.30	3.21	4.77
1.4×10^{-14}	1.84×10^{-15}	-14.74	3.09	4.78
4.55×10^{-14}	6.03×10^{-15}	-14.22	2.99	4.77
1.21×10^{-13}	1.60×10^{-14}	-13.80	2.88	4.79

Table (3)

V_{AC} (v)	$\chi_{eff.}$(emitter) (e.v.)	$\chi_{eff.}$(collector) (e.v.)
0.28	4.77	5.05
0.29	4.78	5.08
0.32	4.77	5.10
0.33	4.79	5.12

FIGURE (7-6) continued

Data for Analysis of Characteristic Plots (continued)

Table (4)

V_{AC} (V)	$V_{AC}+ .3V$ (V)	I_e at $V_{AC}+ .3V$ (A)	$\frac{I_e}{T^2_{py}}$ ($A.^oK^{-2}$)	$\frac{1}{T_{py}}$ ($^oK^{-1}$)	$\frac{I_e}{T^2_{calc}}$ ($A.^oK^{-2}$)	$\frac{1}{T_{calc}}$ ($^oK^{-1}$)
0.28	0.58	5.4×10^{-8}	1.76×10^{-14}	5.72	1.69×10^{-14}	5.62
0.29	0.59	1.63×10^{-8}	5.7×10^{-15}	5.95	5.84×10^{-15}	5.98
0.32	0.62	4.0×10^{-8}	1.5×10^{-15}	6.13	1.35×10^{-15}	6.19
0.33	0.63	1.0×10^{-9}	4.1×10^{-16}	6.39	4.1×10^{-16}	6.41

Table (5)

$Ie_{sat.}$ (A)	$Ie_{Ret.}$ (A)	T^2 ($^oK^2$)	I_e/T^2_{py} sat. ($A.^oK^{-2}$)	I_e/T^2 Ret. ($A.^oK^{-2}$)	$10^4/T$ ($^oK^{-1}$)
2.4×10^{-8}	5.5×10^{-9}	2.82	8.5×10^{-15}	1.95×10^{-15}	5.95
8.0×10^{-9}	1.61×10^{-9}	2.68	3.0×10^{-15}	6.0×10^{-16}	6.11
3.9×10^{-9}	8.0×10^{-10}	2.58	1.53×10^{-15}	2.3×10^{-16}	6.22
1.5×10^{-9}	3.0×10^{-10}	2.48	6.0×10^{-16}	1.2×10^{-16}	6.35

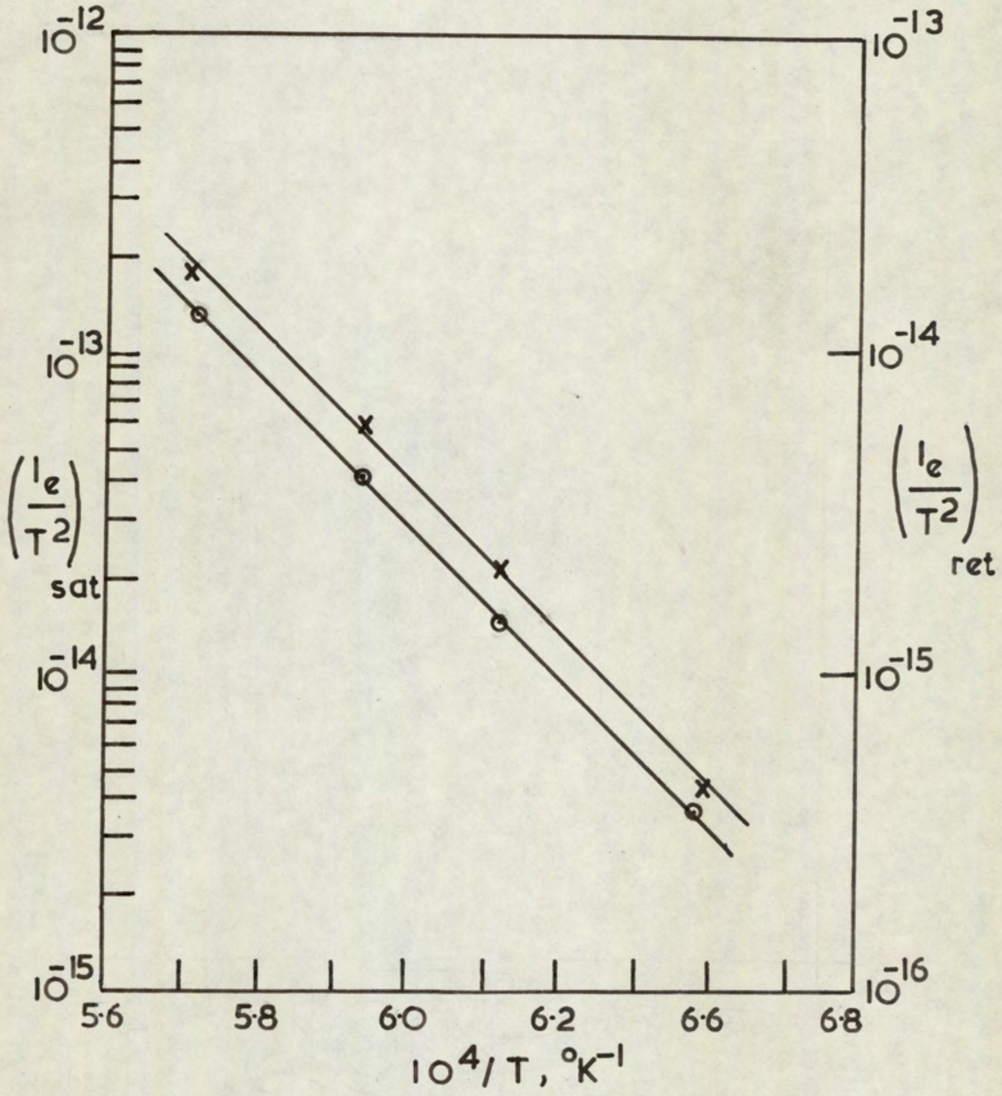

FIGURE (7-7). Richardson Work Function Plots from Characteristic Curves

The values found for the work function of filament (2) (5.09 e.v. c.p.d. method, 5.15 e.v. Richardson method) were consistent, but rather high, and show how traces of contamination by residual gases can affect the observed emission constants.

Repeated flashing and outgassing of this filament reduced the work function value to 423 KJ.mole^{-1} (4.40 e.v.).

Literature work function values for the work function of polycrystalline tantalum show great variance, ranging from 467 KJ.mole^{-1} (4.88 e.v.) (86) to 388 KJ.mole^{-1} (4.03 e.v.).(87) The experimental work function of a polycrystalline material appears to depend greatly upon the pretreatment of the filament, the experimental methods and the method used to analyse the data.

7.4. Dependence of Ta Work Function on Residual Gas Adsorption

Even though the residual gases are only present at pressures of 1 x 10^{-10}mm.Hg. or less, the total amount present in the system, either in the gas phase or adsorbed in the walls, is enough to cause appreciable changes in the work function of the collector surface.

To measure these changes the collector was held at high temperature (> 2200°K) to ensure complete outgassing. It was then cooled to room temperature and the work function change with residual gas adsorption followed by measuring the change in the contact potential as a function of time.

The work function of the emitter (filament (1)), $\chi^{1}_{eff.}$, was calculated to be 448 KJ.mole^{-1} (4.65 e.v.). The contact potential difference measured for the clean collector was - 0.32V., hence, $\chi^{2}_{eff.}$ = 417 KJ.mole^{-1} (4.33 e.v.). (This compares with the value of 423 KJ.mole^{-1} (4.40 e.v.) found in the previous section.

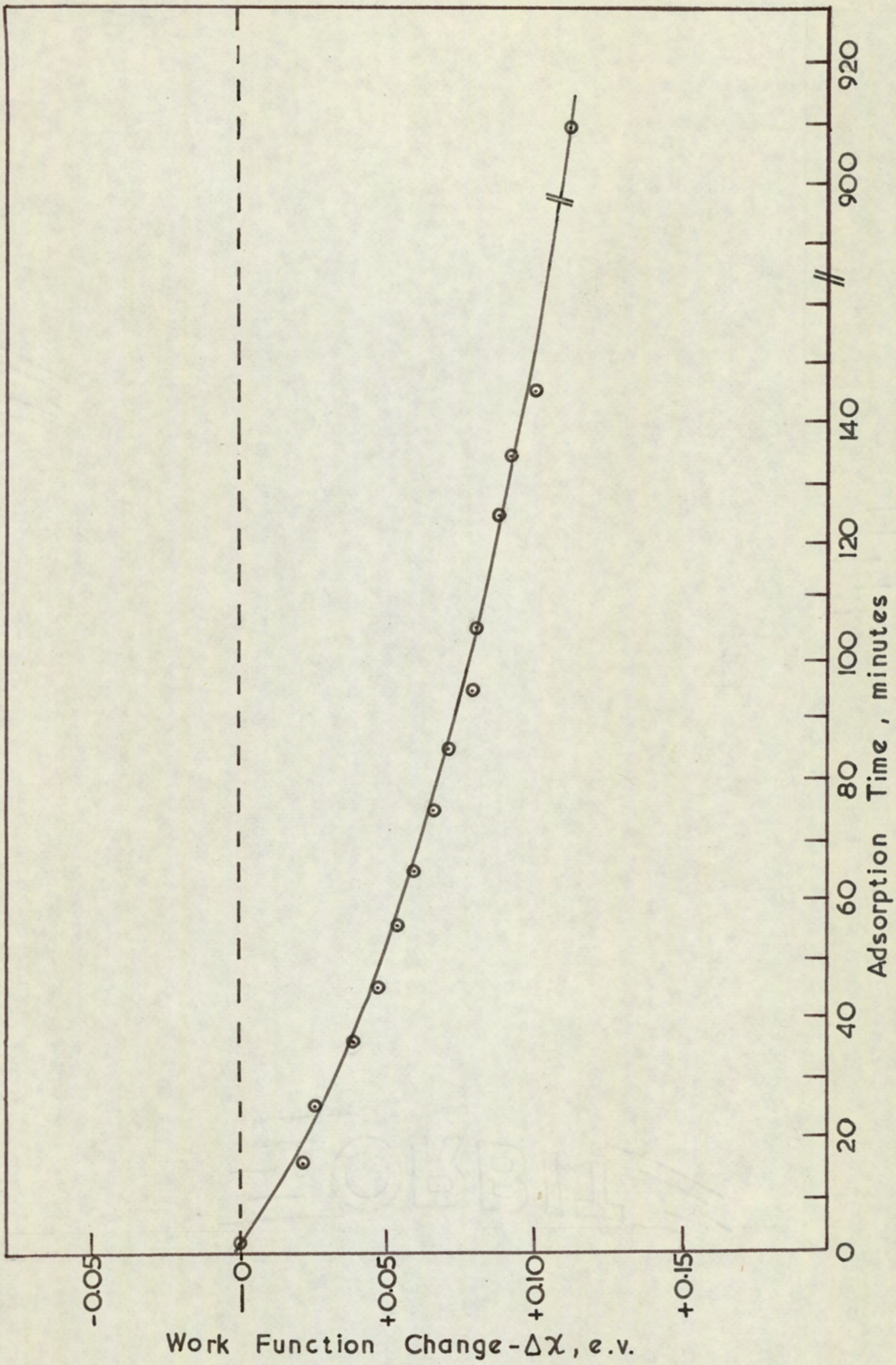

FIGURE (7-8) Work Function Change During Residual Gas Adsorption

The characteristic plot was then recorded at 10 minute intervals for $2\frac{1}{2}$ hours and the results shown in figure (7-8) for experiment 7(b). The contact potential was measured again after 15 hours and was found to have changed by only a small amount. The final value of $\chi^2_{eff.}$ was 427 KJ.mole^{-1} (4.43 e.v.) thus $\Delta\chi = + 10 \pm 2$ KJ.mole^{-1} (+ 0.1 e.v.).

A similar experiment was performed with the roles of the filaments reversed and it was again found that the work function change was small (+ 12 KJ.mole^{-1}) and of the same sign.

These observed work function changes are very small and there could be several reasons for this. It may be that adsorption of the residual gas is negligible for the observation time. Alternatively it may be that appreciable residual gas adsorption does occur but the work function change brought about by this adsorption is very small.

The lowest pressure attainable was 2×10^{-12} mm.Hg. but with one or both filaments operating, because of the cell design, the background pressure was generally $\leqslant 5 \times 10^{-10}$mm.Hg. For this condition the molecular bombardment rate of the filament surface will be 10^{11} molecules.sec.$^{-1}$cm.$^{-2}$ and as the surface is free of adsorbed species the sticking coefficient will be high (typically 0.5) hence coverages approaching a monolayer should be achieved in about two hours (less if dissociative adsorption occurs).

It seems probable then that residual gas adsorption does occur but it causes only a small increase ($\sim + 10$ KJ.mole^{-1}) in the work function of the tantalum filaments.

7.5. The Effect of Iodine and Methyl Iodide Adsorption on the Work Function of Tantalum

The effect of iodine and methyl iodide vapour on the work function of the tantalum filaments was studied in the pressure range $5 \times 10^{-9} - 1 \times 10^{-7}$ mm.Hg and the temperature range 300 - 2000°K for adsorption times up to three hours.

The experimental methods used have been described in section (4.7.3.2). Many of these experiments were carried out in conjunction with thermal desorption experiments described in section (4.7.3.1) in order to correlate work function-surface coverage data.

The experiments were designed to measure the dependence of the work function of tantalum upon exposure to the two gases and upon the temperature of the adsorbate-adsorbent system.

7.5.1. Iodine

The contact potential change during the adsorption of iodine on tantalum was measured at pressures of $1 - 8 \times 10^{-8}$mm.Hg for adsorption times up to two hours.

The results of these experiments were very similar to those found for the adsorption of the residual gases in the previous section. A small positive change in the work function was observed, although in some experiments this change was imperceptible. Some examples are given in table (7-3).

It can be seen that there is no correlation between the observed work function change and the iodine dose thus it seems probable that this change is due to residual gas adsorption.

To determine whether there is a work function change due to iodine alone the dependence of the work function of the I_2/Ta system was studied over the temperature range at which the iodine was known to desorb.

TABLE (7-3)

The Effect of Iodine on the Work Function of Tantalum

Emitter	Collector $\chi_{eff.}$ (e.v.)		$\Delta\chi$ (e.v.)	Dose (10^{-8} mm.Hg)	Pressure
$\chi_{eff.}$ (e.v.)	clean	I_2 pres.	(= $\chi_{I_2} - \chi_{clean}$)	(minutes)	(mm.Hg)
4.62	–	4.69	+ 0.1±0.02	180	2×10^{-8}
4.65	4.59	–			
4.64	4.53	4.66	+ 0.13±0.02	180	6×10^{-8}
4.65	4.23	4.24	+ 0.01±0.02	210	2×10^{-8}
4.65	4.59	4.59	0.0 ±0.02	264	2×10^{-8}
4.47	4.50	4.52	+ 0.02±0.02	20	2×10^{-8}

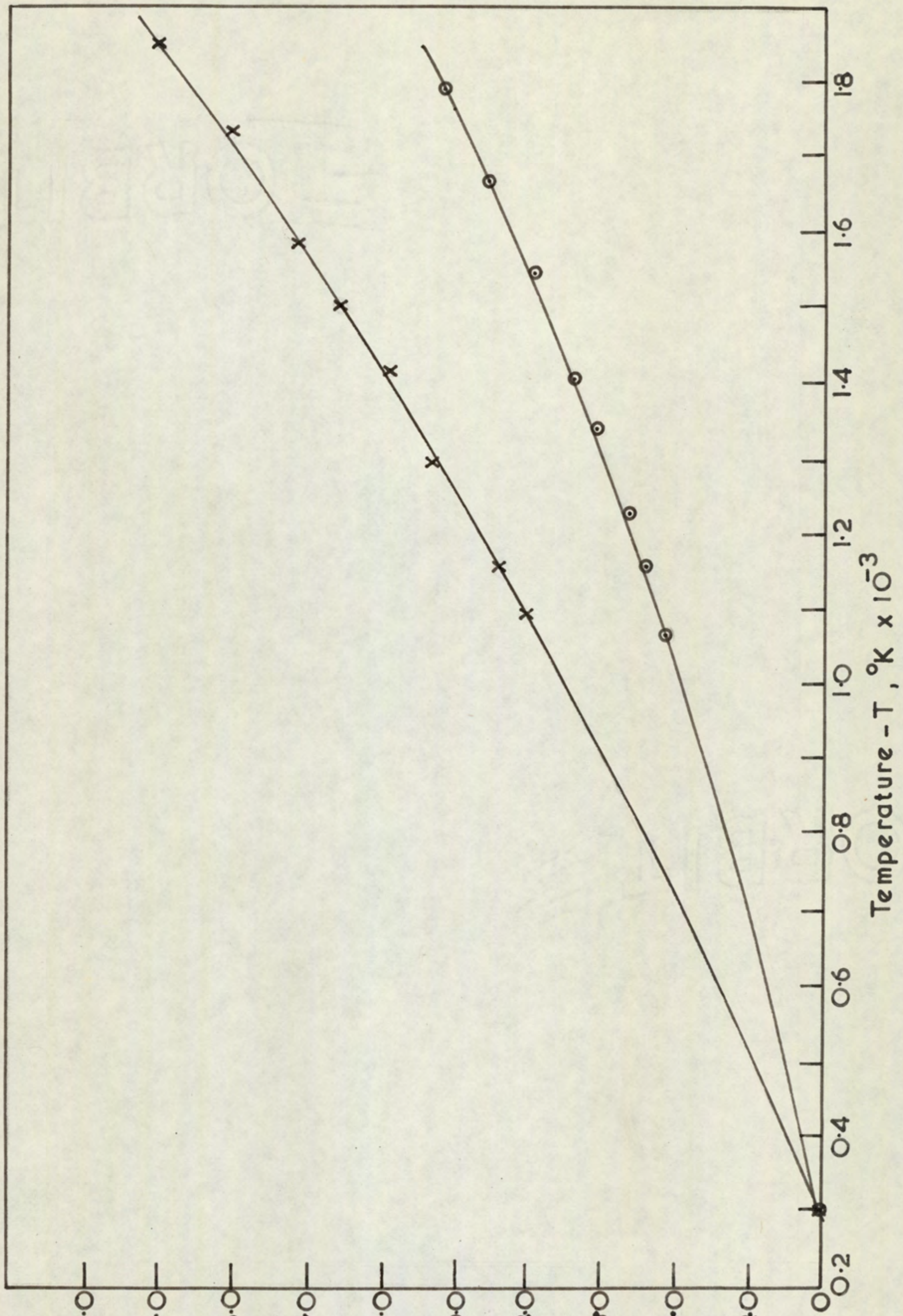

FIGURE (7-9) Filament Current as a Function of Temperature

The temperature of the filaments in this range (300 - 1000°K) was estimated by measuring the temperature pyrometrically down to 1050°K and extrapolating the I_f - T plot to 300°K. These plots are shown in figure (7-9) for both filaments. The estimated error is ± 30°.

Several experiments were carried out in which the iodine was allowed to adsorb onto the filaments for varying times. The characteristic plot was then determined and the change in contact potential difference, as the collector temperature was increased, measured by one of the two methods described in section (4.8.2).

The results are shown in figure (7-10) together with a plot of the desorption rate of iodine as a function of temperature. It can be seen that there is no appreciable work function change over the temperature at which iodine desorbs.

7.5.2. Methyl Iodide

Several experiments, similar to those for iodine, were performed to determine the effect of adsorption of methyl iodide on the work function of tantalum.

The time dependence of the work function was followed at a methyl iodide pressure of 1 x 10^{-7} mm.Hg.

The work function was found to increase during the course of adsorption as shown below.

$\chi_{\text{eff.}}$ emitter (e.v.)	$\chi_{\text{eff.}}$ collector (e.v.)	$\Delta\chi$ (e.v.)	Adsorption time (minutes) (P = 10^{-7} mm.Hg)
4.66	4.47	-	0
4.65	4.51	0.04	15
4.70	4.70	0.23	35
4.65	4.74	0.27	60

The Richardson work function of the emitter was found to be unaffected by the adsorption of methyl iodide.

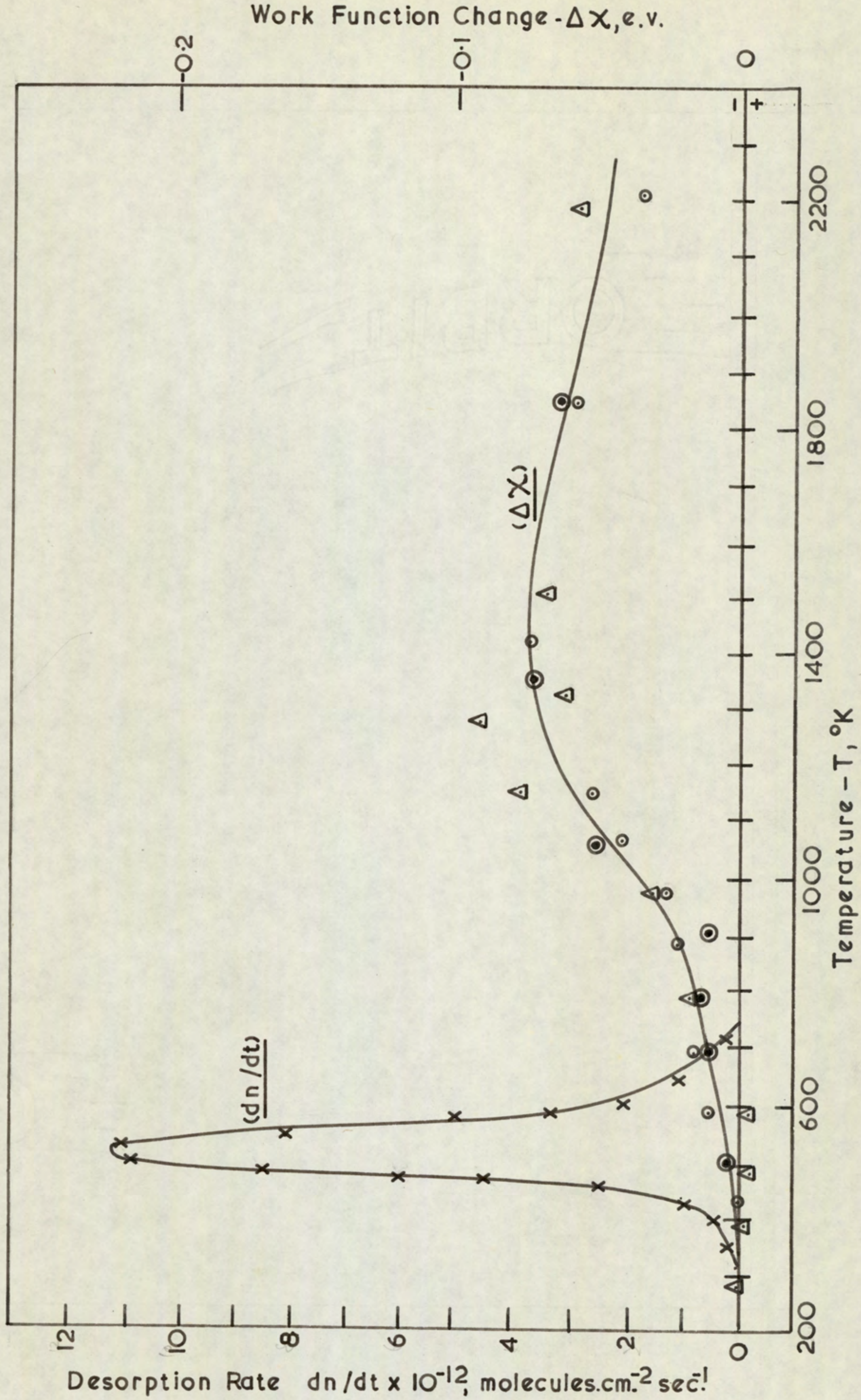

FIGURE (7-10) Work Function Change and Desorption Rate as a Function of Temperature

7.6. Discussion of Work Function Measurements

These measurements must be discussed in conjunction with the results of the thermal desorption experiments which give a measure of the number of adsorbed species responsible for the measured work function changes.

In section (5.2.3) it was concluded that the equilibrium concentration of iodine on the surface was 10^{12} molecules.cm.$^{-2}$ which, assuming 10^{15} adsorbed species.cm.$^{-2}$ to constitute a monolayer, is 10^{-3} of a monolayer. The thermal desorption of methyl iodide showed that similar coverages ($\lesssim 3 \times 10^{-3}$ of a monolayer) were attained, but in this case the desorption peak may not have been due to a unique species because hydrogen, resulting from the decomposition of the methyl group, would desorb with a pressure maximum at 560°K (78,90,91).

This is the same temperature range as the desorption peak found for methyl iodide and iodine (pressure maximum 700°K) but as no splitting of the desorption peak could be discerned and because of the similarity of the two peaks (iodine and methyl iodide) it was concluded that these were due to the same species, molecular iodine.

In the preceding sections the work function changes observed when both iodine and methyl iodide adsorb onto the tantalum filaments were found to be negligibly small compared to the changes caused by residual gas adsorption but this is to be expected because of the low surface coverages encountered.

Measurements have been made (88,89) to determine the work function changes on tungsten surfaces during iodine adsorption but no similar literature data is available for adsorption on tantalum. On tungsten the work function change at low surface coverages (10^{-2} monolayer) was negligibly small, approached -0.4 e.v. at 0.5 monolayer, whilst at higher coverages the work function increased and at saturation reached a value of +0.09 e.v. compared to the clean surface value.

Similar measurements during the adsorption of methane, which adsorbs initially as a methyl radical and a hydrogen atom, showed that both the hydrogen (79) and methane residues (89) contribute to the observed lowered work functions, although again these results apply to higher surface coverages than were encountered in this work.

It has been found in many instances that the extent of adsorption and work function changes are very specific to crystal faces and heats of adsorption and desorption vary similarly (1,6). It is possible that the heat treatment of the tantalum filament, which produced a recrystallised structure in which the average crystallite diameter was 1×10^{-3} cm., resulted in the growth of crystal faces which have relatively low activity towards adsorption of iodine and methyl iodide.

8.0. RESULTS OF MAGNETRON EXPERIMENTS

The first section will deal with the effect of the experimental conditions upon the measured parameters, the next with work function values obtained in the absence of any gas purposely introduced into the vacuum system and subsequent sections with the surface ionisation of iodine and methyl-halogen compounds and the effect these compounds have on the work function of various surfaces.

8.1. Effect of Experimental Conditions

The conditions during an experiment must be such that the saturated emission currents are being drawn both for the ion and electron emission and that in the presence of the magnetic field only the ion current is measured.

8.1.1. Effect of Anode Potential

In the saturated field region there is no space charge between the anode and cathode and the current drawn is independent of the applied voltage except for a small and usually negligible Schottky correction.

Plots of ion and electron currents as functions of the anode-cathode potential difference are shown in figures (8-1) and (8-2) respectively. It can be seen that as the value of the saturation current increases so does the voltage required to achieve saturation but in all cases for the electron current this is achieved before $V_a = 40$v ($=$ 16v.cm.$^{-1}$). The grids were held at an intermediate potential ($\frac{1}{2}.V_a$).

Measurements were made at various values of V_a in the range 50 - 200 volts and the values of the electron affinity and work function were found to be independent of V_a.

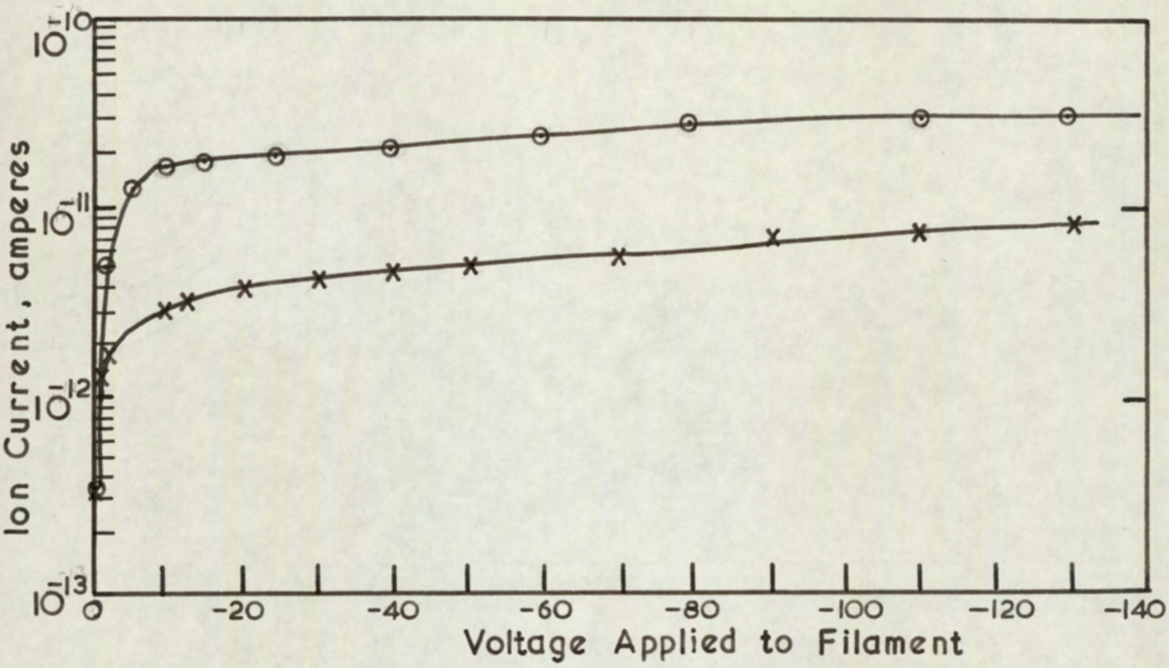

FIGURE (8-1). Dependence of Ion Current upon Applied Voltage

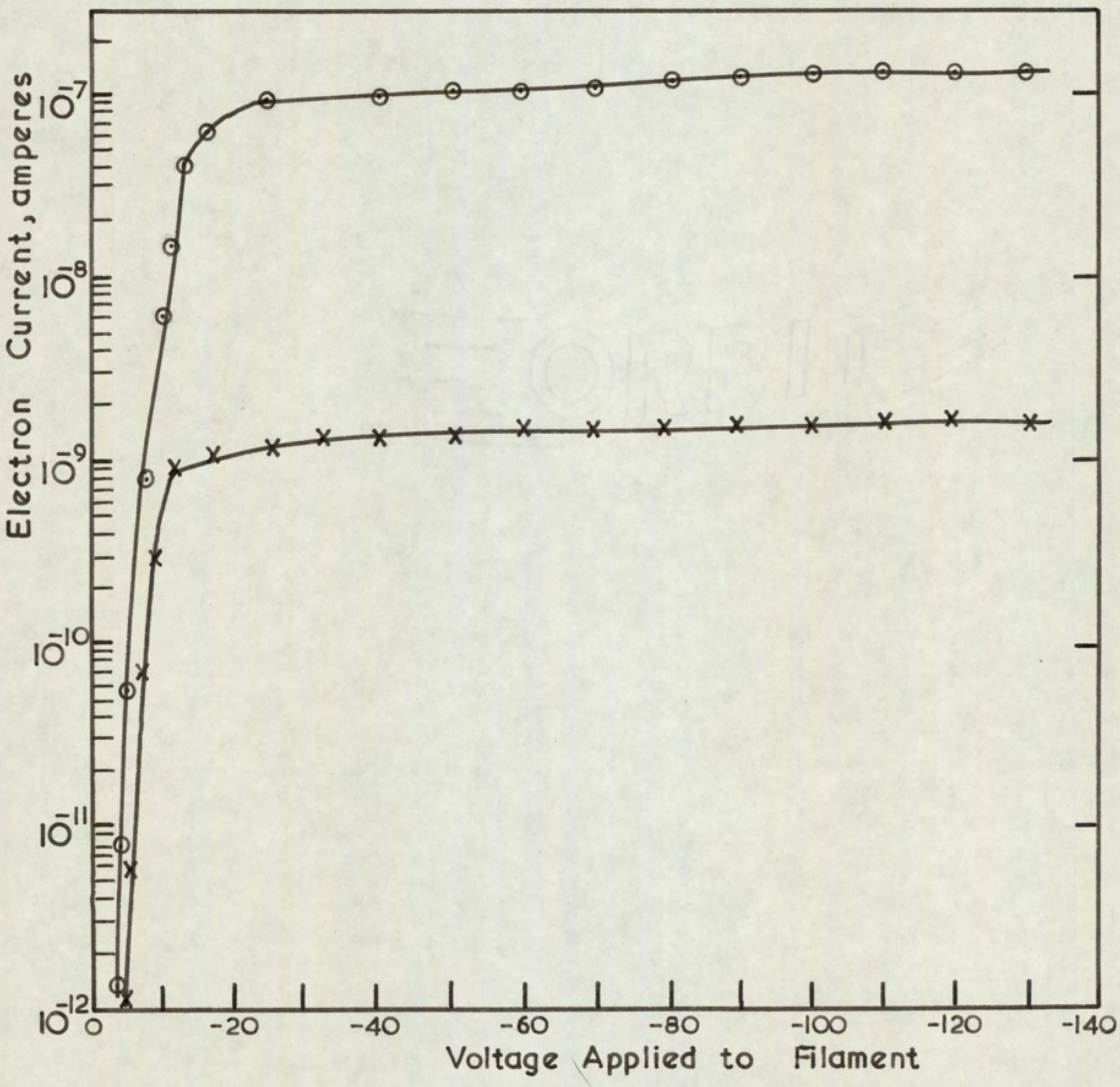

FIGURE (8-2). Dependence of Electron Current upon Applied Voltage

8.1.2. Effect of Magnetic Field Strength

The total thermionic emission current, for various temperatures, is shown as a function of magnetic field density (in gauss) in figure (8-3).

It can be seen, as expected, that there is a sharp reduction in the collected current when the magnetic field reaches a critical cut-off value. This is found to be 26.7 gauss when the accelerating potential is 100 volts (40 $v.cm.^{-1}$) and from these values the quantity e/m for the electron, may be calculated using equation (3-45). The value found using this method is 5.6×10^{17} stat.C(e.s.u.).$gm.^{-1}$, in good agreement with the accepted value of 5.3×10^{17} stat.C(e.s.u.).$gm.^{-1}$.

To ensure that the ion current was independent of the magnetic field strength the usual operating field was at least 200 gauss.

8.2. Work Function Values for Clean Filaments

Several different types of filament material were used in order to determine the effects of the ionising surface in the surface ionisation process. The metals used were tungsten, tantalum, molybdenum and platinum, all of which were in the form of a polycrystalline wire 0.005" in diameter.

It was often found exceedingly difficult to remove all traces of oxide contamination (as shown by high work function values) from the surfaces of the tungsten, tantalum and molybdenum filaments, but such difficulties were not experienced with platinum filaments.

Oxide formation is not important on hot platinum filaments as the only known oxide of platinum, PtO_2, dissociates at 200°C.

Accordingly the clean work function, χ^{**}, of platinum was found to be 443 $KJ.mole^{-1}$ (4.6 e.v.), a value in accord with literature values for polycrystalline platinum.

Initial work function measurements on the other filaments in the presence of the residual gases tended to yield high values, for example, up to 6.3 e.v. for tungsten, but with rigorous heat

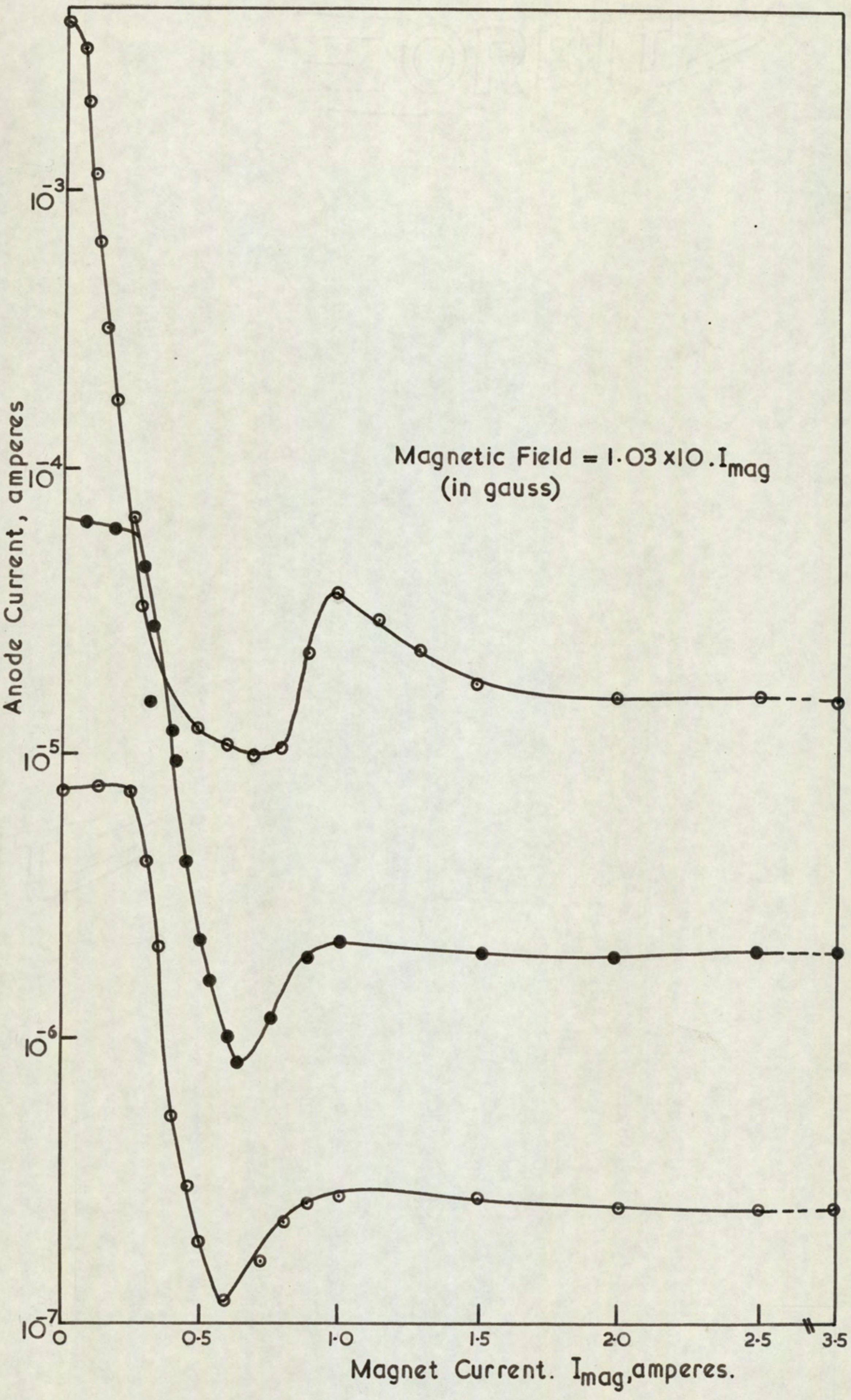

FIGURE (8-3) Dependence of Anode Current on Magnetic Field

TABLE (8-1)

Temperature Dependence of Effective Work Function

Filament Material	Temperature (^{o}K)	χ_{eff} (e.v.)	$\frac{d\chi_{eff}}{dt}$ (e.v. ^{o}K-1)
Pt	1250	4.60	-
	1315	4.60	
	1388	4.60	
	1470	4.60	
W	1555	5.35	-6 x 10^{-4}
	1721	5.25	
	1930	5.12	
	2055	5.05	
Ta	1510	4.65	-6.4x 10^{-4}
	1610	4.63	
	1850	4.48	
	2000	4.35	
Mo	1500	4.84	-5.0 x 10^{-4}
	1650	4.78	
	1875	4.67	
	2100	4.55	

treatment the following values were obtained; W - 472 KJ.mole^{-1} (4.9 e.v.), Ta - 463 KJ.mole (4.8 e.v.) and Mo - 472 KJ.mole^{-1} (4.9 e.v.). These values are somewhat higher than the normal values for clean, polycrystalline emitters (92).

The temperature dependence of the apparent work function may be determined by calculating the effective work function over the experimental temperature range. It can be seen that for platinum, which is not susceptible to oxide contamination, $d\chi_{eff}/dT = 0$. Values for the various filaments are given in table(8-1).

8.3. Surface Ionisation of Iodine

8.3.1. Measurement of Apparent Electron Affinity

The surface ionisation of iodine on various metal filaments has been studied closely and its electron affinity is well known (31). The following experiments were carried out as a check on modifications made on the magnetron and the choice of experimental conditions and also to study the influence of the filament surface on the formation of negative ions from molecular iodine.

Analar grade iodine was used for these experiments but it was further outgassed and purified by vacuum distillation prior to any measurements.

8.3.1.1. Iodine on Tantalum Filaments

The temperature dependence of the electron emission from a tantalum filament prior to the admission of iodine gave an apparent work function, χ^{**} of 544 ± 10 KJ.mole^{-1} (5.0 e.v.) and this value was found to be unchanged by the presence of iodine vapour. The apparent electron affinity, E', for iodine was found, using equation (3-36) to be 310 KJ.mole^{-1} (3.22 e.v.) from an average of three experiments. Typical semi-log plots of (I_e/T^2), I_i and (I_e/I_iT^2) as a function of T^{-1} are shown in figure (8-4).

The results of a similar series of experiments using a filament with an apparent work function of 477 KJ.mole^{-1}, (4.94e.v.) gave an apparent electron affinity of 306 ± 10 KJ.mole^{-1} (3.17e.v.) at an average filament temperature of 1600^{o}K.

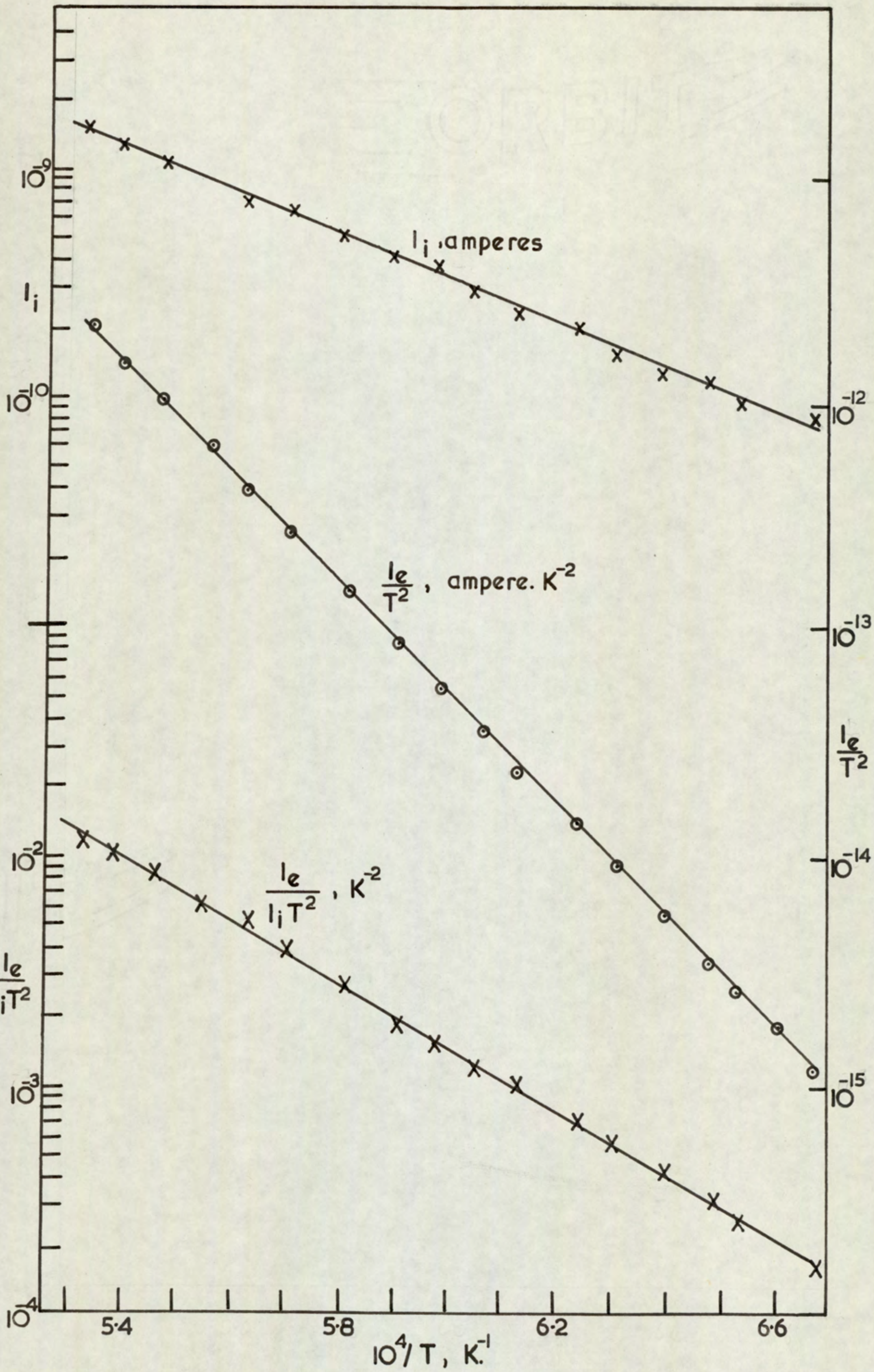

FIGURE (8-4). Iodine – Tantalum. Plots of I_e/T^2, I_i and I_e/I_iT^2 against Reciprocal Temperature

8.3.1.2. Iodine on Molybdenum Filaments

As with tantalum, the apparent work function was higher than the average value for polycrystalline surfaces (4.3 e.v.(92)) but the measured value of the apparent electron affinity was similar to before, 309 KJ.mole^{-1}, (3.21 e.v.), at an average filament temperature of 1600°K and the electron emission was found to be unaffected by the presence of iodine vapour.

8.3.1.3. Iodine on Tungsten Filaments

Oxide contamination was a particular problem with tungsten filaments and a range of work function values were found both in the absence and presence of iodine vapour, but several clear facts emerge. The electron emission was unaffected by the presence of iodine vapour and the apparent electron affinity, which takes into account the value of the electron work function was found to have a constant value of 316 ± 10 KJ.mole^{-1} (3.27 e.v.) at an average filament temperature of 1700°K.

8.3.1.4. Iodine on Platinum Filaments

The average clean surface work function of the platinum filaments used for these experiments was 438 KJ.mole^{-1} (4.55 e.v.) and the work function was found to remain unchanged in the presence of iodine vapour. The apparent electron affinity, however, was found to differ from the almost constant value found previously using the other filament materials.

As shown in figure (8-5) the plot of log (I_e/T^2) against T^{-1} was linear over the temperature range studied but the corresponding ion current plot showed two distinct regions; one at low temperature ($T < 1280$°K) for which E' = 165 KJ.mole^{-1} (1.71 e.v.) and the other at higher temperatures ($T > 1280$°K) for which E' = 96.2 KJ.mole^{-1} (0.99 e.v.) from an average of seven experiments in the temperature range 1100 – 1700°K.

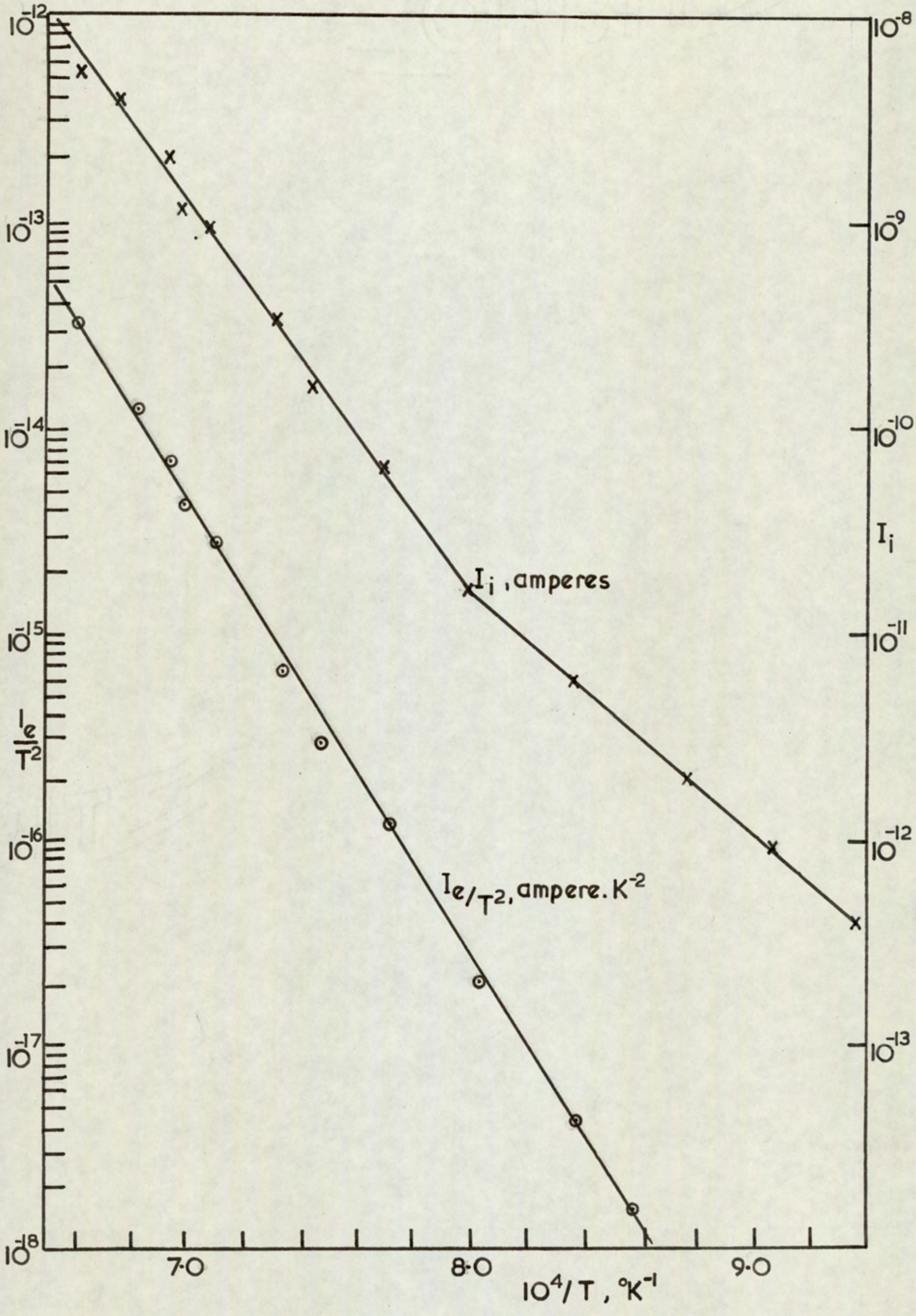

FIGURE (8-5) Iodine-Platinum. Plots of I_e/T^2 and I_i against Reciprocal Temperature

8.3.2. Effect of Iodine on the Thermionic Work Function of the Emitting Surface

In these experiments the filament was thermally cleaned and its temperature set at a specific value (in the range 1150 - 2000°K) before iodine was admitted into the system and its effect on the thermionic emission currents noted. The ion current of course increased drastically but the electron current was found to be unaffected for all of the filament materials studied.

Farragher (49) has considered the effect of strongly adsorbed impurities which do not contribute to the ion current and has shown that impurities will not affect the measured electron affinity even though the work function may be changed.

8.3.3. Discussion of Surface Ionisation of Iodine

The average apparent electron affinity of the iodine atom, as measured from the ratio of the electron and ion currents emitted from tungsten, tantalum and molybdenum filaments as a function of temperature, was found to be 310 (± 3.0) $KJ.mole^{-1}$ (3.22 e.v.). The average filament temperature at which the measurements were carried out was 1600°K.

Many workers have determined the electron affinity of iodine by surface ionisation methods. Typical values obtained were 305$KJ.mole^{-1}$ (93) 316 $KJ.mole^{-1}$ (94), 314 $KJ.mole^{-1}$ (36), 307 $KJ.mole^{-1}$ (42) and 302 $KJ.mole^{-1}$ (31), the average value being 308 $KJ.mole^{-1}$. The values found by photodetachment are generally lower than this, values of 295 $KJ.mole^{-1}$ (95) and 300 $KJ.mole^{-1}$ (96) being typical.

It can be seen that the average value of the apparent electron affinity (310 $KJ.mole^{-1}$) agrees well with the other values found from the surface ionisation of iodine or iodine containing molecules.

Therefore, from equation (3-17) it can be seen, E = E', i.e. the rate determining step in the formation of I^- from iodine molecules is not the adsorption and dissociation of the molecule on the surface but the desorption of the surface atom as a negative ion.

This is to be expected from the equilibrium constant of the surface reaction,

$$I_{2(S)} \rightleftharpoons 2\ I_{(S)} \qquad - \quad (8\text{-}1)$$

at the temperature of the surface which will be given by the ratio n_a/n_m^2, where n_a and n_m are the surface concentrations of the atoms and molecules respectively. The evaluation of the surface equilibrium constant has been undertaken by McCarroll (65) who showed that molecular iodine, in equilibrium with the surface, could not exist on a tungsten surface above 680°K and for the other filaments at similar temperatures.

Therefore molecular iodine impinging on a filament surface at 1100 - 2000°K and becoming accommodated with the surface will behave as atomic iodine.

As the ions are emitted in thermal and charge equilibrium with the surface this suggests that the halogen has a sufficiently long lifetime on the surface to be considered as forming a surface bond.

The nature of this surface bond has been the object of several recent studies of the surface ionisation of the halogens (5,32,43) in which the desorption of negative ions was followed using a modulated molecular beam technique.

The desorption rate of all the ions studied was found to follow a first order Arrhenius expression, the activation energy being independent of the adsorbing species (e.g. for iodine, I_2, ICl, IBr) and dependent only upon the metal surface and the desorbing ion.

The desorption reaction is,

$$(M - I)_{surface} \longrightarrow M_{(s)} + I^-_{(g)} \qquad - \quad (8\text{-}2)$$

The activation energies for various metals are shown below,

System	Bond Broken	E_d (e.v.)	E_d^- (e.v.)
CsI - Mo	Mo - I	3.19	4.38
CsI - Ta	Ta - I	2.66	-

The high negative ion binding energies show that the adsorbed species must be in the form of a covalent metal halogen species.

The suggested mechanism of ion formation for a compound AI will be,

Adsorption,

$$AI_{(g)} + M_{(s)} \longrightarrow A_{(s)} + MI_{(s)} \qquad - (8\text{-}3)$$

(In the case of iodine A also = I)

Desorption,

$$MI_{(s)} \longrightarrow M_{(s)} + I_{(g)} \qquad - (8\text{-}4)$$

$$e_f + MI_{(s)} \longrightarrow M_{(s)} + I^-_{(g)} \qquad - (8\text{-}5)$$

This scheme does not distinguish between the ion and the atom on the surface because of the rapid interchange of the electron between the surface and the halogen.

The desorption energy of the negative ion will be given by,

$$E_d^- = E_d - E + \chi \qquad - (8\text{-}6)$$

where E_d^- and E_d are the desorption energies of the ion and neutral species respectively.

This "single state" theory was assumed in section (3) and most evidence from surface ionisation experiments tends to support this mechanism for negative ion desorption.

It is of interest to note that evidence from positive surface ionisation points to the separate existence of positive ions and neutral species on the surface.

The results were as expected for iodine ion formation on tungsten, tantalum and molybdenum but the apparent electron affinity determined using platinum filaments is not the true electron affinity of the iodine atom. It may be that the adsorption and desorption of iodine neutral species is in equilibrium with the ion emission process and energy terms, other than the electron affinity, have to be considered. The energy values obtained from the I_e/T^2 and $I_i - T^{-1}$ plots are shown in table (8-2) together with the apparent electron affinity values in the temperature range 1050 - 1600°K and using known bond energy values and the electron affinity of iodine, the interpretation of the processes leading to these values should be possible.

TABLE (8-2)

Iodine/Platinum Surface Ionisation Data

Quantity	Energy; $KJ.mole^{-1}$
χ	433
$W < 1280^\circ K$	266
$W > 1280^\circ K$	335
$E' > 1280^\circ K$	98.0
$E' < 1280^\circ K$	167

Several mechanisms may be suggested. If adsorption on the surface is not important but the dissociation of the molecule does form part of the rate determining step, then, assuming one ion is formed from one iodine molecule,

$$E' = E_I - D_{I_2} \qquad - \quad (8\text{-}7)$$

Inserting the appropriate values, the predicted value of E' is 162 KJ.mole^{-1}, in agreement with the experimental value below 1280°K.

Alternatively, if dissociation and adsorption on the surface are important, the apparent electron affinity will be given by,

$$E' = E_I - D_{I_2} + Q_I \qquad - \quad (8\text{-}8)$$

where Q_I, the heat of adsorption of an iodine atom on the platinum surface may be estimated using the method of Stevenson described in section (6-2). It is found to be 150 KJ.mole^{-1} and inserting this into equation (8-8) gives the value of E' to be 311 KJ.mole^{-1}.

It has been reported $^{(97,98)}$ that iodine (and the other halogens) form surface compounds on platinum filaments and at high temperatures ($>$1300°K) the emission of Pt(X) molecules occurs. There was no mass spectrometric evidence for this but it does seem that, as in the present experiments, "anomalous" results have often been observed during the interaction of the halogens with platinum filaments.

Using this information it seems that adsorption, with dissociation on the platinum surface, does occur and that the rate determining step may be the dissociation of the platinum-iodine surface bond. If this is the case the overall energy change will be (E – Q) and using the value for Q_I above (150 KJ.mole^{-1}) and the electron affinity found previously (310 KJ.mole^{-1}) then the expected value of E' is 160 KJ.mole^{-1}. This is in agreement with the observed value and in view of the fact that these anomalous results are only observed with platinum filaments suggests that the platinum surface is in some way involved and this latter mechanism, desorption of ions from an atomic chemisorbed layer, seems reasonable. The first mechanism, involving only dissociation, would be expected to be observed for all of the filament materials if it was important but as seen previously this is not the case.

8.4. Surface Ionisation of Methyl Cyanide, Methyl Bromide and Methyl Iodide

The surface ionisation of these compounds has been studied in order to determine the mechanism of ion formation and the effects of adsorption, either of the methyl group or the electronegative group, on the measured ion and electron currents. This section will concentrate on the extraction of apparent electron affinity values from experimental data assuming the theory outlined in section (3) is adequate.

The effect of these gases on the electron emission properties of the various filaments will be considered in more detail in sections (8-5) and (8-6).

8.4.1. Mass Identification of Ions

The major disadvantage of the magnetron method is that direct identification of the ions produced during the surface ionisation reaction is not possible as the method of mass separation employed is only capable of distinguishing electrons from the heavier, negative ions.

With more complex molecules the molecular ion may not be the only ion formed at the surface as at the temperatures employed (1100 - 2100°K) dissociation of the substrate to form separate species which may themselves attach electrons is quite feasible and has been observed (41,99).

For this reason it is desirable to carry out a mass spectrometric analysis of the ions produced at the filament in conjunction with the normal analysis of the temperature dependence of the thermionic currents. In accord with this the negative surface ionisation mass spectra of the compounds studied were determined qualitatively using an Atlas, AMP 3 quadrupole mass filter equipped with a surface ionisation source and a Faraday cup collector.

As expected, with iodine, only the singly charged I^- ion was detected and similarly in the spectra of the methyl compounds only the ions I^-, Br^- and CN^- could be detected, the CH_3^- ion, if it was formed, was below the detection limit of the mass spectrometer (and I^-, Br^-, $CN^- : CH_3^- > 10^4$).

The ion currents measured in the magnetron are therefore due to a unique ion and the temperature dependence of the corresponding current will give the apparent electron affinity of this ion.

8.4.2. Measurement of Apparent Electron Affinity

8.4.2.1. Methyl Cyanide

This compound was studied on tungsten, tantalum and platinum filaments. The bond strength of the (C-CN) bond is high (426 KJ.mole^{-1}) and from a comparison with previous magnetron work the dissociation energy of this bond would be expected to contribute to the value of the measured electron affinity, E'.

The electron affinity of the cyanide group is well known (305.4 KJ.mole^{-1} (8)) and is used later in calculations.

The experiments showed that on all of the filaments used the ion and electron currents were both exponentially dependent upon reciprocal temperature over the range 1250 - 2100°K for tantalum and tungsten filaments and 1250 - 1800°K for platinum filaments.

Typical plots are shown in figure (8-6) and a summary of the results is given in table (8-3). This shows the apparent work function (χ^{**}) obtained from plots of log (I_e/T^2) against T^{-1}, E', the apparent electron affinity and the pressure at which the determination was made.

The average work functions found for tungsten (410 KJ.mole^{-1}) and platinum (400 KJ.mole^{-1}) are slightly lower than the clean surface values but the work function of tantalum was reduced to a much greater extent. The actual value was dependent upon the exposure of the filament to methyl cyanide vapour (but not the pressure) and approached a limiting value of 360 KJ.mole^{-1}, (3.73 e.v.).

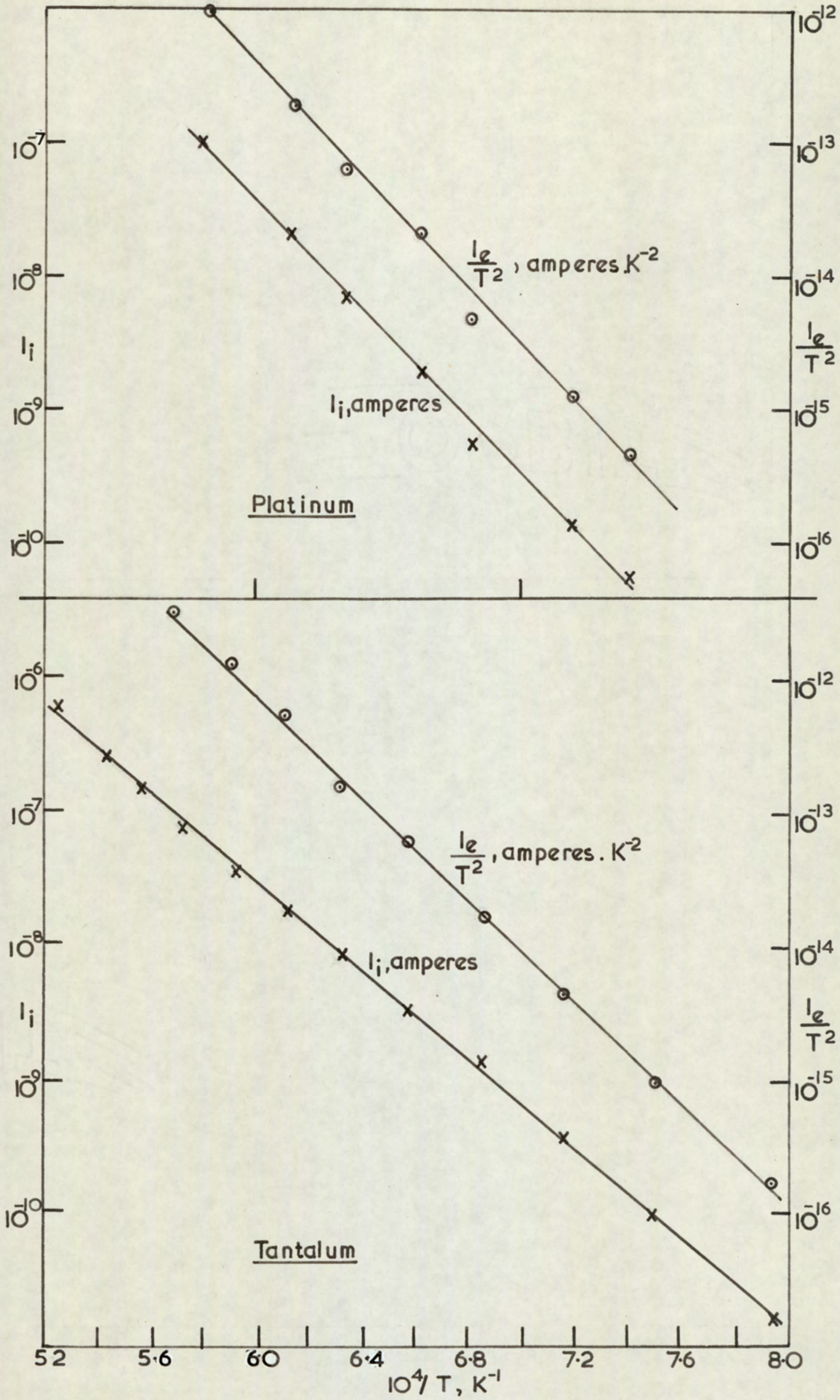

FIGURE (8-6). Methyl Cyanide – Tantalum and Platinum. Plots of I_e/T^2 and I_i against Reciprocal Temperature

TABLE (8-3)

Methyl Cyanide - Summary of Experimental Data

Filament	χ^{**} (KJ.mole^{-1})	E' (KJ.mole^{-1})	P, mm.Hg 1mm.Hg = 0.133N.m^{-2}
Tantalum	296	10.5	6×10^{-5}
	355	21.0	3×10^{-4}
	344	4.6	1×10^{-3}
	358	4.2	2×10^{-3}
	315	18.5	3×10^{-3}
	323	10.9	5×10^{-3}
Average	-	11.5 ± 3.6	-
Tungsten	395	29.3	5.6×10^{-4}
	426	16.8	2.8×10^{-3}
	406	20.9	1.0×10^{-3}
	406	13.0	1.0×10^{-4}
	410	21.0	4.8×10^{-3}
Average	410 ± 7.0	20.1 ± 3.8	-
Platinum	393	4.2	2.0×10^{-3}
	398	0.0	1.0×10^{-5}
	406	8.3	2.0×10^{-4}
	400	6.3	1.6×10^{-3}
	402	-4.2	1.0×10^{-4}
	408	-1.5	8.0×10^{-4}
Average	400 ± 3.4	2.2 ± 2.9	-

8.4.2.2. Methyl Bromide

This compound was again studied on tungsten, tantalum and platinum filaments. The bond strength of the (C-Br) bond is 292 KJ.mole^{-1} which is in the intermediate range where the rate determining step may or may not involve fission of this bond.

The semilog plots of (I_e/T^2) and I_i against reciprocal temperature were found to be linear and the apparent work function and electron affinity values derived from these plots are given in table (8-4) whilst examples are shown in figure (8-7).

The apparent work functions of platinum and tantalum were 390 KJ.mole^{-1} (4.06 e.v.) and 425 KJ.mole^{-1} (4.41 e.v.) respectively and showed no marked dependence upon exposure to methyl bromide. The apparent work function of tungsten however, showed a marked dependence on exposure to the gas although the apparent electron affinity was found to have an approximately constant value.

8.4.2.3. Methyl Iodide

The surface ionisation of this compound was studied using tungsten, tantalum, molybdenum and platinum filaments. The bond strength of the (C-I) bond is low (230KJ.mole^{-1}) and the rate controlling step for ion formation may not involve the breaking of this bond.

Semilog plots of (I_e/T^2) and I_i as a function of reciprocal temperature gave linear plots over substantial temperature ranges. The results are summarised in table (8-5) with examples of the experimental plots in figure (8-8).

Molybdenum and platinum filaments exhibited normal work functions but the apparent work functions found for tantalum and tungsten filaments showed considerable variation with the history of the filament. The temperature dependence of the ion current however varied in the same manner as that of the electron emission and the apparent electron affinity was found to be independent of these effects.

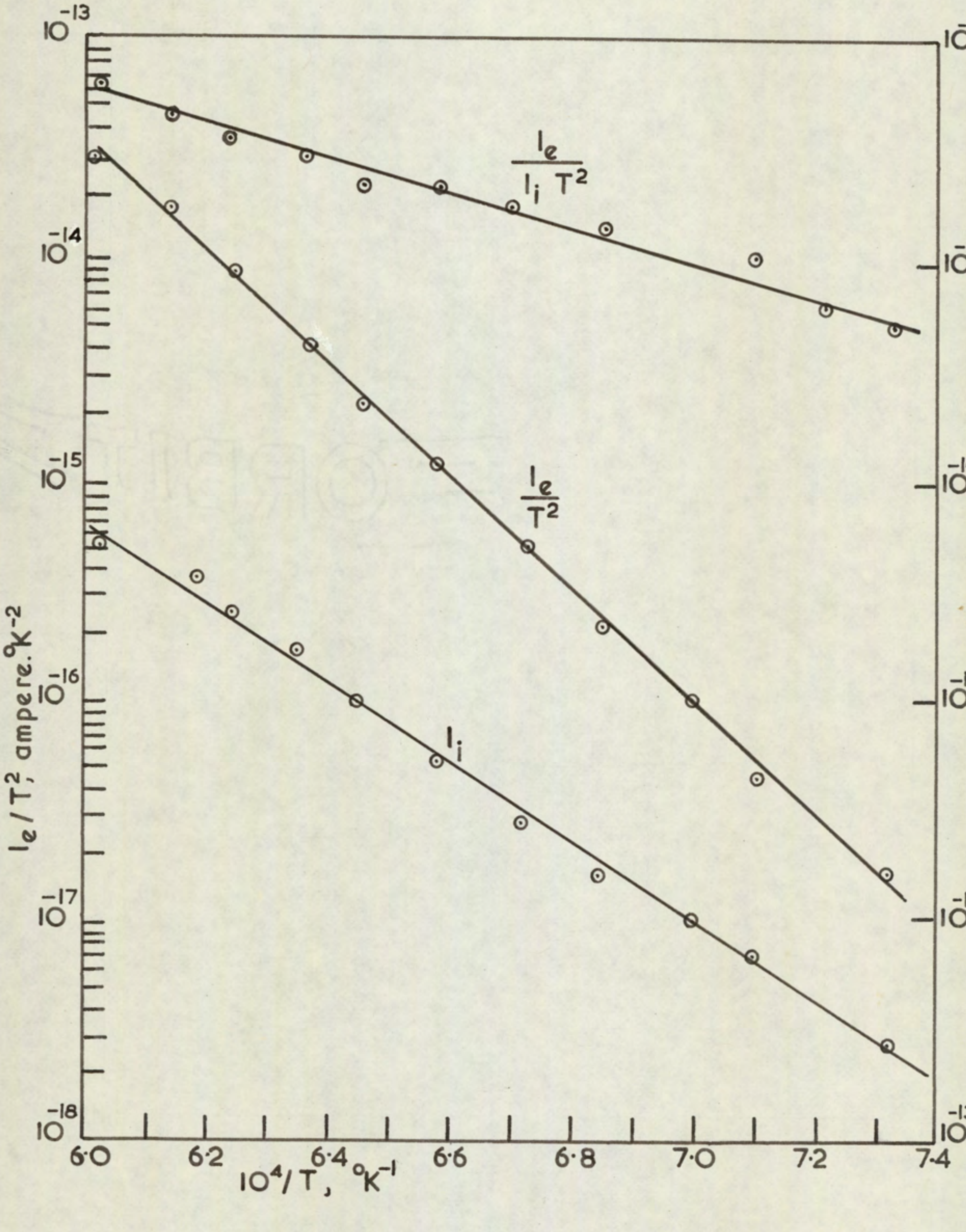

FIGURE (8-7) Methyl bromide–tantalum. Plots of I_e / T^2, I_i and $I_e / I_i T^2$ against reciprocal temperature

TABLE (8-4)

Methyl Bromide - Summary of Experimental Data

Filament	χ^{**} (KJ.mole^{-1})	E' (KJ.mole^{-1})	P, mm.Hg. 1mm.Hg = 0.133Nm^{-2}
Tantalum	435	172	5.0×10^{-4}
	410	176	4.0×10^{-4}
	394	164	1.2×10^{-3}
	444	162	8.5×10^{-5}
	426	167	1.0×10^{-4}
	439	169	1.2×10^{-4}
Average	425 ± 11.5	168 ± 2.6	-
Tungsten	448	52.4	6.0×10^{-5}
	262	83.0	6.0×10^{-4}
	287	61.0	2.8×10^{-3}
	297	65.0	4.0×10^{-3}
	329	64.2	1.0×10^{-3}
	328	60.0	3.1×10^{-3}
Average	-	64.4 ± 6.3	-
Platinum	388	49.7	6.0×10^{-4}
	394	52.3	2.5×10^{-4}
	390	39.6	1.0×10^{-3}
	394	54.4	1.5×10^{-4}
	378	46.4	1.0×10^{-3}
Average	390 ± 4.0	49.9 ± 3.8	-

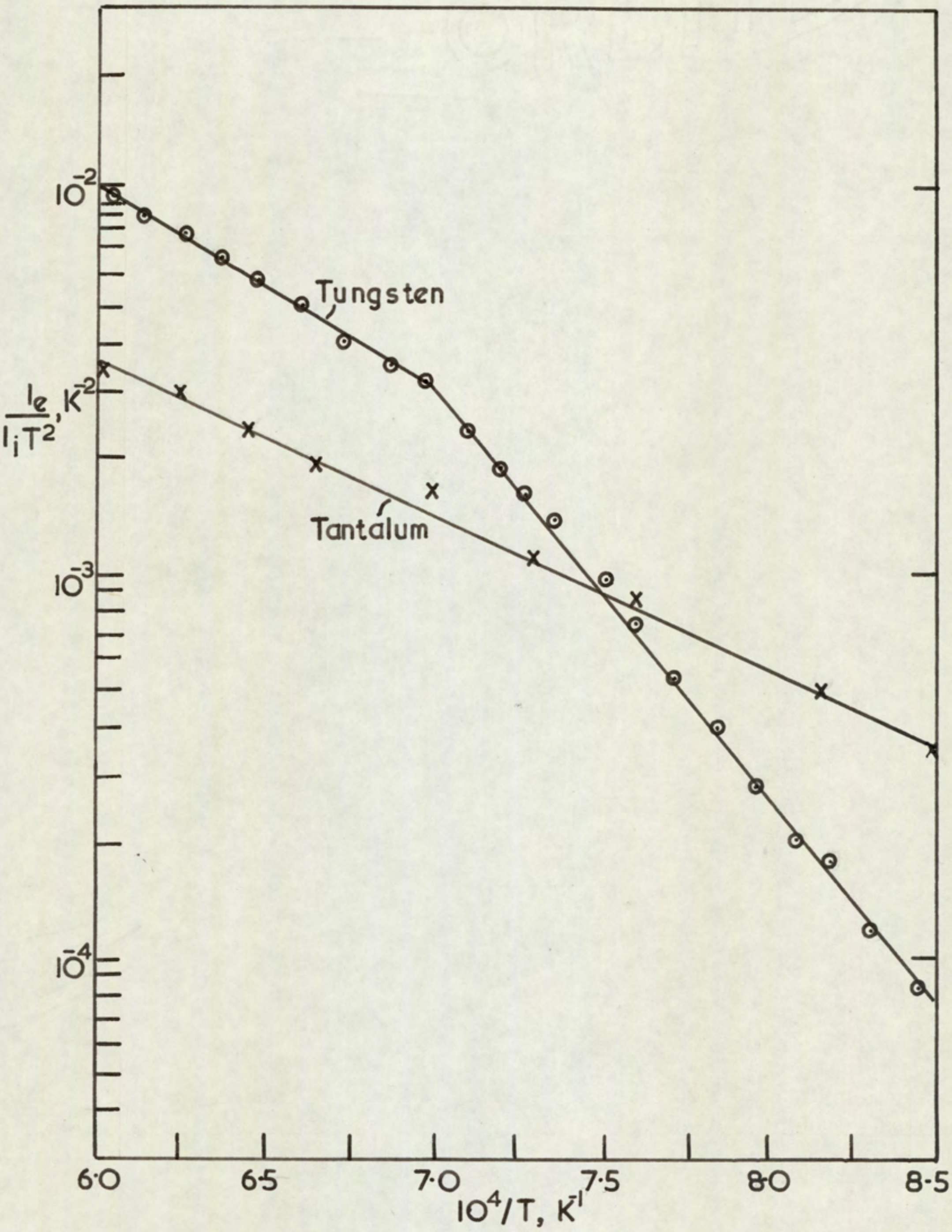

FIGURE (8-8) Methyl Iodide. Plots of $I_e/I_i T^2$ for Tungsten and Tantalum Filaments.

TABLE (8-5)

Methyl Iodide - Summary of Experimental Data

Filament	χ** (KJ.mole^{-1})	E' (KJ.mole^{-1})		P, mm.Hg 1mm.Hg = 0.133Nm^{-2}
		< 1460°K	> 1460°K	
Tungsten	422	209	92.0	5×10^{-5}
	388	184	75.0	7×10^{-5}
	415	214	87.5	8×10^{-5}
	390	195	75.2	2×10^{-4}
	401	207	71.0	1×10^{-3}
Average	402± 9	204	80.1	-
Molybdenum	438	174		1×10^{-5}
	468	186		4×10^{-5}
	440	184		1×10^{-4}
	423	197		7×10^{-5}
	440	193		1×10^{-4}
Average	442± 11	187± 5.3		-
Tantalum	254	78.1		1×10^{-5}
	271	64.8		3×10^{-5}
	276	83.7		8×10^{-5}
	293	79.5		1×10^{-4}
	258	58.3		1×10^{-4}
Average	-	71.8± 6.7		-

The apparent electron affinity values found for the iodine negative ion on these filaments was not particularly reproducible because carbide formation during the course of an experiment gave rise to changing surface conditions.

8.4.3. Discussion of Apparent Electron Affinity Values - Estimation of the Heat of Adsorption of the Methyl Radical

Table (8-6) gives a summary of the apparent electron affinity values found for the compounds CH_3I, CH_3CN and CH_3Br for the various filament materials used.

Mass spectrometric analysis (section (8-4-1)) of these systems showed that only the ions CN^-, Br^- and I^- are to be expected in any abundance from the surface ionisation of these compounds.

The dissociation energies of the CH_3-X and the CH_2X-H bonds and the electron affinities of X are shown in table (8-7). It is obvious from a comparison of these affinities and the experimental values that the rate determining step for ion emission is not the desorption of the negative ion.

As the ions formed by surface ionisation are in equilibrium with the surface and adsorption and dissociation must be occurring on the surface then a mechanism involving these steps may be postulated. Referring to figure (3-1) and equation (3-5), the apparent electron affinities for the two possible alternative mechanisms will be given by,

(a) $E' = E - D$, where dissociation of the CH_3X bond occurs with the simultaneous formation of X^- but the adsorption and desorption of the methyl radical is not involved in the overall energetics.

(b) $E' = E - D + Q$, in this case the rate determining step of the mechanism is a concerted reaction involving the simultaneous formation of X^-, breaking of the CH_3-X bond and formation of the surface-methyl bond and therefore the heat of adsorption of this radical must be included in the overall energy change.

Columns (4) and (5) in table (8-6) show the values of E' expected if mechanism (a) describes the ion formation and the value of Q_T if mechanism (b) were correct, respectively.

TABLE (8-6)

Summary of Results from the Surface Ionisation of Methyl Bromide, Iodide and Cyanide (all values in KJ.mole^{-1})

(1) Substrate	(2) Filament	(3) $E_T^\ddagger$	(4) (E–D)	(5) E'–(E–D) $Q_T(CH_3)$	(6) $Q_o(CH_3)$
CH_3CN	Ta	11.5	-122	133	118
	W	20.1	-122	142	131
	Pt	2.2	-122	124	108
CH_3Br	Ta	169	44	125	117
	W	64.4	44	–	–
	Pt	50.0	44	–	–
CH_3I	Ta	71.8	69	–	–
	W<1460	204	69	135	123
	W>1460	80.1	69	–	–
	Mo	187	69	118	109

TABLE (8-7)

Electron Affinity and Bond Energy Data for Methyl Bromide, Iodide and Cyanide (all values in KJ.mole^{-1})

Substrate	E_X	D_{CH_3-X}	D_{CH_2X-H}
CH_3Br	336	292	430
CH_3I	306	236	430
CH_3CN	305	427	430
CH_3	104	–	–

This value of Q_T, the heat of adsorption of the methyl radical at the average filament temperature, must be corrected to 0°K (8) and values are shown below for the various filaments.

Filament	Q_o (KJ.mole^{-1})
Tungsten	126
Tantalum	118
Molybdenum	109
Platinum	107

The bond strength of several atomic carbon-metal surface bonds have been estimated. The value for platinum carbide (100) is 274 KJ.mole^{-1}, whilst corresponding values for tungsten, tantalum and molybdenum are 340, 333 and 322 KJ.mole^{-1} respectively, but values for metal-methyl bonds would be expected to be considerably less than this value.

The fact that Q_o is similar for all three methyl compounds and the value for the different filament materials shows the expected trend does suggest that a similar mechanism is in operation and that this involves a metal-adsorbate bond.

If the mechanism involves dissociative chemisorption in the rate determining step then the mechanism followed would be expected to be dependent upon the strength of the CH_3-X bond. This determines the degree of dissociation of the molecule at the temperature of the filament which will be expected to be different for CH_3CN (D = 426 KJ.mole^{-1}), methyl bromide (D = 292 KJ.mole^{-1}) and methyl iodide (D = 230 KJ.mole^{-1}). High values for both $D(CH_3-X)$ and $Q_o(CH_3)$ will tend to favour a mechanism involving dissociative chemisorption.

Accordingly, the log (I_e/I_iT^2) against T^{-1} plots for methyl cyanide are linear throughout the whole temperature range (1150 -

2000°K) whereas the results for methyl bromide and iodide are strongly dependent upon the filament material used and the temperature range.

From the experimental data in table (8-6) the two mechanisms suggested may be distinguished. For methyl cyanide (Ta, W, Pt), methyl bromide (Ta) and methyl iodide (W, $<$ 1460°K; Mo) mechanism (b) is followed and a value for the heat of adsorption of the methyl radical is obtained. It has been predicted $^{(64)}$ that Q_o should be dependent upon the heat of sublimation of the metal and this trend is observed ($W > Ta > Mo > Pt$).

This type of mechanism was also suggested by Ritchie and Wheeler $^{(101)}$ who have studied the surface ionisation of several methyl compounds on tungsten. The compounds studied were CH_3NO_2, CH_3I, CH_3CN and CH_3NH_2 but no mass spectrometric analysis was carried out to determine the major ions present.

This is vitally important with nitromethane and methylamine because of the possibility of more than one ion being formed (NO_2^-, NO^-; NH_2^-, NH^-) and also, in the latter case, because the CH_3 and NH_2 groups have almost identical electron affinities (104 and 107 KJ.mole^{-1} $^{(8)}$) and therefore might be expected to make comparable contributions to the total ion current.

The results for methyl iodide show marked disagreement with Q_o $^{(\text{Ritchie \& Wheeler})}$ = 200 ± 10 KJ.mole^{-1}. However, the results for methyl cyanide are directly comparable and recalculating Ritchie and Wheeler's result for methyl cyanide, using the accepted value of the electron affinity of the cyanide group, gives $Q_o(CH_3)$ on tungsten to be 150 ± 10 KJ.mole^{-1}. Although this agreement is not good it may be accounted for, as may possibly the methyl iodide result, by the different methods of preparing and properties of the polycrystalline surface.

For methyl bromide (W, Pt) and methyl iodide (Pt, Ta; W, $>$ 1460°K) the experimental value of E' approximates to the calculated value of (E - D) and it appears that mechanism (a) is followed.

There is some evidence for the existence of a surface methyl group. During the study of the surface ionisation of γ picolene$^{(105)}$ (4-methyl pyridine) a peak was observed which could only be attributed to the CH_3O^- ion (m/e = 31.0).

This peak was observed initially but disappeared after prolonged heating of the filament, suggesting that the ion is formed from a surface methyl group and oxygen and oxide impurities which are gradually removed. This is direct evidence for at least the transient existence of a surface methyl group.

It has also been shown that the initial reaction in the adsorption of methane, the reaction to form CH_3(ads) and H(ads) (in this case I(ads)) is rapid, whilst the further reaction, $CH_3(ads) \longrightarrow CH_n(ads)$, (where n = 2,1,0) is slow.

8.5. Pressure Dependence of Thermionic Currents

8.5.1. General Considerations of Pressure Measurement

The experimental relationship between the ion current and the pressure can be written in the form,

$$\log I_i = \log P^x + C \qquad - \quad (8\text{-}9)$$

where C is a constant. Experimental values of x are given in table (8-8).

The experimental slope of the ion current-pressure plots will however depend to some extent upon the method chosen to measure the pressure. For example, in a Penning discharge gauge the true pressure is related to the ion current in the gauge by the relationship,

$$I_+ = Kp^n \qquad - \quad (8\text{-}10)$$

The actual value of k and n will depend upon the gauge and the ambient gas and the gauge will only read the true pressure for the gas (usually dry air) for which it has been calibrated. The extent of the error must be determined experimentally.

Three types of gauge were used to cover the pressure range 10^{-7} - 1 mm.Hg; a Penning discharge gauge, a Pirani gauge and a "Baratron" capacitance bridge gauge. The Penning gauge, useful in the range 10^{-4} - 10^{-7} mm.Hg depends for its operation upon the

TABLE (8-8)

PRESSURE DEPENDENCE OF ION CURRENTS

Filament / Substrate	Tantalum	Tungsten	Molybdenum	Platinum
I_2	1.16	1.2	1.2	1.25
MeCN	0.89	0.95	-	0.80
MeBr	0.92	1.00	-	0.95
MeI	0.97	0.98	0.95	1.00

ionisation of gas molecules in an unstable plasma discharge and the relation between the true and indicated pressures is more likely to depend upon the chemical characteristics of these molecules than the other gauges used.

The Baratron gauge, useful in the range 1 x 10^{-5} mm.Hg, is a differential pressure gauge, requiring an auxiliary vacuum system, but the sensitivity of the gauge depends only upon the number of gas molecules striking a flexible diaphragm (one arm of a capacitance bridge) and is therefore relatively insensitive to the actual gas species, depending only on the quantity $(M)^{-\frac{1}{2}}$.

The Pirani gauge, useful in the range 10^{-1} - 5 x 10^{-4} mm.Hg, operates again on a bridge principle, but in this case a resistance bridge, one arm of which is heated (120°C). The heat conduction away from the filament and hence its resistance will depend upon the pressure of gas surrounding the filament.

For the gases used in these experiments the coincidence of the indicated pressures of the Pirani and Baratron gauges, which only depend upon physical characteristics, was close, whereas the Penning gauge showed pressures at variance (– 50%) with these above 1 x 10^{-4} mm.Hg.

8.5.2. Iodine

The pressure dependence of the iodine negative ion currents for a series of temperatures and for different filaments is shown in figures (8-9) to (8-12) for tungsten, tantalum, molybdenum and platinum respectively.

In the region where the ion current is linearly dependent upon the pressure the following slopes were obtained,

Ta - I_2; 0.94, 1.30, 1.35, 1.00, 0.95; average 1.16 amp.mm.Hg^{-1}

Pt - I_2; 1.40, 1.20, 1.15, 1.18; average 1.23 amp.mm.Hg^{-1}

The slopes for tungsten and molybdenum were more difficult to estimate because at low iodine pressures, below the value at

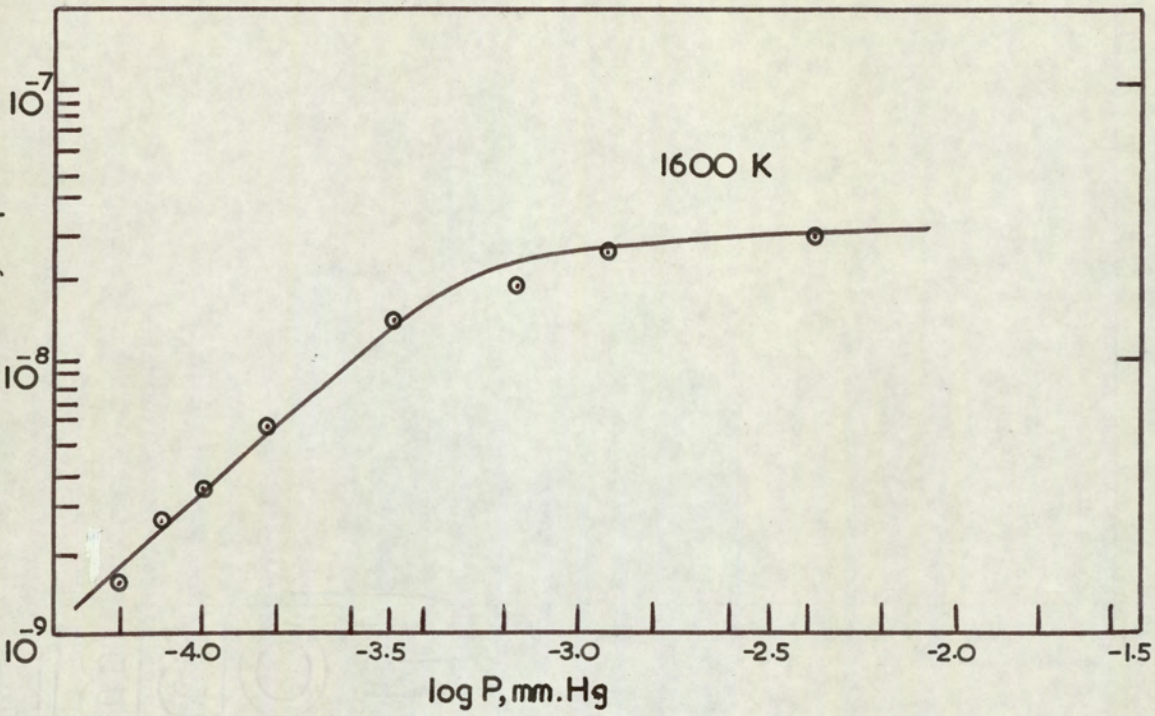

FIGURE (8-9) Iodine-Tungsten. Pressure Dependence of Ion Current

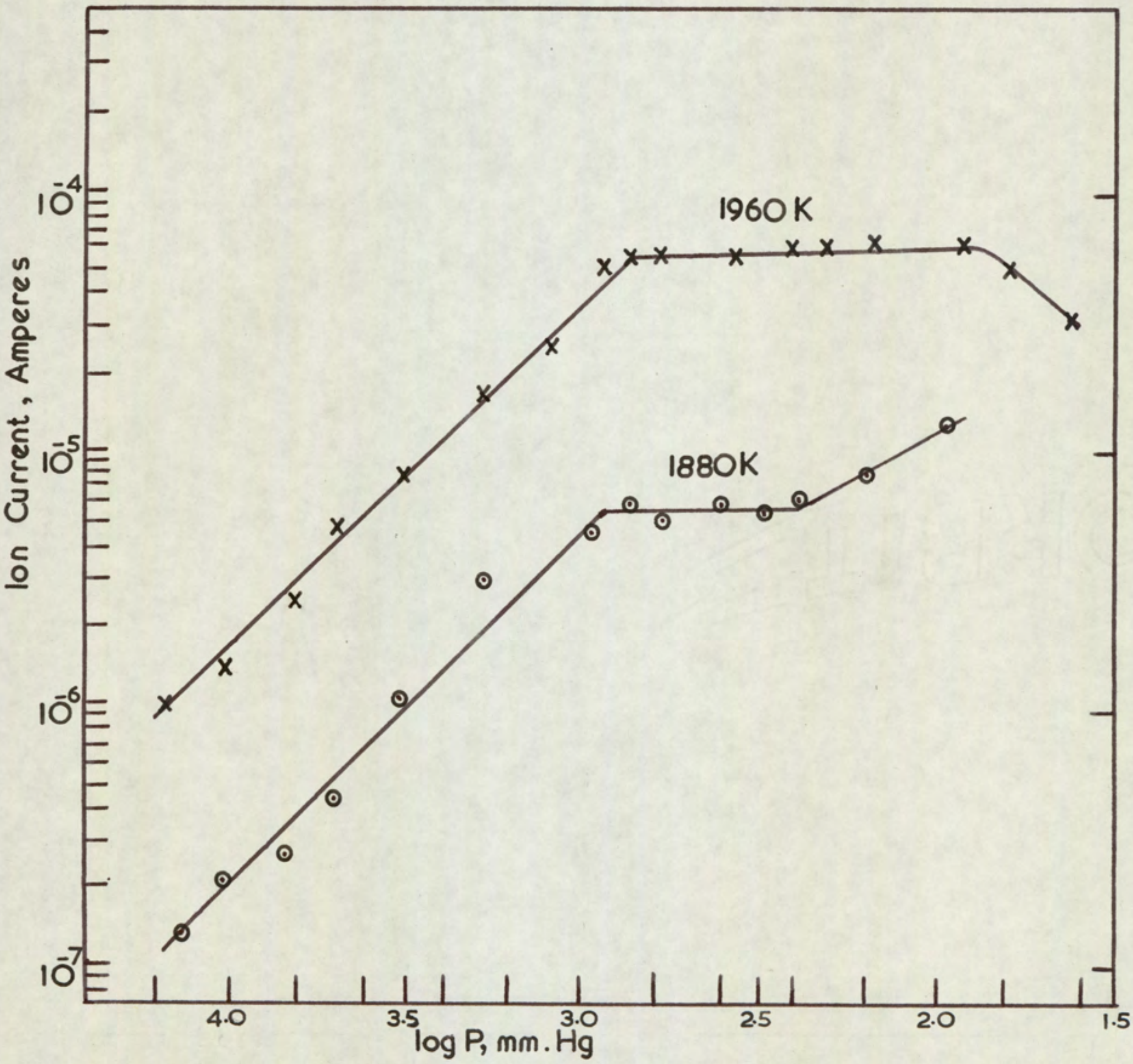

FIGURE (8-10) Iodine - Tantalum. Pressure Dependence of Ion Current

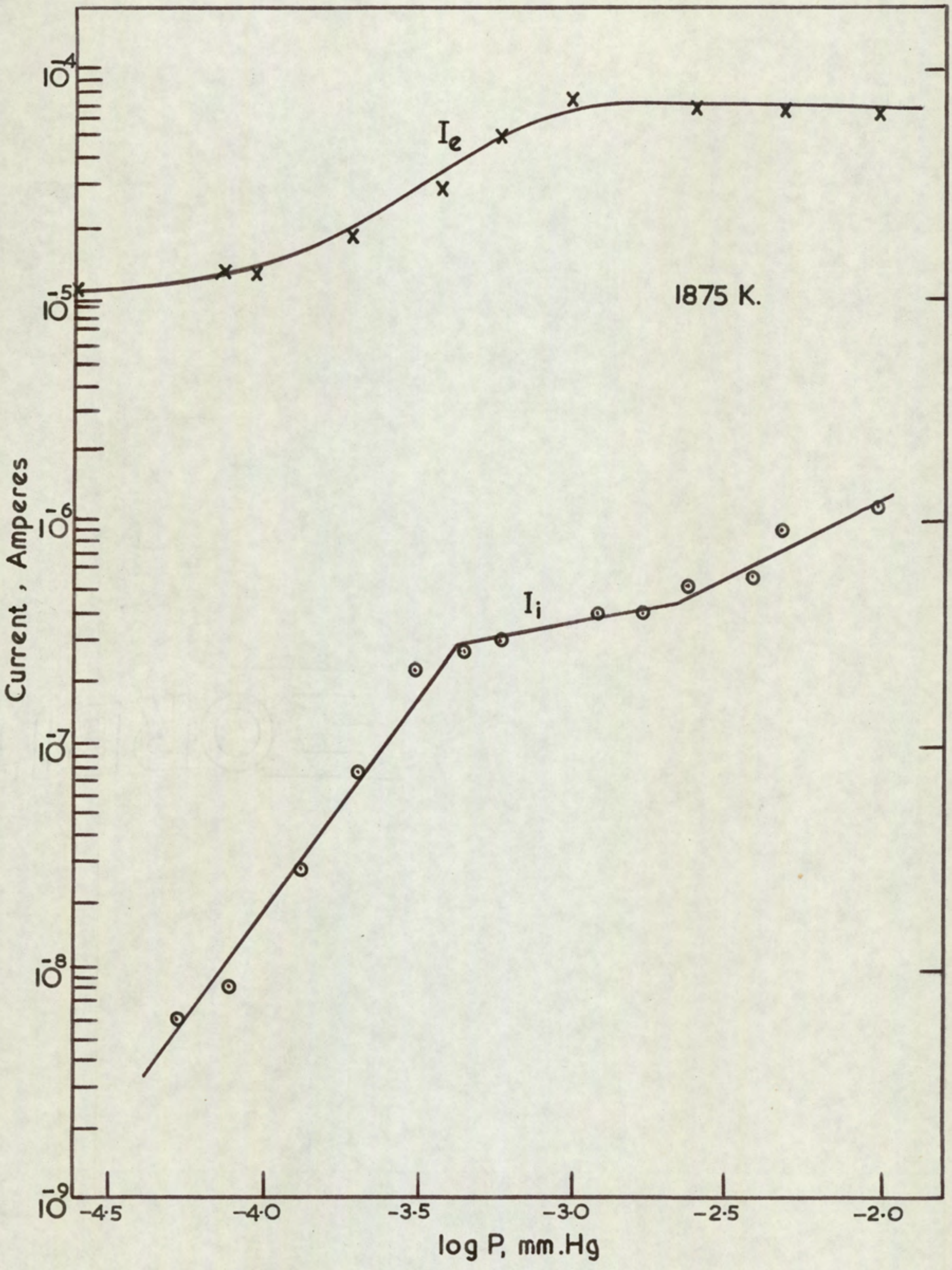

FIGURE (8-11) Molybdenum - Iodine . Pressure Dependence of Ion and Electron Currents

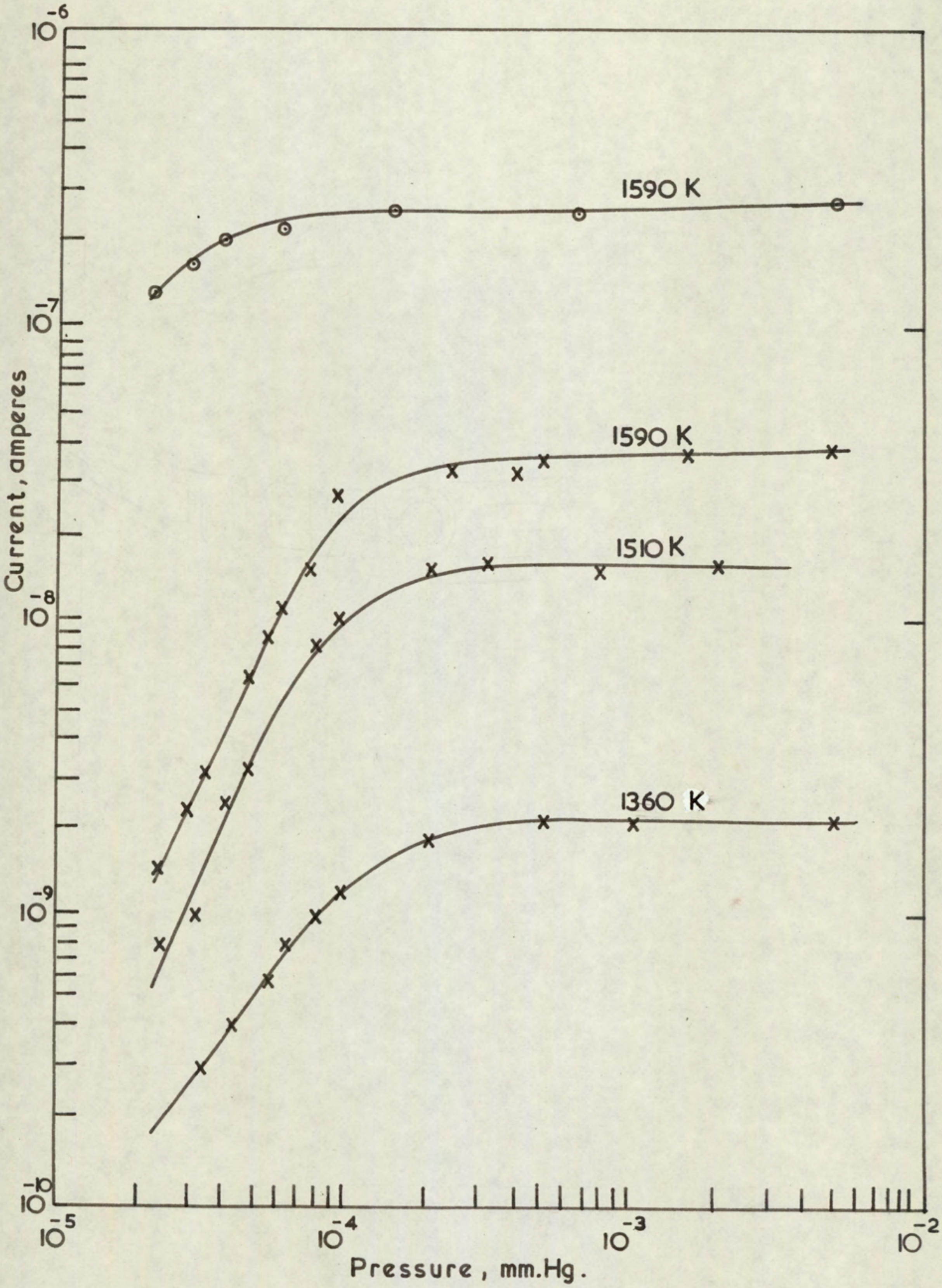

FIGURE(8-12). Iodine – Pressure dependence of ion (X) and electron (⊙) currents emitted from a platinum filament which the knee in the ion current occurred, the electron current was also found to decrease. The work function is therefore increasing and hence the ion current decreases more rapidly than expected. If this decrease in work function is taken into account, then for W-I_2 and Mo-I_2 the value of dI_i/dP is found to be 1.2 amp.mm.Hg.$^{-1}$.

8.5.3. Methyl Cyanide

These plots, several of which are shown in figures (8-14) and (8-15) were of a similar form to the iodine plots with a linear region of characteristic slope up to a pressure of 4 x 10^{-3} mm.Hg, whilst above this pressure the ion current showed no pressure dependence. The inflexion point occurred at a similar point for the tantalum, tungsten and platinum filaments.

The actual slopes were 0.89 for tantalum, 0.95 for tungsten and 0.82 for platinum. This suggests that ion formation is occurring via a similar mechanism for all three filaments and that again log I_i is directly proportional to log P, the error in the exponent being due to the different gauge sensitivity for air and methyl cyanide.

An interesting, though not readily explainable, phenomenon was observed for methyl cyanide on platinum. This is shown in figure (8-16). It was found that if the temperature of a new filament did not exceed 1400°K and methyl cyanide was allowed into the system at some temperature below this, then as the pressure was increased a maximum in the ion and electron currents was observed at 3 x 10^{-5} mm.Hg (the ion current increased by up to two orders of magnitude). This effect was quite reproducible and repeatable for different platinum filaments as long as the temperatures did not exceed 1400°K but heating above this caused an irreversible change and the maximum could no longer be detected. This could be due to an irreversible structural change or the desorption above this temperature of some surface impurity which reacts with the methyl cyanide.

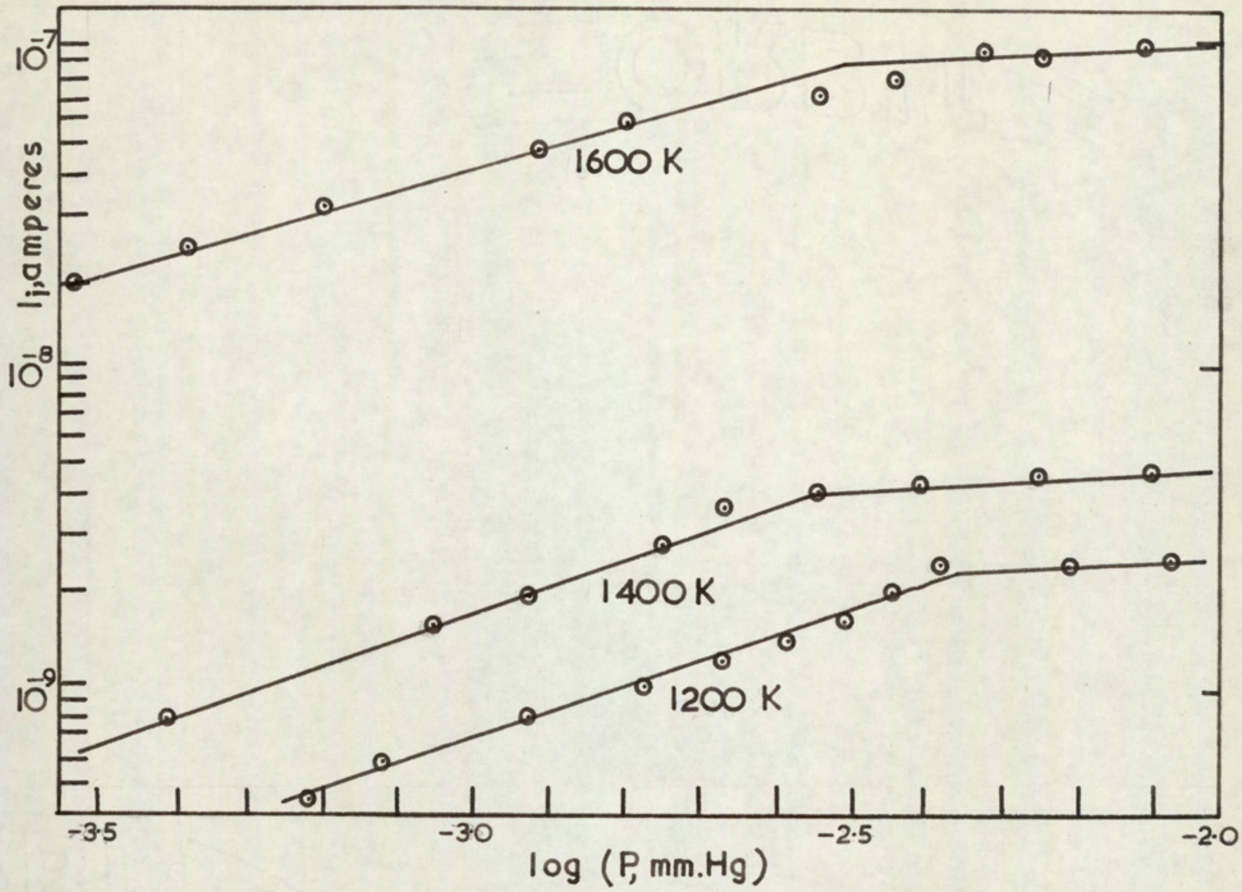

FIGURE (8-14) Methyl Cyanide-Tantalum Pressure Dependence of I_i

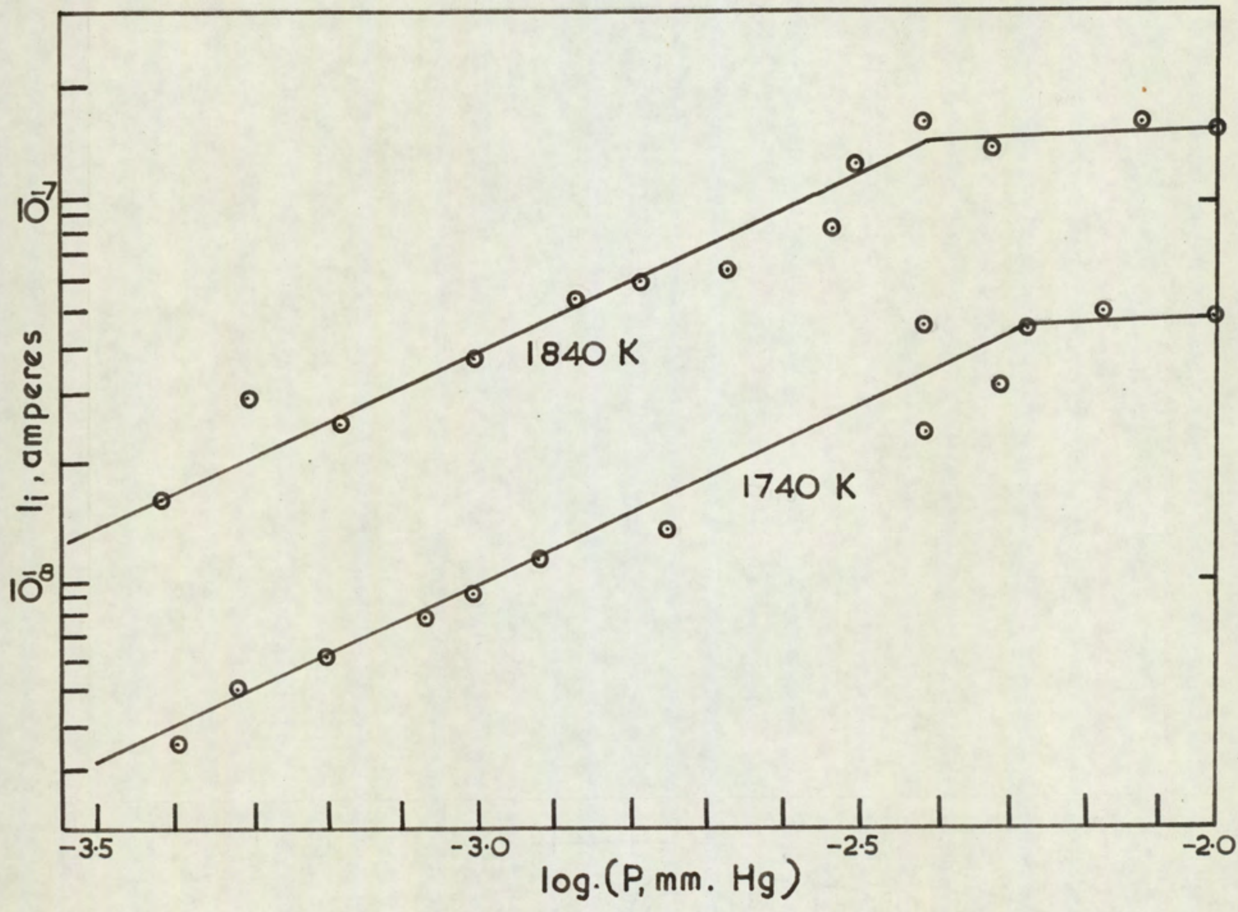

FIGURE (8-15) Methyl Cyanide-Tungsten. Pressure Dependence of I_i

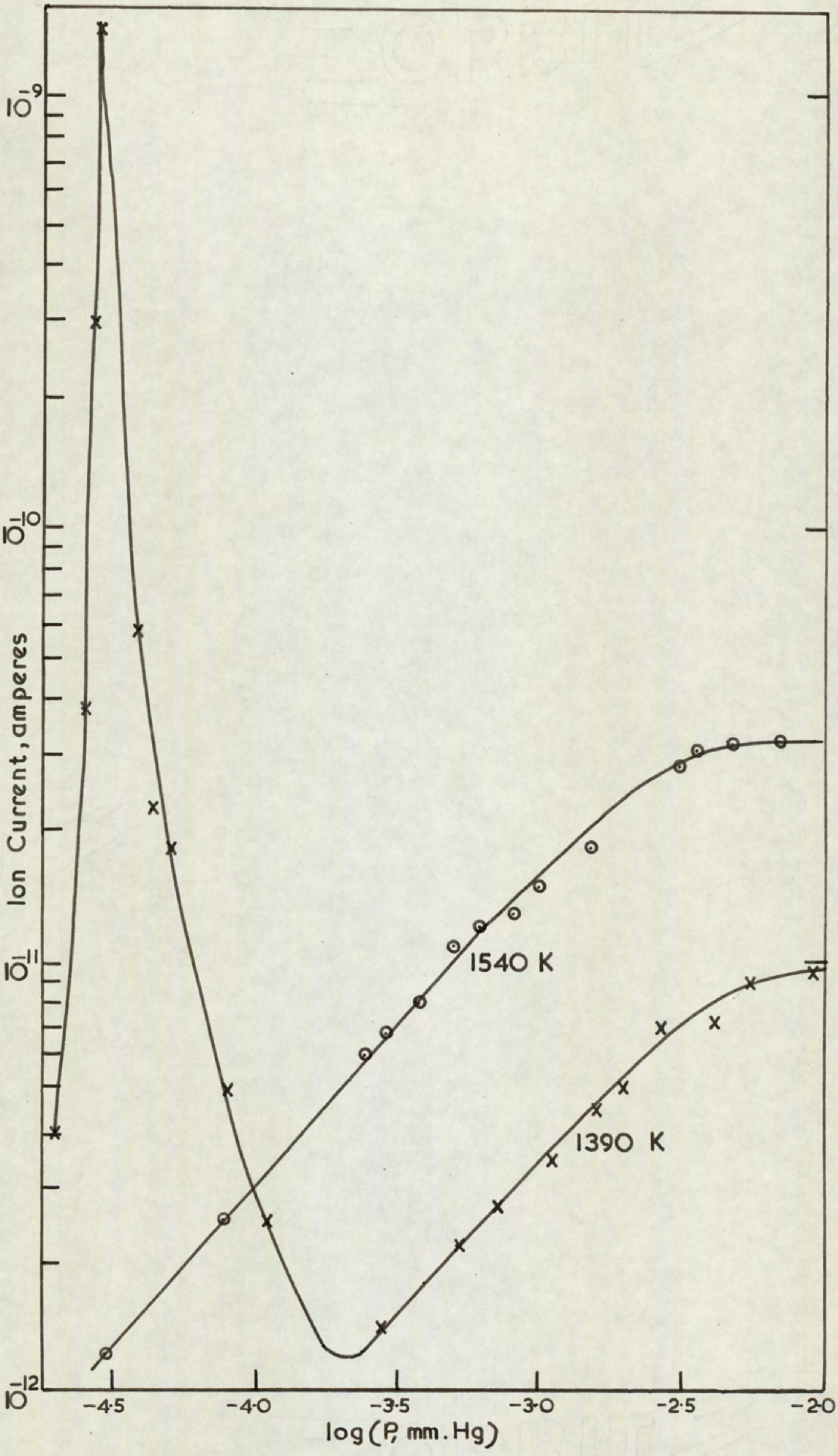

FIGURE (8-16). Methyl Cyanide-Platinum. Pressure Dependence of Ion Current

8.5.4. Methyl Bromide

8.5.4.1. Methyl Bromide on Tantalum, Tungsten and Platinum Filaments

These results were quantitatively similar to the methyl cyanide results, slopes of (dI_i/dP) of approximately unity being observed for the different filament materials. The actual values were tungsten, 0.95; tantalum, 0.92 and platinum, 0.95. No maxima similar to that observed for the thermionic currents from platinum filaments when methyl cyanide was introduced could be detected.

Plots are shown in figures (8-17) for tungsten and (8-18) for tantalum where it can also be seen that the electron current is sensibly independent of the pressure of methyl bromide in the experimental pressure range.

8.5.4.2. Methyl Bromide on Tantalum Carbide Filaments

Initial experiments were obtained on pure metal filaments which, after suitable heat treatment and recrystallisation, do not readily form a carbide. The results below were obtained using a tantalum carbide filament produced by heating a new tantalum filament in the vapour of methyl bromide.

The pressure dependence of the thermionic currents shown in figure (8-19) was found to be similar to that for the TaC-MeI system. It can be seen that the electron current is sensibly independent of pressure until a certain critical pressure, which is temperature dependent, is reached and it then decays exponentially with time.

The ion current, below 1.5×10^{-3} mm.Hg, was found to be linearly dependent upon the pressure (slope, $dIi/dP = 1.05$ amp.mm.Hg^{-1}) until this same critical pressure was reached at which point it also decayed exponentially with time.

The rates of decay of the thermionic currents were not studied in great detail but the current-time plots were similar in form and gave similar rate constants to those determined for the TaC-MeI system which was studied in greater detail.

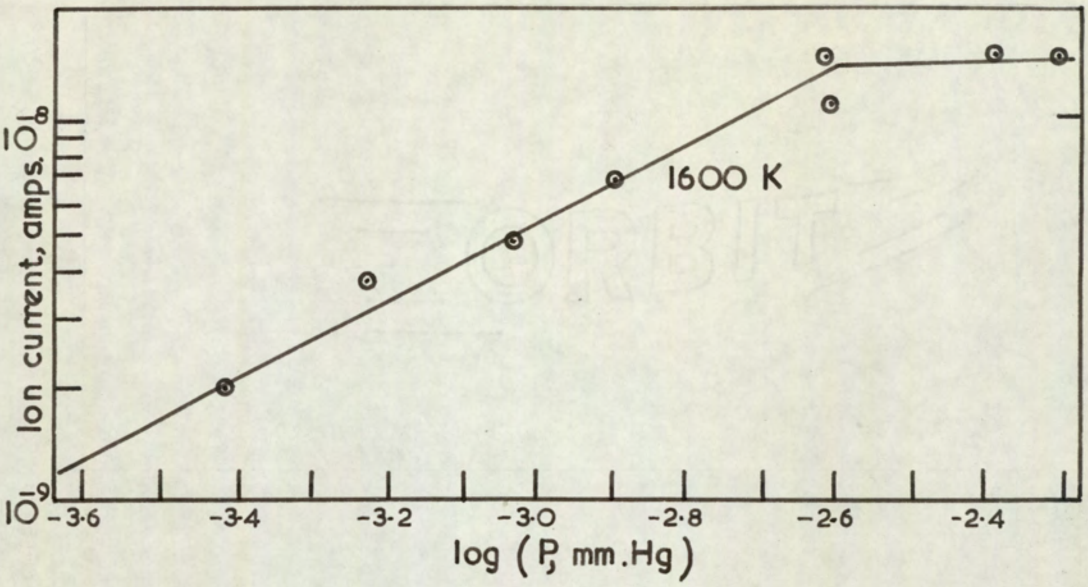

FIGURE (8-17) Methyl Bromide - Tungsten. Pressure Dependence of Ion Current

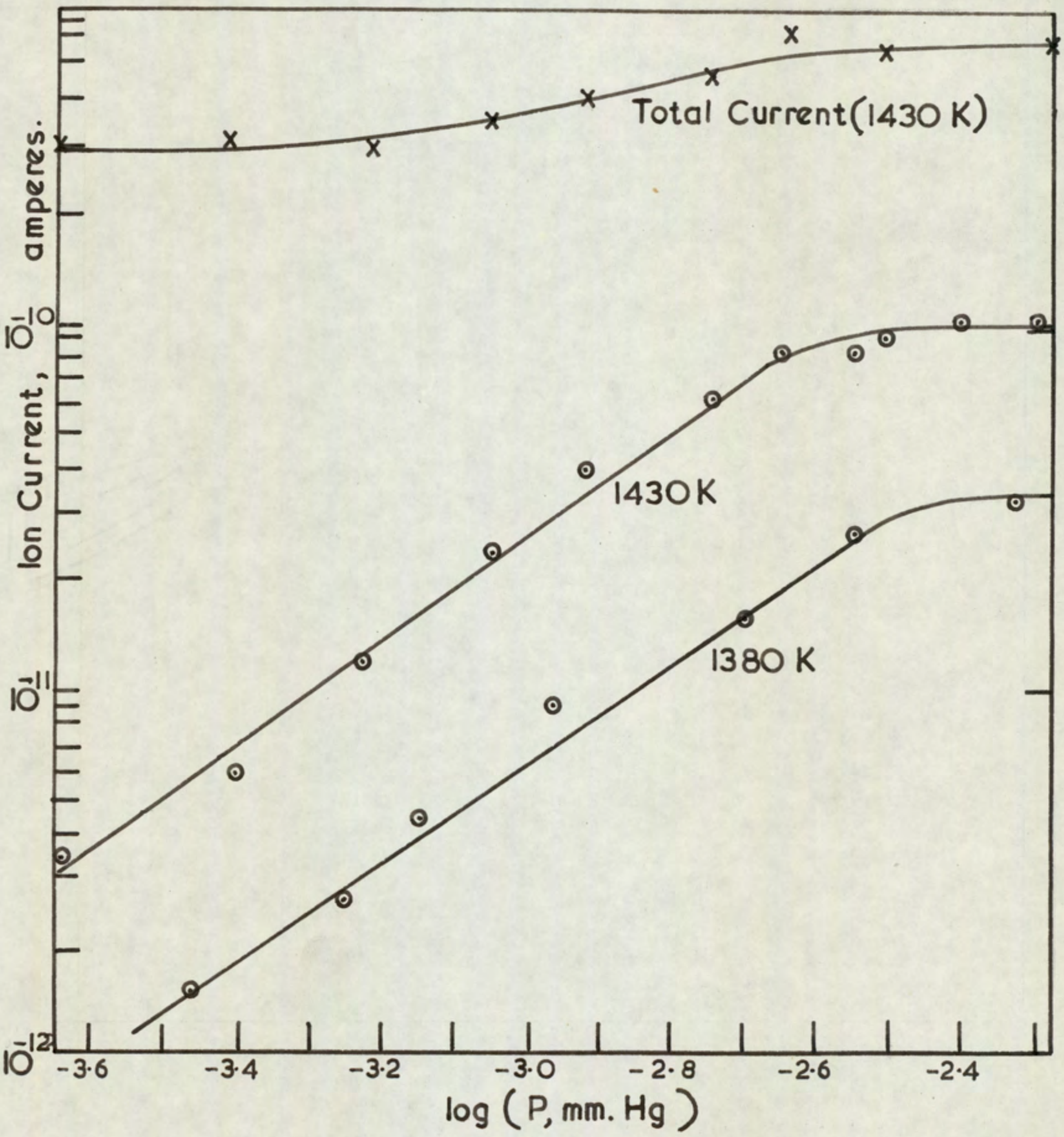

FIGURE (8-18) Methyl Bromide - Tantalum. Pressure Dependence of Ion Current

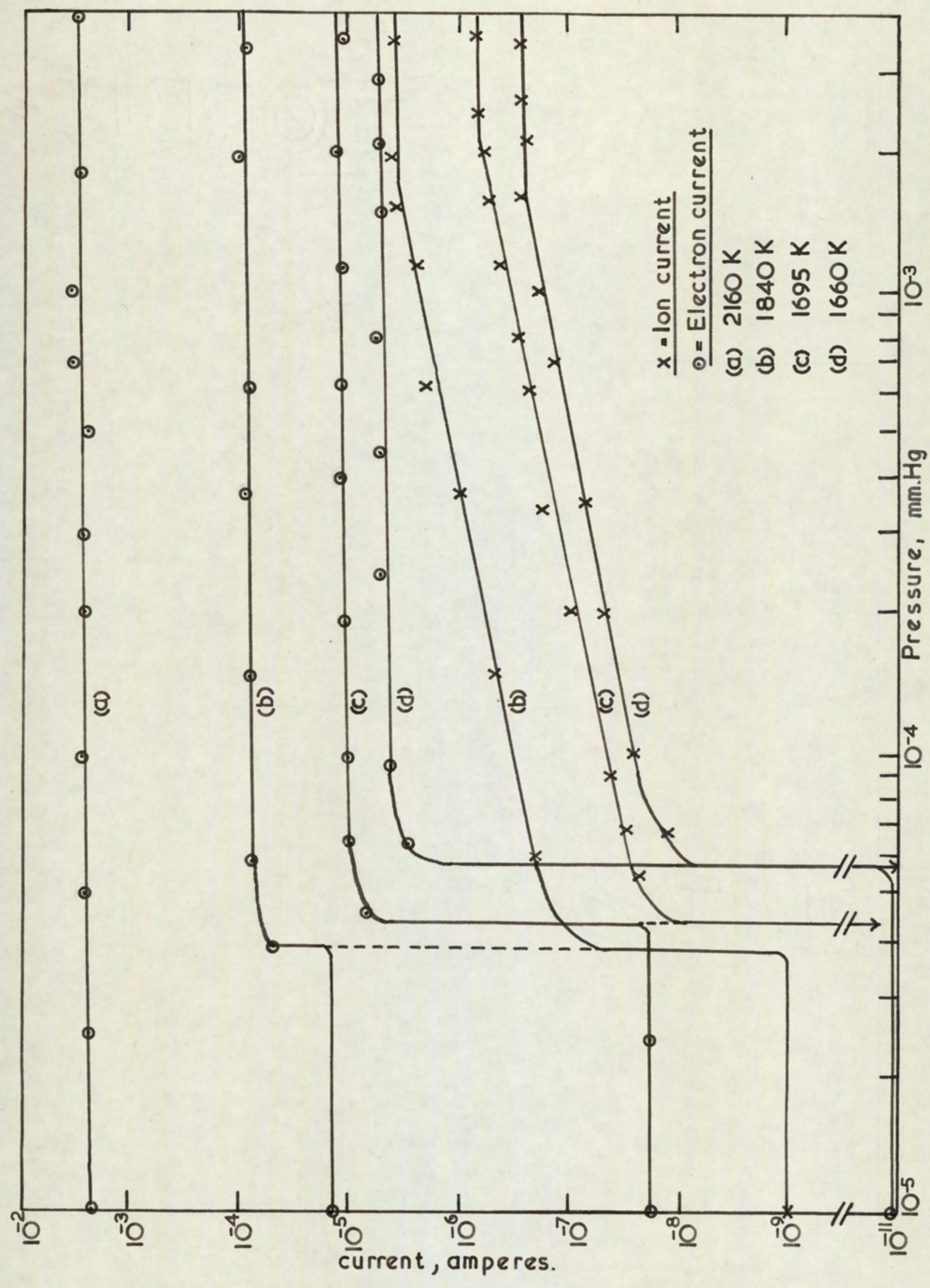

FIGURE (8-19) Methyl Bromide-Tantalum Carbide. Pressure Dependence of Thermionic Currents

8.5.5. Methyl Iodide

8.5.5.1. Pressure Dependence of Thermionic Currents

These results were similar to the other methyl compounds on tungsten, platinum and molybdenum filaments although saturation was not attained until higher pressures. The observed values of dI_i/dP were 0.98 (W), 0.97 (Mo) and 1.00 (Pt) and typical results are shown in figure (8-20).

The results obtained using tantalum filaments however show a considerable dependence upon the pretreatment of the filament.

If the filament was cleaned, outgassed and recrystallised in vacuo and then the methyl iodide admitted, results very similar to those above were obtained. This is shown in figure (8-21), the pressure dependence of the ion current giving a slope of 0.97 amp.mm.Hg^{-1}.

The electron current was found to be pressure dependent below 10^{-4} mm.Hg^{-1} but the change was small, corresponding to an effective work function change of $\lessapprox$ 20 KJ.$mole^{-1}$.

If however a new filament was cleaned and outgassed in methyl iodide vapour, the electron emission was found to be increased and if the pressure dependence of the thermionic currents was studied different behaviour was observed. If the pressure dependence was studied by decreasing the pressure in a stepwise fashion then it was found that at a certain critical pressure a drastic decrease in the thermionic currents occurred. The opposite effect was observed by increasing the substrate pressure and a small hysteresis effect was present if the process was carried out cyclicly. This is shown in figure (8-22) and is believed to be due to a kinetic effect, the hysteresis diminishing with increasing duration of the experiment. The critical pressure was found to be temperature dependent, as shown in figure (8-23) for various plots at different temperatures.

8.5.5.2. Kinetics of the Decay of the Ion and Electron Currents

The kinetics of change in the thermionic emission currents were studied further by two different methods.

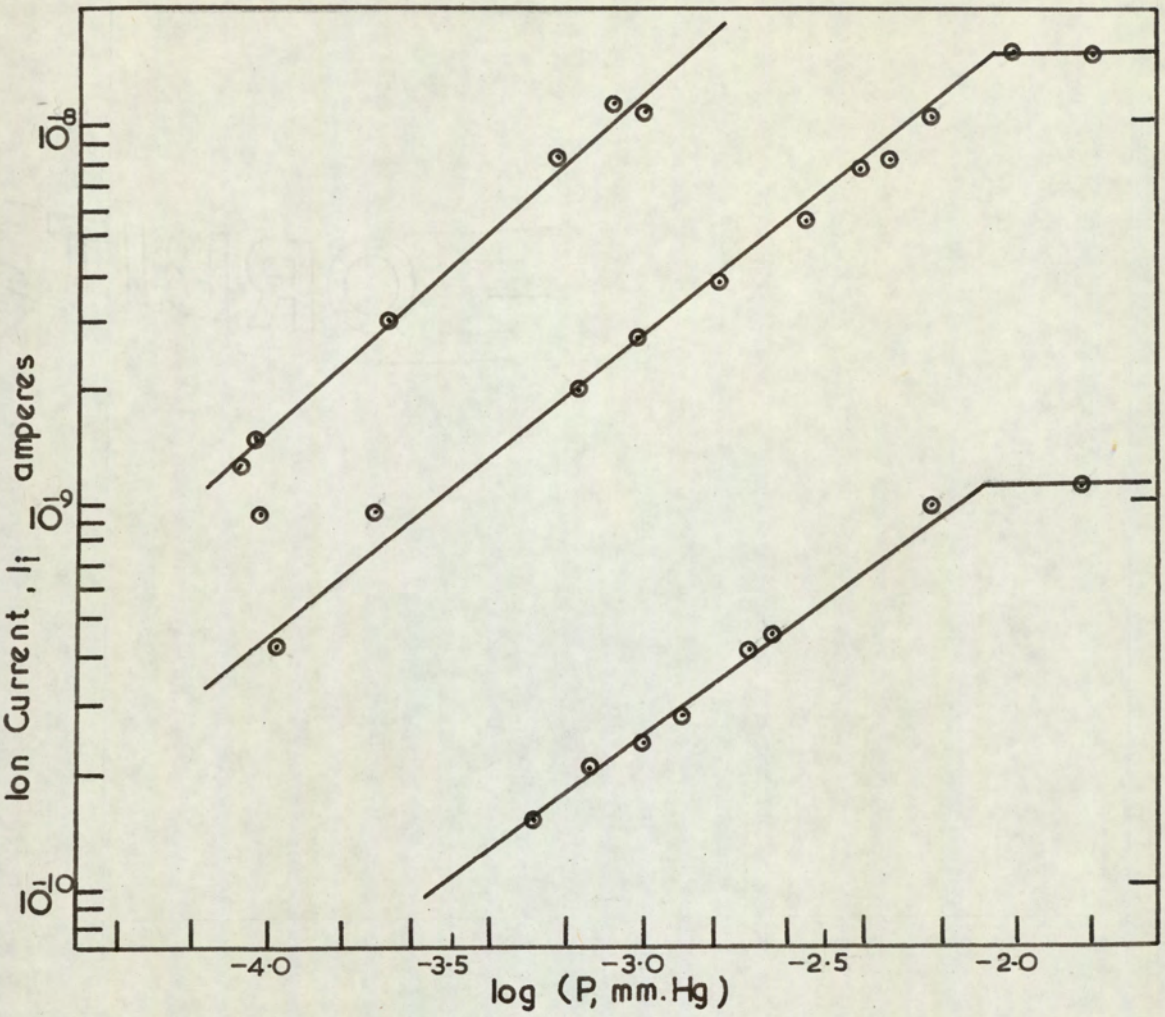

FIGURE(8-20) Methyl Iodide-Tungsten. Pressure Dependence of Ion Current

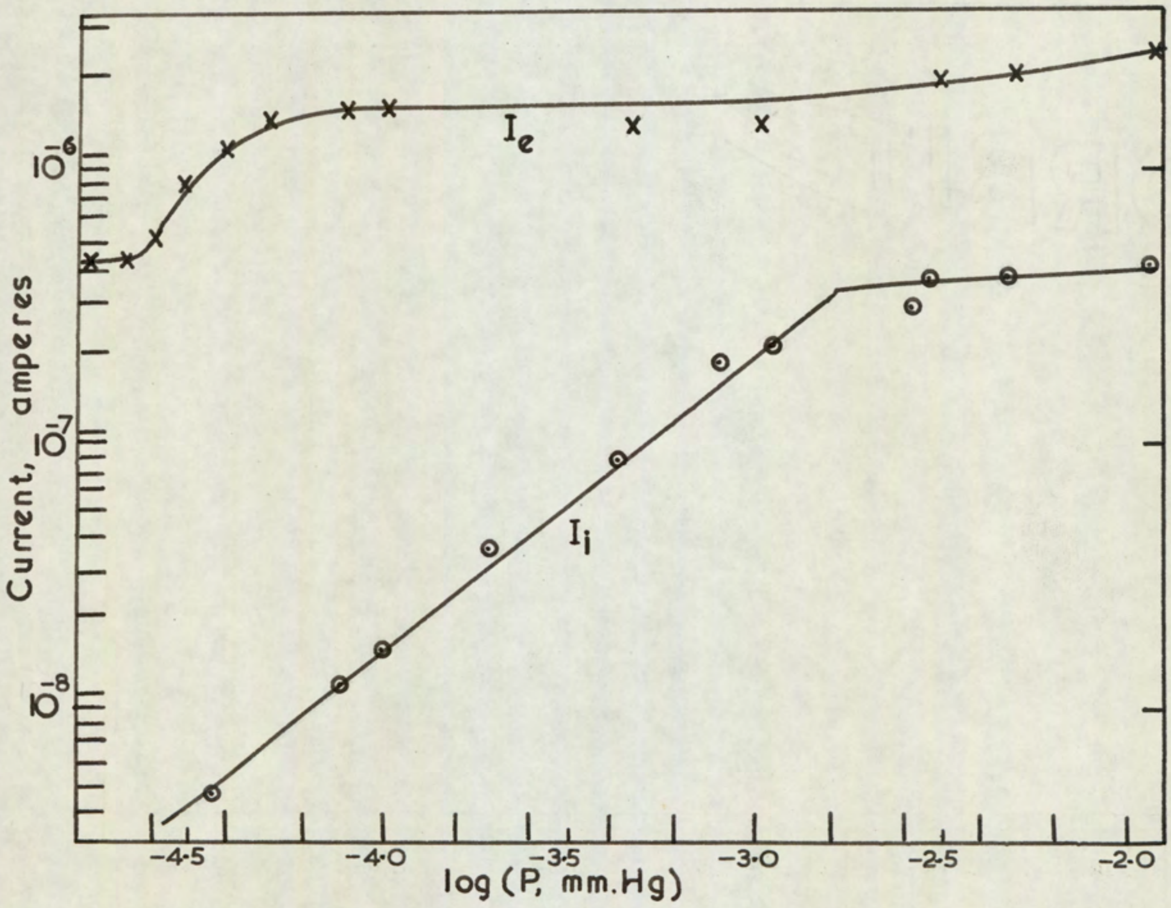

FIGURE (8-21) Methyl Iodide-Tantalum. Pressure Dependence of Thermionic Currents

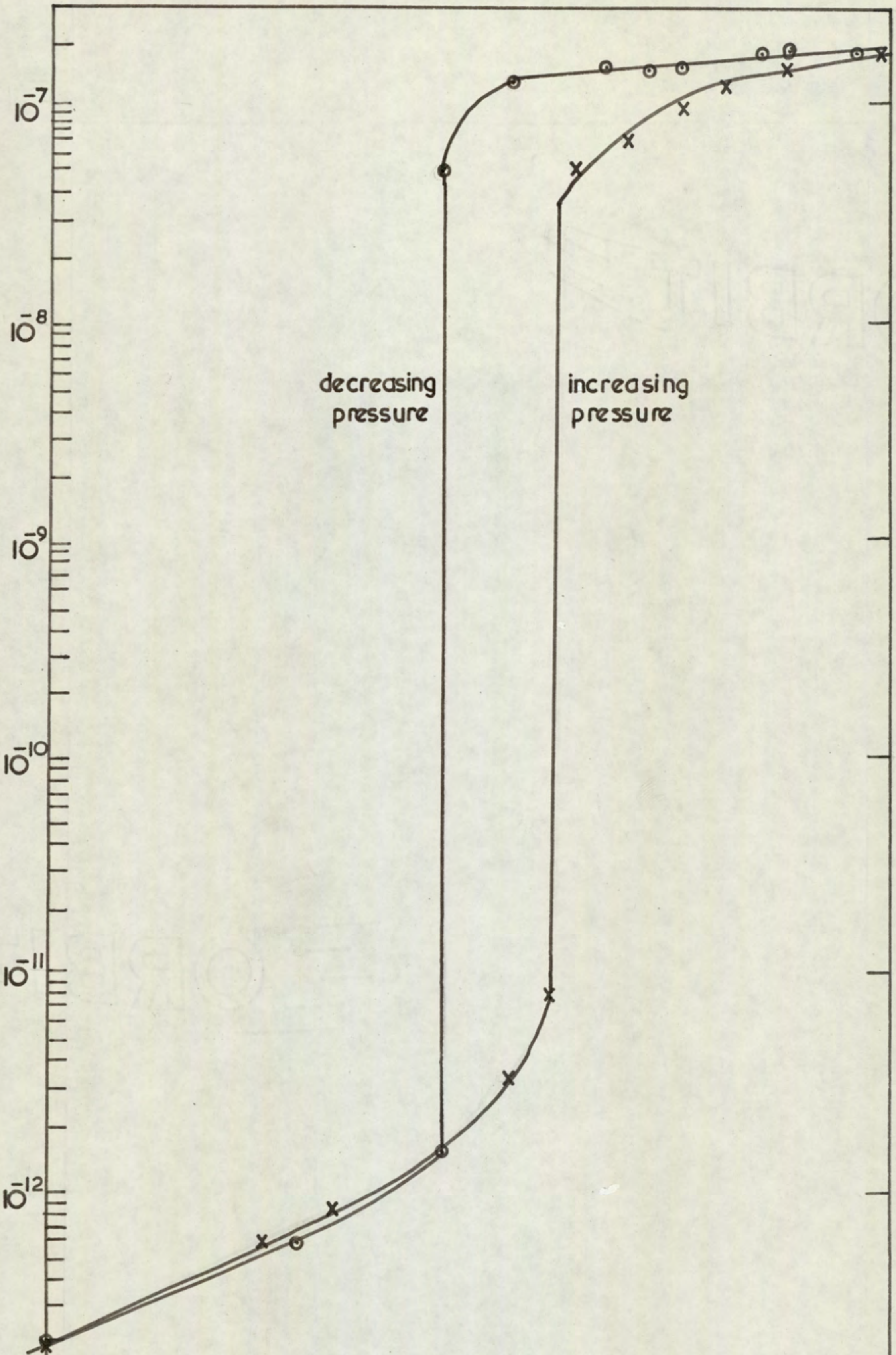

FIGURE (8-22) Methyl Iodide – Tantalum Carbide. Pressure Dependence of Thermionic Current showing Hysteresis Effect

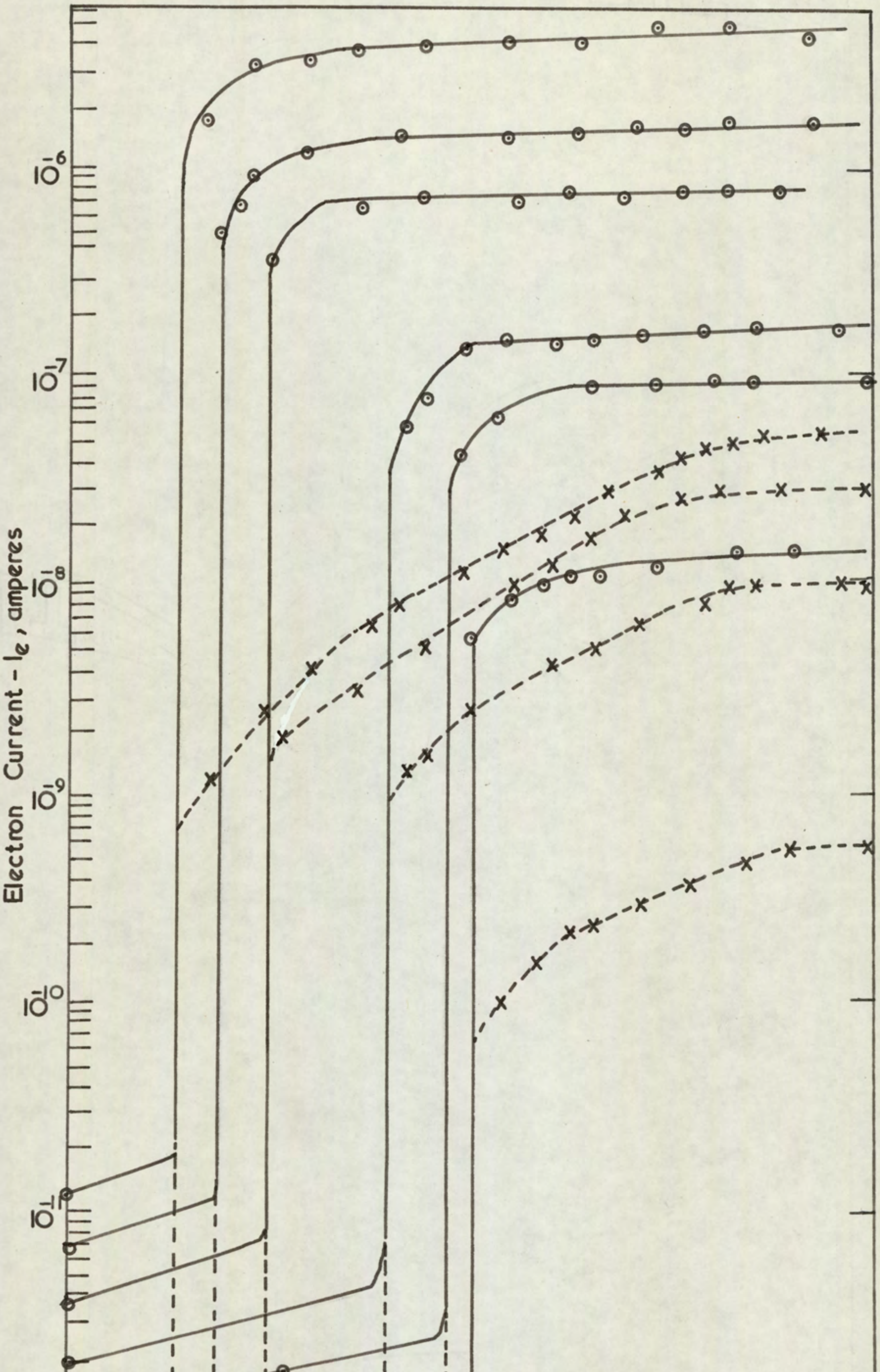

FIGURE (8-23) Methyl Iodide-Tantalum Carbide. Pressure Dependence of Thermionic Currents at Various Temperatures

In the first method the decay of the ion and electron currents was followed by slowly decreasing, at a constant rate, the pressure of methyl iodide until a value was reached at which these currents became time, as well as pressure, dependent. The pressure was then held constant at this value and the decay of the current followed using a combination of an AVO D.C. amplifier and a chart recorder. These results are shown for various temperatures in figures (8-24) and (8-25) for the electron and ion currents respectively. The analysis of these results is complicated as the ambient pressures (and hence the equilibrium surface concentrations) as well as the temperature are different for each set of results.

These currents showed the opposite (but not mirror image) type of behaviour when the pressure was increased from the background value to a pressure at which saturation occurs. An example is shown in figure (8-26).

In order to remove the complications mentioned above a different experimental method was employed. At each temperature the filament was saturated (I_e and I_i both independent of pressure) with gas. The flow of gas was then rapidly interrupted and the pressure reduced to the background value.

Initial experiments showed the rates of decay for both electron and ion currents were more rapid than in the previous experiments and it was necessary to construct a measuring system with a more rapid response. This system consisted of an integrated circuit logarithmic D.C. amplifier (Analogue Devices type 755P) used in conjunction either with an oscilloscope or a chart recorder. The plots obtained from such a system will yield directly, for a first order reaction, the rate constant.

It was decided to concentrate on the decay, rather than the increase in the thermionic currents for several reasons. Plots obtained of these currents when the pressure was increased were found not to be simple first order, as were the decay plots. There was an initial rapid increase, followed by a rather slower

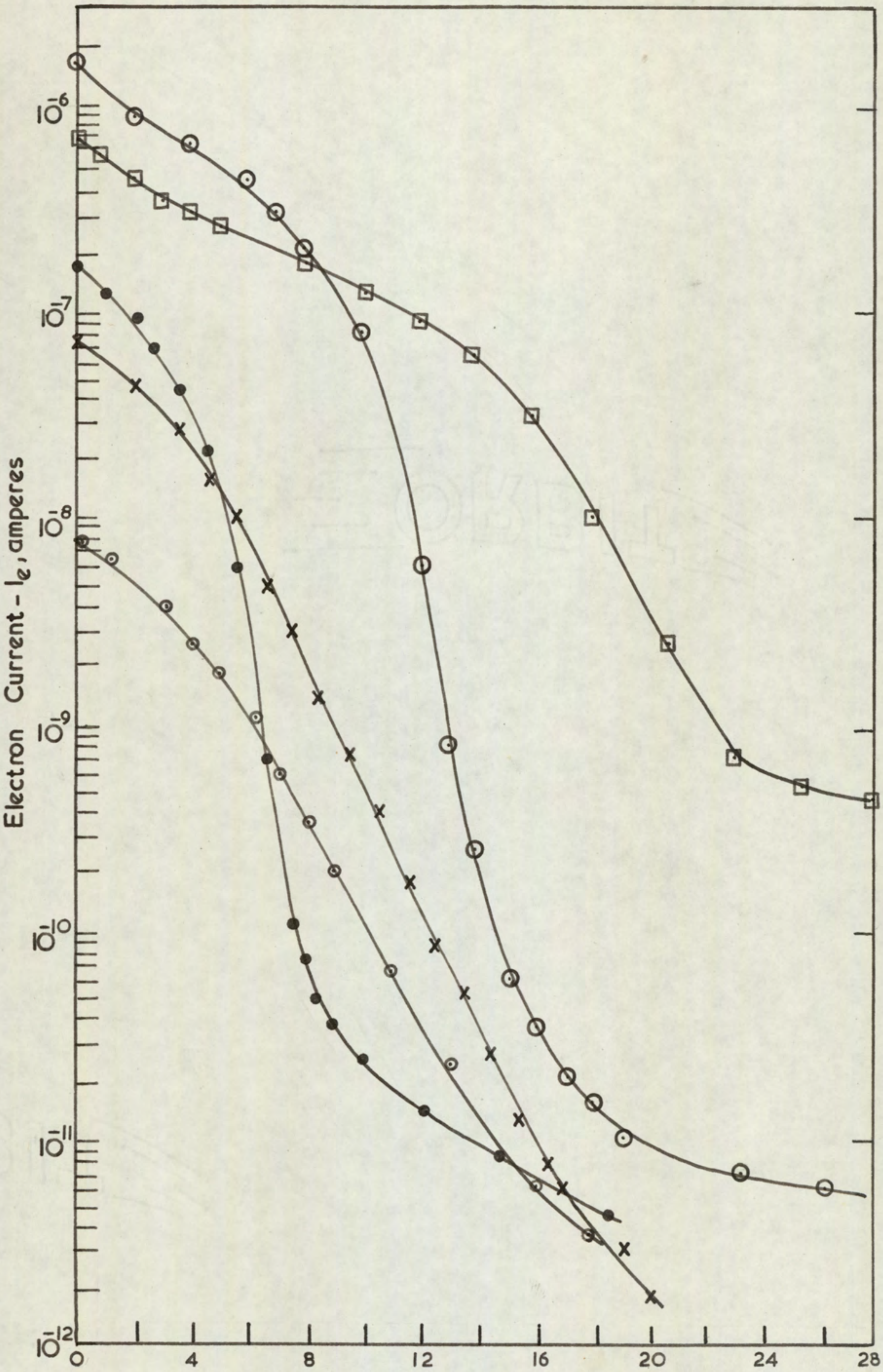

FIGURE (8-24) Methyl Iodide - Tantalum Carbide. Time Dependence of Electron Current at Critical Pressure

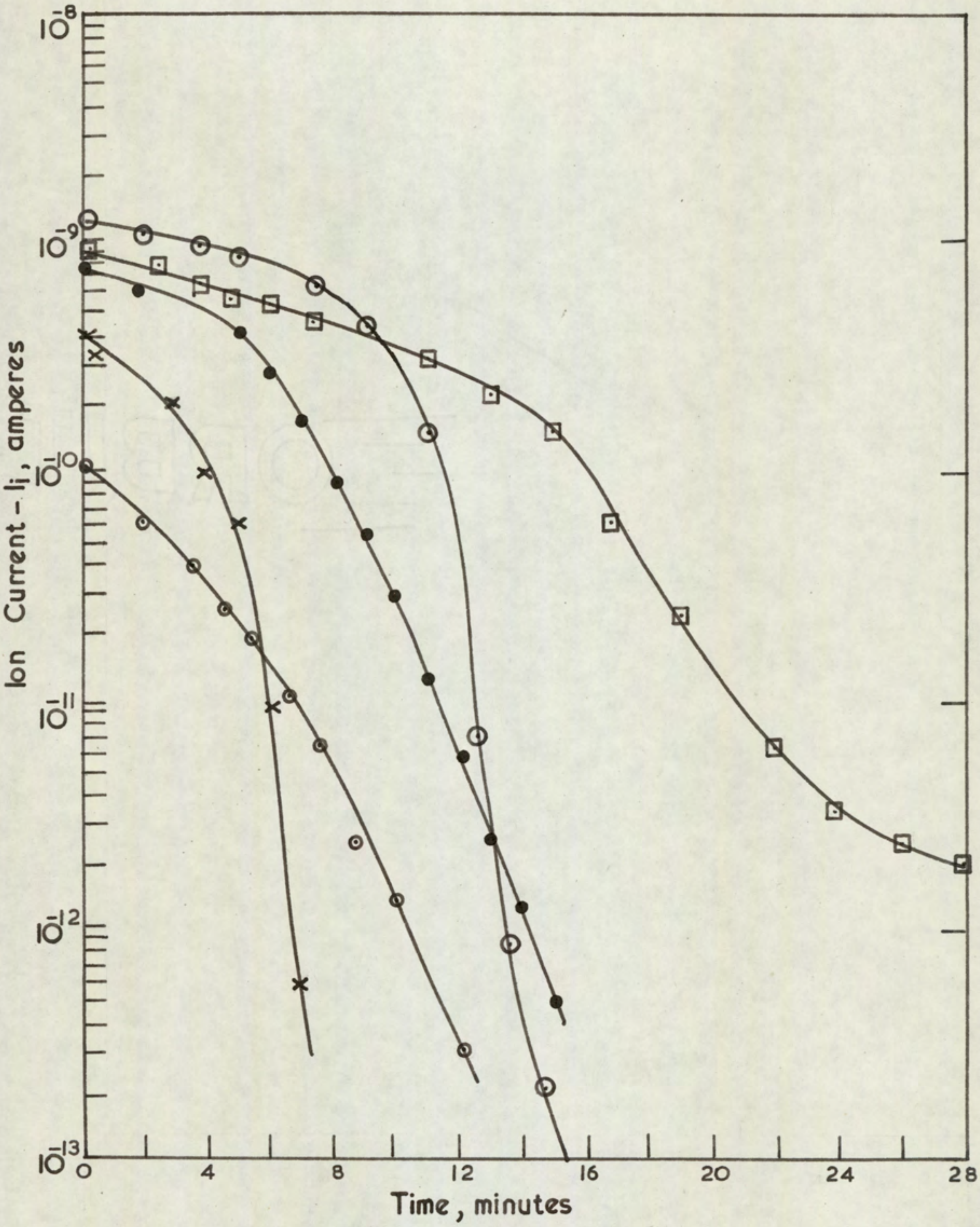

FIGURE (8-25) Methyl Iodide – Tantalum Carbide. Time Dependence of Ion Current at Critical Pressure

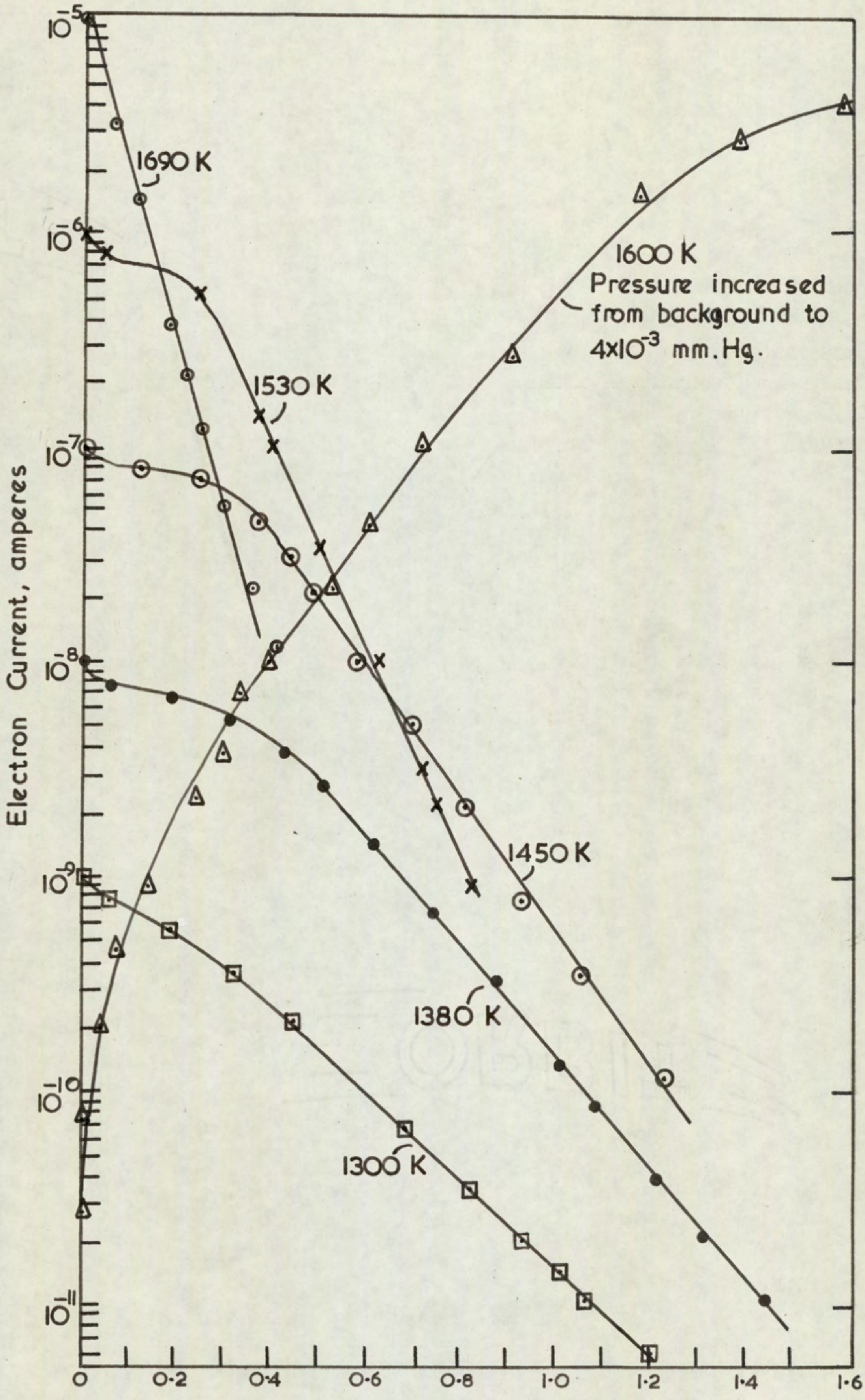

FIGURE (8-26) Methyl Iodide - Tantalum Carbide. Time Dependence of Electron Current increase, neither region yielding a linear log (I_e) - t plot. Also experimentally it was difficult to increase the pressure from the background level (where it is also difficult to ensure a reproducible background condition) to a given pressure, at a constant repeatable rate.

It was found convenient to follow the decay of the electron current using the chart recorder in conjunction with the logarithmic amplifier. Experiments were carried out at different temperatures and these showed that after an initial induction period the reaction was first order. Several plots of log I_e against time are shown in figure (8-26) and using the rate constants for a series of such plots the activation energy may be obtained from a plot of log k against T^{-1}. An example is shown in figure (8-27) and the average for several plots was 163 ± 10 KJ.mole^{-1}.

A similar series of experiments were carried out to determine the decay kinetics of the ion current. This current was found to decay much more rapidly than the electron current ($\leqslant 1$ sec. for completion) and therefore an oscilloscope, with facilities for photographic recording was employed. Examples of the traces obtained are shown in figure (8-28). It can be seen that again, after an initial induction period, these plots of log I_i against time are linear. The rate constants obtained from these semilog plots are shown in figure (8-29) plotted as a function of T^{-1}.

The decay of the ion current will depend upon many factors. The rate of ion production depends upon the surface concentration of ion precursors which will normally be an equilibrium value depending upon the pressure of gas above the surface. When the gas pressure is reduced to its background level the equilibrium surface concentration will be correspondingly lower. However, the rate of removal of gas phase species is of a similar magnitude or slower than the rate of decay of the ion current. A further complication to the analysis of this rate data is that the rate of desorption of negative ions depends upon the work function of the surface which has previously been shown to be changing during the experiment.

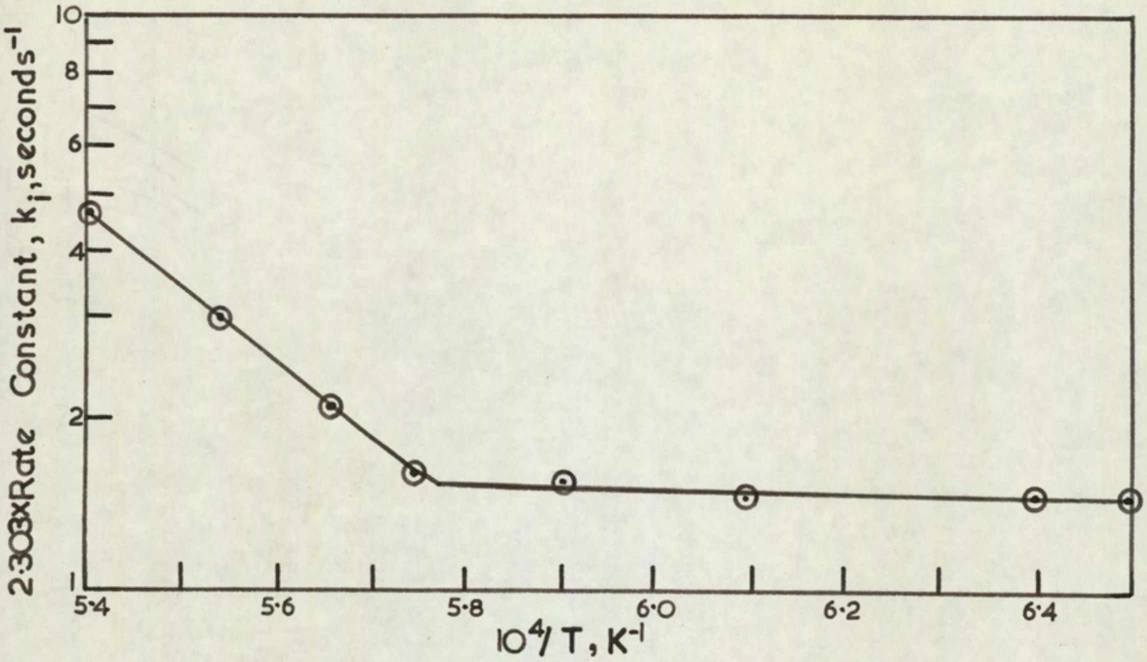

FIGURE (8-29) Rate Constant for Decay of Ion Current against T^{-1}

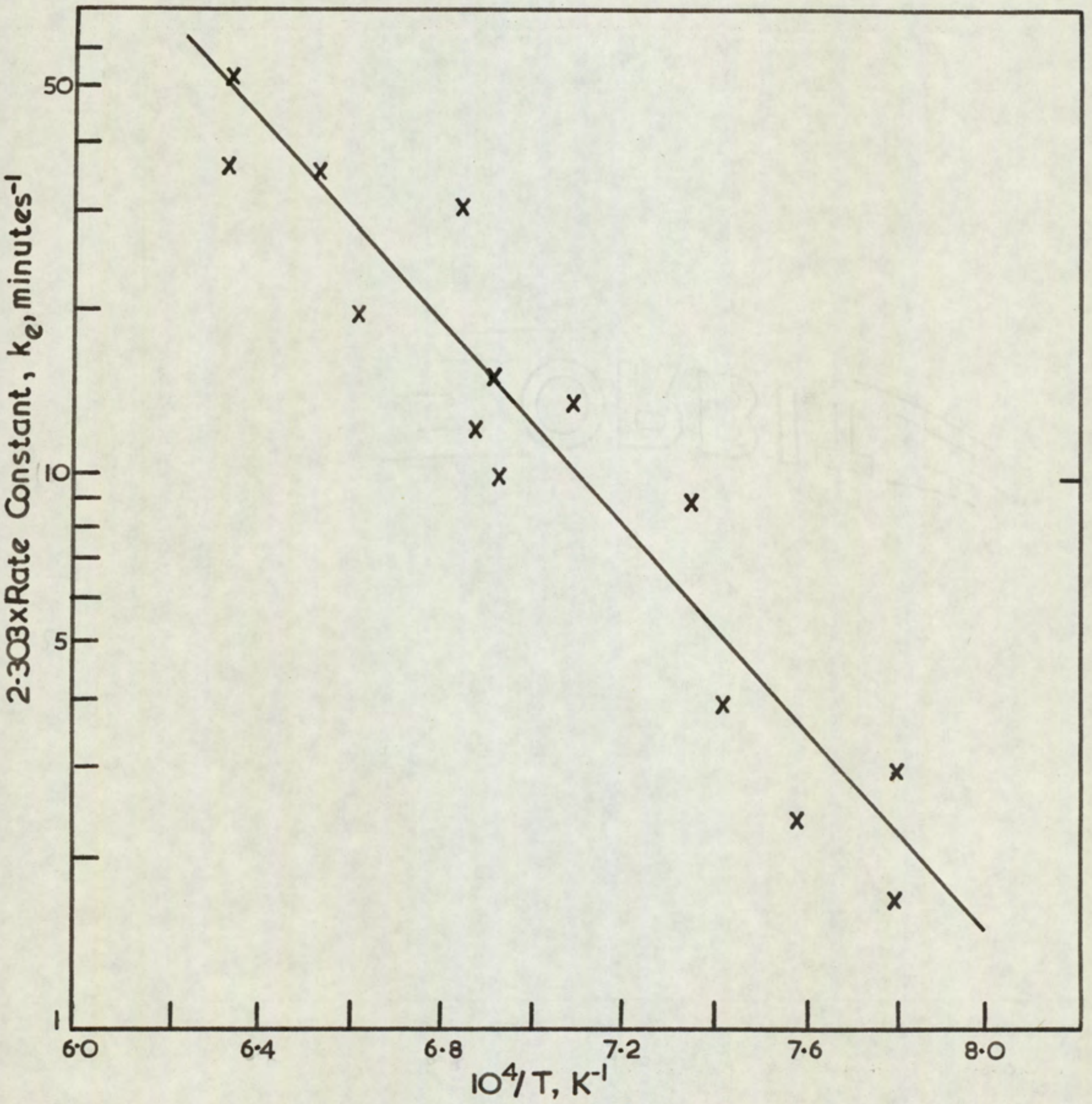

FIGURE (8-27) Rate Constant for Decay of Electron Current against T^{-1}

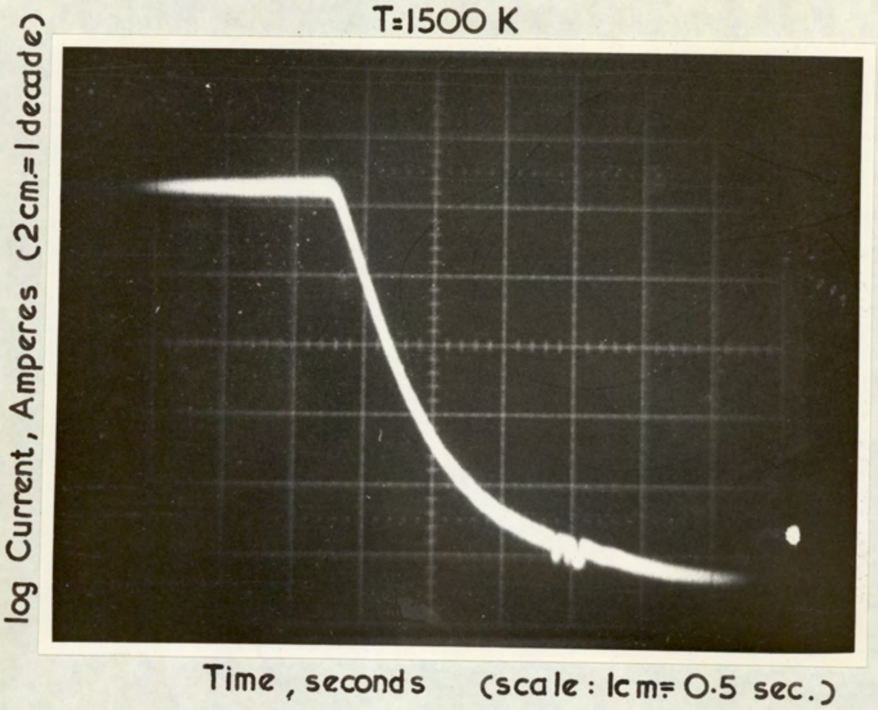

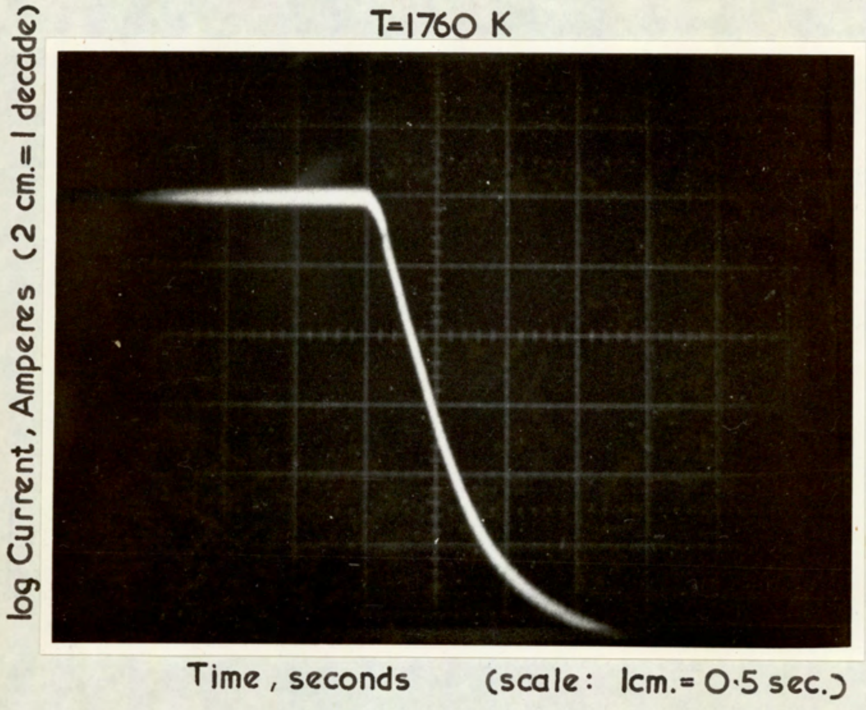

FIGURE (8-28) Oscilloscope Traces of Ion Current Decay

The difference in the rate constants for the decay of the ion and electron currents shows that the ion precursor (I) is not causing the electron current changes as the ion current diminishes very rapidly, although the species involved must be initimately related to the adsorption-dissociation reaction of the methyl iodide.

This is also supported by the results of the pressure dependence plots, the electron current attaining a saturated value before the ion current. This is discussed further in section (8-6).

8.5.6. Discussion of Pressure Dependence Plots

The relationship between the ion current and pressure is given in equation (3-35) which states

$$J_i = P. \frac{[C_s].\ e}{h} \cdot \frac{F_i^{\ddagger}\ F_a^{\ddagger}}{F_g\ F_d^{\ddagger}} \exp\left(-\frac{(\chi - E)}{RT}\right) \quad - (3\text{-}35)$$

or more simply, $J_i \propto P$, for the case of a monatomic gas or for a substrate that gives a single ion.

If dissociation occurs and the substrate molecule gives rise to more than one ion, e.g. $X_2 \rightarrow 2X^-$, then the ion current will show a square root dependence upon the pressure.

All of the experimental plots of log I_i against log P showed a linear characteristic at low pressures with a slope of approximately unity, departures from this slope being accounted for by differences in the gauge sensitivity for dry air and the substrate vapours. At higher pressures, the actual value dependent upon the substrate and filament, the ion current was independent of the pressure in the system. The onset of saturation was independent of temperature indicating the adsorption processes were non-activated.

In the case of iodine on platinum, saturation of the ion current occurred at 1×10^{-4} mm.Hg. This value is much lower than found for the other systems but it should be remembered that iodine also gave anomalous results from the temperature dependence plots. Both of these results suggest a more complex reaction is occurring with iodine on this filament than the other filament materials.

At a pressure of 1×10^{-4} mm.Hg, 1.2×10^{16} molecules.cm.$^{-2}$sec.$^{-1}$ are striking the surface and if a sticking coefficient of 0.4 is assumed, then at saturation the rate of adsorption will be 5×10^{15} molecules.cm.$^{-2}$sec.$^{-1}$. The adsorption process is non activated and since the adsorption-desorption processes are in equilibrium and also the desorption rate of ions (typically 10^{12} ions cm.$^{-2}$sec.$^{-1}$ for Pt/I) is much less than that of neutrals the desorption rate will be very near 5×10^{15} molecules.cm.$^{-2}$sec.$^{-1}$ (or 10^{16} atoms.cm.$^{-2}$sec.$^{-1}$).

The desorption rate of iodine atoms will be given by,

$$\left(-\frac{dn}{dt}\right) = n_s \cdot \frac{kT}{h} \cdot \frac{F^{\ddagger}}{F_{initial}} \cdot \exp\left(-\frac{E_d}{RT}\right) \qquad - \quad (8\text{-}11)$$

For atomic desorption, $F^{\ddagger}/F_{initial} \simeq 1$ and E_d is estimated to be 153 KJ.mole^{-1} therefore n_s, the surface concentration may be evaluated as a function of temperature. At a typical filament temperature of 1400°K, $n_s = 10^{11}$ atoms cm.$^{-2}$ and the assumption, in section (3), that ion formation occurs from a sparce layer (a monolayer = 10^{15} atoms.cm.$^{-2}$) appears to be valid.

The inflexion point for the other systems (I_2 and CH_3X on Ta, W, Mo) occurred at higher pressures, typically around 2×10^{-3} mm.Hg ($3\text{-}4 \times 10^{17}$ molecules.cm.$^{-2}$sec.$^{-1}$). The fact that it is the same for all these systems suggests that saturation of some physical adsorption state is occurring. This state will be the precursor to the chemisorbed state from which ion emission occurs.

8.5.6.2. Anomalous Effects at High Pressures

In some experiments, depending on the temperature (and hence the electron flux) and the vapour present the ion current (and electron current in some instances) above 5×10^{-3} mm.Hg was again found to be pressure dependent. This is believed to be due to gas phase reactions which affect the number of charge carriers reaching the anode.

Such reactions are,

(a) Electron attachment by low energy electrons. The yield for this process will depend upon the electron current and the pressure.

(b) Electron impact ionisation with the formation of a positive ion and an electron/collision. The yield will again be dependent upon the electron current and the pressure.

(c) Gas phase collisions between negative ions formed at the filament and neutral species causing electron detachment. The loss will depend upon the ion current and the pressure.

The negative ion current for ions formed by electron attachment will be given by,

$$J_g^- = \sigma_i^= J_e \, n \, d \qquad - \quad (8\text{-}12)$$

where $\sigma_i^=$ = cross section for formation of negative ions

J_e = electron current density. In the coaxial magnetron the anode current, I_e, is related to the current density at any point by

$$J_e = I_e/2\pi rl$$

where l is the length and r the radius of the collector.

J_g^- = negative ion current for ions formed by attachment

n = density of gas molecules

d = electron path length.

Calculations, however, using the attachment cross sections for iodine(102) and other substrates (103) show that even at high pressures and temperatures the negative ion current from this source is 40 - 50 times lower than the surface ion current.

The formation of positive ions by electron impact will effectively reduce the negative ion current collected by the anode as the electrons formed simultaneously will be lost to the grids. The positive ion current will be given by,

$$J_g^+ = \sigma_i^+ + J_e n d \qquad - \quad (8\text{-}13)$$

In a typical experiment the ion current decreases from 1×10^{-4} amperes at $P = 5 \times 10^{-3}$ mm.Hg to 1×10^{-5} amperes when $P = 1 \times 10^{-2}$ mm.Hg ($\Delta I_i = 9 \times 10^{-5}$ amperes). Using the above equation the calculated decrease is 8×10^{-5} amperes in good agreement with the experimental decrease.

These effects only exhibit themselves at high pressures ($> 5 \times 10^{-3}$ mm.Hg) and therefore it is important that thermionic measurements are only made at pressures below this.

8.6. Thermionic Emission from Metal and Metal Carbide Filaments in the Presence of Methyl containing Compounds

In this section it will be attempted to collect and rationalise the experimental emission data (the pressure and temperature dependence of the ion and electron currents) for the various filaments in the presence of the methyl compounds.

The most important factor in determining the emission properties of a particular filament appears to be whether or not carbide formation occurs and if it does, the physical structure of this carbide.

8.6.1. Platinum Filaments

The emission properties (magnitude of electron emission and intercept on the $\ln(J_e/T^2)$ axis as $1/T \rightarrow 0$) of this filament material were found to be most reproducible.

The clean surface work functions were readily obtained and no large changes in electron emission in the presence of either the halomethanes or iodine were observed. Typical $\log (J_e/T^2) - T^{-1}$ plots for platinum both clean and in the presence of the gases above are shown in figure (8-30).

The table below gives the apparent work function, χ^{**} and A^{**} values. It can be seen that there is a slight decrease in the work function for the halomethanes.

System	χ^{**} (KJ.mole^{-1})	A^{**} (A.cm.$^{-2}$°K^{-2})
Pt	443	160.0
Pt/I_2	440	80.3
Pt/CH_3I	397	0.8
Pt/CH_3Br	390	1.0
Pt/CH_3CN	400	7.0

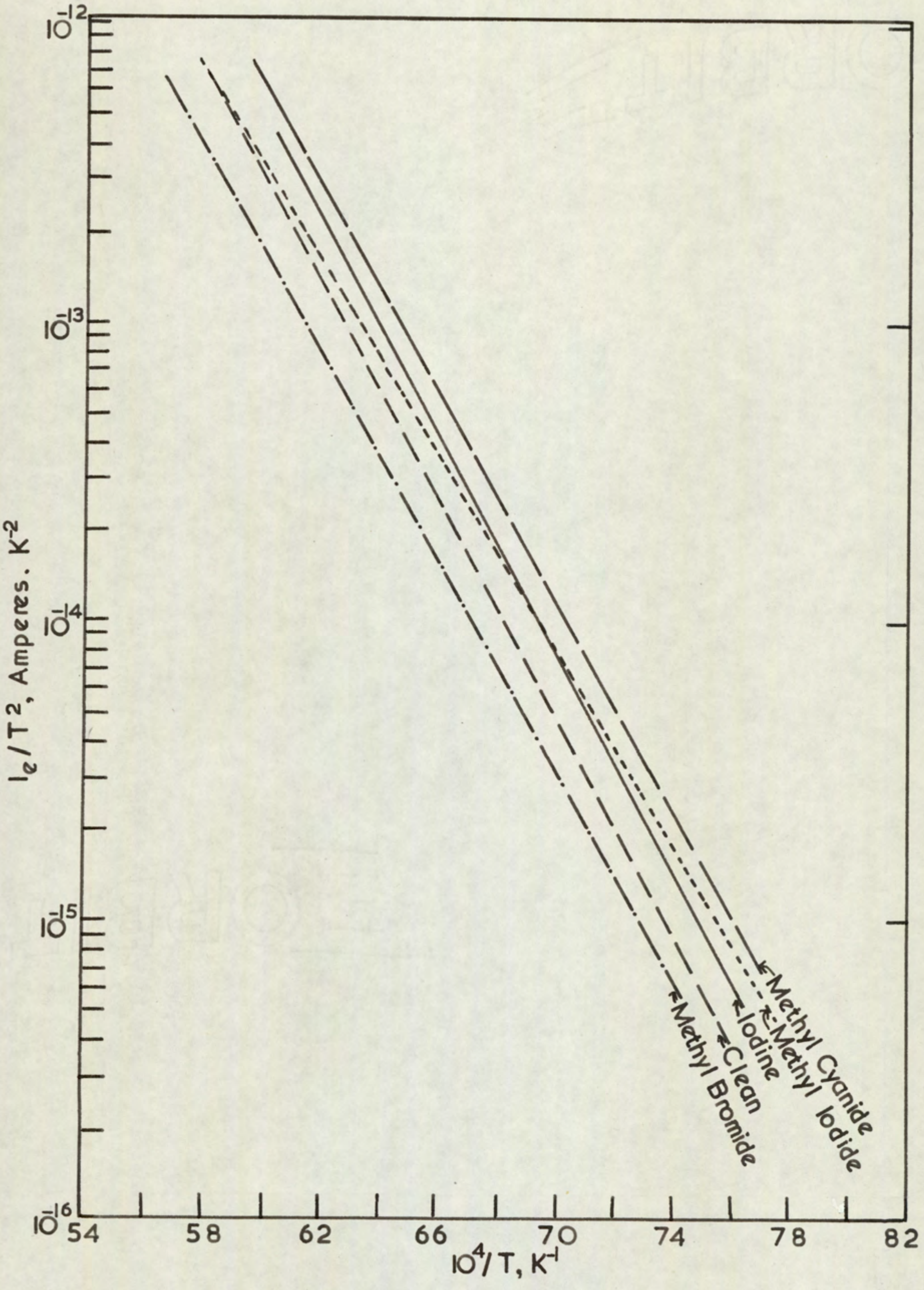

FIGURE (8-30) Plots of I_e/T^2 against $10^4/T$ for Platinum in the presence of Various Gases

8.6.2. Tantalum and Tantalum Carbide Filaments

The results obtained using Ta, W and Mo filaments are somewhat complicated by the formation of carbides due to the decomposition of the methyl group (and also the cyanide group).

Tantalum and tantalum carbide filaments were studied using X-ray crystallography, electron microprobe analysis and electron microscopy.

8.6.2.1. The Electron Microprobe Analyser

This technique was used to determine the presence, or absence, of iodine occluded in the filament. It cannot be used to determine the presence of carbon as the method is insensitive below atomic number 11 (Na).

No iodine (detectability limit 0.1%) could be detected and tantalum was found to be the only element present.

8.6.2.2. X-Ray Analysis

X-ray powder diffraction photographs of the different types of filament were obtained and immediate differences were discernable. Drawings of these photographs are shown in figure (8-31).

The powder photographs of the filaments that produced enhanced emission were found to exhibit arcs of uniform density showing the material to be uniformly polycrystalline whereas the photographs produced by the other type of filament, which showed normal behaviour, were found to exhibit discontinuous arcs showing that the individual crystallites are relatively large.

An estimate may be made of the size of the crystallites from the density and distribution of the individual spots (104) and using this criterion the crystallites appear to be in the range $8 \times 10^{-3} - 2 \times 10^{-2}$ cm. compared to the filament diameter of 2.5×10^{-2} cm.

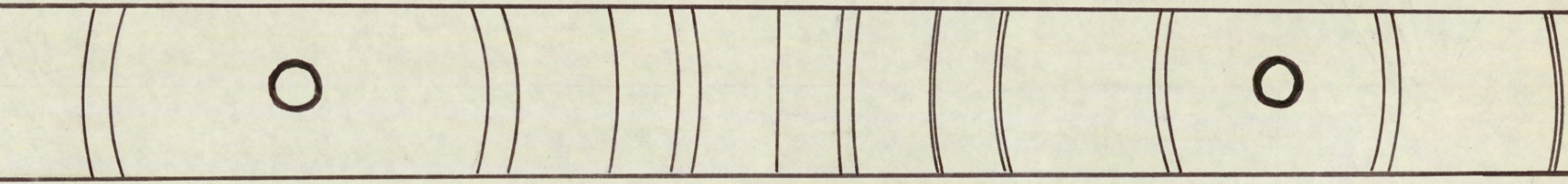

Tantalum Carbide , $TaC_{0.98}$

Tantalum

FIGURE (8-31) Diagrams of X Ray Powder Diffraction Photographs of Tantalum & Tantalum Carbide

In both cases the sections of the filaments studied were taken from the central portion of the measuring region to ensure comparability.

From a knowledge of the powder camera dimensions and the separation of the arcs on the photograph, $\sin\theta$ (where θ = angle of diffraction) values may be calculated and hence, using the Bragg equation, the corresponding d_{hkl} values. This data is shown in tables(8-9) and (8-10).

It was suspected that the filament showing normal behaviour (filament (1)) was tantalum whilst the other filament (filament (2)) was believed to be tantalum carbide (either TaC or Ta_2C). A search of the ASTME powder data file revealed that this was correct. The agreement between the d_{hkl} values of filament (1) and pure tantalum (file number 4-0788) and also between filament (2) and a substance analysed as $TaC_{0.98}$ (file number 19-1292) as shown in table (8-10)was excellent although the relative intensities were not in agreement. The colour of the carbide was reported to be golden yellow which was exactly the colour of the filaments after suitable treatment with methyl iodide.

Tantalum has a body centred cubic lattice ($h + k + l = 2n$) with the lattice spacing, a = 0.3306 nm. The carbide has a face centred cubic lattice with some carbon vacancies and a lattice spacing of 0.4456 nm.

Line doubling was found to be an important feature of these powder photographs, especially at high diffracting angles and because it occurs with both filaments, one of which is completely polycrystalline whilst the other contains larger, orientated crystallites, it appears that the splitting is caused by absorption of the X-rays. This absorption will be non uniform as the cylindrical filaments present a non-uniform cross section to the diffracted rays.

TABLE (8-9)

ANALYSIS OF POWDER PHOTOGRAPH _ FILAMENT (1)

2x		sin θ	d	R.I.	d_{hkl}	hkl
(cm)			(nm)	literature values		
7.72	19 16	0.3299	0.2337	100	0.2338	110
11.10	27 42	0.4648	0.1659	21	0.1653	200
13.95	34 49	0.5712	0.1350	38	0.1350	211
16.50	41 10	0.6583	0.1171	13	0.1169	220
17.00	47 35	0.7383	0.1044	19	0.1045	310
14.56	53 40	0.8056	0.09549	7	0.0943	222
14.50	53 50	0.8073	0.09569			
11.78	60 36	0.8713	0.08828	29	0.08835	321
11.69	60 50	0.8732	0.08848			
8.59	68 34	0.9308	0.08257	4	0.08265	400
8.42	68 59	0.9330	0.08282			
3.67	80 50	0.9872	0.07790	–	–	–
3.29	81 47	0.9879	0.07809			

TABLE (8-10)

ANALYSIS OF POWDER PHOTOGRAPH - FILAMENT (2)

2x		sin θ	d	R.I.	d_{hkl}	hkl
(cm.)			(nm.)	literature values		
7.0	17°28	0.300	0.2570	100	0.2571	111
8.12	20°16	0.3464	0.2225	65	0.2227	200
11.75	20°19	0.4898	0.1574	45	0.1575	220
14.06	35°5	0.5748	0.1341	40	0.1344	311
14.75	36°49	0.5995	0.1286	14	0.1287	222
16.39	49°6	0.7558	0.1020	18	0.1022	331
16.37	49°8	0.7562	0.1019			
15.70	50°49	0.7752	0.09945	20	0.9962	420
15.69	50°51	0.7755	0.09940			
12.80	58°4	0.8486	0.09084	20	0.9094	422
12.77	58°8	0.8492	0.09078			
10.40	64°3	0.8992	0.08573	20	0.8574	511,333
10.32	64°14	0.9006	0.08561			
4.80	78°1	0.9782	0.07881	10	0.7876	440
4.50	78°46	0.9808	0.07859			

Tantalum filaments which had been subjected to treatment with other gases were also studied. These gases were methyl bromide, methyl cyanide, cyanogen iodide (105) and iodine.

As with methyl iodide it was found that a filament subjected to heat treatment and recrystallisation prior to the admission of methyl bromide remained as pure tantalum throughout a series of experiments and powder photographs again show the presence of large individual crystallites.

Other experiments in which a filament with a pre-adsorbed film of methyl bromide was heated in the presence of the vapour of this compound produced a carbide filament identical with filament (2).

The introduction of methyl cyanide and cyanogen iodide (105) also produced tantalum carbide. In the case of methyl cyanide a filament similar to filament (2) could be produced by suitable pre-treatment but for both cyano-compounds the recrystallised tantalum filaments converted more readily to TaC than those discussed above for methyl iodide and bromide, presumably because of the action of the CN group.

Electron photomicrographs show TaC filaments produced by this latter route tended to retain the crystalline nature of the heat treated filament.

8.6.2.3. Electron Microscopy

Electron microscope photographs of selected filaments were obtained using a Cambridge 'Stereoscan' scanning electron microscope. Examples are shown in figures (8-32) to (8-36).

The high emission, $TaC_{0.98}$ filament exhibited an extremely granular structure whilst the pure Ta filament showed large crystallites approaching the size of the filament.

It can be seen that the surface area of the metal filament can be approximated to the geometrical area but that of the carbide must be much greater than this value because of the

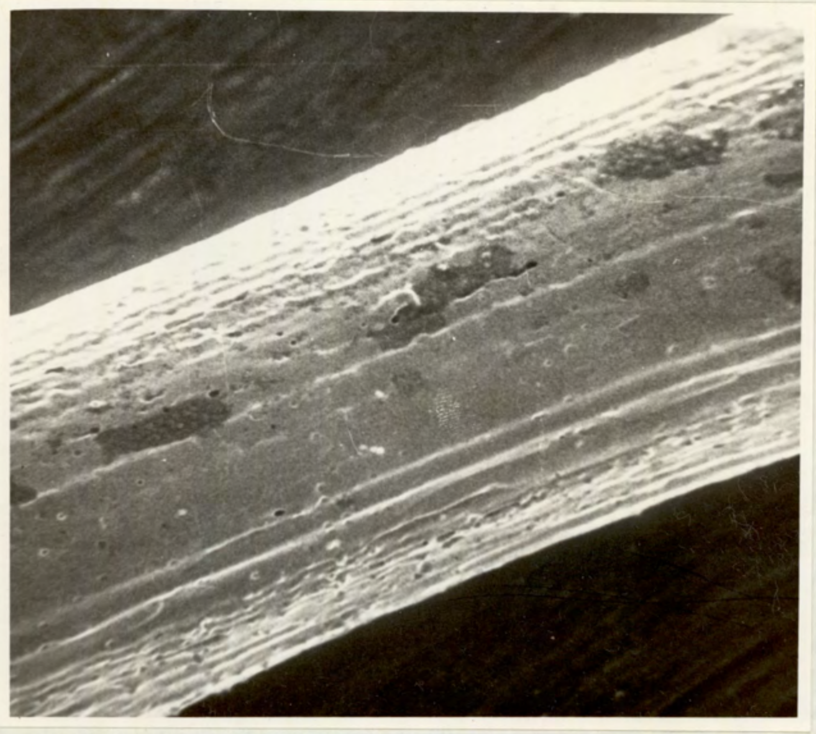

FIGURE (8-32) Tantalum Filament (x500)

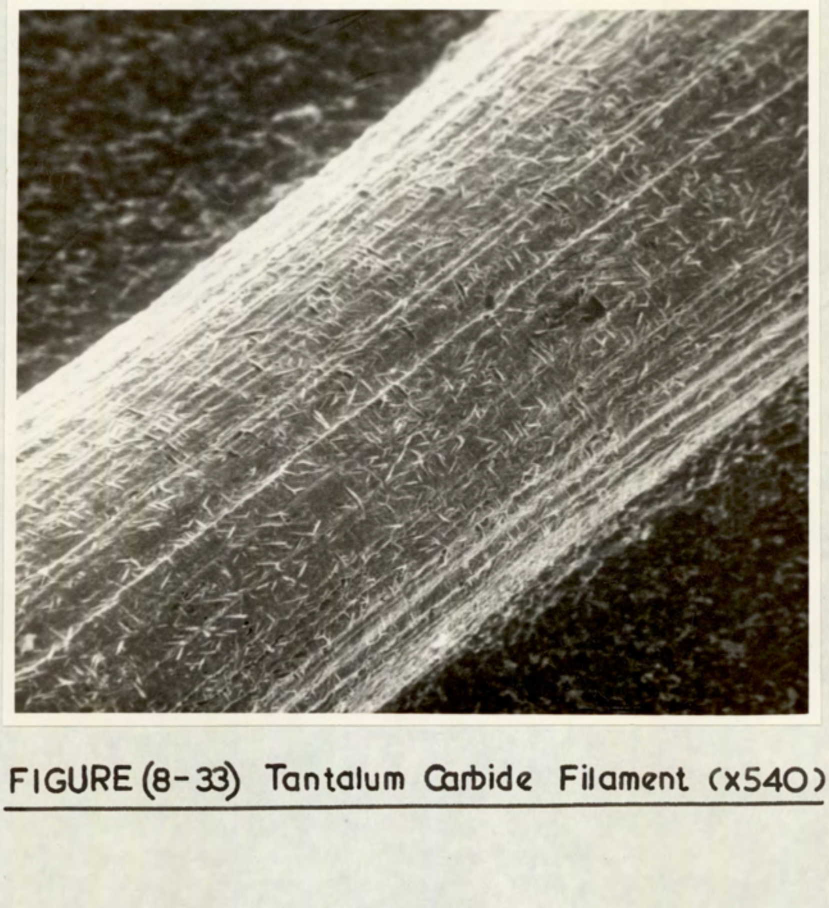

FIGURE (8-33) Tantalum Carbide Filament (x540)

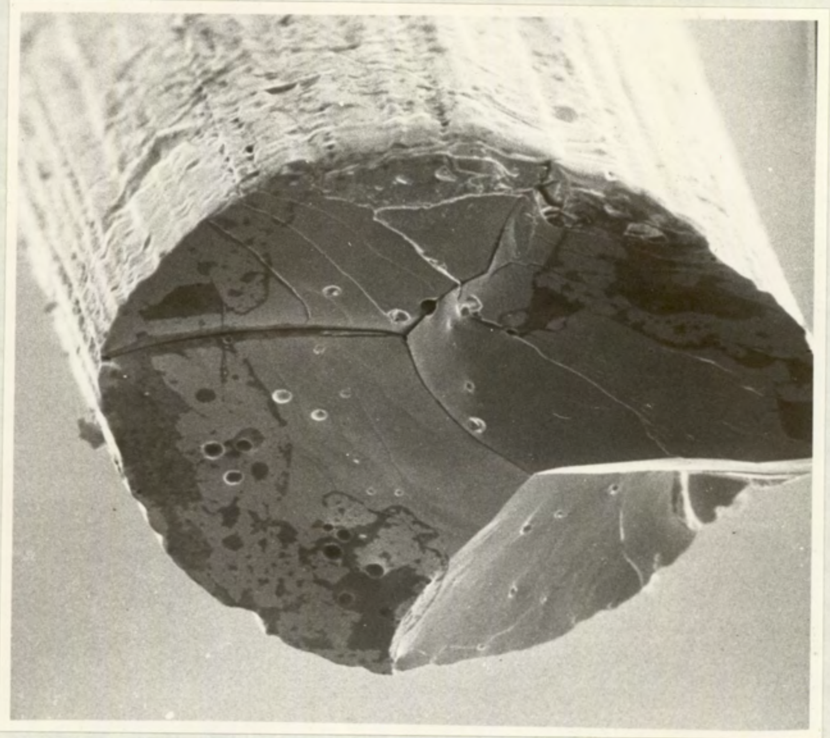

Tantalum Filament

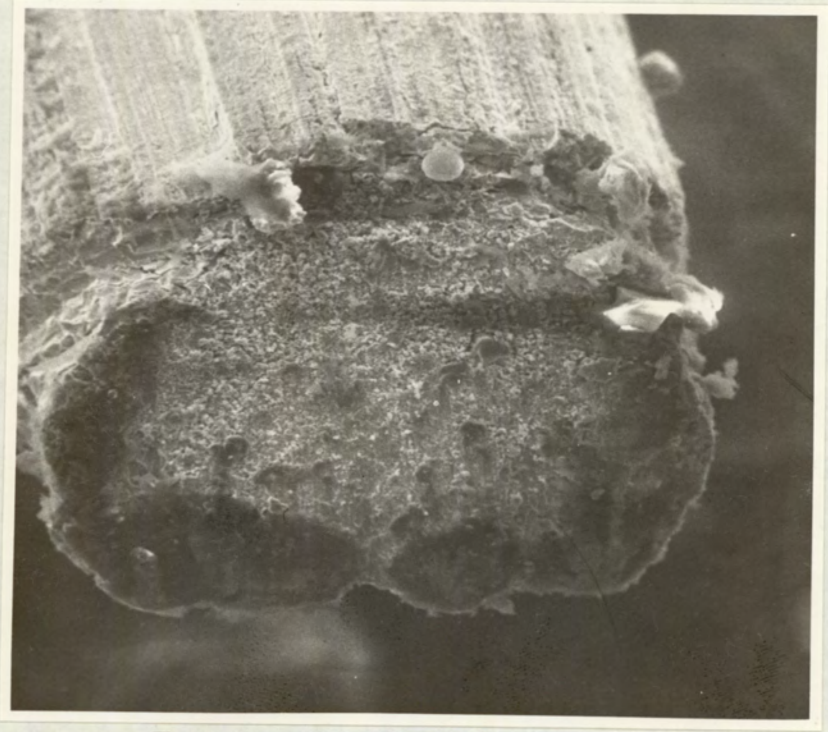

Tantalum Carbide Filament

FIGURE (8-34). Cross Sectional Views of Filaments (x750)

Tantalum Filament

Tantalum Carbide Filament

FIGURE (8-35) Cross Section and Surface Views (x3000)

Tantalum Filament

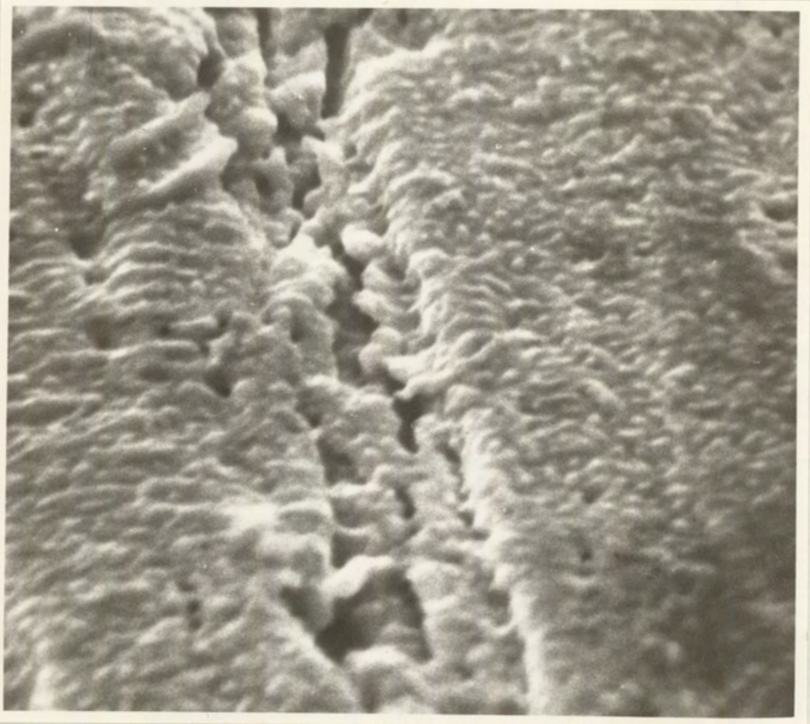

Tantalum Carbide Filament

FIGURE (8-36) Surface Views of Filaments (x3100) extreme surface roughness and as the photograph (figure (8-36)) at high magnification shows it would be extremely difficult to estimate the surface area.

The surface area will affect the thermionic current and this may account for the small differences in electron and ion emission encountered for different filaments formed under apparently similar conditions.

8.6.2.4. Thermionic Emission from Tantalum and Tantalum Carbide Filaments

The initial experiments with methyl iodide using tantalum filaments produced results which were apparently extremely complex. However, once it was realised that carbide formation was occuring and that the carbide had different thermionic properties to the pure metal, the situation was somewhat simplified.

Initially, the apparent work function value obtained for the Ta/CH_3I system was 213 KJ.mole^{-1} (2.21 e.v.). Several more experiments were carried out at low pressures ($\leqslant 10^{-4}$ mm.Hg) and it was found that the work function increased over the duration of these experiments until a limiting value was reached (380 KJ.mole^{-1} (3.95 e.v.)). These results are shown in figure (8-37).

Similar results were obtained with Ta/CH_3CN where the work function was initially 295 KJ.mole^{-1} (3.06 e.v.) but increased with exposure to methyl cyanide over the duration of several experiments to a limiting value of 360 KJ.mole^{-1} (3.73 e.v.).

In both cases the filaments were initially pure tantalum whilst analysis after the final experiments showed them to be completely converted to carbide.

Subsequent experiments, in which the filaments were fully converted to carbide prior to any quantitative measurements, gave work function values similar to the limiting cases above.

It is useful to compare the electron emission from the filaments in the several limiting cases; pure recrystallised

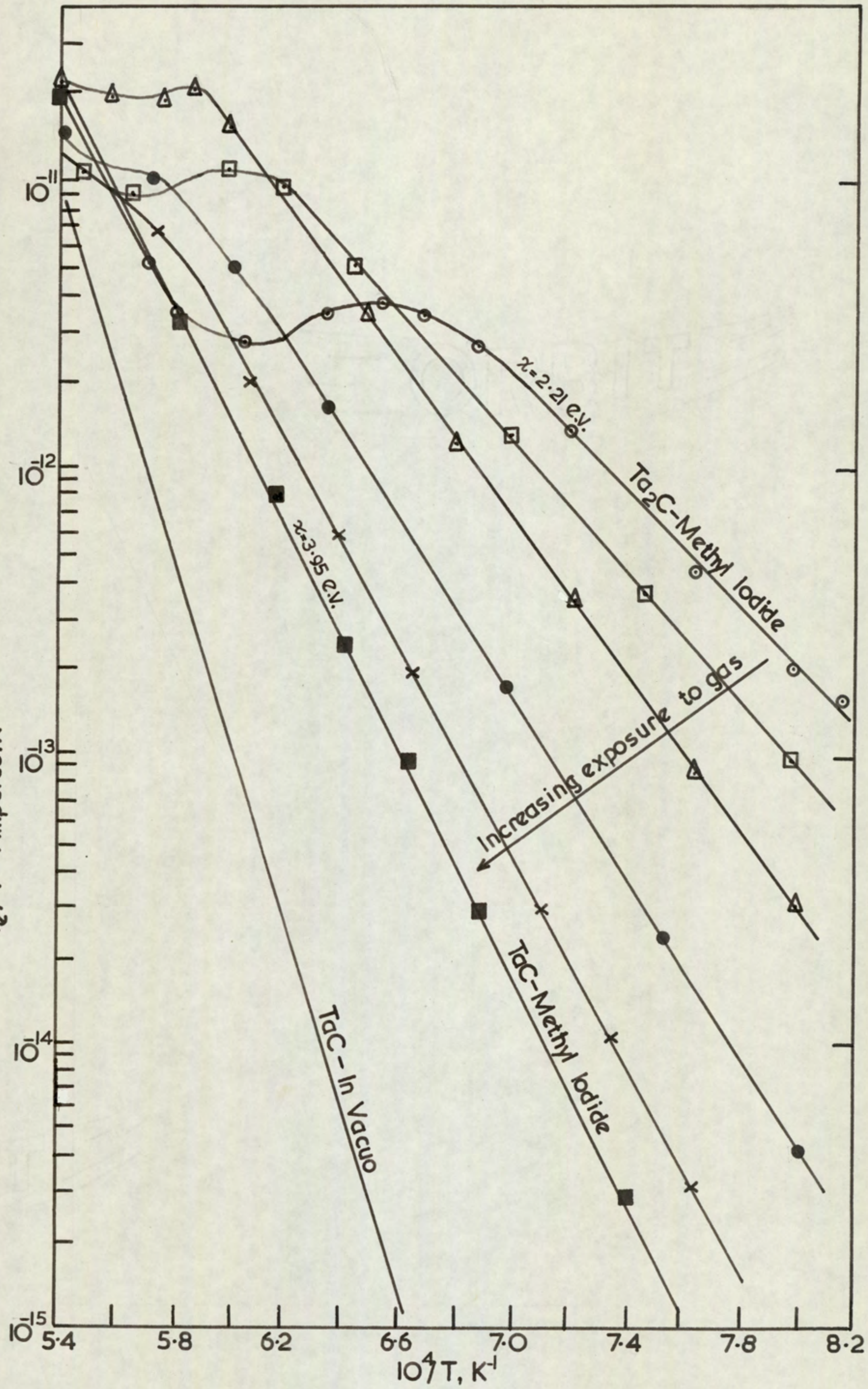

FIGURE (8–37) Apparent Work Function Plots for Tantalum Carbides tantalum, clean tantalum carbide ($TaC_{0.98}$) and the same filaments saturated with methyl iodide, methyl bromide and methyl cyanide and the work function values for these are shown in table (8-11).

The average value for recrystallised tantalum in the vapour of the three methyl compounds (431 ± 10 kJ.mole^{-1}) is close to the value found for the same type of filament material under ultra high vacuum conditions in section (7-3) (442 KJ.mole^{-1}).

The work function of tantalum carbide was dependent upon the methyl compound present, but in all cases the I_e/T^2 against reciprocal temperature plots were linear in the range 1300 - 2000°K whilst in vacuo the emission for the same filaments showed a discontinuity at 1750 ± 30°K. Above this temperature the emission approached that of the CH_3X/TaC system but below it the emission showed a much greater temperature dependence equivalent to a work function of ~ 900 KJ.mole^{-1}, the actual slope varying for different filaments. This value, however, is thought not to be a true work function as the surface conditions are changing.

Figure (8-38) shows plots of the ion and electron emission from tantalum and tantalum carbide filaments in methyl bromide vapour. The apparent electron affinity of the bromide ion obtained from the slopes of the I_e/T^2 and $I_i - T^{-1}$ plots on the carbide filaments was different to the value found on tantalum filaments (167 KJ.mole^{-1}) and was also found to be dependent upon the pressure of the substrate, as shown in figure (8-39) where the slope of the ion and electron currents are seen to vary independently with pressure. This effect was not found with the metal filaments and points to a more complex ion formation reaction.

To identify the role the methyl group played in producing the low work function surface, several experiments were performed in

TABLE (8-11)

Work Functions of Tantalum and Tantalum Carbide

Surface	Substrate	χ, KJ.mole^{-1}
Ta	-	459
TaC > 1780°K	-	405
TaC < 1780°K	-	718
Ta	MeI	426
Ta	MeBr	436
Ta	MeCN	432
TaC	MeI	380
TaC	MeBr	318
TaC	MeCN	342

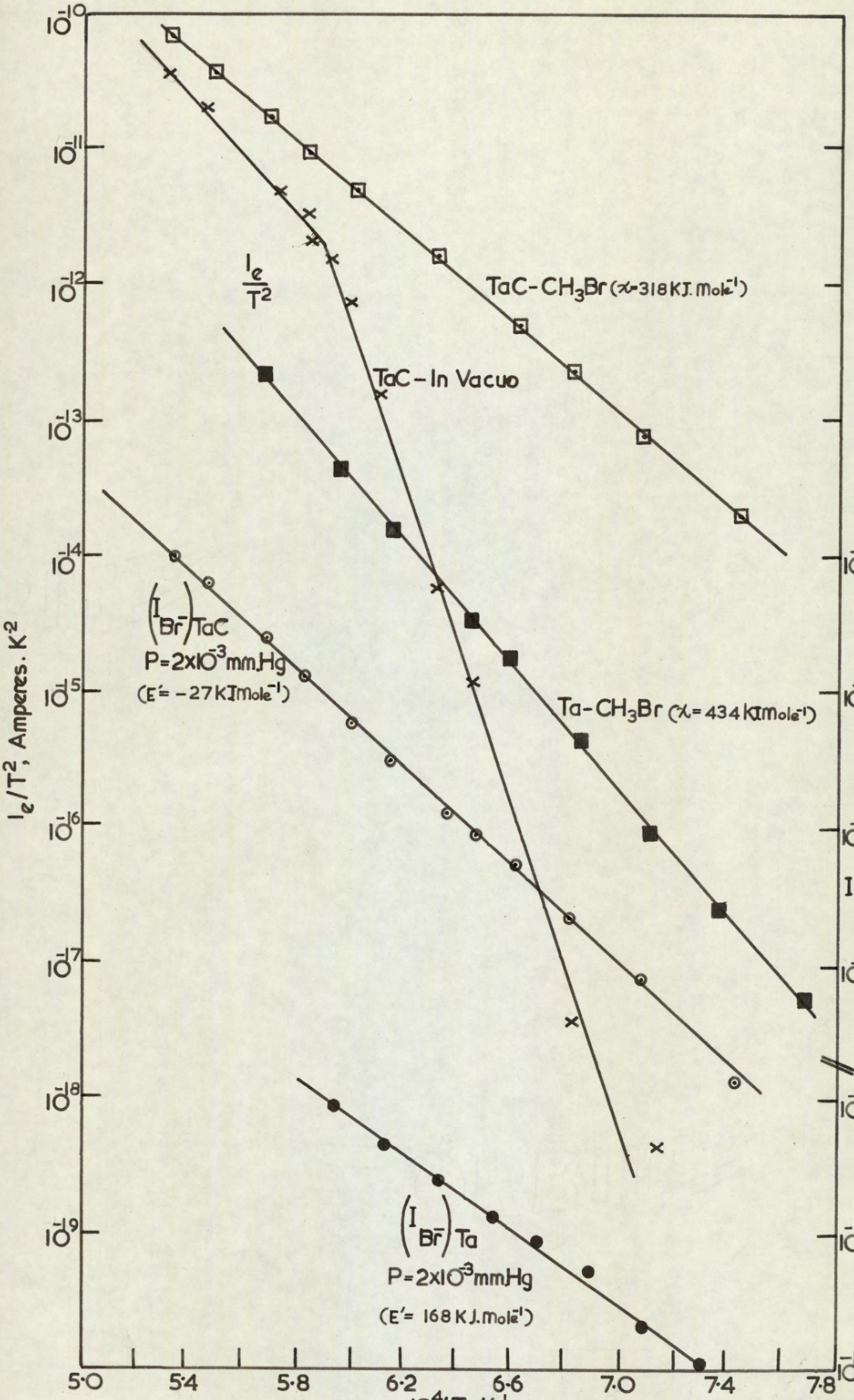

FIGURE (8-38) Ion and Electron Emission from Tantalum and Tantalum Carbide in Methyl Bromide Vapour

FIGURE(8-39) Pressure Dependence of Ion and Electron Emission from Tantalum Carbide in Methyl Bromide Vapour

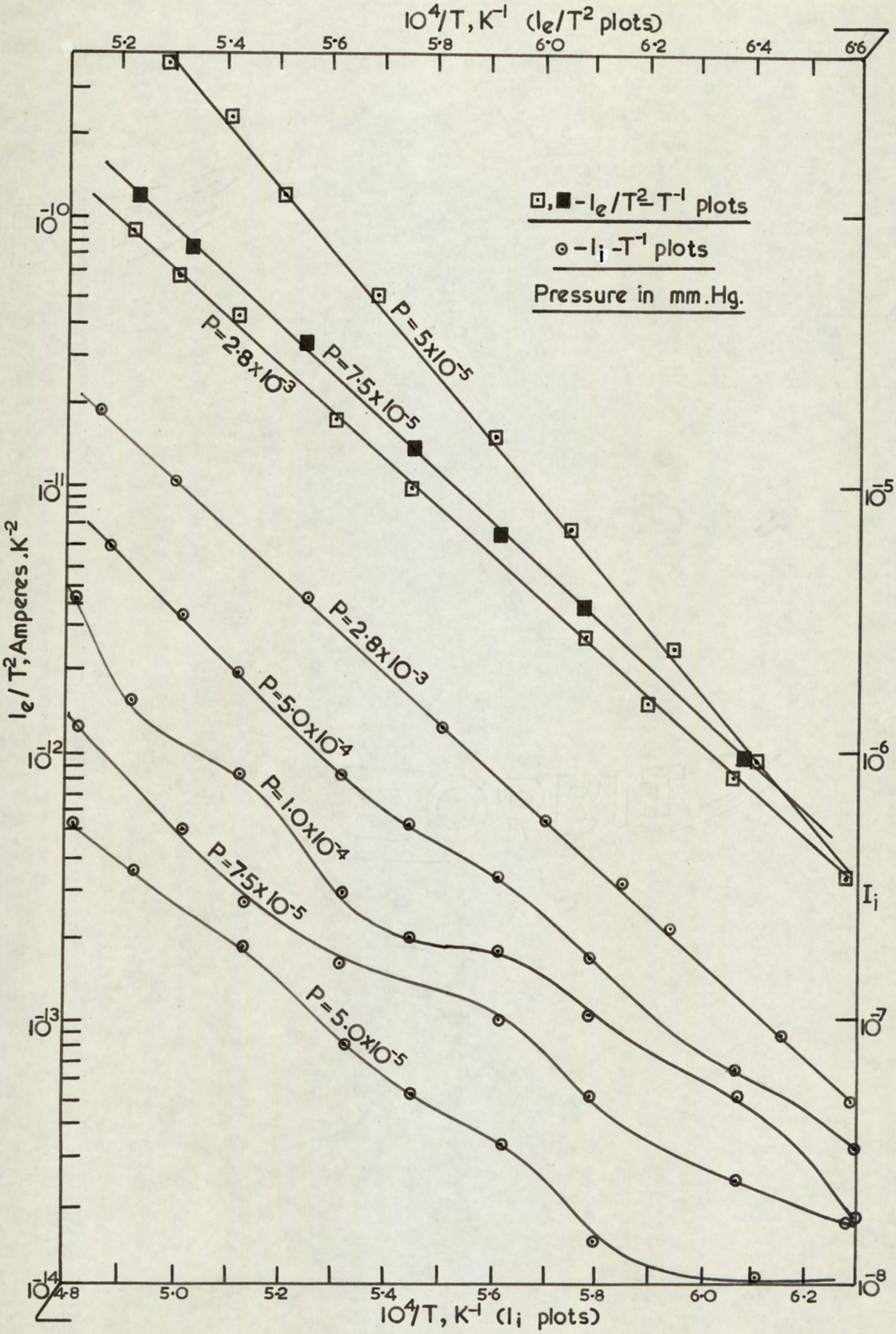

which the work functions of filaments which had been pretreated with methyl iodide or bromide were determined in the presence of iodine vapour at several pressures.

As expected, the electron emission followed closely that of the clean tantalum carbide filament, the break in the curve being exactly reproduced. This is shown in figure (8-40) where the electron and ion emission from tantalum carbide in iodine vapour is compared with the emission from the same filament in methyl iodide vapour. The complex temperature dependence of the ion current from iodine shows the complex, heterogeneous nature of the emitting surface.

These results show that the presence of the methyl group, or other carbon containing group, is essential to produce the high emission below 1750°K. Lowered work functions have also been observed when tetracyanoethylene interacts with tantalum filaments (49) to form a carbide filament.

When the vapour of CH_3X was removed from the system it was possible to follow the decay of the thermionic currents from their equilibrium value for the CH_3X/TaC system to their background levels. When the flow of a gas to a filament emitting ions formed from the gas molecules is halted, the adsorption-desorption equilibrium is disturbed and the ionic emission (electrons and ions) reverts back to its original level before the gas was introduced, normally very rapidly ($t_{\frac{1}{2}} \sim 10^{-2}$ sec.(43)).

A rapid decay was observed for the ion current from the TaC/CH_3I system but the electron current, below 1750°K, was found to decay, via a first order reaction, much more slowly than expected. The activation energy for this decay was 162 $KJ.mole^{-1}$ ($\Delta H_o = 143$ $KJ.mole^{-1}$).

The decay of the ion current can be related directly to the initial surface concentration and can be expressed by the relation,

$$N_i = \int_{t_o}^{t} k_i n_o \exp(-k_i t) \, dt \qquad - (8\text{-}15)$$

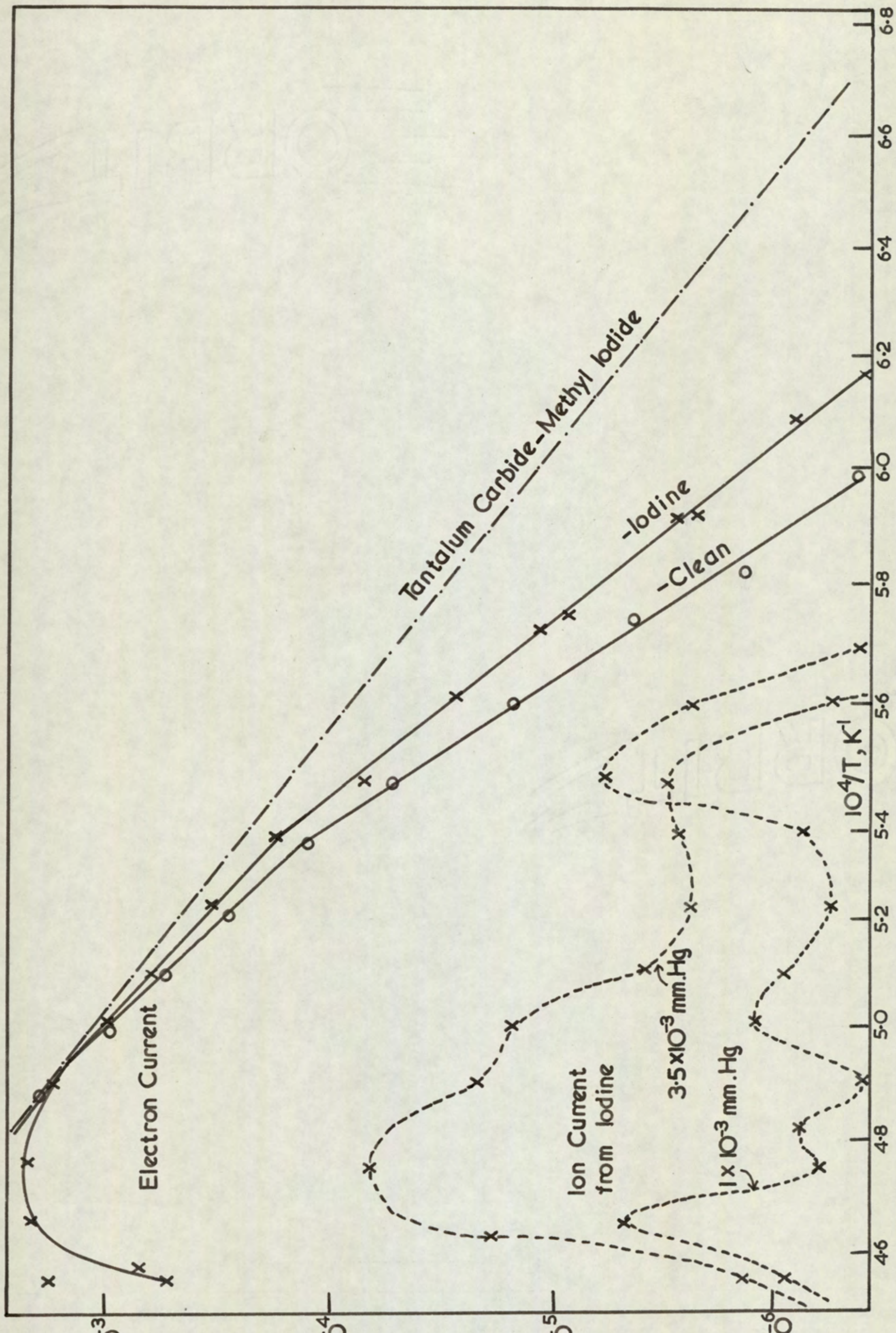

FIGURE (8-40). Thermionic Emission from Tantalum Carbide where N_i = number of ions emitted

t_o = time gas flow halted

n_o = surface concentration at $t = t_o$

This can be simplified by letting t_o = zero time.

$$\frac{N_i}{(N_i)_o} = \exp(-k_i t) = \frac{I_i}{(I_i)_o} \qquad - \quad (8\text{-}16)$$

Similarly, for the electron current,

$$\frac{I_e}{(I_e)_o} = \exp(-k_e t) \qquad - \quad (8\text{-}17)$$

From the temperature dependence of k_e the activation energy was determined.

The reaction followed, that of the decay of the electron current, is however only a secondary process, and the primary process, that causing the change in emission properties, must be considered.

As the emission current is exponentially dependent upon the work function, if the surface consists of patches of different work functions then the measured emission will be weighted in favour of the patches of low work function.

If the electron emission is reduced then it can be shown that this will not occur until a monolayer coverage is approached. For example, if the work function of a particular patch (1) is 1 e.v. lower than another patch (2), then at 1400°K $J_1/J_2 = 4 \times 10^3$, thus for equal emission the fractional area of patch (1) would be 2.5×10^{-2}, hence $\theta = 0.975$.

It was shown above that the presence of a carbonaceous vapour was necessary to produce a low function for TaC below 1750°K. There are two explanations for this;

(1) The emission properties of TaC measured in the presence of CH_3X are due to the modification of the surface dipole layer by CH_n and this species has a long lifetime

on the surface. In this case the activation energy for electron decay will be the desorption energy of this species. The desorption reaction may be,

$$CH_{3(ads)} \longrightarrow CH_{3(g)} \quad (E_A = Q_{CH_3}) \qquad - (8\text{-}18)$$

or

$$CH_{3(ads)} + CH_{3(ads)} \longrightarrow C_2H_{6(g)} \qquad - (8\text{-}19)$$

(2) The emission measured in the presence of CH_3X is the is the 'clean' surface emission from TaC (as is found with pure tantalum) but below 1750°K, in the absence of CH_3X, a surface film of high work function forms. This is most probably a film of carbon. If CH_3X is introduced over such a surface ($\theta \rightarrow 1$) then several chemical reactions can occur to remove this adsorbed layer.

$$CH_3I_{(g)} \longrightarrow CH_{3(ads)} + I_{(ads)} \qquad - (8\text{-}20)$$

$$CH_{3(ads)} \longrightarrow CH_{n(ads)} + (3 - n)\, H_{(ads)} \qquad - (8\text{-}21)$$

$$C_{(ads)} + mH_{(ads)} \longrightarrow CH_{m(ads)} \qquad - (8\text{-}22)$$

$$CH_{m(ads)} \longrightarrow CH_{m(g)} \qquad - (8\text{-}23)$$

$$CH_{m(ads)} + CH_{n(ads)} \rightarrow C_2H_{x(g)} \qquad - (8\text{-}24)$$

(e.g. C_2H_2, C_2H_4, C_2H_6)

The ideas in (2) seem to be supported by the evidence available. The emission properties of many metal carbides have been measured (44,92,106) and as shown in the next section the values found for $TaC_{0.98}$ correspond to the values measured in the presence of the CH_3X compounds.

The heat of adsorption of the methyl radical on tantalum carbide is difficult to estimate because of the inherent inhomogeneity of the surface. However, if it can be assumed to bond only to tantalum surface atoms then in section (8.4.3) $Q_{(CH_3)}$ on tantalum was estimated to be 117.5 $KJ.mole^{-1}$ (1.23 e.v.) This is lower than the measured activation energy and such a low value for the heat of desorption of similar magnitude to that found for the experimental activation energy would, in any case, lead to rapid depletion of the adsorbed layer at the temperatures employed. The abundance of reactions by which the adsorbed carbon layer can be removed could explain the form of the emission-time plot after the gas is reintroduced into the system (see figure (8-26)).

The electron micrographs of the carbide filaments showed them to be granular with a large number of crystallites and hence a large interfacial area. This has been observed previously (106).

It seems probable that the carbon surface layer is formed by the diffusion of carbon, which has been formed by the decomposition of the methyl group followed by diffusion into the filament, along the interfacial boundaries, back to the filament surface. This diffusion process, which is likely to be the rate determining step, will exhibit first order kinetics. However, when the vapour of CH_3X is present, once the carbon diffuses to the surface it is removed by chemical reaction.

There are three types of diffusion to consider, solid diffusion, through vacancies in the crystal lattice; interface diffusion, along grain boundaries and mechanical defects and surface diffusion.

The activation energy for solid diffusion of carbon in tantalum carbide has been measured and although there is some discrepancy, values of 360 $KJ.mole^{-1}$ (107) 355 $KJ.mole^{-1}$ (108)

375 KJ.mole^{-1} (109) and 380 KJ.mole^{-1} (110) having been obtained by various workers, the average value is far higher than the experimental activation energy (163 KJ.mole^{-1}).

However, it has been shown (111) that the types of diffusion are closely related, the only difference being the number of bonds broken and it has been shown that E_A (solid diff.) = 2 x E_A (surface diff.) and 1.5 x E_A (interface diff.).

The diffusion of carbon in tantalum has also been studied and found to proceed with an activation energy of 217 KJ.mole^{-1} so that the corresponding interface diffusion energy will be 163 KJ.mole^{-1}. It is possible that carbon diffusion on tantalum carbide proceeds entirely on a path involving only tantalum surface atoms.

8.6.3. Tungsten and Molybdenum Filaments

The interaction of these filaments with the compounds under discussion has not been investigated as fully as the Ta/TaC system but the results do suggest that carbide formation does occur under certain conditions.

Experiments using molybdenum were only carried out for iodine and methyl iodide and normal work functions (448 KJ.mole^{-1} (4.68 e.v.) and 438 KJ.mole^{-1} (4.58 e.v.) respectively) were observed. However the results were complicated by a break in the emission curve at 1570°K, which is believed to be due to a phase change (113).

In the case of tungsten filaments, which were used with all of the gases, lowered work function values were observed with methyl bromide (328 KJ.mole^{-1} (3.41 e.v.)), methyl cyanide (393 KJ.mole^{-1} (4.07 e.v.)) and methyl iodide (404 KJ.mole^{-1} (4.18 e.v.)) compared with the clean surface value of 448 KJ.mole^{-1} (4.65 e.v.).

It was also found that the work function of tungsten (or tungsten carbide) was dependent initially upon the exposure to the methyl compound as shown below in table (8-12).

TABLE (8-12)

Experiment	KJ.mole^{-1}
1	448
2	262
3	287
4	297
5	329
6	328

Initially the filament was pure tungsten but during the course of the experiments it was converted to tungsten carbide. This carbide has also been reported to be formed by the interaction of tetracyanoethylene with tungsten filaments (49).

8.6.4. Discussion of Thermionic Emission Properties of Refractory Metal Carbides

The emission properties of refractory metal carbides have been studied by several groups of workers (106,114,115). These carbides are of considerable interest in thermionic conversion processes because of their combination of low work functions and high melting points (e.g. TaC m.p. = 4150°K (116)).

Work function measurements on these carbides have been collected (44,92) and are shown in table (8-13). The values found are always lower than the pure metal (or carbon itself which has a work fumction of 452 KJ.mole^{-1} (4.7 e.v.)) and where several studies have been carried out considerable variation in the experimental emission properties has resulted. It can be seen however that these values encompass the experimental work functions found for tantalum carbide.

TABLE (8-13)

EMISSION PROPERTIES OF CARBIDES

Carbide	χ, KJ.mole^{-1}	A, A.cm.$^{-2}$°K^{2}	Ref. & Comment
TaC	294	2.1	(115) powder
TaC	303	0.3	(115) coated on W fil.
TaC	305	0.22	(114) carburised fil.
TaC	351	-	(92) coated on W fil.
TaC	370	-	(92) coated on W fil.
TaC	363	-	(92) Powder 1400°K
TaC	351	-	(92) Powder 2000°K
W_2C	250	-	(92) Field emission
WC	344	-	(92) Field emission
MoC	365	-	(92) Carburised fil.
Mo_2C	371	-	(92) Carburised fil.

In the case of tantalum, carburisation in dilute hydrocarbon gases is reported to be rapid above 2300°K (114). The carbon initially deposited on the surface diffuses, principally along grain boundaries, to form a thin, porous surface skin of Ta_2C which is then converted to TaC.

The diffusion of carbon in this initial reaction is quite rapid (114) proceeding with an activation energy of 80.5 ± 26 $KJ.mole^{-1}$. The material does not become homogeneous until the carburisation is complete.

The work function values of both the monocarbide, WC and the dimetal carbide, W_2C have been reported (92). Initially W_2C (χ= 250 $KJ.mole^{-1}$, (2.60 e.v.)) is formed but upon addition of more carbon, WC (χ= 344 $KJ.mole^{-1}$, (3.60 e.v.)) results.

The mechanism of growth, $M \rightarrow M_2C \rightarrow MC$, appears to be similar both for tantalum and tungsten.

It has also been noted (106) that there is a correlation between microstructure and thermionic emission. For a given carbide the Richardson work function was found to increase as the grain size decreased although no quantitative measurements were given.

Using the information above the dependence of the work function of tantalum and tungsten to exposure to the CH_3X vapours can be explained. It can be seen from table (8-13) for W/CH_3Br that initially the clean surface work function (448 $KJ.mole^{-1}$) was obtained but after this initial exposure to methyl bromide the apparent work function dropped to 262 $KJ.mole^{-1}$, a value very near that reported for W_2C (250 $KJ.mole^{-1}$). Then over the duration of several experiments the apparent work function increased until it reached a stable value of 329 $KJ.mole^{-1}$, a value which is comparably close to the literature value for the apparent work function of WC (344 $KJ.mole^{-1}$ (3.6 e.v.)).

The work function values of all the carbide filaments in the vapours of methyl bromide, cyanide and iodide have been found to be reduced compared to the corresponding metal filaments. The saturated electron current density emitted from a homogeneous surface of work function χ_o can be written,

$$J_o = \bar{d}_o AT^2 \exp(-\chi_o/RT) \qquad - \qquad (8\text{-}25)$$

where $\bar{d}_o (=(1 - \bar{r}))$ is the transmission coefficient.

The experimental pre-exponential factor, A^{**} $(= \bar{d}A)$ like the work function, was also found to be reduced as shown in table (8-14) below and a contributory cause may be the lowering of the transmission coefficient for emission from the carbide compared to that of the metal.

TABLE (8-14)

Apparent Work Functions and Pre-exponential Factors for Ta and TaC

System	χ^{**} KJ.mole^{-1}	$\log_{10}A^{**}$, A.cm.$^{-2}$deg.$^{-2}$
Ideal surface	-	+ 2.08
Ta	430	+ 1.06
TaC	256	- 2.30
TaC	328	- 0.80
TaC	341	- 0.11
TaC	359	+ 0.20

The emission properties of the carbide/CH_3X system can be discussed further by supposing the surface can be considered as a metal surface having an adsorbed carbon layer, probably involving carbon from the carbide lattice as well as adsorbed

CH_n ($n = 3,2,1,0$) species which modifies the potential barrier and hence the transmission coefficient for electron and ion emission.

The emission equation for the carbide, work function χ_c, can be written,

$$J_c = \bar{d}_c \theta A T^2 \exp(-\chi_c/RT) \qquad - \quad (8\text{-}26)$$

where $\chi_c = \chi_o + \Delta\chi$

Then, letting $\bar{d}_c/\bar{d}_o = \alpha$ and combining equations (8-25) and (8-26),

$$\frac{J_c}{J_o} = \alpha\,\theta \exp(-\Delta\chi/RT) \qquad - \quad (8\text{-}27)$$

The temperature dependence of J_c/J_o will be determined by $\Delta\chi$ as θ is independent of temperature. This is to be expected as the carbides are extremely stable at the temperatures employed. This can be experimentally verified by rearranging equation (8-27) to give,

$$RT \ln\left(\frac{J_c}{J_o}\right) = RT \ln(\alpha\theta) - \Delta\chi \qquad - \quad (8\text{-}28)$$

Plots of this relation were found to be linear showing $(\alpha\theta)$ to be independent of temperature.

The transmission coefficients in equation (8-25) and equation (8-26) have been calculated by Fowler (117) and are given by,

$$\bar{d}_o = 2(\pi kT/\chi_o)^{\frac{1}{2}} \qquad - \quad (8\text{-}29)$$

$$\bar{d}_c = \frac{8\left[\pi kT(\chi_o + \Delta\chi)\right]^{\frac{1}{2}}}{\chi_o} \exp\left(-\frac{4}{3}\left[\frac{8\pi^2 m(-\Delta\chi)}{h^2}\right]^{\frac{1}{2}}.1\right) \qquad - \quad (8\text{-}30)$$

Therefore,

$$\alpha = 4\left(\frac{\chi_o + \Delta\chi}{\chi_o}\right)^{\frac{1}{2}} \exp\left(-\frac{4}{3}\left(\frac{8\pi^2 m(-\Delta\chi)}{h^2}\right)^{\frac{1}{2}}.1\right) \qquad - \quad (8\text{-}31)$$

Plots of the relation in equation (8-28) were used to obtain $(\alpha\theta)$ and hence, assuming $\theta = 0.5$, the width of the barrier, l, may be estimated using equation (8-31) and these values are shown in table (8-15) together with the experimental work function changes $(\chi_o - \chi_c)$ and the dipole moment/surface bond associated with these work function changes, calculated using equation (2-7). The final column of this table shows the value of D/l which is a measure of the charge on the surface layer and is reasonably constant.

TABLE (8-15)

Substrate	$-\Delta\chi$ KJ.mole^{-1}	D Debye	l nm.	D/l
CH_3I	23	0.27	0.4	0.68
CH_3CN	61	0.44	0.63	0.69
CH_3Br	85	0.53	0.65	0.78

The values of l obtained are consistent with the barrier extending over the first layer of surface atoms and adsorbed methyl layer.

The interpretation of the work function changes is difficult as the observed work function depends not only upon the formation of a carbide but also upon the gas present above the surface; for example the following table, (8-16), shows the work functions, observed under various conditions, for a particular filament.

TABLE (8-16)

Substrate	χ, KJ.mole^{-1}
CH_3I	371
CH_3Br	317
In vacuo $>$1700°K	400
In vacuo $<$1700°K	1160

The reactions producing surfaces having these work functions are complex and it is difficult with the information available to characterise these surfaces more fully.

9.0. CONCLUSIONS AND CORRELATION OF MAGNETRON, THERMAL DESORPTION AND CONTACT POTENTIAL MEASUREMENTS

The magnetron method yields information about the rates of emission of electrons and negative ions and the energy changes involved in the rate determining steps of these reactions.

For ion emission these energy changes may include not only the electron affinity of the desorbing ion but also heats of dissociation and adsorption of the substrate or decomposition products of the substrate.

The results obtained for the surface ionisation of iodine and methyl iodide, bromide and cyanide using tantalum, tungsten, molybdenum and platinum filaments have indicated that the mechanism of the ion formation reaction is very specific to the metal-substrate combination and also the temperature of the filament.

The study of ion formation for molecular iodine on tungsten, tantalum and molybdenum filaments showed that iodine behaves as a monatomic gas on the filament surface, the rate determining step being desorption of the negative ion. The electron affinity found for these results agreed well with literature values.

For the same reaction on platinum filaments the mechanism was more complex and found to be dependent upon temperature. The low temperature mechanism was shown to involve the breaking of the surface bond in the rate determining step.

On energetic grounds and with a knowledge of at least a transient existence of the surface methyl group, a mechanism for surface ionisation of the methyl compounds involving simultaneous fission of the CH_3-X bond (where X = I, Br, CN), desorption of X^- and adsorption of the methyl radical can be postulated. Using known values for bond energies and electron affinities a consistent value for the heat of adsorption of the methyl radical was obtained (table 8-6).

The thermal desorption method yields information about the desorption of neutral particles and the energy changes involved in the rate determining step of these reactions.

If iodine and methyl iodide are allowed to adsorb onto a tantalum filament at 300°K and then the adsorbed products desorbed by rapidly raising the temperature of the filament, the observed desorption traces were very similar and a quantitative analysis showed the desorbing species to obey a similar rate equation.

From these results it was concluded that the adsorption of iodine and methyl iodide on tantalum produces surface iodine atoms and that these are mobile on the surface, but that it is energetically more favourable for the iodine to be desorbed and to a certain extent exist on the surface as iodine molecules. No desorption peak that could be attributed to atomic iodine was observed although the magnetron results showed that at high temperatures the iodine exists predominantly as atoms.

Work function measurements, both in the ultra high vacuum system at low temperatures (300 - 1000°K) and in the magnetron at temperatures above this, showed that at low surface coverages (measured by the thermal desorption technique) and also at high temperatures, the work function changes caused by iodine and the methyl compounds were small for recrystallised metal filaments.

It was found however that the adsorption and decomposition of the methyl compounds on a filament that had not been previously heat treated produced a carbide filament having markedly different thermionic properties to the parent metal. Both the ultra high vacuum system filaments and tantalum filaments that had been recrystallised in the magnetron prior to gas admission showed a high immunity to carbide formation even at high temperatures. Electron micrographs showed the growth of relatively large crystallites in these filaments and therefore it seems that attack, initially for formation of M_2C and later MC, occurs along defects and grain boundaries which will be more numerous before heat treatment.

The emission properties of tantalum carbide in particular have been studied in detail and found to depend upon temperature and also the gas present. This has been interpreted from kinetic as well as steady state thermionic emission measurements in terms of complex surface reactions of carbon residues formed from the decomposition of the methyl group.

REFERENCES

1. Hayward, D. O. and Trapnell, B. M. W., "Chemisorption", 2nd Edition, (Butterworth - London, 1964).
2. Robinson, W. N., "Physical Principles of Ultra High Vacuum and Equipment", (Chapman and Hall - 1968).
3. Redhead, P. A., Hobson, J. P. and Kornelsen, E. V., "The Physical Basis of Ultra High Vacuum", (Chapman and Hall - 1968).
4. Glasstone, S., Laidler, K. J. and Eyring, H., "The Theory of Rate Processes", (McGraw-Hill - New York, 1941).
5. Scheer, M. D., Fine, J. and McKinley, J. D., Surf. Science, (1972) 30 258.
6. Redhead, P. A., Trans. Far. Soc., (1961) 57 641.
7. Beeck, O., Disc. Far. Soc., (1950) 8 118.
8. Page, F. M., Goode, G. C., "Negative Ions and the Magnetron", (Wiley - 1969).
9. Garner, W. E. and Veal, F. J., J. Chem. Soc., (1935) 1487.
10. Farnsworth, H. E., Schlier, R. E. and Dillon, J. A., J. Phys. Chem. of Solids, (1959) 8 116.
11. Allen, J. A., Revs. Pure and Appl. Chem. (Aust.),(1954) 4 133.
12. Frakenburg, W. G., J. Am. Chem. Soc., (1966) 66 1827.
13. Rideal, E. K. and Trapnell, B. M. W., Proc. Roy. Soc. (1951) A205 409.
14. Becker, J. A. and Hartmann, C.D., J. Phys. Chem., (1953) 57 153.
15. Ehrlich, G., J. Chem. Phys., (1961) 34 29.
16. Hickmott, T. W., J. Chem. Phys., (1960) 32 810.
17. Eisinger, J., J. Chem. Phys., (1959) 40 412.
18. Redhead, P.A., Vacuum, (1962) 12 203.
19. Brennan, D., Hayward, D. O. and Trapnell, B. M. W., Proc. Roy, Soc. (1960) A256 81.
20. Kisluik, P., J. Phys. Chem., (1959) 31 1605.
21. Sams, J. R., Costabaris, G. and Halsey, G. D., J. Phys. Chem., (1960) 64 1689.
22. Ehrlich, G., J. Appl. Phys., (1961) 32(1) 4.
23. Erents, K., Grant, W. A. and Carter, G., Surf. Sci., (1965) 3 480.
24. Hobson, J. P. and Redhead, P. A., Trans. 4th Int. Vacuum Congress, (1968).

25. Hansen, S. R. and Mimeault, V. J., "Experimental Methods in Catalytic Research", 217-264, (Academic Press N.Y. - 1968).

26. Petermann, L. A., Nuovo Cimento, (Supplement), (1967), 5(2) 364 - 373.

27. Madey, T. A. and Yates, Y. T., J. Vacuum Science and Tech., (1971), 8 (4) 525.

28. Kutsenko, E. N., Russ. Tech. Physics, (1971), 41 (5) 1063.

29. Langmuir, I. and Kingdon, K. H., Phys. Rev. (1929), 34 129.

30. Persky, A., Greene, E. F. and Kuppermann, A., J. Chem. Phys., (1968) 49 2347.

31. Ionov, N. I., "Surface Ionisation and its Applications - Progress in Surf. Science", Ed. S. E. Davison, (Pergamon - 1972).

32. Scheer, M. D. and Fine, J., Advances in Applied Mechanics, Suppl. 5, 2 (1969) (6th Symp. Rarefied Gas Dyn.).

33. Zandberg, E. Ya. and Ionov, N. I., "Surface Ionisation" N.T.I.S. Springfield V. A. (T.T. - 70 - 51048), (1971).

34. Kaminsky, M., "Atomic and Ionic Impact Phenomena on Metal Surfaces" (Springer-Verlag) (1965).

35. Zamel, J., J. Chem. Phys. (1958) 28 410.

36. Glockler, G. and Calvin, M. J., J. Chem. Phys. (1936) 4 492.

37. Sutton, P. P. and Mayer, J. E., J. Chem. Phys. (1935) 3 20.

38. Page, F. M., Trans. Far. Soc., (1960)56 1742.

39. Zandberg, E. Ya., Sov. Phys. - Tech. Phys. (1972) 17 (4) 665.

40. Page, F. M. and Chamberlain, A . T., unpublished work.

41. Herron, J. T., Rosenstock, H. M. and Shields, W. R., Nature (1965) 206 611.

42. Bailey, T. L., J. Chem. Phys. (1958) 28 792.

43. Dugan, J. L. G., Diss. Abs. (B), (1972) 32 (9) 5129.

44. Riviere, J. C., "Solid State Surface Science" - ed. M. Green, (Marcel Dekker - New York - 1969), 1 179-289.

45. Culver, J. and Tompkins, F. C., Adv. in Catalysis (1959) 10 67.

46. Hensley, E. B., J. Appl. Phys. (1961) 32 301.

47. Herring, C. and Nichols, M., Rev. Mod. Phys. (1949) 21 185.

47a Beck, A. J., Handbook of Vacuum Physics, 2 (2), "Thermionic Emission", (Pergamon Press - 1966).

48. Shelton, H., Phys. Rev. (1957), 107 1553.

49. Farragher, A. L., (1966) Ph.D. Thesis - University of Aston in Birmingham.

50. Branscomb, L. M., Seman, M. L. and Steiner, B., J. Chem. Phys. (1962) 37 1200.

51. Berry, R. S., Reimann, C. W. and Spokes, G. N., J. Chem. Phys. (1962) 37 2278.

52. Ionov, N. I., Sov. Phys. J.E.T.P., (1948) 18 96.

53. Zandberg, E. Ya., Ionov, N. I., Paleev, V. I. and Tontegode, A. Ya., Sov. Phys. - Tech. Phys. (1962) 32 503.

54. Ionov, N. I. and Katataev, V. I., Sov. Phys. - Tech. Phys. (1962) 32 626.

55. Zazula, P. and Wilhelmsson, H., Arkiv Fysik (1963) 24 511.

56. Ritchie, B. and Wheeler, R., J. Phys. Chem., (1966) 70 173.

57. Chaikovskii, E. F., Mel'nik, L. G. and Pyatigorskii, G. M., Soviet Phys. - Tech. Phys. (1970) 15 (1) 163.

58. Page, L. and Adams, N. I., "Principles of Electricity", 4th edition, (D. Van Nostrand - 1969).

59. Worthing, A. G., J. Franklin Institute (1922) 194 597.

60. Martinez, J. M. and Madjid, A. H., J. Appl. Phys. (1970) 41 5322.

61. Malter, L. and Langmuir, D. B., Phys. Rev. (1939) 55 743.

62. De-Vos, J. C., Physica (1954) 20 690.

63. International Critical Tables, Vol. 5.

64. Eley, D. D. et al., Proc. Roy. Soc. (A) (1969) 314 301 (and many references in ref. (1)).

65. McCarroll, B., J. Chem. Phys. (1967) 47 5077.

66. McCarroll, B., J. Appl. Phys. (1969) 40 (1) 1.

67. Jennings, T. A., (1971) Ph.D. Thesis - University of Aston in Birmingham.

68. Hill, M. P., Lecchini, M. A. and Bethica, B. A., Trans. Far. Soc. (1966) 62 229.

69. Lange, W. J., Singleton, J. H. and Erikson, D. P., (1966) 3 303, 319, 338.

70. Young, J. R. and Hession, F. P., (1963) 10th National Vac. Symp., p.234 (Macmillan).

71. Crawley, D. J. and De Chernatony, L., Vacuum (1970) 20 389.

72. Bryant, P. J. and Gosselin, C. M., J. Vac. Sci. Tech., (1966) <u>3</u> 350.
73. Redhead, P. A., Symposium on Electron and Vacuum Physics (Hungary) (1962) 89.
74. Cope, O. J., Vacuum (1968) <u>18</u> 665.
75. Melton, C.E., "Principles of Mass Spectrometry and Negative Ions", (Dekker N.Y. - 1970).
76. Greenburg, J., PHys. Rev. (1958) <u>112</u> (6) 1898.
77. Wang, G. C. Y. and Lee, C. Y., "Thermophysical Properties of High Temperature Solid Materials" (section 101-0012) Ed. Y. S. Toulaukian (Macmillan N.Y. - 1970).
78. Rye, R. R., J. Chem. Phys. (1969) <u>50</u> (8) 3585.
79. Hopkins, D. J. and Shah, D. R., Vacuum (1972) <u>22</u> 267.
80. Burns, R. A., Ph.D. Thesis - Iona State University (1970), (Diss. Abs. <u>31q</u> 5284 B, (1971)).
81. Wright, P. G., Ashmore P. and Kemball, C., Trans. Far. Soc. (1958) <u>54</u> 1692.
82. Yates, J. T. and Madey, T. E., J. Vac. Sci. Tech. (1972) <u>9</u>(2) 672.
83. Eley, D. D., Disc. Far. Soc., (1950) <u>8</u> 34.
84. Stephenson, D. P., J. Chem. Phys., (1955) <u>23</u> 203.
85. Eley, D. D. et al., Proc. Roy. Soc. (1969) <u>A.314</u> 319.
86. Tontegode, A. Ya., and Zandberg, E. Ya., Sov. Phys. - Tech. Phys. (1966) <u>10</u> 1162.
87. Munick, R., La Boge, W. and Coomes, E., Phys. Rev. (1950) <u>80</u> 887.
88. Jowlett, C. and Hopkins, B., Surface Science (1970) <u>22</u> 405.
89. Duell, M. and Moss, R., Trans. Far. Soc. (1965) <u>61</u> 2262.
90. A rmstrong, R. A. and Legget, M. R., Surface Science (1971) <u>24</u> 404.
91. Tamm, P. W. and Schmidt, L. D., J. Chem. Phys. (1969) <u>51</u> 5352.
92. Fomenko, V. S., "Handbook of Thermionic Properties", Ed. E. V. Samsonov (Plenum Press - 1966).
93. Page, F. M., Trans. Far. Soc., (1961) <u>57</u> 359.
94. Mayer, J. E. and Sutton, P. P., J. Chem. Phys. (1934) <u>2</u> 145.
95. Berry, R. S. and Reimann, G. W., J. Chem. Phys. (1963) <u>38</u> (1540).
96. Morrison, J. D. et al., J. Chem. Phys. (1960) <u>33</u> 821.

97. Müller, E., Ann. Physik (1932) 14 831.

98. Kalandyk, S., Acta. Phys. Polonica (1934) 3 165.

99. Zandberg, E. Ya., Sov. Phys. - Tech. Phys., (1972) 17(4) 665.

100. Morgan, A. E., Trans. A mer. Crystall. Assoc. (1968) 4 59.

101. Ritchie, B. and Wheeler, R., J. Phys. Chem. (1966) 70 113.

102. Biondi, M. A., and Fox, R. E., Phys. Rev. (1960) 109 2112.

103. Christophorou, L. G. and Compton, R. N., Health Physics, (1967) 13 1277.

104, Azaroff, L. V. and Buerger, M. J.,"X-Ray Crystallography - The Powder Method", (McGraw Hill - 1958).

105. Chamberlain, A. T., private communication.

106. Ingold, J. H., J. Appl. Phys., (1963) 34 2033.

107. Resnick, R. and Seigle, L., Trans. Met. Soc. AIME., (1966) 236 1732.

108. Resnick, R. et al., Trans. Met. Soc. AIME., (1965) 233 1915.

109. Brizes, W. F., U. S. At. Energy Comm., WANL-TNR-205 (1967) (C.A. 68 43386b).

110. Fromm et al., Z. Metallk. (1966) 57 808.

111. Eyring, H. and Stean, A. E., J. Phys. Chem., (1940) 44 955.

112. Suziki et al., Bull. Tokyo Inst. Technol., (1969) 90 105.

113. Hansen, M., "Constitution of Binary Alloys", 2nd edition, (McGraw Hill - 1958) 370.

114. Eckstein, B. H. and Forman, R., J. Appl. Phys., (1962) 33(1) 82.

115. Goldwater, D. L., and Haddad, R. E., J. Appl. Phys. (1951) 22 70.

116. Redmond, B. and Smith, E. N., Metal Trans., 185 987.

117. Fowler, R. H.,"Statistical Mechanics", (C. U. P.- 1936).

-o-